 ANL-7639

VARIABLE TEMPERATURE RODDED ZONE PROJECT: DESIGN SUMMARY REPORT

R. A. Lewis, K. D. Dance, J. F. Meyer,
E. F. Groh, and E. M. Bohn

BASE TECHNOLOGY

RETURN TO REFERENCE FILE
TECHNICAL PUBLICATIONS
DEPARTMENT

U of C-AUA-USAEC

ARGONNE NATIONAL LABORATORY, ARGONNE, ILLINOIS

Prepared for the U.S. ATOMIC ENERGY COMMISSION
Division of Reactor Research and Development
under Contract W-31-109-Eng-38

The facilities of Argonne National Laboratory are owned by the United States Government. Under the terms of a contract (W-31-109-Eng-38) between the U. S. Atomic Energy Commission, Argonne Universities Association and The University of Chicago, the University employs the staff and operates the Laboratory in accordance with policies and programs formulated, approved and reviewed by the Association.

MEMBERS OF ARGONNE UNIVERSITIES ASSOCIATION

The University of Arizona
Carnegie-Mellon University
Case Western Reserve University
The University of Chicago
University of Cincinnati
Illinois Institute of Technology
University of Illinois
Indiana University
Iowa State University
The University of Iowa
Kansas State University
The University of Kansas
Loyola University
Marquette University
Michigan State University
The University of Michigan
University of Minnesota
University of Missouri
Northwestern University
University of Notre Dame
The Ohio State University
Ohio University
The Pennsylvania State University
Purdue University
Saint Louis University
Southern Illinois University
The University of Texas at Austin
Washington University
Wayne State University
The University of Wisconsin

NOTICE

This report was prepared as an account of work sponsored by the United States Government. Neither the United States nor the United States Atomic Energy Commission, nor any of their employees, nor any of their contractors, subcontractors, or their employees, makes any warranty, express or implied, or assumes any legal liability or responsibility for the accuracy, completeness or usefulness of any information, apparatus, product or process disclosed, or represents that its use would not infringe privately-owned rights.

Printed in the United States of America
Available from
National Technical Information Service
U.S. Department of Commerce
5285 Port Royal Road
Springfield, Virginia 22151
Price: Printed Copy $7.60; Microfiche $1.45

ARGONNE NATIONAL LABORATORY
9700 South Cass Avenue
Argonne, Illinois 60439

ERRATA TO

ANL-7639

VARIABLE-TEMPERATURE RODDED ZONE PROJECT:
DESIGN SUMMARY REPORT

1. On cover, title page, and page 13, please change authors to read:

   R. A. Lewis, K. D. Dance, J. F. Meyer,
   E. F. Groh, and E. M. Bohn

2. Replace page 250 with the attached new page 250.

November 26, 1973

ACKNOWLEDGMENTS

We wish to acknowledge the contributions of the following persons to the Variable Temperature Rodded Zone and to the writing of this report:

Applied Physics Division

C. E. Till, G. K. Rusch, D. M. Smith, D. J. Kilsdonk, T. W. Johnson, R. D. Shields, W. J. Grajek, F. L. Willis, and D. R. MacFarlane.

Electronics Division

W. P. McDowell, J. M. Paul, A. L. Winiecki, and H. W. Helenberg.

Plant Engineering Division

L. J. Kelly.

Central Shops Department

J. J. McKinney, A. A. Frigo, E. F. Bielick, D. A. Cassidy, R. F. Hall, E. F. Lewandowski, and the other shop personnel in the Building 316 and Building 20 shops who made valuable contributions to this project.

Laboratory Director's Office

F. H. Martens.

Engineering and Technology Division

T. J. Lucitt and R. A. Banike.

TABLE OF CONTENTS

	Page
ABSTRACT	13
1. INTRODUCTION	13
1.1 Scope of This Document	13
1.2 Reference Documents	14
2. PURPOSE AND OBJECTIVES OF THE VTRZ DESIGN	16
2.1 Experimental Reactor-physics Requirements	16
2.2 The VTRZ Concept	21
2.3 VTRZ Design Criteria	22
3. DESIGN STANDARDS	25
3.1 Earthquake Resistance Standards	25
3.2 Structural Materials	27
3.3 Design-basis Stress Limits	28
3.3.1 Components with Maximum Operating Temperature below 800°F (425°C)	28
3.3.2 Components with Maximum Operating Temperature above 800°F (425°C)	29
3.4 Design-basis Operating Parameters	30
3.4.1 Inner (heatable) Matrix Assembly	31
3.4.2 Outer Matrix Assembly	32
3.5 Prototype Testing Requirements	32
4. DESIGN DESCRIPTION	33
4.1 Brief Overall Design Description	33
4.2 Normal (unheatable) ZPR-6 and -9 Critical Facilities and Plate-type Fuel Drawers	38
4.3 Oxide Fuel Rods	45
4.4 Calandria Cans	51
4.5 Heatable Zone Facility	56
4.5.1 Procurement Quality Assurance	56

TABLE OF CONTENTS

Page

4.5.2 Outer Matrix Bridge Structure 59
4.5.3 Inner (heatable) Matrix Assembly 66
4.5.4 Insulation-annulus Components. 85
4.5.5 Argon Loop System 89
4.5.6 Air-cooling Systems. 114
4.5.7 Electrical Power System. 121
4.5.8 Temperature Instrumentation. 127
4.5.9 Component Failure Monitors 134
4.5.10 VTRZ-ZPR Reactor-scram System. 140
4.5.11 Heater-power-interlock System 143
4.5.12 Alarm System 146
4.5.13 Room-temperature Operation of the Heatable Zone . 147
4.5.14 Miscellaneous Auxiliary VTRZ Components 153
4.5.15 Experimental Equipment 157

5. HEAT-TRANSFER ANALYSES AND TESTS 160

5.1 Room-temperature Operation of Calandria-can Assemblies with $(Pu,U)O_2$ Fuel Rods 160

5.1.1 Plutonium-alpha Self-heating. 160
5.1.2 Inner-matrix Air-cooling System 160
5.1.3 Heat-transfer Analysis: Oxide Fuel Rods to Cooling Air 162

5.2 Elevated-temperature Operation of the Fuel-rod-loaded Calandria-can Assemblies in VTRZ Heatable Zone 163

5.2.1 Summary of VTRZ Heated Operation. 163
5.2.2 Heat Transfer within Calandria Cans 166
5.2.3 Heat Transfer between Calandria Cans 168
5.2.4 Heat Capacities. 169
5.2.5 General Heatup 169
5.2.6 Equilibrium Operation 170
5.2.7 Cooldown 172
5.2.8 Front-cover Exposure 173
5.2.9 Air Cooling of Outer Matrix 175

6. STRESS ANALYSES AND TESTS. 177

6.1 Stress Analyses and Tests of the Oxide Fuel Rods 177

6.1.1 Fuel-rod Mechanical Characteristics 177
6.1.2 Fuel-rod Stress Analysis 178
6.1.3 Fuel-rod Operational Tests. 181

TABLE OF CONTENTS

Page

6.2 Stress Analyses and Tests of Calandria Cans 184

6.2.1 Mechanical Characteristics of Calandria Cans 184
6.2.2 Stress Analyses of Calandria Cans 185
6.2.3 Operational Testing of Calandria Cans 187

6.3 The Inner Matrix Assembly 189

6.3.1 Stress Analysis. 189
6.3.2 Inner-matrix-assembly Seismic Analysis 192
6.3.3 Inner-matrix-assembly Prototype Load Tests 194

6.4 Ball Mounts 194

6.4.1 Ball-mount Stress Analysis. 194
6.4.2 Corrosion of Ball-mount Insert Plate and Ball Material 200
6.4.3 Ball-mount Tests 201

6.5 Inner-matrix-assembly Cover Plates 204

6.5.1 Front Cover 204
6.5.2 Service Housing 207

6.6 Outer Matrix Assembly and Central Zone Bridge. 207

6.6.1 Stress Analysis of Outer-matrix-assembly and Central-zone-bridge Combination. 207
6.6.2 Load Testing in VTRZ Prototype 209
6.6.3 Comparison of Calculated and Measured Outer-matrix-assembly Stress-load-deflection Values 210
6.6.4 Stress Analysis of the Reactor-knee Constraints. . . . 213

7. GAS-FLOW ANALYSES AND TESTS 215

7.1 Argon Loop. 215

7.1.1 Argon-loop-flow Pressure-drop Analysis 215
7.1.2 Analysis of High-pressure Relief System. 217
7.1.3 Argon-loop Prototype Experience. 219

7.2 Cooling-guard-ring (CGR) System. 220

7.3 Inner-matrix-cooldown (IMCD) System 221

8. INSTRUMENTATION ANALYSES AND TESTS 223

8.1 Heater Fuses 223

TABLE OF CONTENTS

Page

8.1.1 Analyses of Heater-fuse Operation 223
8.1.2 Prototype Tests of Heater Fuses 224

8.2 Calandria-can Overheat Detection. 225

8.2.1 Analysis of Calandria-can Overheat Monitoring System 225
8.2.2 Prototype Testing of Calandria-can Overheat Monitoring System 229
8.2.3 Effect of Thermocouple Burnouts on System Operation. 230

8.3 Calandria-can Failure Monitor. 231

8.4 Fuel-rod Failure Monitors 231

8.4.1 Helium Fuel-rod Failure Monitor. 231
8.4.2 Plutonium-alpha Fuel-rod Failure Monitor 234

8.5 Monitoring of Argon Cover-gas Purity. 239

8.6 Inner-matrix-assembly Expansion Monitor. 240

9. NUCLEAR ANALYSES FOR TYPICAL VTRZ ASSEMBLIES 242

9.1 VTRZ Reference Assemblies 242

9.2 Operational Characteristics of Reference VTRZ Assemblies. 244

9.3 Calculations of Core-distortion Effect 246

ACKNOWLEDGMENTS 250

REFERENCES 251

LIST OF FIGURES

No.	Title	Page
1.	Typical ZPR Fuel and Diluent Plates	17
2.	Typical Loaded ZPR Plate-type Fuel Drawer	18
3.	Pictorial View of ZPR-6 Fast Critical Facility	19
4.	Calculated Maximum Acceleration Response of a Damped Spring-mass Oscillator to the Design-basis Earthquake	27
5.	Typical Plate-type Fuel Drawer, Calandria Cans, and Oxide Fuel Rods	34
6.	VTRZ in ZPR-6	35
7.	Section View of VTRZ	36
8.	Perspective Cutaway View of Single VTRZ Half-zone	37
9.	Line Drawing of ZPR-6 Fast Critical Facility	39
10.	Plates and Blocks for ZPR-6 and -9	44
11.	Three Loaded ZPR Drawers	45
12.	Fuel Rod	46
13.	Square and Triangular Calandria Cans	53
14.	Square-cross-section Calandria Cans	54
15.	Welding Pattern Used in Outer Matrix Assembly	61
16.	Side View of Outer Matrix Assembly	63
17.	Rear View of Outer Matrix Assembly	64
18.	Central Zone Bridge	65
19.	Inner-matrix Assembly	67
20.	Typical Square Matrix Tube	67
21.	Cutout for Radial Access Hole	68
22.	Triangular Tubes	69
23.	Summary of Inner-matrix Weld	70
24.	Inner-matrix Jacket	71
25.	Front Cover of Inner Matrix	73
26.	Service Housing	74
27.	Inert-gas (argon) Circulation Pattern within Inner-matrix Envelope	75

LIST OF FIGURES

No.	Title	Page
28.	Calandria-can Positioner Clips	76
29.	Thermocouple and Heater-bus Wiring within Wiring Space	78
30.	Inner-matrix Flange and Service-housing Heaters	79
31.	Inner-matrix Cooldown Duct System	80
32.	Inner-matrix Jacket, Ball Mount, Axial Guides, and Motion-restrainer Positions	82
33.	Ball Mount	83
34.	Inner-matrix Complex	84
35.	Insulation-annulus Configuration, Rear View	85
36.	Insulation-annulus Configuration, Side View	86
37.	Schematic of Argon Loop System	90
38.	"Purge" and "Normal" Mode Schematic of VTRZ Argon Loop System	91
39.	Pneumatic-valve Digital-logic Circuitry	95
40.	Simplified Argon Loop System	97
41.	Argon-loop-system Typical Monitor Assembly	98
42.	Typical Thermocouple Sensor and Housing	102
43.	AEC Filter and Housing	103
44.	VAC Dri-Train with VTRZ Modifications	105
45.	Purifier in Regeneration Station	106
46.	Front Panels--Flow and Pressure Control	107
47.	Manual Normal-mode Pressure Control in Reactor Cell	109
48.	Semiautomatic Normal-mode Pressure Control in Reactor Cell	109
49.	Semiautomatic Normal-mode Pressure Control in Control Room	110
50.	Automatic Normal-mode Pressure Control	110
51.	High-pressure Relief System	112
52.	Low-pressure Relief System	114
53.	Cooling Guard-ring System	115

LIST OF FIGURES

No.	Title	Page
54.	Inner-matrix Cooldown System	116
55.	Outer-matrix Cooling System	117
56.	Schematic of VTRZ Electrical Power System	122
57.	Detail--Electrical Power-distribution System for VTRZ Inner-matrix-assembly Heaters	123
58.	Installation of VTRZ Electrical System in ZPR-6 Cell	124
59.	Thermocouple Location Scheme for Calandria-can Overheat Requirement	128
60.	Thermocouple Location Scheme with "Complete Redundancy"	129
61.	Typical Thermocouple Location Scheme for Insulation Annulus and Outer Matrix	130
62.	VTRZ Temperature Instrumentation	132
63.	Plutonium-alpha Monitor	135
64.	Helium Monitor Assembly	138
65.	VTRZ Scram System	141
66.	Heater-power-interlock System	144
67.	VTRZ Alarm System	148
68.	VTRZ Display Panel	149
69.	VTRZ Dual-purpose Rod-mounting Plates	154
70.	Knee Constraint	156
71.	Calculated Total Differential Pressure across Matrix for Three 12-in. Calandria Cans per Tube per Reactor Half; Matrix Cooling-air System	161
72.	Calculated Matrix Cooling-air Temperature Rise across 72-in.-long, $(Pu,U)O_2$-fueled, Calandria-can Core	162
73.	Design-reference Inner-matrix Cartridge-heater Array	164
74.	Alternative Inner-matrix Cartridge-heater Array	164
75.	Calculated VTRZ Heatup Pattern	170
76.	VTRZ Equilibration from Uniform Power Reduction from 32 to 2 kW	171
77.	Axial-motion-restrainer Bracket	191

LIST OF FIGURES

No.	Title	Page
78.	Lower Ball-mount Bracket	196
79.	Upper Ball-mount Bracket	197
80.	Final Outer Weldment; Deflections and Stresses for Design Load of 19,800 lb	209
81.	Configuration for Prototype-outer-matrix Load Test	211
82.	Deflection vs Load in Single Row of Welded Matrix Tubes	212
83.	Deflection vs Load in Prototype Outer Weldment	213
84.	Argon-loop Flow Resistance	216
85.	VTRZ Dri-Train Blower Curves for Pressure-drop Analysis	216
86.	Flow Resistance for High-pressure Relief System	218
87.	Cooling-guard-ring Flow-pressure Curves	221
88.	Inner-matrix-cooldown Flow-pressure Curves	222
89.	Fuse-testing Oven	226
90.	Zonal Configuration for VTRZ-1	243
91.	Zonal Configuration for VTRZ-2	243
92.	Radial Flux and Adjoint-flux Distributions for VTRZ-1	246
93.	Radial Flux and Adjoint-flux Distributions for VTRZ-2	246

LIST OF TABLES

No.	Title	Page
1.	Probabilities That the Design Ground Motion and the Two Times Ground Motion Will and Will Not Be Exceeded at Least Once in N Years	26
2.	VTRZ Design-basis Earthquake-induced Acceleration Loads	27
3.	Design Working Stress Limits for VTRZ Components To Be Constructed of Type 304 or 304L Stainless Steel and To Have Maximum Operating Temperatures below 800°F (425°C)	29
4.	Design Working Stress Limits for Type 304 or 304L Stainless Steel Components with Maximum Operating Temperatures above 800°F (425°C)	30
5.	VTRZ Design-basis Operating Parameters	31
6.	Summary of Physical Characteristics of ZPR-6 and -9	41
7.	Inventory of Fissile and Fertile Material Plates	44
8.	Inventory of UO_2 Fuel Rods	47
9.	Inventory of $(Pu,U)O_2$ Fuel Rods	48
10.	Specific Impurity Limitations in Oxide Fuel Pellets	49
11.	Inventory of Calandria Cans	56
12.	VTRZ Heatable Zone Facility Procurement	57
13.	Welding-procedure Qualification, Operator Qualification, and Periodic Tests	59
14.	Argon-loop-system Valve Configurations	94
15.	VTRZ Scram Conditions and Circuitry	142
16.	VTRZ Heater-interlock Conditions and Circuitry	145
17.	VTRZ Heater-interlock Conditions and Ranges	146
18.	VTRZ Alarm Conditions and Circuitry	150
19.	VTRZ Alarm Conditions and Ranges	152
20.	Calculated Pu-alpha Self-heating in $(Pu,U)O_2$ Fuel Rods	160
21.	Calculations of Calandria-can Temperatures Resulting from Transfer of Pu-alpha Decay Heat from $(Pu,U)O_2$ Fuel Rods to Cooling Air around Calandria Cans	162
22.	Operating Temperatures in Calandria Cans Containing Heaters	167
23.	Calandria-can-heater Power Restrictions and Recommendations	167

LIST OF TABLES

No.	Title	Page
24.	Heat Transfer between Adjacent 2 x 12-in. Calandria-can Faces	168
25.	Calculated Heat Leakage from Inner Barrel to Outer Matrix at 550°C Operating Temperature	175
26.	Oxide Fuel-rod Bursting Temperatures	181
27.	Fuel-rod Exposure Tests for Various Temperature and Pressure Conditions	182
28.	Heatable (Type H) Calandria-can Thermal-cycling Tests	187
29.	Results of Calandria-can Overheat Tests	188
30.	Summary of Argon-loop Pressure-drop Analysis	215
31.	Capabilities of VTRZ High-pressure Relief System	218
32.	Summary of Cooling-guard-ring Pressure-drop Analysis	220
33.	Summary of Inner-matrix-cooldown Pressure-drop Analysis	221
34.	Summary of Fuse Testing for VTRZ	224
35.	Summary of Helium-monitor Prototype Testing	233
36.	Regional Cell Patterns in Reference Assemblies	242
37.	Reference Assembly VTRZ-1	243
38.	Reference Assembly VTRZ-2	243
39.	Criticality Parameters and Reactivity Coefficients for Reference Assemblies	245
40.	Material Worths	246
41.	Real and Adjoint Flux at Center of VTRZ for VTRZ-2 with and without Insulation Zone	247
42.	Reactivity Effect due to Collapse of Insulation Zone	248

VARIABLE TEMPERATURE RODDED ZONE PROJECT: DESIGN SUMMARY REPORT

by

R. A. Lewis, K. D. Dance, J. F. Meyer,
E. F. Groh, and E. M. Bohn

ABSTRACT

This report summarizes all aspects of the design of the Variable Temperature Rodded Zone (VTRZ) and the principal engineering analyses and laboratory tests upon which the design is based. The VTRZ design described in this report represents the design at the end of the formal Design and Development Phase. Changes made in the VTRZ design as a result of experience gained in the preoperational testing will be described in a later document. This report provides a systematic reference source on VTRZ design for use in subsequent installation, operation, maintenance, and modification phases of the VTRZ project.

1. INTRODUCTION

1.1 Scope of This Document

This document summarizes all aspects of the design of the Variable Temperature Rodded Zone (VTRZ) and the principal engineering analyses and laboratory tests upon which the design is based. The purpose of the VTRZ in the overall ANL Critical Experiments Program is discussed, and the specific design criteria and design standards that have been applied are described. Technical descriptions of the design of all major VTRZ subcomponents and subsystems are included. The principal engineering analyses and tests carried out as part of the VTRZ design are summarized to provide a complete design description.

The VTRZ design described in this report represents the design at the end of the formal Design and Development Phase of the project. It is probable that some, at least minor, changes will be made in the design as a part of experience gained during installation and preoperational testing.

The primary purpose of this report is to provide a systematic reference source on VTRZ design for use in subsequent installation, operation, maintenance, and (possibly) modification phases of the VTRZ project. Secondarily, this report provides supporting documentation for the VTRZ Final Safety Analyses Report (ANL-7638).

1.2 Reference Documents

The following list contains the principal documents used during the VTRZ design work or resulting from the design work:

(1) W. Y. Kato et al., Final Safety Analysis Report on the Use of Plutonium in ZPR-6 and -9, ANL-7442 (Feb 1970).

This document governs the operation of the ZPR-6 and -9 facilities and was used as the basic reference document concerning ZPR-6 and -9 operating procedures and limits.

(2) R. A. Lewis, Quality Assurance Program, Variable Temperature Rodded Zone Project, Heatable Zone Facility (Sept 29, 1969) (VTRZ Project Document).

This document, specifically approved by the AEC-RDT, governed the design phase of the heatable zone portion of the VTRZ (i.e., all except the design of the oxide fuel pins and the calandria cans).

(3) A. B. Shuck et al., Reactor Fuel Specification: Enriched Uranium Dioxide Fuel Rods for Zero Power Reactors, RF-B3a,b (ZPR).

This document governed the procurement and ANL inspection of all of the various types of oxide fuel rods.

(4) R. A. Lewis et al., Variable Temperature Rodded Zone Project, Final Safety Analysis Report, ANL-7638 (to be published).

(5) VTRZ Design File (VTRZ Project Document).

This document contains copies of all design analyses, test procedures, test result reports, and other design data generated by the project.

(6) VTRZ Quality Assurance File (VTRZ Project Document)

This document contains copies of all communications relating to VTRZ project quality assurance except those related to the calandria cans.

(7) VTRZ Administrative File (VTRZ Project Document)

This document contains copies of all communications relating to VTRZ budgets, personnel assignments, and schedules except those related to the calandria cans.

(8) VTRZ Calandria Can File (VTRZ Project Document)

This document contains copies of all documents related to quality assurance and administration of the calandria cans.

(9) Procurement Specifications

The following documents were generated by the VTRZ design phase to control the procurement of the VTRZ:

a. Oxide Fuel Pin Procurement Specifications

(1) ANL Specification No. RF-B2b,c (ZPR), Reactor Fuel Specification, Uranium-Plutonium Dioxide Fuel Rods for Zero Power Reactors.

(2) ANL Specification No. RF-B3a,b (ZPR), Reactor Fuel Specification, Enriched Uranium Dioxide Fuel Rods for Zero Power Reactors.

(3) ANL Specification No. RF-C2d (ZPR), Reactor Fuel Specification, Depleted Uranium Dioxide Fuel Rods for Zero Power Reactors.

b. ANL Specification No. RF-C1c (ZPR), Calandria for Variable Temperature Rodded Zone

c. Heatable Zone Procurement Specifications

(1) ANL Specification No. ANL-3605-RP, Specification for Heatable Zone Facility, Mechanical Section, Variable Temperature Rodded Zone Project.

(2) ANL Specification No. ANL-315-36-RP, Specification for Procurement of Components for Electrical Power Section, Heatable Zone Facility, Variable Temperature Rodded Zone Project.

(3) ANL Specification No. ANL-SY215-RP, Specification for Variable Temperature Rodded Zone Project, Heatable Zone Project, Heatable Zone Facility, Instrumentation and Control Section Equipment.

(4) ANL Specification No. ANL-IGL-RP, Specification for Heatable Zone Facility, Inert Gas Loop Section, Variable Temperature Rodded Zone Project.

2. PURPOSE AND OBJECTIVES OF THE VTRZ DESIGN

2.1 Experimental Reactor-physics Requirements

The study of the core physics of large fast-breeder-reactor designs through critical experiments is a fundamental part of the overall fast-breeder-reactor development program in the United States. At present, these critical experiments are devoted primarily to studies of large dilute liquid-metal-cooled fast-power-breeder (LMFBR) designs. The critical experiment program is being carried out principally at Argonne National Laboratory using the ANL ZPR-3, -6, -9, and ZPPR facilities.

The design of the Argonne ZPR critical facilities is based on the assumption of room-temperature (zero-power) operation in which the fast-reactor critical mockups are built up from an inventory of reactor component materials in the form of thin plates. The reactor inventory contains large numbers of thin plates, typically 1/16 to 1/2 in. thick, 2 in. high, and 2-8 in. long, of materials needed in fast-reactor assemblies: for example, Pu-U alloy, enriched and depleted uranium, depleted U_3O_8, depleted UO_2, stainless steel, sodium, and Fe_2O_3. The plates are canned in stainless steel where this is appropriate. Figure 1 illustrates typical ZPR mockup material plates. Fast-breeder-reactor critical assemblies of various compositions can be constructed by mixing appropriately chosen numbers and types of mockup plates in ZPR fuel drawers, as shown in Fig. 2, and loading the drawers into the matrix tubes of the ZPR facilities, as shown in Fig. 3. The ZPR fuel drawers are nominally 2 in. square by 15-33 in. long and are inserted into matrix tubes $2\frac{1}{2}$ to 5 ft long, depending on the ZPR facility. All plate cladding, fuel drawers, and matrix tubes to be used in conjunction with the VTRZ are 304 stainless steel.

The ZPR facilities are of a split-table design, as shown in Fig. 3. This design was chosen for loading convenience and to obtain a large margin of reactor shutdown reactivity.

From the standpoint of reactor physics, the cores of fast breeder power reactors presently being designed differ from the ZPR critical mockups in two ways: configuration and temperature. The fast-power-breeder cores consist of mixed PuO_2-UO_2 fuel rods, clad in stainless steel (Type 304 or 316), and set in a tight lattice with liquid sodium flowing between the rods. The fuel rods typically operate at about 550°C surface temperature and 2500°C central temperature.

Over the broad central range of the neutron spectrum typical of fast breeder reactors, from about 10 keV to 1 MeV, the differences in core configuration, or heterogeneity, between the ZPR plate cores and the fast-breeder-reactor rodded cores have very little significance because of the small cross sections and, therefore, the relatively long mean free paths;

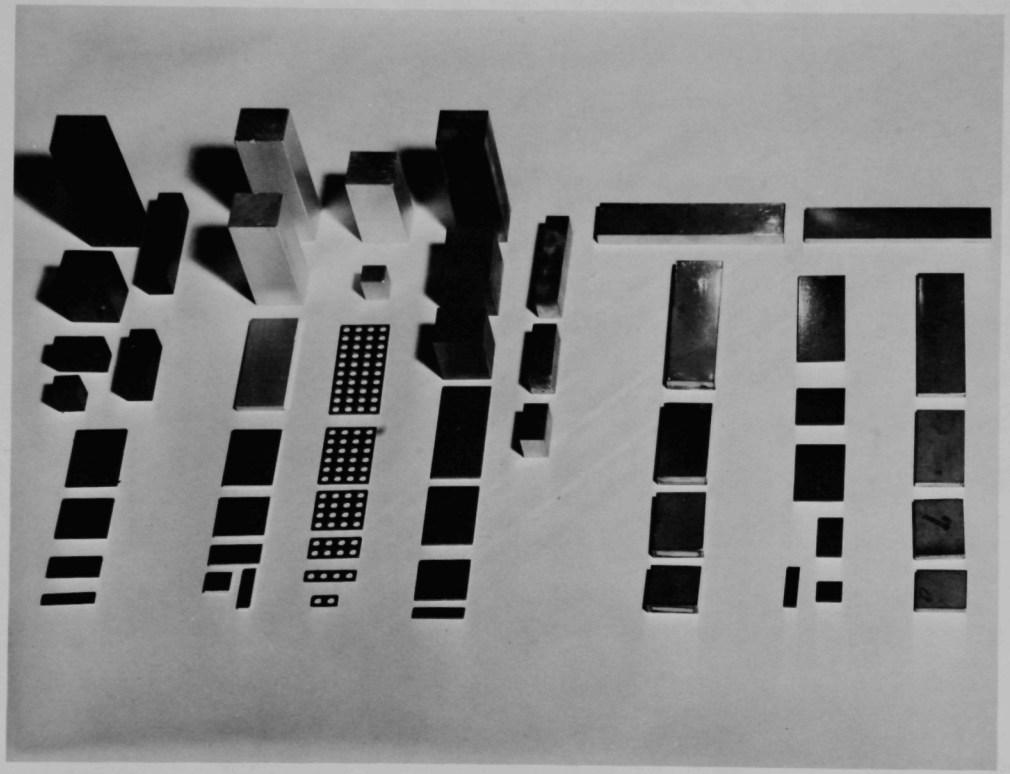

Fig. 1. Typical ZPR Fuel and Diluent Plates. ANL Neg. No. 112-9993.

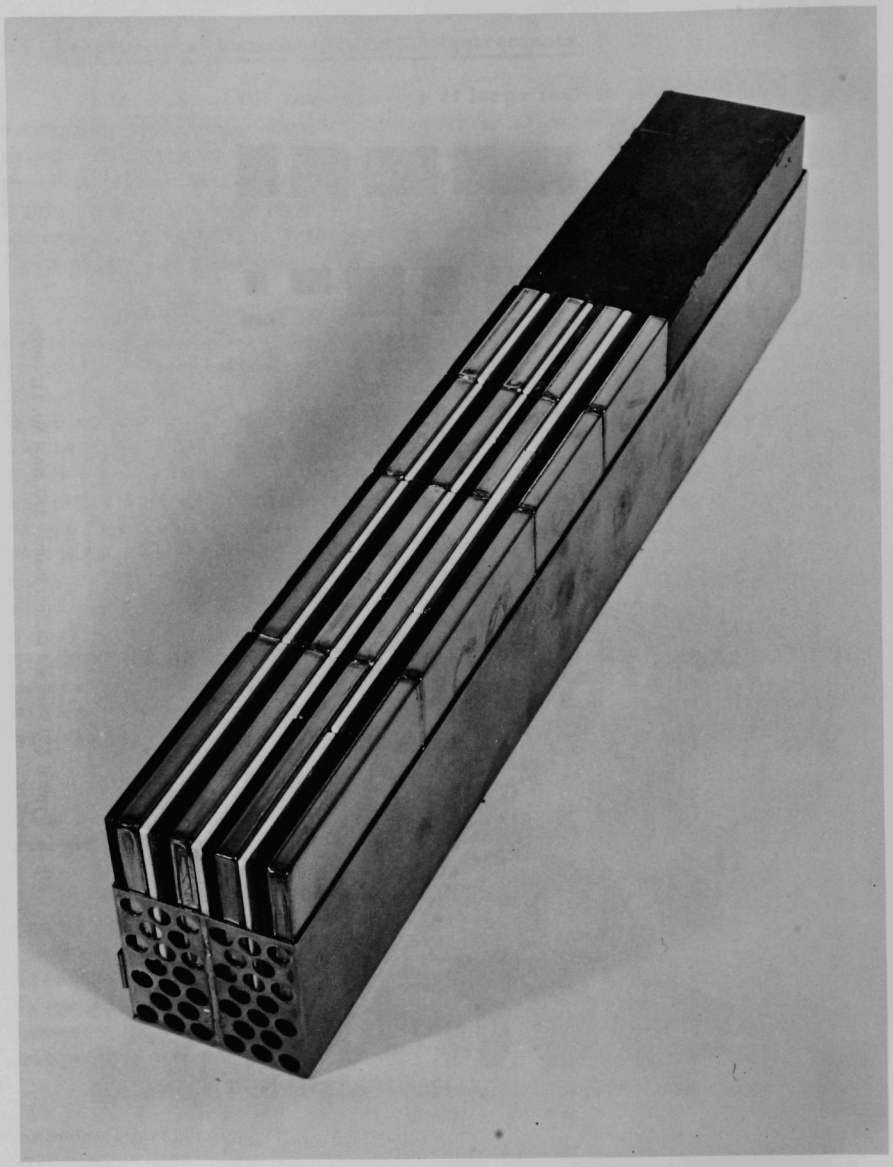

Fig. 2. Typical Loaded ZPR Plate-type Fuel Drawer. ANL Neg. No. 112-5038.

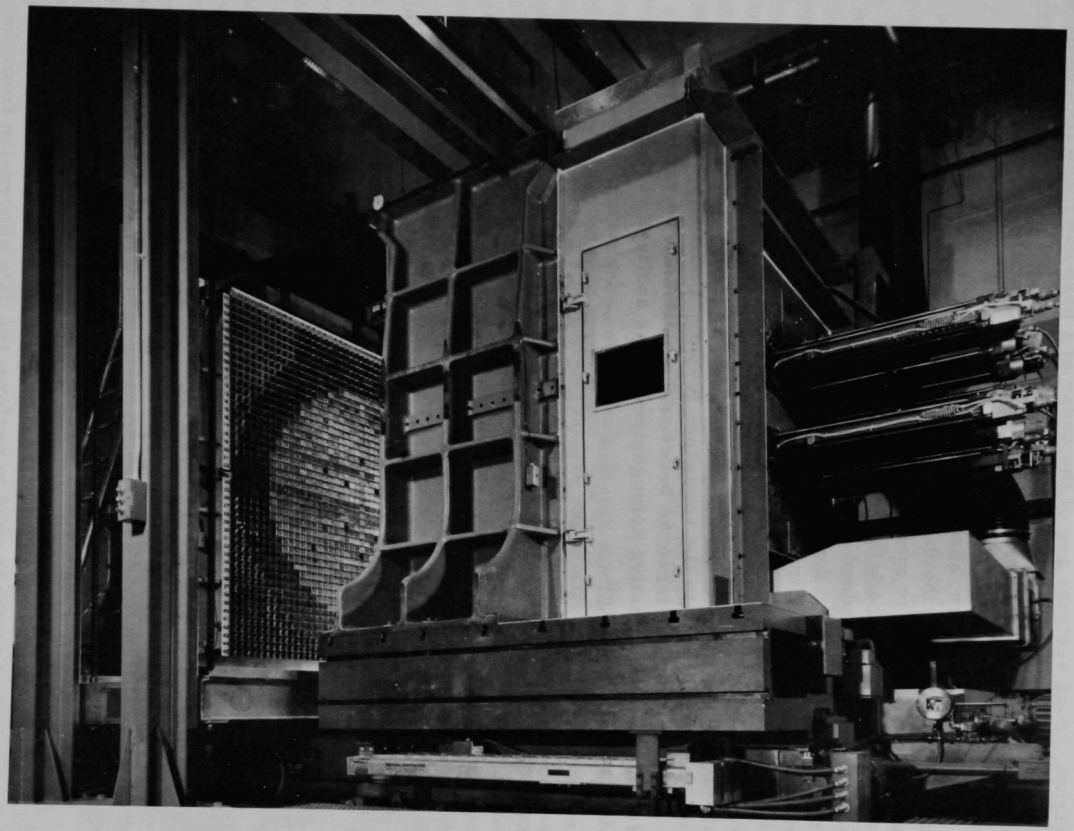

Fig. 3. Pictorial View of ZPR-6 Fast Critical Facility

i.e., in this energy range, which constitutes the bulk of the spectrum, the fast reactor is essentially homogeneous from a physics standpoint, regardless of the detailed core configuration. In this midrange of the fast-reactor spectrum, cross sections are of the order of 1 barn and mean free paths are of the order of 10 cm. However, above 1 MeV and below 10 keV, the exact configuration of the fast core does have an effect on the core physics.

At high energies, above 1 MeV, the effects of configuration are principally a result of the differences in fast-fission probabilities caused by the differences in the manner in which the ^{239}Pu (or ^{235}U) primary fission source is arranged, spatially, relative to other ^{239}Pu (or ^{235}U) or to fast-fissionable ^{238}U. In rodded configurations, the ^{239}Pu, ^{238}U, and oxygen are intimately mixed within the fuel pins; in the plate configurations, these components are generally separated spatially. Below 10 keV, the configurational effects on core physics are a result of the occurrence of large resonance cross sections, most significantly in ^{238}U, which cause very large neutron-spectrum perturbations localized in space (to the ^{238}U-containing plates) and in energy (to the resonance levels). Considered in another way, the configurational differences between the plate and rod cores result in differences in the effective homogenized cross sections of the cores above 1 MeV and below 10 keV.

The temperature differences between the ZPR assemblies and operating fast power reactors mean essentially that the ZPR assemblies mockup fast power reactors at room temperature rather than at operating conditions. Three effects of significance to core physics occur as a fast reactor is heated to operating temperature: an approximately 15% reduction in sodium density in the core, changes in low-energy cross sections (resonances) due to the Doppler effect, and gross core expansion of about 3% in volume.

On the basis of reactor-analysis calculations and small-scale heterogeneity measurements, the differences in configuration and temperature between hot-rodded fast-power-reactor cores and ZPR plate assemblies are not considered to be serious impediments to the acquisition, from the ZPR plate assemblies, of most integral reactor-core physics data needed to support efficient and accurate fast-reactor design calculations. However, it is now felt that systematic experimental studies of the plate-rod-temperature difference effects, as an associated part of the plate Critical Experiments Program, are needed for the following reasons:

(1) Calculated plate-versus-rod-heterogeneity differences amount to 1-3% in k depending on the core. It is important to verify the accuracy of the analytical methods used to perform the data conversion from the plate assemblies, in which they are measured, to the hot-rodded cores, in which they are needed.

(2) The effects of configurational and temperature differences at high and low energies are expected to be sufficient to have a significant effect on two important fast core parameters: the sodium-void and Doppler reactivity coefficients. This is due to the fact that these coefficients are sensitive to the details of the reactor neutron and adjoint spectra.

2.2 The VTRZ Concept

The purpose of the VTRZ project was to design, develop, and procure the necessary special equipment that would permit systematic comparative experimental studies of the reactor-core physics differences between hot-rodded fast-power-breeder cores and ZPR room-temperature plate-form critical mockups of these reactors. The basic concept of the VTRZ project was that an inventory of heatable oxide fuel rods and fuel-rod mounting assemblies would be acquired that could directly replace ZPR plate-fuel drawers in the ZPR matrix and that would be exactly matched to the composition of specific plate cores selected for study; i.e., the rodded assembly would differ from the plate assembly only in configuration, not in composition.

Two ZPR plate cores have been selected for the plate-rod-temperature studies out of the series of UO_2 and PuO_2-UO_2 LMFBR cores planned in the ANL Critical Experiments Program. The UO_2 core (ZPR-6 Assembly 6) is a 5/1 fertile-to-fissile ratio sodium-cooled assembly and the PuO_2-UO_2 core (ZPR-6 Assembly 7) is a 6.5/1 fertile-to-fissile ratio (plutonium, 11.5% ^{240}Pu) sodium-cooled assembly.

Oxide fuel rods and fuel-rod mounting assemblies have been ordered that exactly match the compositions of the two selected ZPR plate assemblies. The fuel rods are 3/8-in.-dia, 6-in.-long units clad in Type 304L stainless steel. The fuel-rod mounting assemblies are 2-in.-square, 12-in.-long Type 304L stainless steel, calandria cans, which can be filled with varying amounts of sodium to match the room-temperature plate cores and also to simulate cores at elevated temperature and with different amounts of sodium voiding. The fuel rods and calandria cans are designed to fit directly into ZPR matrix tubes replacing regular ZPR fuel drawers. For experimental flexibility, fuel rods containing depleted UO_2 and also fuel rods of high fissile enrichment are to be acquired, in addition to the fuel rods necessary for the direct plate-rod comparisons. Except for the calandria, which are loaded full of sodium at room temperature, all calandria cans and fuel rods are designed for heating to 600°C. This temperature limitation arises from the need to use Type 304 stainless steel to match that used in the ZPR plate cores.

For room-temperature plate-rod comparisons, the fuel-rod-calandria-can assembly can directly replace plate-fuel drawers in the regular ZPR matrix. For elevated temperature measurements, a special,

insulated, electrically heated, 25-cm-radius, 360-liter matrix section replaces the central portion of the regular ZPR matrix. This heatable zone facility contains a regular ZPR matrix structure. The plate-fuel drawers are unheatable; only the rod-calandria assemblies may be heated.

Although direct rod-versus-plate reactivity comparison measurements and intracell reaction-rate distribution measurements will be made on the room-temperature rod-calandria assemblies, the bulk of the experiments to be performed with the VTRZ equipment will be central-reactivity-worth measurements on a variety of materials--particularly, central sodium worth and ^{238}U Doppler. The basic idea is that the rod-calandria zone will be used to set up central real and adjoint spectra in which central-reactivity-worth measurements can be made. Because of the difficulties involved in subtracting expansion coefficients, measuring the Doppler coefficient of the VTRZ by direct measurement of the overall reactivity change of the reactor on heating up the entire heatable zone will probably not give a very precise result. This measurement will, however, be done to supplement other measurements.

The basic set of plate-rod-temperature comparison measurements will be repeated in a sequence of four assemblies to provide a basis for the separation of configurational and temperature effects:

(1) Plate core cold.

(2) Rod-calandria core cold with sodium matched to plate core.

(3) Rod-calandria core cold with sodium matched to hot-rodded core.

(4) Rod-calandria core hot.

2.3 VTRZ Design Criteria

The following is a list of the principal VTRZ design criteria derived from the experimental physics requirements, ZPR compatibility requirements, and general safety considerations. Where the basis of a criterion is not obvious from the foregoing discussion an explanation is given.

(1) The heatable zone should be ~25 cm in radius and contain ~360 liters of usable volume.

It is highly desirable to have a region for experiments in the center of the VTRZ, of about 6-in. (15-cm) radius, in which the neutron spectrum is essentially that of a full-size (single-zone) reactor having the same composition, configuration, and temperature as the VTRZ. Some additional radius is necessary as a neutron-spectrum buffer zone between

the experimental zone and the outer regions of the reactor in order to equilibrate the incoming neutron spectrum to that of the VTRZ. On the other hand, it is desirable to minimize the VTRZ size as much as possible, consistent with achieving the purposes of the experiment, to reduce inventory costs. Consideration of the typical 10-cm transport mean free paths at energies above 100 keV in these reactors, leads to a VTRZ radius of about 25 cm. There is considerable experimental evidence that 25 cm is an adequate radius for the VTRZ. The principal experimental evidence comes from a series of zoned reactor cores (ZPR-6 Assemblies 4Z, 5, and 6; and ZPR-9 Assemblies 11, 12, 18, and 19) in which central-reactivity-measurement results were compared in driven central zones of varying radius and in the full-size equivalent of these small zones. A VTRZ axial length of 72 in. (giving a 360-liter volume) was chosen to accommodate typical LMFBR core heights with a 12-in. axial blanket (depleted-UO_2 fuel rods) on each end.

(2) The heatable zone should contain regular ZPR matrix tubes. Plate-fuel drawers will not be heated.

This is to permit direct plate-fuel drawer and rod-calandria assembly replacements.

(3) Type 304 or 304L stainless steel shall be used for all components in the heatable zone, except where other materials are necessary for structural reasons. The maximum heatable-zone operating temperature should be set at the highest temperature consistent with the use of Type 304 (or 304L) stainless steel.

Limitation to Type 304 or 304L stainless steel is a result of the basic requirement that the rod-calandria assemblies and the heatable zone itself exactly match the ZPR plate assemblies. All plate cladding, fuel drawers, and matrix tubes in the regular ZPR assembly inventory is Type 304 stainless steel. As discussed below, the use of Type 304 or 304L stainless steel limits maximum operating temperatures to the range 550-650°C.

(4) The heatable zone is to be thermally isolated from the surrounding (plate-form) reactor core. The temperature of the reactor core adjacent to the VTRZ should be limited to a value consistent with structural strength requirements, and provisions should be made to stabilize this temperature so as to avoid excessive reactivity drifts.

(5) Due to the presence of high-temperature sodium and plutonium fuel rods in the heated zone, a gastight inert-gas-filled envelope should be provided around the zone to prevent sodium fires, in the event of sodium leakage out of the pin assemblies, and to contain the plutonium contamination in the event of a fuel-rod failure.

(6) The VTRZ should be heated electrically in such a way as to provide maximum flexibility of heating and sufficient heater power to achieve operating temperature in about 2 hr. The rate of thermal equilibration after achieving operating temperature should not be excessive compared to this heat-up time. These times are dictated by the normal 8-hr working shift. The temperature distribution should be controlled so that, at equilibrium, the heated zone is essentially isothermal.

(7) Provision should be made for cooling the heatable zone to a comfortable handling temperature over some reasonable period, of the order of 24 hr.

(8) The heatable zone should be split, on its axial midplane, into two equal subzones. The subzones should be provided with appropriate mounting arrangements so as to place one at the center of the movable reactor half and one at the center of the stationary reactor half. The mounting arrangement should cause the mating surfaces of the two halves of the heated zone to remain together and aligned during heated operation.

(9) Provision must be made for the support of the reactor materials above the insulated cavity containing the heatable zone (however, see Criterion 13).

(10) The VTRZ design should provide maximum flexibility and accessibility for experiments, consistent with safety. Provision for thermally isolated central reactivity measurements should be made.

(11) Remote control and monitoring of the VTRZ should be provided in the reactor control room.

(12) Provision for removal of plutonium-alpha decay heat should be made so that plate-fuel drawers or rod-calandria assemblies containing plutonium can be maintained at room temperature within the heatable zone when this is desirable.

(13) The amount and type of insulating and structural material between the heated zone and the surrounding core should be strictly controlled to minimize the perturbing effect on the neutron spectrum in this region.

(14) Operating material stress limits should be set with reasonable factors of safety considering the published material yield strengths, creep strengths, and the degree to which stress calculations have been verified with direct prototype tests.

3. DESIGN STANDARDS

3.1 Earthquake Resistance Standards

In the design of structures to resist the effects of earthquakes, the usual procedure is to require the structure to support certain acceleration-induced loads, in addition to the dead loads on the structure, within the design stress limits of the structure. The acceleration-induced loads may act vertically, up or down, and/or horizontally in any direction. The magnitudes, directions, and points of application of the acceleration-induced loads are based upon the assumed earthquake magnitude, the assumed ground-motion spectrum, and a dynamic analysis of the response of the structure to these assumed vibrations.

The VTRZ will be operated in either the ZPR-6 or the -9 Fast Critical Assembly. These assemblies are located in Building 316 on the ANL Site near Lemont, Illinois. No dynamic earthquake response analysis has ever been carried out for Building 316. A complete analysis is available, however, for the Argonne Advanced Research Reactor (AARR) Building,[1] which was to have been built about 350 m NNW of Building 316.

A complete dynamic earthquake-response analysis consists of four steps: First, a design earthquake-magnitude and ground-motion spectrum is postulated on the basis of site seismic history, geology, and acceptable probabilities that stronger earthquakes will not occur in given periods of time. Second, the resonant frequencies and damping factors of the soil-structure combination under consideration are calculated; in this analysis, the structure is assumed rigid and resting on an elastic soil base. Third, the internal resonant frequencies and resting damping factors of the structure itself are calculated. Fourth, the acceleration-induced loads at various points in the structure are calculated as the structure responds to the assumed input ground motion.

Based upon the AARR earthquake-response analysis report,[1] the acceleration-induced loads calculated for the AARR Building are applicable to Building 316. This conclusion is based upon the fact that the soil-structure resonant modes are the dominant effects in determining acceleration loads and these modes are primarily a result of the estimated soil-elasticity parameters. These elasticity parameters are identical for Building 316 and AARR because of the proximity of the AARR site. The importance of the internal-building-structure resonant frequencies in determining acceleration-induced loads is much less than the importance of the soil-structure resonances because the latter corresponds much more closely to the major earthquake frequency band. However, the designs of Building 316 and the AARR Building are sufficiently similar so that the internal building resonance frequencies should be nearly the same.

Reference 1 describes the method used for calculating earthquake-induced loads in the AARR structural design. Because of the apparent applicability of the AARR analysis to Building 316 and the VTRZ structure, the AARR analysis has been adopted as the basis for VTRZ earthquake-resistance design. The AARR-VTRZ earthquake design standard and its basis are summarized in the subsequent paragraphs of this section.

The VTRZ earthquake-design standard may be briefly stated as follows: The VTRZ-ZPR-6 structure shall be designed to accommodate the vertical and horizontal acceleration loads induced by the design-basis earthquake, in addition to all dead loads present, within normal design-working stress limits. The VTRZ-ZPR-6 structure shall also be designed to accommodate two times the vertical and horizontal acceleration loads, in addition to the dead loads present, within the yield stress of the materials of the structure.

The design-basis earthquake is defined as an earthquake of undefined epicenter location that results in a maximum (horizontal) ground acceleration at the VTRZ site of 0.075 g and exhibits the same ground-motion history as the May 18, 1940, El Centro, Calif., earthquake. The probabilities of the occurrence of such an earthquake at the VTRZ site are estimated in Ref. 1 on the basis of available seismic-activity historical data. Using the design standard stated in the previous paragraph, the probabilities of exceeding stress limits are shown in Table 1 (p. III-10 of Ref. 1). To further characterize the design-basis earthquake, it is calculated in Ref. 1 that a simple damped spring-mass oscillator exposed to the design-basis earthquake would respond with maximum accelerations, as shown in Fig. 4, as a function of oscillator resonant period and percent of critical damping. The oscillation of Fig. 4 would continue over the 1-3-min earthquake length.

It is estimated in Ref. 1 that reasonable soil-elasticity assumptions for the AARR-VTRZ site lead to soil-structure resonant frequencies in the range of 0.7-0.9 sec (5% critical damping). To be conservative, the 0.7-sec period is assumed (see Fig. 4) to be the actual resonant frequency.

TABLE 1. Probabilities That the Design Ground Motion and the Two Times Ground Motion Will and Will Not Be Exceeded at Least Once in N Years

	1	20	50
Probability of not reaching working stresses	0.99987	0.9978	0.9943
Probability of reaching working stress	0.00013	0.0022	0.0057
Probability of not yielding	0.99995	0.9990	0.9975
Probability of yielding	0.000046	0.001	0.0025

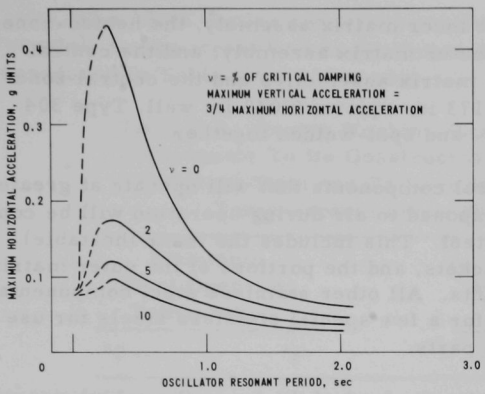

Fig. 4

Calculated Maximum Acceleration Response of a Damped Spring-mass Oscillator to the Design-basis Earthquake

Reference 1 shows that with the assumption of the 0.7-sec soil-structure period and conservative internal-structure resonant frequencies, the resulting earthquake-induced accelerations applicable to the VTRZ environment are 0.19 g horizontally and 0.07 g vertically. These accelerations are based on the assumption that the VTRZ equipment has natural periods of <0.1 sec and damping >0.5% of critical; these are easily achieved limits. Table 2 summarizes the earthquake-acceleration load criteria used in the VTRZ design; some additional acceleration has been arbitrarily added to approximately account for whatever differences might exist between the AARR Building and Building 316.

TABLE 2. VTRZ Design-basis Earthquake-induced Acceleration Loads[a]

	Vertical Acceleration, g	Horizontal Acceleration, g
Design to accommodate within design stress	0.1	0.2
Design to accommodate within yield stress	0.2	0.4

[a]VTRZ equipment must have natural resonant periods less than 0.1 sec and damping greater than 0.5% of critical damping.

3.2 Structural Materials

As discussed in detail below, the principal structural (i.e., load-carrying) components of the VTRZ are the inner (heatable-zone) matrix

assembly, the jacket enclosing the inner matrix assembly, the heated-zone-to-outer-matrix ball mounts, the outer matrix assembly, and the central zone bridge. The inner and outer matrix assemblies and the central zone bridge consist of regular ZPR (2.173 in. square, 0.040 in. wall, Type 304 stainless steel) matrix tubes tack- and spot-welded together.

All welded and/or structural components that will operate at greater than 100°C and will normally be exposed to air during operation will be constructed of Type 304L stainless steel. This includes the inner (heatable) matrix jacket, the ball-mount brackets, and the portions of the outer matrix assembly supporting the ball mounts. All other stainless steel components will be Type 304 or 304L, except for a few special stainless steels for use in making bolts, dowels, and spun parts.

The ball mounts that transfer the load of the inner (heatable) matrix assembly to the outer matrix assembly contain nickel-based super alloy (In-718) insert plates and tungsten carbide balls designed for high strength and oxidation resistance. The ball mounts operate in air between the heated and unheated portions of the VTRZ.

All structural components are described in detail in Chapter 4.

3.3 Design-basis Stress Limits

3.3.1 Components with Maximum Operating Temperature below 800°F (425°C)

Design stress limits for VTRZ components with maximum operating temperatures below 800°F (425°C) have been based upon the Design Stress Intensity values listed in Table N-421 of the ASME Boiler and Pressure Vessel Code, Section III, for Nuclear Vessels. For Types 304 and 304L stainless steel below 100°F, these design-stress-intensity values are two-thirds of the minimum 0.2% offset yield strength for the material. The minimum yield strength for Types 304 and 304L stainless steel to be used in the VTRZ is controlled through the specification that the material must be purchased and verified against ASTM standards. The principal load-carrying components of the VTRZ that operate in the temperature range covered by this section (i.e., below 800°F) in fact operate below 100°F.

The ASME Boiler and Pressure Vessel Code (Section III), Paragraph N-414, permits the combination of the tensile and bending stress in a component to reach 1.5 of the design stress intensity, i.e., such that the extreme fibers of a stainless steel beam reach the 0.2% offset yield. This has not been permitted in VTRZ design. The maximum combined tensile and bending stress in any VTRZ component is limited to the ASME code (Table N-421) design-stress-intensity values for the highest operating temperature of the component.

The ASME Boiler and Pressure Vessel Code, Section III (Nuclear Vessels), design stress values for Types 304 and 304L stainless steel are reproduced in Table 3 for reference.

TABLE 3. Design Working Stress Limits for VTRZ Components To Be Constructed of Type 304 or 304L Stainless Steel and To Have Maximum Operating Temperatures below 800°F (425°C)[a]

Maximum Metal Operating Temperature		Maximum Design Working Stress Limit, psi	
°C	°F	304	304L
38	100	20,000	16,700
93	200	20,000	16,700
149	300	19,800	16,500
204	400	17,600	14,700
260	500	16,400	13,600
315	600	15,600	13,000
389	700	15,100	12,600
426	800	14,800	12,300

[a]Stress limits correspond to design stress levels given in Table N-421 of ASME Boiler and Pressure Vessel Code (Section III, Nuclear Vessels).

3.3.2 Components with Maximum Operating Temperature above 800°F (425°C)

Stress limits are based on creep strengths for all components (except the ball-mount inserts and balls) having maximum operating temperatures at or above 800°F (425°C). The design working stress limit is taken as the typical 0.00001%/hr creep-rate stress level for the material at the maximum operating temperature of the component. This creep rate is equivalent to 1 mil/in. of creep in 10,000 hr or 0.88 (mil/in.)/yr. Table 4 lists the design stress limits adopted for VTRZ design for Types 304 and 304L stainless steel.

The VTRZ ball-mount design is a special case of VTRZ equipment operating above 800°F (425°C). A satisfactory stress-analysis technique was not found that adequately described the situation in the ball mounts in which the balls, caught vertically between plates, carry a vertical load under rolling conditions with a simultaneous significant vertical temperature gradient. Although an approximate stress-analysis theory was applied to this situation to roughly guide the design, the design is basically justified on direct full-scale rolling tests that were performed under various loads

and temperature gradients that scope the operating conditions. The ball-mount design is discussed fully in Sec. 6.4 of this report. The maximum design working load for the ball-mount plates and ball combination is less than one-third of the ultimate failure load as determined by actual tests under operating conditions.

TABLE 4. Design Working Stress Limits for Type 304 or 304L Stainless Steel Components with Maximum Operating Temperatures above 800°F (425°C)

Temperature		Stress for Rupture in 10,000 hr, 1000 psi		Design Working Stress Limit (stress for 0.00001%/hr creep rate), 1000 psi	
°C	°F	304	304L	304	304L
482	900	38.6	39.9	17.4	-
538	1000	27.8	26.1	11.3	10.1
593	1100	18.3	15.2	7.0	6.9
650	1200	11.2	9.2	4.0	3.7

3.4 Design-basis Operating Parameters

This section lists the design-basis operating load and temperature parameters on the basis of which the VTRZ has been designed; i.e., these parameters must be accommodated within the design working stress limits discussed in Sec. 3.3. The following paragraph contains a brief description of the VTRZ to orient the reader. A detailed design description is given in Chapter 4.

The VTRZ consists of two, essentially mirror image, half-zones--one half-zone to be mounted in the movable reactor half and the other half-zone in the stationary reactor half. The two half-zones are structurally independent. Each VTRZ half-zone consists of an inner (heatable) matrix assembly, an outer matrix assembly, and a 2-in.-thick annular insulation and cooling guard-ring space between the two matrix assemblies. The matrix assemblies are weldments composed of regular ZPR 2.173-in.-square, 0.040-in.-wall matrix tubes tack- and spot-welded together. An inner matrix assembly consists of 57 full-size and 12 partial matrix tubes, 3 ft long (enclosed in a jacket), in a general octagonal cross-section barrel shape. The inner matrix assembly is supported within an octogonal cross-section hole, 24 in. across and 4 ft long, by ball mounts that span across the 2-in. annular space between the assemblies. The principal purpose of the outer matrix assembly is to support the load of the reactor core above the heatable inner matrix, i.e., it is essentially a bridge over the heatable zone.

Table 5 summarizes the VTRZ design-basis parameters.

TABLE 5. VTRZ Design-basis Operating Parameters[a]

Inner Matrix Assembly	
Maximum total deadweight resting on the ball mounts of each half-zone	5000 lb
30,000-hr operating temperature	600°C
100-hr operating temperature	650°C
Outer Matrix Assembly	
Maximum total weight to be loaded into the matrix tubes above the 11-matrix-tube-wide cavity in the outer matrix assembly of each half-zone (approximately uniformly distributed)	18,000 lb
Maximum operating temperature for load-carrying portions	95°C

[a]The dead-load parameters do not include the earthquake-induced loads of Table 2. These acceleration loads must be added to the dead loads of this table for use in design calculations.

3.4.1 Inner (heatable) Matrix Assembly

The inner (heatable) matrix assembly of each half-zone will be approximately octagonal in cross section, about 20 in. across the flats, and contain a 3-ft matrix assembly. The matrix will consist of 57 full-size matrix tubes plus 12 partial (triangular) matrix tubes. Normal reactor core mockup drawers weigh about 10 lb/ft, depleted uranium weighs 32.4 lb/ft, and the matrix tubes weigh about 1.1 lb/ft. Based upon the weights of prototype equipment, the following breakdown is typical of a normal half-zone inner matrix assembly loading (assuming three 12-in. calandria cans per matrix tube loaded with oxide fuel pins):

Half-zone inner matrix assembly, including jacket	450 lb
Rear assembly cover	80 lb
Front assembly cover	5 lb
Mockup core materials (57 + 12 x 1/2)(3)(10)	1890 lb
	2425 lb

To accommodate a maximum flexibility in inner-matrix-assembly loading for experimental purposes, a design half-zone inner-matrix total dead loading on the ball mounts of 5000 lb has been set.

The intended maximum bulk average operating temperature of the VTRZ inner (heatable) matrix assembly is 550°C. To achieve this, it is necessary to permit the temperatures at some points to reach about 580°C. A high-temperature alarm will be set for temperatures exceeding 580°C. For equipment protection, the VTRZ automatic control system will be set to eliminate all electrical heating if an indicated temperature above 600°C is noted and to cause a reactor scram if such a temperature is noted. The inner matrix assembly and associated equipment have been designed for continuous operation at 600°C and abnormal operation up to 650°C for up to 100 hr. The design-basis lifetime of the VTRZ at 600°C has been taken as 30,000 hr (3.4 yr).

3.4.2 Outer Matrix Assembly

The outer matrix assembly bridges over the 24-in.-wide cavity needed for the heatable inner matrix assembly. The critical design parameter is the total deadweight of reactor mockup material that must be supported above the 24-in. (11-matrix-tube)-wide cavity. The design-basis dead load has been taken as 18,000 lb approximately uniformly distributed in the matrix tubes above the cavity. A design temperature limit of 200°F (95°C) has been taken for the load-carrying portions of the outer matrix assembly and for the plate-form reactor materials in it.

3.5 Prototype Testing Requirements

The performance characteristics of all principal structural, safety, and control systems are to be verified by prototype or startup tests before use of the systems in critical ZPR reactor assemblies.

4. DESIGN DESCRIPTION

4.1 Brief Overall Design Description

A brief overall description of the VTRZ design is included in this section to provide orientation for the subsequent sections that give detailed descriptions of each subsystem.

The VTRZ equipment consists of an inventory of oxide fuel rods; an inventory of fuel-rod mounting assemblies, called calandria cans because of their through-tube design; and a heatable zone facility. The oxide fuel rods are designed to be used at any temperature from room temperature to a maximum of 600°C. The inventory of fuel rods includes depleted-UO_2 rods, 16- and 46%-enriched-UO_2 rods, and 15 and 30% plutonium mixed PuO_2-UO_2 rods. The calandria can inventory includes cans filled with sodium at room temperature, designed for use only at room temperature; cans approximately 85% filled at room temperature, designed for heating to a maximum of 600°C; and empty cans, designed for use in sodium-void measurements. The VTRZ Heatable Zone Facility is a complex assembly designed to replace the central portion of the ZPR-6 or -9 matrix with a special insulated and heatable matrix unit.

The oxide fuel rods and the calandria can units are designed so that they may be used in the regular ZPR matrix, at room temperature, as well as in the Heatable Zone Facility. It is, in fact, intended that many of the plate-versus-rod heterogeneity comparison experiments will be carried out in the regular ZPR matrix at room temperature completely independent of the Heatable Zone Facility. The regular ZPR plate fuel drawers may be used in the Heatable Zone Facility, as part of comparison measurements, but they will not be heated.

The oxide rods and rod-mounting calandria can assemblies are shown in Fig. 5, where they are compared to the regular ZPR plate-type fuel drawers. The oxide rods are all of one size, viz., nominally 3/8-in. OD by 6 in. long with 12-mil Type 304L stainless steel cladding. The calandria cans are Type 304L stainless steel and nominally 2 in. square outside by 12 in. long with sixteen 10.5-mil wall through-tubes sized to contain the clad fuel rods.

The Heatable Zone Facility consists basically of an insulated heatable zone, called the inner matrix assembly; an outer bridge unit, called the outer matrix assembly; and several auxiliary systems for air cooling, inert gas, electrical power, and instrumentation. Figure 6 shows the Heatable Zone Facility installed in ZPR-6. Figure 7 is a section view, normal to the horizontal axis, of the inner and outer matrix assemblies. Figure 8 shows a perspective cutaway view of a single VTRZ half-zone.

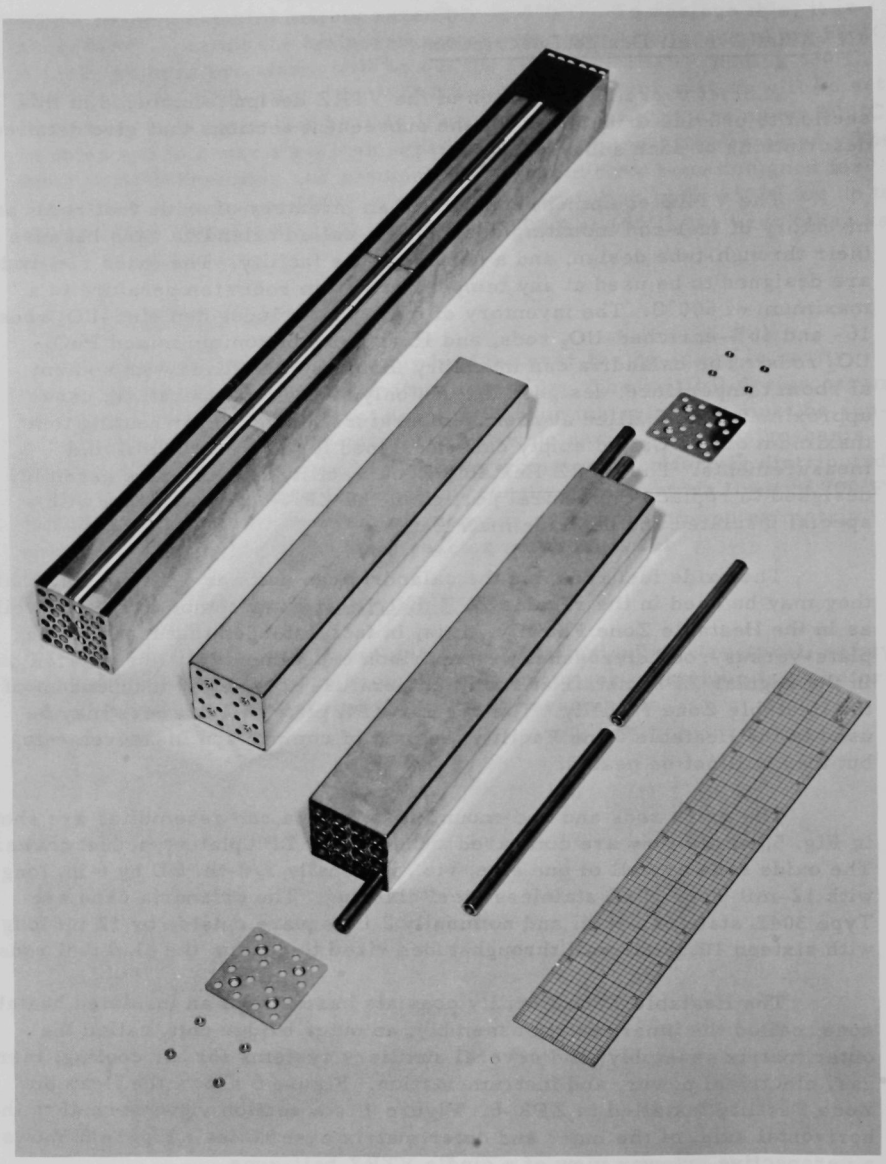

Fig. 5. Typical Plate-type Fuel Drawer, Calandria Cans, and Oxide Fuel Rods. ANL Neg. No. 116-3.

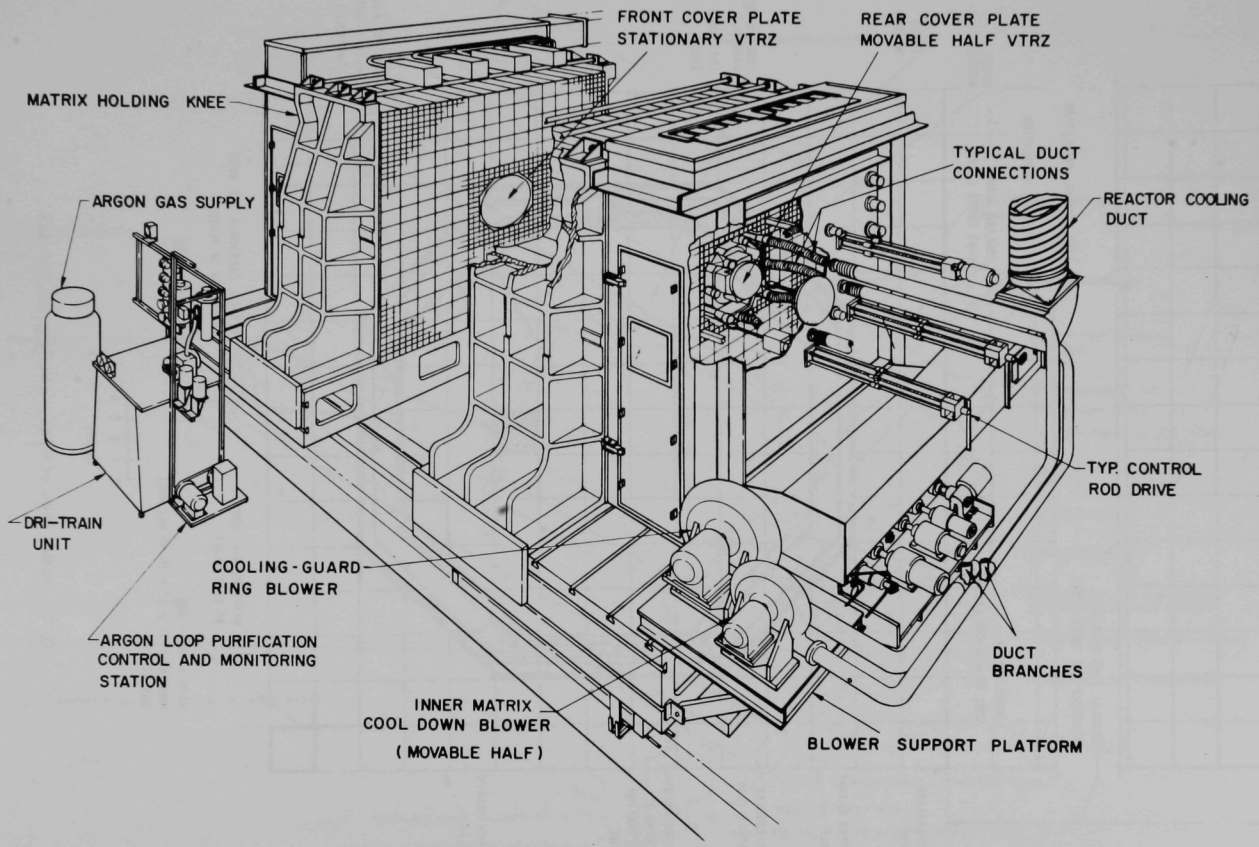

Fig. 6. VTRZ in ZPR-6. ANL Neg. No. 116-420 Rev. 1.

The inner (heatable) matrix assembly consists of a region in the shape of a right cylinder with an octagonal cross section, approximately 20 in. inside across the flats of the octagon and 6 ft long, split normal to its long axis into two 3-ft "half-zone" sections, one mounted in the center of each reactor half and mating at the reactor midplane when the halves come together. Each half-zone contains a matrix structure, which consists of regular ZPR (2.093 in. square inside by 40-mil wall) Type 304 stainless steel matrix tubes welded together and mounted horizontally. The matrix structure is supported and enclosed by an octagonal barrel. When operating at room temperature, with either plate or rodded fuel, the inside of the zone may be cooled, if necessary, by circulating air through the zone in exactly the same manner, and using the same equipment, as is described in ANL-7442. In the heatable configuration, the heatable zone is isolated from the reactor cell by gastight front and rear covers on each half-zone, and a high-purity argon atmosphere, at a slightly negative pressure with respect to the cell, is provided within each half-zone. These precautions minimize the consequences if a leak occurs in a plutonium fuel rod or in a sodium-filled calandria can.

Each heatable half-zone of the VTRZ is supported radially by 10 brackets arranged, five on each side, along the horizontal midplane of the half-zone and attached to the outside of the barrel enclosing the heatable matrix. The brackets are shown in Figs. 7 and 8. The weight of the heatable zone is transmitted through the brackets to a special welded bridge assembly, composed mainly of regular ZPR matrix tubes, which operates at room temperature and is designed to carry the load of the reactor core above the heatable zone as well as the weight of the heatable zone itself. Expansion of the heatable zone radially and axially is permitted by ball mounts in the support brackets and is controlled by radial and axial restraints and guides attached to the front and along the bottom of the heatable zone. A 2-in.-thick, radial, insulation and air cooling, guard-ring annulus separates the heatable zone from the outer bridge assembly.

The inner matrix assembly is heated by 3/8-in.-dia Inconel-clad electrical cartridge heaters of various lengths up to 36 in. The heaters will replace fuel rods in selected calandria can fuel tubes. The number of heaters will be selected on the basis of the requirements of the particular experiment being performed.

4.2 Normal (unheatable) ZPR-6 and -9 Critical Facilities and Plate-type Fuel Drawers

The ZPR-6 and -9 facilities are split-table-type critical assemblies consisting of one stationary and one movable table, as shown in Fig. 9. Each reactor table is 3.7 m (12 ft) wide and 2.4 m (8 ft) long and rests on a cast steel bed. An array of square cross-section tubes may be stacked horizontally on each table to form a matrix for fuel assemblies. A maximum of

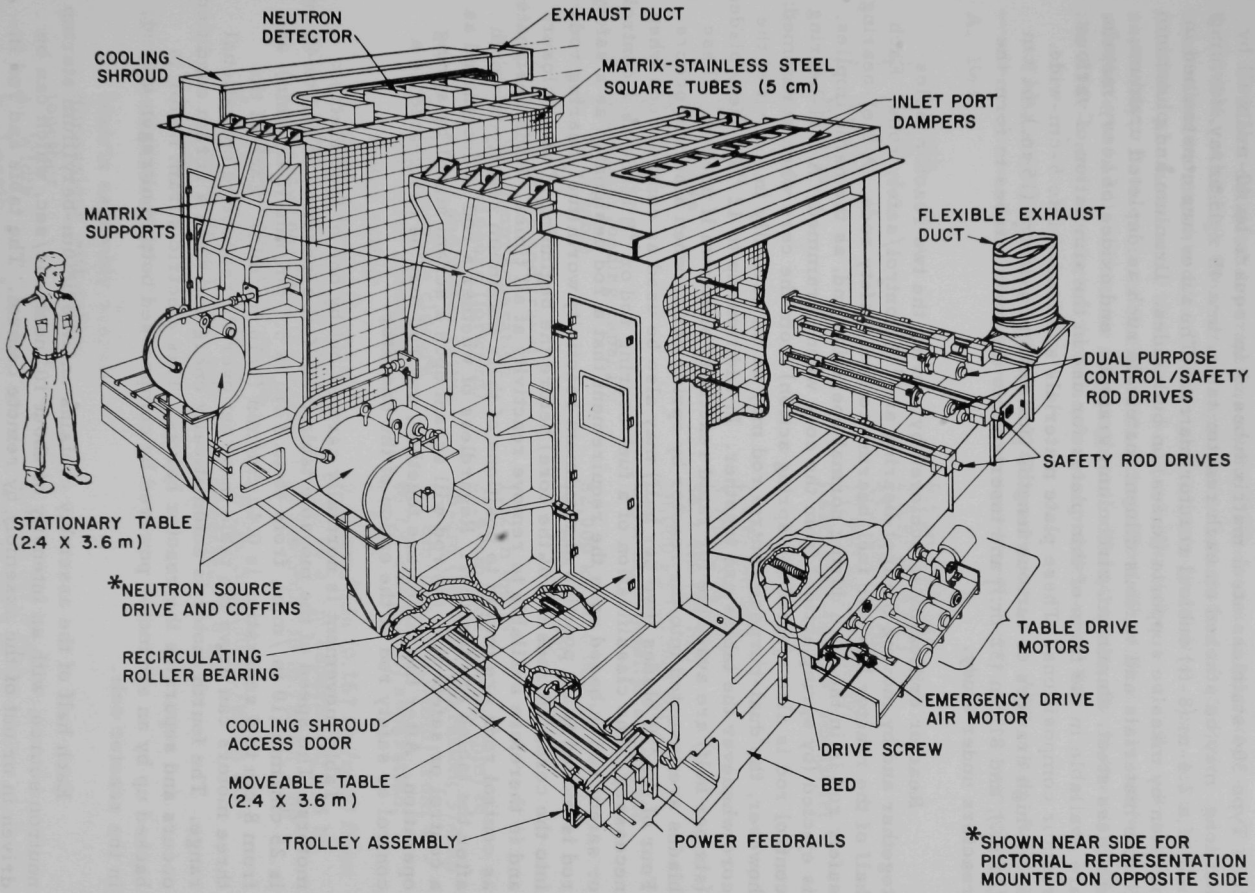

Fig. 9. Line Drawing of ZPR-6 Fast Critical Facility

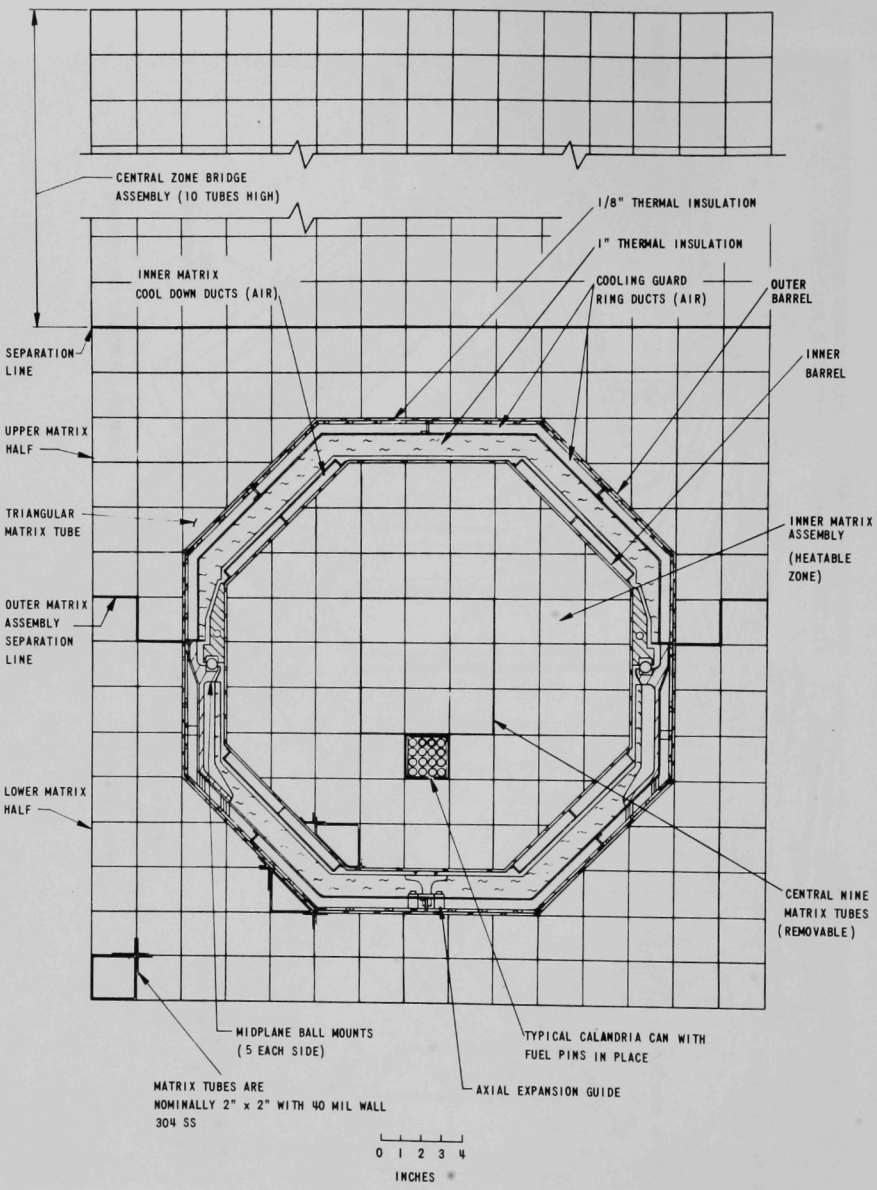

Fig. 7. Section View of VTRZ. ANL Neg. No. 116-429.

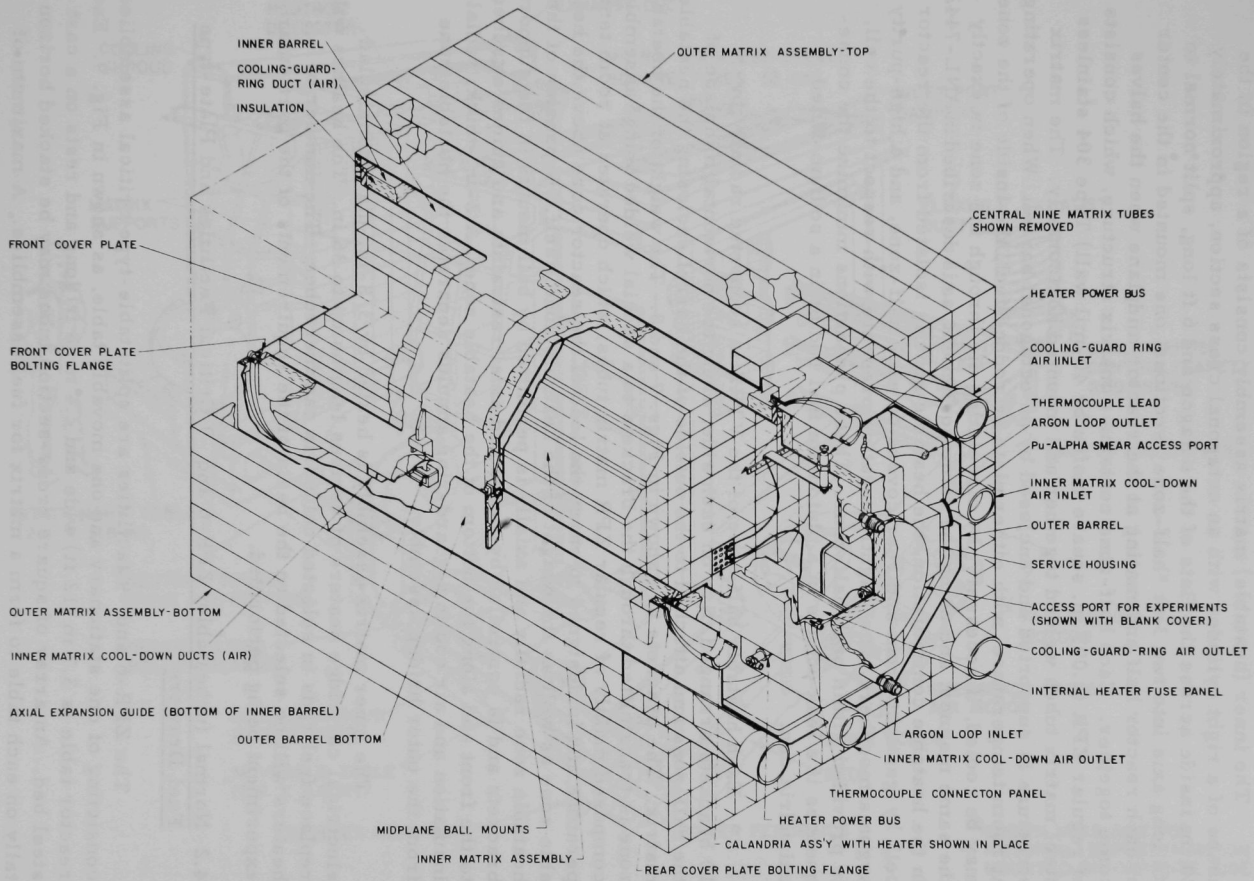

Fig. 8. Perspective Cutaway View of Single VTRZ Half-zone. ANL Neg. No. 116-419.

2025 Type 304 stainless steel matrix tubes, 2 in. square by 40-mil wall by 4 ft long, may be stacked on each reactor table, in a 45 x 45 array, forming half of a 2.4-m (8-ft) cubical reactor matrix. The tubes are constrained in position by massive supports (knees) on both sides. Uranium and plutonium fissile materials and various diluent materials such as depleted uranium, stainless steel, aluminum, zirconium, graphite, and oxides of heavy metals are available in the form of thin plates for use in the simulation of various reactor compositions. These plate materials are loaded into 5-cm-wide, 5-cm-high drawers of various lengths [for example, 38 cm (15 in.), 61 cm (24 in.), and 81 cm (32 in.)] and inserted into the matrix tubes to form the reactors under study.

Reactor criticality is achieved by moving the two reactor tables together and by moving the fuel-bearing and ^{10}B control/safety rods. Each half of the reactor has five fuel-bearing control/safety rods. A fuel-bearing safety rod is in the core during normal operation and, as the name implies, is ejected (by spring action) from the core when scrammed. A fuel-bearing control rod is also ejected (by spring action) from the core when scrammed; however, the dual-purpose control rod may be in, partially in, or out of the core whenever the tables are together. In addition, up to 12 ^{10}B safety blades (six per half) are available for rapid reactivity shutdown if needed. These blades are inserted into the reactor by spring action when a scram occurs. Four of the ^{10}B blades (two per half) may also be used as control rods when necessary. The classification of a fuel-bearing rod or ^{10}B blade as a control or safety rod is based upon the requirement that a rod designated as a safety rod is moved to its position of maximum reactivity worth (fuel-bearing rods into the core, ^{10}B rods out of the core) before the beginning of table closure and is therefore available to remove reactivity at all times. Rods designated as control rods are moved to positions of their maximum reactivity worth after the tables are together. Regardless of whether a rod is designated as a control or safety rod, the rod will scram upon a scram signal by spring operation. After the tables are together, any rod may be designated as a control or safety rod at the option of the operator.

Table movement is normally carried out by one of four electric motors. The speed of the movable table from full separation of 152 to 46 cm is 25 cm/min (10 in./min), from 46 to 8 cm is 5.1 cm/min (2 in./min), and from 8 cm to 0 separation is 0.42 cm/min (1/16 in./min). Each of the three motors can drive the table in or out over its respective operational range. The fourth motor is automatically energized when a scram condition occurs and separates the reactor halves. This electric scram motor is backed up by an air motor powered by compressed bottled nitrogen stored in the reactor cell.

Each half of the assembly contains an americium-beryllium startup neutron source, with an intensity of about 10^7 neutrons/sec, which can be driven in or out of the assembly by remote control. The table and rod instrumentation and associated nuclear instrumentation are located remote from the reactor in the control room.

More detailed descriptions of the ZPR-6 and -9 facilities appear in Refs. 2-6. Although the matrix supports and control-rod mounting plate have been sized to match a 2.4-m^3 (8-ft cube) matrix assembly, only minor modifications are necessary to make a 3 x 3 x 2.4-m (10 x 10 x 8-ft) matrix assembly. Each table is designed to carry about 82 metric tons, which is adequate to handle all cores contemplated. The physical characteristics of the ZPR-6 and -9 reactor facilities are summarized in Table 6.

TABLE 6. Summary of Physical Characteristics of ZPR-6 and -9

A. Bed	
1. Length	6.5 m (256 in.)
2. Width	2.6 m (103 in.)
3. Height	43.2 cm (17 in.)
4. Weight	17,500 kg (38,550 lb)
5. Material	Cast, high-tensile, semisteel
B. Tables	
1. Length	2.4 m (96 in.)
2. Width	3.7 m (144 in.)
3. Thickness	54.7 cm (18 in.)
4. Weight	10,000 kg (22,000 lb)
5. Material	Cast, high-tensile, semisteel
6. Maximum loading capacity	
a. Each table	82,000 kg (180,000 lb)
b. Total	164,000 kg (360,000 lb)
7. Table drive and travel	
a. Maximum separation	1.52 m (60 in.)
b. Fast closure (forward) speed and motor rating	25.4-cm/min (10-in./min) to 46-cm (18-in.) separation; 3/4 hp
c. Intermediate closure (forward) speed and motor rating	5.1 cm/min (2 in./min) from 46- to 7.6-cm (3-in.) separation; 1/2 hp
d. Slow closure (forward) speed and motor rating	0.42 cm/min (0.167 in./min) from 7.6- to 0-cm separation; 1/4 hp
e. Fast separation (reverse) speed and motor rating	76 cm/min (30 in./min); 1 hp
f. Emergency separation speed, motor type, and rating	76 cm/min (30 in./min); air-operated; 0.9 hp
C. Matrix Assembly	
1. Matrix assembly overall dimensions with tables together	
a. Width	2.48 m (97.8 in.)
b. Length	2.44 m (96.3 in.)
c. Height	2.48 m (97.8 in.)

TABLE 6 (Contd.)

2. Matrix assembly on one table	
a. Width	2.48 m (97.8 in.)
b. Length	1.22 m (48.1 in.)
c. Height	2.48 m (97.8 in.)
3. Tube bundles	
a. 25 tubes/bundle	Five rows and five columns
b. Size	1.22 m length; 27.6 cm square
c. Total number of bundles	162
d. Number per half	81
e. Total number of tubes	4050
f. Tube dimensions	1.22-m (48.0-in.) length; 5.52-cm (2.173-in.) width and height
g. Tube material	Type 304 stainless steel
D. Control and Safety Rods	
1. Fueled rods	
a. Number	Five per half
b. Material	Core composition
c. Drive motor and rating	27 V dc; 1/20 hp
d. Scram drive	Spring-loaded
e. Spring compression	306-kg (675-lb) primary spring; 45-kg (100-lb) secondary spring
f. Length of stroke	61 cm (24 in.)
g. Scram time	
15 cm (6 in.)	95-100 msec
90% of full stroke	250 msec
h. Approximate maximum reactivity addition rate	0.04 \$/sec [0.01% ($\Delta k/k$)/sec with β_{eff} = 0.004]
i. Overall dimension of control drawer	
Length	1.03 m (40.7 in.)
Width	5.24 cm (2.064 in.)
Height	5.22 cm (2.055 in.)
Wall thickness	0.12 cm (0.048-0.051 in.)
2. Boron rods	
a. Number	Six per half
b. Absorber	^{10}B
c. Normal drive	27-V dc electric motor
d. Maximum reactivity addition speed	0.25 cm/sec (0.1 in./sec)
e. Scram drive	Loaded spring
f. Spring compression	181 kg (400 lb)
g. Length of stroke	76 cm (30 in.)
h. Scram time to 90% of full stroke	90 msec

TABLE 6 (Contd.)

i. Outside dimensions of ^{10}B safety rod	
Width	4.92 cm (1.935-1.940 in.)
Length	78.4 cm (30.88 in.)
Thickness	0.95 cm (0.370-0.380 in.)
Length of ^{10}B area	71.1 cm (28 in.)
E. Neutron Source Assembly	
1. Number	One per half
2. Neutron source strength	10^7 neutrons/sec
3. Source	Am-Be
4. Source drive motor	Reversible, 1/6 hp, 1725 rpm, 115 V ac
a. Feed speed	184 cm/min (72.3 in./min)
b. Time to travel from coffin to full insertion	1 min, 42 sec
5. Source position	
a. Along radial direction	Core-blanket interface
b. Distance from matrix interface	
Location 1	10.2 cm (4.03 in.)
Location 2	20.4 cm (8.03 in.)
6. Source coffin size	61-cm (24-in.) diameter

To have a high degree of flexibility in the compositions and geometries to be studied on the ANL fast critical facilities ZPR-3, -6, -9, and ZPPR, the Laboratory's inventory of fissile, fertile, structural, and coolant materials are in plate form. The plates used in the core are 2 in. high, have nominal thickness of 1/32, 1/16, 1/8, 1/4, and 1/2 in., and are of varying lengths in inch increments. Examples of such plates appear in Fig. 10. Blocks having thicknesses of 1 and 2 in. are also included in the inventory for use in the blanket or reflector region of the reactors. The materials used in the ANL fast critical facilities are of standard dimensions so that the materials may be used interchangeably in all four facilities. All materials are color-coded or stamped with identifying marks for ease of identification.

A typical drawer loading is shown in Fig. 11, where three drawers are shown loaded with fuel, fertile material, and sodium cans.

The Laboratory maintains a large inventory of fissile materials for use in ZPR-3, -6, and -9 and ZPPR. The uranium fuel inventory is about 2300 kg of ^{235}U; the total plutonium inventory is in excess of 3000 kg. The general dimensional and isotopic characteristics of the fuels available to ZPR-6 and -9 are listed in Table 7.

TABLE 7. Inventory of Fissile and Fertile Material Plates

Material	Nominal Dimension, in.	Total Quantity, kg	Clad	Comments
1. 93% ^{235}U	(1/32, 1/16, 1/8) x 2 x (1, 2, 3)	2,560	Unclad	
2. 20% ^{235}U	1/16 x 2 x (1, 2, 3)	180	Unclad	
3. 31% ^{235}U	1/8	83	Unclad	
4. 98.9 wt % Pu, 1.1 wt % Al	1/8	210	SS	95% ^{239}Pu, 4.5% ^{240}Pu
5. 98.9 wt % Pu, 1.1 wt % Al		17.4	SS	72% ^{239}Pu, 21.9% ^{240}Pu
6. 20 wt % Pu, 77.5 wt % U, 2.5 wt % Mo	1/4	175	SS	91% ^{239}Pu, 8.5 % ^{240}Pu
7. 28 wt % Pu, 69.5 wt % U, 2.5 wt % Mo	1/4	2,900	SS	88% ^{239}Pu + ^{241}Pu, 12% ^{240}Pu 1425 kg available 7/68 2300 kg available 1/69 2625 kg available 7/69 2900 kg available 10/69
8. 36 wt % Pu, 61.5 wt % O, 2.5 wt % Mo	1/4	190	SS	73% ^{239}Pu + ^{241}Pu, 27% ^{240}Pu, available 2/69
Depleted uranium	1/16, 1/8	20,000	Unclad	
Depleted-uranium blocks	2, 5	154,000	Unclad	

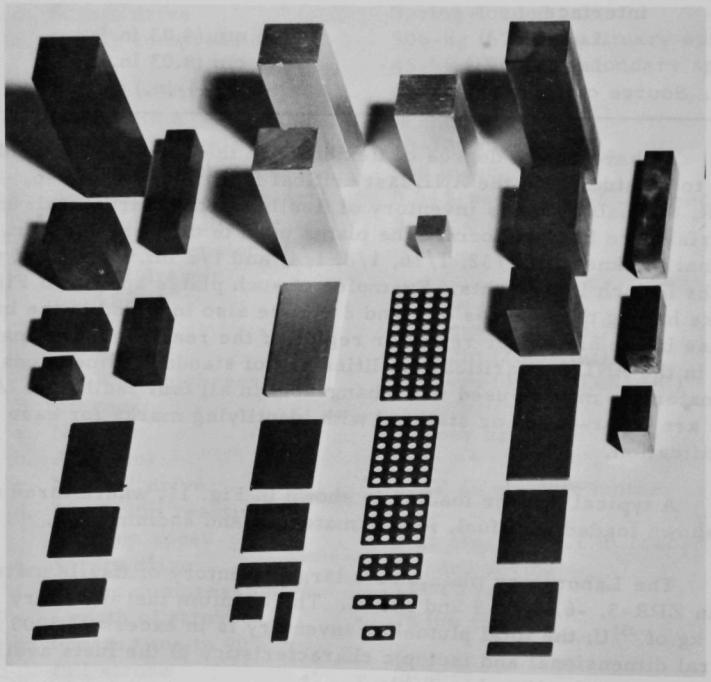

Fig. 10. Plates and Blocks for ZPR-6 and -9. ANL Neg. No. 112-9993B.

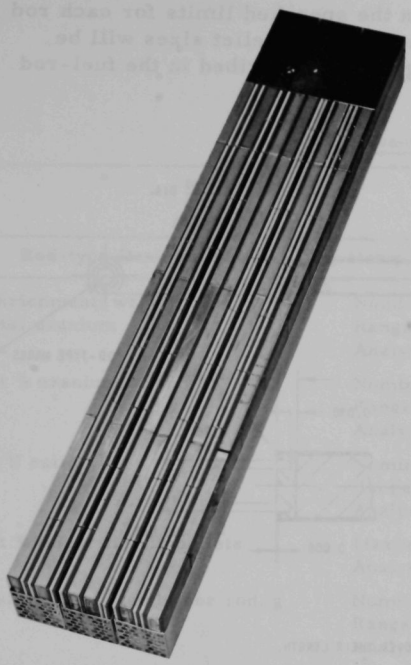

Fig. 11. Three Loaded ZPR Drawers. ANL Neg. No. 112-6846.

4.3 Oxide Fuel Rods

The oxide-fuel-rod inventory is being acquired commercially from the Kerr-Magee Corp. of Oklahoma City under the quality-assurance plan and the three procurement specifications listed in Sec. 1.2 (3 and 9a). The principal fuel-rod dimension, composition, weight, inspection, testing, and record specifications are summarized in this section. Reference should be made to the fuel-rod quality-assurance plan and to the specifications for complete dimensional and compositional descriptions and for details of the fabrication, assembly, inspection, and analytical quality controls applied to the fuel rods. Each completed fuel rod will carry a serial number through which a complete in-process and final record of the component weights, internal and external dimensions, and component compositions of the individual rod will be obtainable from the records to be delivered by the manufacturer with the rods.

All the oxide fuel rods have the same construction and are, nominally, the same size. The principal external dimensions are summarized in Fig. 12. Each fuel rod consists of a stack of sintered UO_2 or PuO_2-UO_2 pellets clad in a seamless tube with welded-in end plugs; a cup-shaped spacer is included within the cladding at one end of the pellet stack. The tubing, end plugs, and internal spacer are all carefully analyzed Type 304L stainless steel; the seamless tubing for all the fuel rods was obtained from a single vacuum-melt batch and therefore has identically the same composition. The end-plug welds are by the Tungsten Inert Gas (TIG) process. Fuel-rod-type designations are stamped on both end plugs, in addition to the fuel-rod serial number on the tube, in order to facilitate identification; for example, a stamped "D" designates the depleted UO_2 rods.

The individual oxide pellets are required to be approximately right cylinders, but do not have specific dimensional specifications except as follows: Each pellet must pass through a 0.3480-in.-dia gauge longer than the pellet. The total pellet stack height must be 5.720 ± 0.030 in. Chips, cracks, and pits must be below specification maximums. And the total

weight of the oxide stack must be within the specified limits for each rod type as discussed below. Some data on the actual pellet sizes will be available from the ANL inspection program as described in the fuel-rod quality-assurance program.

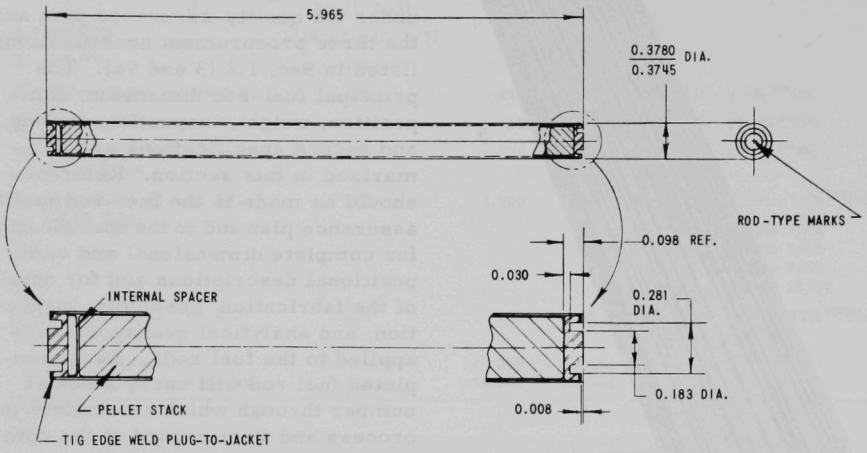

NOTES:

1. THE FINISHED RODS MUST BE STRAIGHT WITHIN 2 mils OVER THEIR LENGTH.
2. THE FINISHED RODS MUST PASS THROUGH A 0.3810-in. DIA x 6.5 in. LONG CYLINDRICAL GAGE BY GRAVITY FORCE ONLY.

Fig. 12. Fuel Rod. ANL Neg. No. 116-431.

The sequence of fuel-rod fabrication is approximately as follows: The tubes are cut to length from 0.3780/0.3760-in.-OD, 0.012 ± 0.0005-in.-wall, Type 304L stainless steel tubing. The first end plug, with type designation already affixed, is welded in. The pellet stack is made up and inserted in the tube, and a selected spacer added so that less than 5 mils of free axial length remains when the final end plug is inserted. Just before the final end-plug weld, the interior of the rod is flushed and backfilled with an argon-helium gas mixture at 1 atm absolute pressure. The specifications require that the argon-helium gas mixture must contain at least 50 vol % helium and not more than 10 ppm H_2O and 30 ppm O_2. The final end plug is then welded in. This final end plug has a special double-dot designation, which designates the spacer end--for example, ·D·.

The specification requirements for the weight and composition of each oxide fuel-rod type now planned for the ZPR inventory are summarized in Table 8 for the UO_2 types and in Table 9 for the PuO_2-UO_2 types. The 16%-enriched UO_2 fuel rods are matched in composition to the basic uranium plate-form comparison core to be used for plate-versus-rod measurements, i.e., ZPR-6 Assembly 6. The 46%-enriched-UO_2 rods are

TABLE 8. Inventory of UO_2 Fuel Rods

Attribute		UO_2 Fuel-rod Type		
		Depleted	16%	46%
Rod-type Designation (end-plug stamp)		D	A	B
Enrichment; wt % ^{235}U of total uranium	Nominal[a]	0.22	16.40	46.50
	Range[a]	±0.02	±0.05	±0.05
	Analysis[a]	±0.02	±0.05	±0.05
Wt % uranium of pellets	Nominal[b]	87.6 min	88.14	88.14
	Range[b]	≥87.6	+0.06, -0.74	+0.06, -0.74
	Analysis[b]	≥87.6	±0.30	±0.30
O/U ratio	Nominal	2.00	2.00	2.00
	Range	±0.02	±0.02	±0.02
	Analysis	±0.01	±0.01	±0.01
Wt % impurities in pellets	Maximum	0.50	0.50	0.50
	Analysis	-[c]	±0.10	±0.10
Pellet-stack weight per rod, g	Nominal[b]	89.29	90.50	90.50
	Range[b]	±1.50	±1.50	±1.50
	Analysis[b]	±0.005[c]	±0.005	±0.005
304L SS cladding weight per rod, g	Nominal[d]	12.3	12.3	12.3
	Analysis[d]	±0.01	±0.01	±0.01
Uranium weight per rod, g	Nominal[e]	78.2	79.8	79.8
Oxygen weight per rod, g	Nominal[e]	10.9	10.5	10.5
^{235}U weight per rod, g	Nominal[e]	0.17	13.05	37.00
Approximate total number of rods in inventory		14,600	11,500	4,500
Approximate total ^{235}U inventory, kg		-	150	167

[a]Value must be within "Range" of "Nominal" and be measured within "Analysis" (2σ).
[b]Pellet and pellet-stack weights include impurities.
[c]Total uranium in pellet stack must be known to ±0.01 g.
[d]Cladding weight is not directly specified. This is a calculated value. Cladding weight will be determined by difference method to ±0.01 g.
[e]These values are calculated from the nominal value assuming 0.25 wt % impurities.

TABLE 9. Inventory of $(Pu,U)O_2$ Fuel Rods

Attribute			$(Pu,U)O_2$ Fuel-rod Type		
			15%	30%	High-240
Rod-type Designation (end-plug stamp)			F	G	H
Uranium isotopic composition, wt % ^{235}U of uranium		Nominal[a]	0.22	0.22	0.22
		Range[a]	±0.02	±0.02	±0.02
		Analysis[a]	±0.02	±0.02	±0.02
Plutonium isotopic composition, wt % of plutonium	239	Nominal	86.40	86.40	67.30
		Range	±0.80	±0.80	±0.60
	240	Nominal	11.50	11.50	25.93
		Range	±0.50	±0.50	-0.18, +0.35
	241	Nominal	1.70	1.70	5.26
		Range	-0.70, +0.80	-0.70, +0.80	-0.23, +0.33
	242	Nominal	0.25	0.25	1.42
		Range	0.25	0.25	-0.08, +0.10
	238	Nominal	0.05	0.05	0.09
		Range	±0.05	±0.05	±0.02
Wt % ^{239}Pu + ^{241}Pu of pellets		Nominal[b]	11.67	23.38	11.67
		Range[b]	±0.17	±0.27	±0.17
		Analysis[b]	±0.08	±0.08	±0.08
Wt % total (U + Pu) of pellets		Nominal	88.05	88.05	88.05
		Range	±0.40	±0.40	±0.40
Wt % plutonium of pellets		Analysis	±0.07	±0.07	±0.07
Wt % uranium of pellets		Analysis	±0.03	±0.03	±0.03
O/(Pu + U) ratio		Nominal	1.98	1.98	1.98
		Range	±0.02	±0.02	±0.02
		Analysis	±0.01	±0.01	±0.01
Wt % impurities in pellets		Maximum	0.50	0.50	0.50
		Analysis	±0.10	±0.10	±0.10
Pellet stack weight per rod, g		Nominal[b]	89.60	89.40	89.60
		Range[b]	±1.30	±1.50	±1.30
		Analysis[b]	±0.005	±0.005	±0.005
304L SS cladding weight per rod, g		Nominal	12.3	12.3	12.3
		Analysis	±0.01	±0.01	±0.01
^{239}Pu + ^{241}Pu weight per rod, g		Nominal[c]	10.46	20.90	10.46
Plutonium weight per rod, g		Nominal[c]	11.87	23.68	14.42
Uranium weight per rod, g		Nominal[c]	67.02	55.04	64.47
Oxygen weight per rod, g		Nominal[c]	10.49	10.46	10.49
Approximate total number of rods in inventory			12,700	5,900	1,600
Approximate total fissile (^{239}Pu + ^{241}Pu) inventory, kg			133	116	20

[a]Value must be within "Range" of "Nominal" and must be measured to within "Analysis" (2σ). If no range is specified, the quantity is not directly specified.
[b]Pellet and pellet-stack weights include impurities.
[c]These values are calculated from nominal values assuming 0.25 wt % impurities.

intended for general use, and their composition was chosen to give the same fertile-to-fissile ratio as the combination of one 1/16-in.-thick enriched-uranium plate and one 1/16-in.-thick depleted-uranium plate. The 15% $(Pu,U)O_2$ rods are matched in composition to the basic plutonium plate-form core to be used in the plate-versus-rod comparison measurements. The 30% $(Pu,U)O_2$ rods have exactly twice the fissile content of the 15% rods, so that the combination of one 30% rod and one depleted-UO_2 rod matches the fertile-to-fissile ratio of the 15% rod; this attribute will be used in comparing the properties of single and mixed enrichment rods. The high 240 $(Pu,U)O_2$ rods have the same fertile-to-fissile ratio as the 15% rods but with 26 wt % rather than 11.5 wt % ^{240}Pu in the plutonium.

In addition to the general requirement that the fuel pellets contain less than 5000 ppm (0.50 wt %) impurities (i.e., other than plutonium, uranium, and oxygen), specific limitations were placed on certain elements for either nuclear or chemical reasons. These limitations are listed in Table 10.

TABLE 10. Specific Impurity Limitations in Oxide Fuel Pellets

Element	Maximum ppm by Weight	Element	Maximum ppm by Weight
Hydrogen	10	Samarium, Europium, Gadolinium, Dysprosium, Lithium	Sum 10
Beryllium	20		
Boron	20		
Aluminum	1200		
Silicon	200	Sodium, Potassium	Sum 400
Titanium	500		
Copper	400	Cobalt, Tungsten, Tantalum	Sum 100
Niobium	250		
Molybdenum	600		
Carbon	200	Chlorine, Fluorine	Sum 100
Nitrogen	200		

The UO_2 pellets are produced by oxidation of uranium enriched to the value needed (i.e., it is not formed by mixing depleted and enriched UO_2), so that the microhomogeneity of this material is ensured. The $(Pu,U)O_2$ will be produced by coprecipitation (i.e., simultaneous precipitation) of the PuO_2 and UO_2 from a solution containing the correct Pu/U ratio for each required

rod type. Although the coprecipitation technique inherently produces a more uniform product than the more standard blending technique (i.e., mixing PuO_2 and UO_2), there is no guarantee of microhomogeneity. The specifications require the $(Pu,U)O_2$ to be controlled so that at least 99% of the plutonium in the pellets occurs as solid solution $(Pu,U)O_2$ or as agglomerates or particles of PuO_2 less than 125 μ in size. Not more than 1% of the plutonium can occur as agglomerates or particles, containing twice the average plutonium content of the pellets, having a diameter larger than 250 μ. The $(Pu,U)O_2$ microhomogeneity specifications will be enforced during the production run through the use of alpha-radiograph standards based upon X-ray microprobe analysis.

Each pellet must pass through a 0.348-in.-dia cylindrical gauge, longer than the pellet, and be visually inspected (against standards) for chips, pits, and cracks. Pellet edge chips may not exceed a 1/16-in. depth, as measured from the end or cylindrical surfaces, and pits in any surface may not exceed 0.032-in. diameter by 0.020 in. deep. The total chipped and pitted area may not exceed 5% of the cylindrical or end surface of a pellet. Pellet dimensions are controlled by process control, accomplished through periodic sampling and measurement. The process control must give a 95% confidence that 95% of the pellets produced are within the following dimensional limits:

(1) The difference between maximum and minimum pellet diameters shall not be more than 0.006 in.

(2) The difference between maximum and minimum pellet lengths shall not be more than 0.004 in.

(3) The linear density, i.e., pellet weight divided by the maximum length, must be between 15.30 and 16.30 g/in. for the depleted UO_2, 15.40 and 16.40 g/in. for the $(Pu,U)O_2$, and 15.50 and 16.50 for the enriched UO_2.

After each pellet stack is made up within the required weight and length, a 1-lb axial load is placed on the stack and the stack height is measured. With the 1-lb load applied, no gap may exist that will allow a 0.005-in. feeler gauge to be inserted more than 1/8 in. between pellets.

One major concern during the design and procurement of the oxide fuel rods was the possibility that outgassing from the pellets would raise the internal rod pressure high enough to distort the rods at their maximum 600°C operating temperature. The specifications required such process controls as necessary to ensure that when the fuel rods are heated to 600°C the total internal pressure would not exceed 300 psig. This maximum 600°C internal pressure has been verified by destructively testing periodic samples of rods. The results of the internal pressure tests on the UO_2 rods

have shown that the pressure within the rods at 600°C is only about 3 atm absolute (i.e., only the pressure expected from the argon-helium fill gas), indicating essentially no outgassing of the pellets. Similar results are expected for the $(Pu,U)O_2$ rods.

All fuel rods are helium leak-checked at room temperature as a part of the final inspection procedure. In addition, the $(Pu,U)O_2$ rods are helium leak-checked at 600°C. The $(Pu,U)O_2$ fuel rods are checked for external alpha contamination after final welding and again three days later. A maximum of 10 dpm alpha, above background, is permitted on a wipe sample and 500 dpm alpha, above background, for fixed surface contamination.

Each oxide fuel rod delivered to ANL will be accompanied by complete weight, composition, and dimensional records. The most significant data for ZPR use will be punched into IBM cards, one card for each rod. The cards may be used for automated inventory manipulation. The data punched on the rod card will be the following:

(1) Fuel-rod identification number.

(2) Gross weight.

(3) Pellet-stack weight.

(4) Oxygen weight.

(5) Plutonium weight.

(6) ^{238}Pu weight.

(7) ^{239}Pu weight.

(8) ^{240}Pu weight.

(9) ^{241}Pu weight.

(10) ^{242}Pu weight.

(11) Uranium weight.

(12) ^{235}U weight.

(13) ^{238}U weight.

(14) Impurities, ppm.

All weights are in grams to the nearest 0.01 g.

4.4 Calandria Cans

An inventory of oxide fuel-rod mounting assemblies, generally referred to as "calandria cans" because of their construction, is being procured from the ANL Central Shops Department. When the procurement is

complete, the inventory will include calandria cans of two different physical sizes and approximately four different sodium loadings. The two physical sizes consist of nominally 2-in.-square, 16-tube cans intended for use in the regular-size ZPR matrix tube and roughly triangular, 10-tube cans intended for corner positions in the heated zone; all cans will be 1 ft long. The square-cross-section cans will be capable of containing 32 fuel rods; the triangular-cross-section cans, 20 fuel rods.

The physical configuration and principal dimensions of the calandria cans are summarized in Fig. 13. Figure 14 shows a photograph of a typical square-cross-section can. The cans are constructed entirely of Type 304L stainless steel. All tubes in all calandria are made from a single, well-characterized, vacuum melt of Type 304L stainless steel. All the sheet stock for the outer jackets, headers, internal spacers, and rod retainer plates is taken from a separate, well-characterized, single vacuum-melt of Type 304L stainless steel. The rod-retainer fasteners, studs, and nuts are normal air-melt Type 304L stainless steel, but of known composition.

Construction of the calandria cans is approximately as follows: The tubes are cut to length, and the three tube spacers are positioned over the tubes. (A small number of the calandria cans in the inventory have two internal tube spacers.) The spacers are square sheets with outer square dimensions matching the internal dimensions of the can jacket and with internal square cutouts matching the outside diameter of the tubes. The spacers serve two purposes: positioning and supporting the tubes and supporting the can jacket. Next, the two end headers are positioned on the ends of the tube-spacer bundles, and the tube-to-header welds (GTAW) are made. The studs, used to attach the rod-retainer plates onto the ends of the cans, are stud-welded to the headers before the headers are welded to the tube bundle. The can jackets are made in two U-shaped halves and welded (GTAW) together along the 1-ft axial dimension. Next, the tube-spacer-header assembly is inserted into the jacket, and the jacket-to-header weld (GTAW) is made. A round sodium-fill hole, in one of the flat jacket surfaces, is left open for subsequent sodium filling. At this point, the assembly is dimensionally inspected, helium leak-checked, and transferred to the sodium-filling facility. After sodium filling, the cans are transferred to an evacuated tank in which plugs are welded-in (electron beam) to close the sodium-fill holes. The cans go through a final dimensional check, weld inspection, and radiographic inspection.

The calandria tubes are 0.3875/0.3895-in. ID with 0.0110/0.0100-in. wall thickness and are cut to 11.938 (+0.000, -0.003) in. for use in the cans. The final inspection of the tubes in the completed, sodium-loaded, calandria cans requires that a cylindrical steel gauge 0.3855/0.3852 in., 7 in. long, and straight within 0.0004-in. runout, shall fall through each tube under its own weight. The fuel rods must pass a 0.3810-in.-dia, 6.5-in.-long fall-through gauge; thus a minimum 5.3 mils of diametral clearance is enforced between

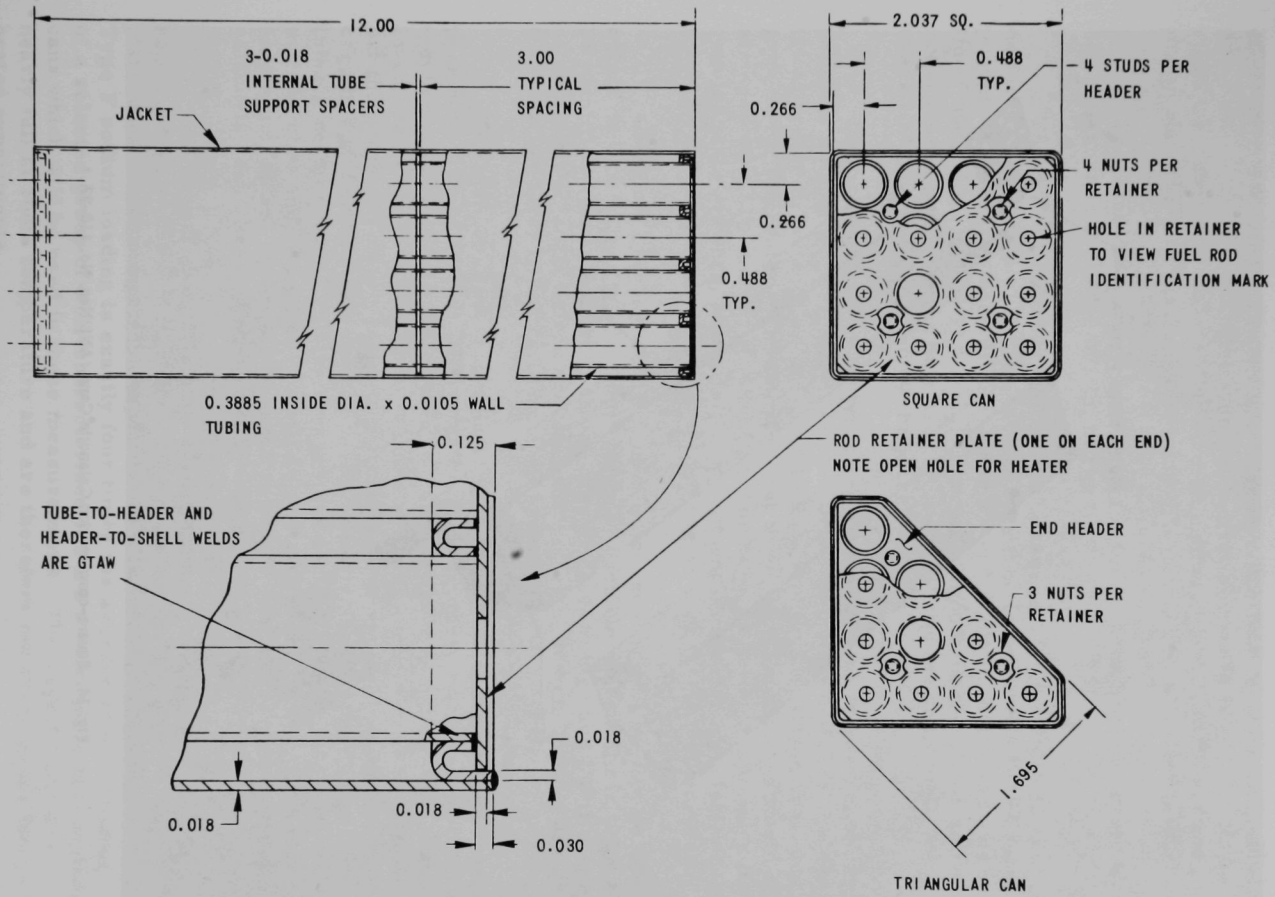

Fig. 13. Square and Triangular Calandria Cans. ANL Neg. No. 116-430.

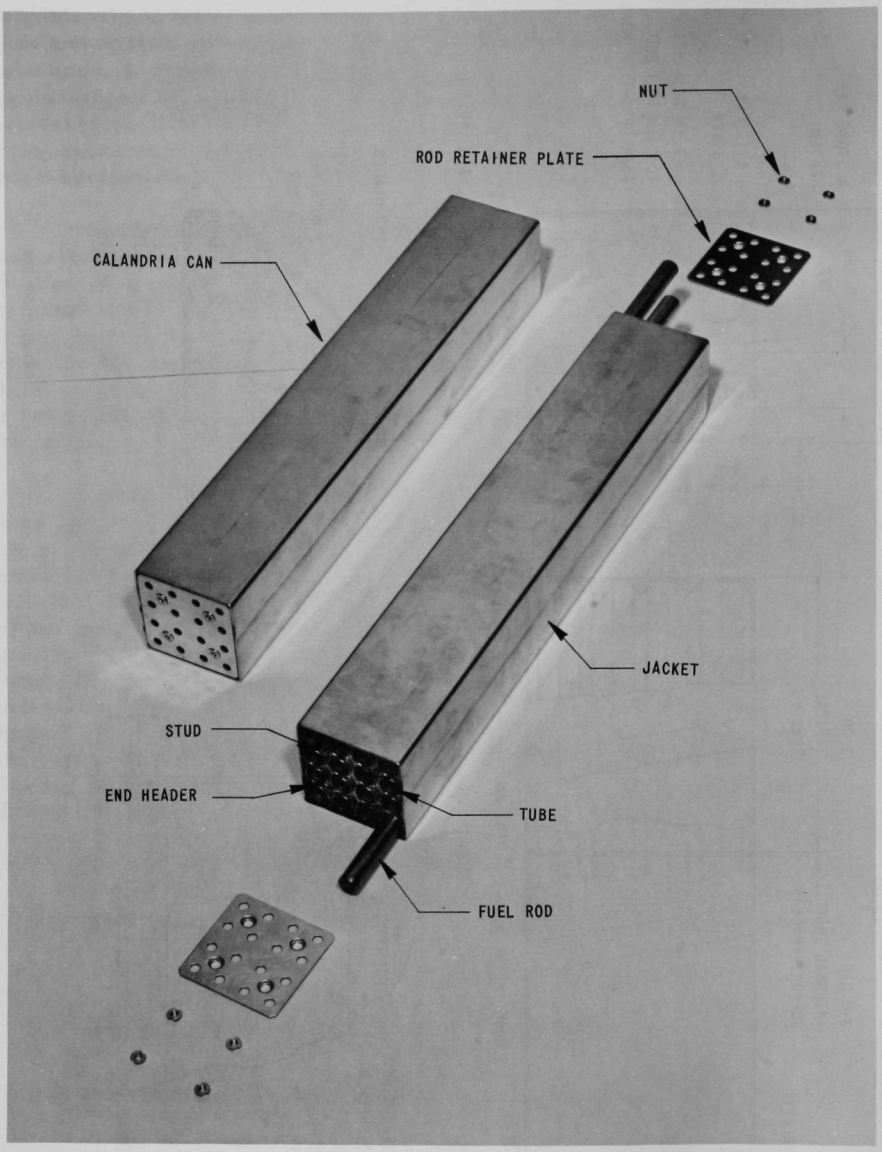

Fig. 14. Square-cross-section Calandria Cans. ANL Neg. No. 116-2A.

effective rod outside diameter and calandria-can-tube inside diameter. In practice, the rod-to-calandria-tube diametral clearance is greater than this, since the maximum rod-cladding outside diameter is 0.3780 in. and the minimum calandria-tube inside diameter is 0.3875 in., i.e., a 9.5-mil gap.

The Type 304L sheet stock used for the jackets, headers, spacers, and rod retainers is 0.019 ± 0.001 in. thick.

The overall length of the calandria cans is 12.000 ± 0.007 in. and is defined by the length of the can jacket. The tube length and header design provide that the tube ends are recessed 0.030 ± 0.002 in. below the outer lip of the jackets. This 30 ± 2-mil space accommodates the 19 ± 1-mil-thick rod-retainer plate and the nuts used to fasten it onto the can, within the overall 12-in. length defined by the jacket.

Two rod-retainer plate types are provided in the inventory; one type provides an open hole for the placement of a 3/8-in.-dia cylindrical electrical heater in one of the four central tubes, and the other type does not provide for the heater. The intent is that the rod-retainer plates would be stamped with ZPR matrix tube location numbers, in the form now used for regular plate drawers, so that after attachment of the retainer plates there would be a definite matrix-position marking on each loaded calandria can.

Complete process and final inspection records will be kept on each calandria can so that the detailed history of each component of each can will be identified with an engraved serial number (1/4 in. high and 1 mil deep) at the time the jacket halves are welded together; a sodium loading designation is added after filling, as described below.

The number, size, sodium filling, and weights of the calandria cans presently planned for the ZPR inventory are summarized in Table 11. The number of cans of each type, given in Table 11, is only approximate. The inventory has been chosen to provide an adequate number of cans to carry out the projected plate-versus-rod comparison measurements in a central core of approximately 25-cm equivalent radius and with a 6-ft length (3 ft in each reactor half). This reference core contains 57 full-size (i.e., square) matrix tubes and 12 partial (triangular) matrix tubes. A 6-ft loading therefore requires 342 square-cross-section and 72 triangular-cross-section calandria cans; these numbers, with 10% spares, are being procured.

The Type F calandria cans are designed to exactly match the homogenized sodium composition of the plate cores to be used in the plate-versus-rod comparison experiments. To be more precise, the Type F sodium loading is exactly four times the average sodium loading of a selected group of well-characterized 1/2 x 2 x 6-in. plate-type sodium cans which will be used in these measurements. The Type F cans are nearly full at room temperature and are therefore not intended for use in heated experiments.

TABLE 11. Inventory of Calandria Cans

Can Type	Type Designation	Sodium Loading,[a] g			Stainless Steel,[b] g				Approximate Number in Inventory
					Assembly[c]		Single Rod Retainer[d]		
		Nominal	Range	Measurement Precision	Nominal	Measurement Precision	Nominal	Measurement Precision	
Square Cross Section									
Full at 20°C	F	330.0	±1.0	±0.01	579.0	±0.01	8.0	±0.01	375
6-in. axial fill	SF	165.0	±1.0	±0.01	579.0	±0.01	8.0	±0.01	65
Full at 550°C	H	300.0	±1.0	±0.01	579.0	±0.01	8.0	±0.01	375
Empty	V	-	-	-	579.0	±0.01	8.0	±0.01	375
Triangular Cross Section									
Full at 20°C	F	206.3	±1.0	±0.01	363.0	±0.01	5.0	±0.01	80
6-in. axial fill	SF	103.2	±1.0	±0.01	363.0	±0.01	5.0	±0.01	15
Full at 550°C	H	187.5	±1.0	±0.01	363.0	±0.01	5.0	±0.01	80
Empty	V	-	-	-	363.0	±0.01	5.0	±0.01	80

[a]Sodium loadings are specified to be within "Range" of "Nominal" and to be measured within "Measurement Precision" (2σ).
[b]Stainless steel nominal weights are only approximate; these values are not directly specified.
[c]"Assembly" includes jacket, two headers, three spacers, all tubes, and fill plug.
[d]Loaded assemblies use two retainer plates and eight nuts; this value is for one retainer plate plus four nuts.

The Type SF cans have precisely half the sodium loading of the Type F cans and have been loaded so that the sodium is solidified in one end of the can, i.e., so that there is approximately a 6-in. void in one end of the can. This can type is intended for use in sodium-void coefficient experiments; sufficient cans are being procured to produce a 6-in.-deep planar void across the reference rodded core. The Type V, voided, cans will also be used in sodium-voiding experiments. The Type SF cans are not intended for heating; the Type V cans can be heated.

Type H cans are designed to be full at 550°C and have a reduced sodium loading over the Type F cans to allow for sodium expansion on heating. The inside gas space on all the can types is evacuated so that gas pressure buildup during heating does not occur.

4.5 Heatable Zone Facility

4.5.1 Procurement Quality Assurance

Procurement of the VTRZ Heatable Zone Facility has been governed by the four specification documents listed in Sec. 1.2(9)c. The procurement was divided into four units on the basis of logical separation and the principal

fabrication and assembly contractor. Table 12 summarizes the four VTRZ Heatable Zone Facility procurement units and the principal and secondary construction responsibilities.

TABLE 12. VTRZ Heatable Zone Facility Procurement

Procurement Unit	Components Included in Unit	Principal Construction Responsibility	Secondary Construction Responsibility
Mechanical	This unit covers all components within the ZPR assembly matrix, the special dual-purpose control-rod mounting plates, and the external cooling-air duct-blower systems. The major subassemblies in this section are: a. Inner (heatable) zone: matrix, internal thermocouple and heater wiring, barrel, front and rear covers. b. Internal insulation and cooling air system. c. Outer matrix and central zone bridge structure. d. Special dual-purpose control-rod mounting plates. e. External cooling-air duct-blower systems.	Central Shops Department	-
Inert Gas (argon) Loop	This unit includes all components of the inert-gas system used to maintain a high-purity argon cover gas within the heatable zone during operation above room temperature. The components include the circulation pumps, valves, piping, gas-purification systems, and the mechanical components of the temperature controls and gas-purity monitoring equipment (He, H_2O, O_2, Pu α) external to the rear cover of the heatable zone.	Applied Physics Division	Central Shops Department
Instrumentation and Control	This unit includes all inert-gas loop instruments; reactor scram circuitry; heater interlock circuitry; off-normal alarm circuitry; controls for heaters, inert gas, and cooling systems; and monitoring of temperature, inert-gas purity, air and argon flow rates, and heated zone pressure.	Electronics Division	-
Electrical	This unit includes all components of the electrical-power-supply system in the ZPR cell. This includes transformers, circuit breakers, power controllers, and wiring to supply the heaters, in-cell instruments, and blowers.	Applied Physics Division	CPFF Contractor

All materials to be used in the VTRZ construction are rigidly controlled through the quality-assurance procedures required by the specification documents. Manufacturer's certification of chemical composition and mechanical properties and also traceability from procurement to finished part are required for all materials. Materials that are particularly important are subjected to ANL overchecks on composition, for example, structural materials and the thermal insulation. (Hydrogen contamination is to be prevented in the thermal insulation.)

The specification documents require extensive in-process and final inspections and tests of all of the VTRZ equipment. This includes dimensional inspections, leak tests, welder and weld qualification, and instrument operational tests. In-process weld control is particularly important because, even though load-versus-deflection tests can and will be done on the completed assemblies, it is essentially impossible to inspect the welds on the completed assembly since most of them are internal to the final structure.

The welding contractor is required through the specifications to establish procedures for all weld types to be performed. This includes procedures for the following: Gas Tungsten Arc Welds (GTAW's) for butt, fillet, plug, matrix tube, and matrix subassembly welds; Resistance Spot Welds (RSW's); Capacitor Discharge Stud Welds (CDSW's); and Electron Beam Welds (EBW's). The welding procedures and test records must show all essential variables affecting the welding-process cycle and the replication of welds. In addition, the welding procedures and welding operators must be qualified for each type weld through tests to be made on material, weld-joint configuration, and conditions that are identical to the construction of the VTRZ weld joints. Table 13 lists the required welding-procedure qualification, operator qualification, and periodic tests to be made. As shown in the table, periodic tests on resistance spot welds and capacitor-discharge stud welds must be made during production using test materials. These sample test welds are required to be approved by a weld inspector, other than the welder, before resuming production. All periodic test results and samples must be retained for review by a representative of the VTRZ Project.

In response to the significant increase in the formality required in quality assurance associated with ANL work, specific quality-assurance requirements have been included in the VTRZ specification documents. These provisions require the Contractor to provide a quality-control organization to supervise and control all quality functions required for the manufacture of the VTRZ assemblies. Personnel performing the quality-control functions must have well-defined responsibility, authority, and organizational freedom to identify and evaluate quality problems and to initiate, recommend, or provide solutions. A complete description of the organization and functions of the Contractor's quality-control organization must be submitted to the VTRZ Project for review and approval before the start of fabrication work. The Contractor is required to provide a comprehensive quality-control plan specifically for the manufacture of the VTRZ assemblies. This

plan must include written procedures for the control of all quality functions and must include scheduled checkpoints and audits to periodically evaluate the effectiveness of the quality program. The plan must also include descriptions of all control forms to be used, procedures for indoctrination and qualification of personnel, procedures for material control, procedures for control of test equipment, all inspection procedures, material-traceability procedures, and nonconforming-material control procedures.

TABLE 13. Welding-procedure Qualification, Operator Qualification, and Periodic Tests

Procedure Tests	Procedure Qualification, in.	Operator Qualification, in.	Periodic Tests
1. Conventional (GTAW) 1/8 Stock	16	8	-
a. Transverse tension (butt)	4	2	-
b. Bend test (butt and fillet)	4	2	-
c. Metallographic (butt and fillet)	4	2	-
2. Plug Weld (GTAW)	8	4	-
a. Metallographic	4	2	-
3. GTAW Matrix Subassembly	10	5	-
a. Metallographic	6	3	-
4. Resistance Spot Weld (RSW)	34	17	4/50[a]
a. Shear	20	10	1
b. Metallographic	10	5	1
5. Capacitor Discharge Stud Weld (SW)	18	6	4/50[a]
a. Torsion test	9	3	1
b. Metallographic	6	2	1
6. Electron Beam Weld (EBW)	24	8	-
a. Transverse tension	3	3	-
b. Bend test	3	3	-
c. Metallography	2	2	-

[a]Four test welds on sample materials at start of each day's production and at intervals of 50 production welds.

4.5.2 Outer Matrix Bridge Structure

The purpose of the outer matrix bridge structure is to create a central cavity in the ZPR matrix into which the heatable zone can be placed with minimum disruption of the regular ZPR matrix pattern. Since structural support members around the inner (heatable) matrix assembly would be an appreciable perturbation on the regular ZPR tube matrix, the design concept of a welded bridge structure composed of ZPR matrix tubes was used. The welded-tube outer matrix bridge structure is designed to support a maximum load of 19,800 lb while maintaining all stresses within the stress-limit standards given in Sec. 3.2. The 19,800-lb maximum load consists of a dead load of 18,000 lb (Table 5) and a seismic loading of 1800 lb (Table 2).

The outer matrix bridge structure is constructed of Type 304 stainless steel and consists of two identical half-zone units, one for each half of the reactor, corresponding to the heatable half-zones. The bridge structure is designed to permit plate-type fuel drawers to be loaded into regular ZPR matrix tubes immediately around the insulation annulus separating the inner (heatable) matrix assembly from the outer matrix assembly. Each half-zone unit of the outer matrix bridge structure is itself composed of two parts; viz., the outer matrix assembly forming the octagonal hole for the heatable inner matrix assembly and the central zone bridge, which aids in the support of the load above the outer matrix assembly. The outer matrix assembly and central zone bridge are shown in cross section in Fig. 7.

Each half-zone outer matrix bridge structure replaces the central 375 regular 4-ft-long matrix tubes in each reactor half (the outer matrix assembly replaces 225 tubes; the central zone bridge replaces 150 tubes) and is itself constructed of ZPR (2.093-in.-square inside dimension by 40-mil wall thickness) matrix tubes.

A 0.120-in.-thick Type 304L stainless steel liner, called the "outer barrel," is attached to the inside surface of the octagonal cross-section cavity in the outer matrix assembly and constitutes the physical outer surface of the VTRZ insulation annulus. The outer barrel adds stiffness to the entire outer matrix assembly and provides a strong stiff area for mounting the ball-mount brackets that support the inner matrix assembly. (The ball-mount brackets are described in Sec. 4.5.3.)

The outer barrel is approximately 24 in. across the flats and is attached to the matrix tubes of the outer matrix assembly by arc-welding 1/8-in. pins attached to the outer-matrix-assembly matrix tubes into 1/4-in. holes in the outer barrel. The 1/8-in. pins are resistance-welded to the matrix tubes. This method of attachment of the outer barrel to the outer matrix assembly provides a large area of attachment while minimizing the possibility of damaging the 40-mil matrix tubes. There are typically 20 welded-pin attachments between the outer-matrix-assembly matrix tubes and the outer barrel in each of its hexagonal sides. The welded-pin attachments are typically 4 in. apart and run in two axial lines from the front to the back of the outer barrel. The axial lines of attachment are typically each 1 in. from the corners of the hexagonal outer barrel. For additional strength, the top edge of the bottom half of the outer barrel is fillet-welded to the adjacent matrix tubes to provide additional strength and stiffness at the points at which the ball-mount brackets are attached to the inside of the outer barrel along the horizontal midplane. The locations of the outer-barrel weld attachments to the outer matrix tubes are shown in Fig. 15.

The outer matrix assembly to which the outer barrel is welded is constructed from regular ZPR matrix tubes. However, immediately adjacent to the outer barrel, the matrix tubes are reduced in length from the usual

4-ft ZPR matrix tube to approximately 3 ft. The actual tube lengths are shown in Fig. 15. The reduction in tube length is at the rear of the outer matrix assembly and allows space for the inner-matrix rear cover and for the cooling guard-ring air ducting. The outer matrix assembly corresponding to each half-zone is constructed in two halves; an upper and a lower half. The split between the halves is just above the inner-barrel support brackets with a step-up between the first and second matrix tubes laterally. To allow convenient disassembly of the VTRZ, the upper and lower halves of the outer matrix assembly are not welded together.

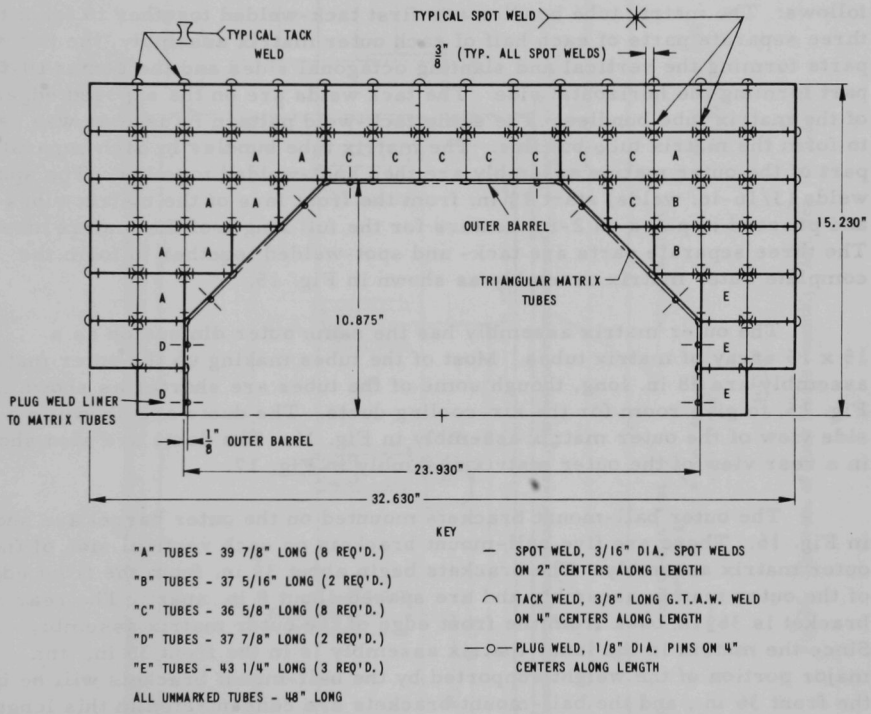

Fig. 15. Welding Pattern Used in Outer Matrix Assembly

To match the hexagonal shape of the outer barrel, the matrix tubes of the outer matrix assembly that are adjacent to the 45° sloping surfaces of the outer barrel are special triangular matrix tubes. There are 12 of these special matrix tubes in each half-zone outer matrix assembly; each is constructed from 40-mil-thick Type 304 stainless steel, as are the regular matrix tubes.

The outer matrix assembly is constructed of individual bundles of matrix tubes as shown in heavy lines in Fig. 15. The individual bundles are spot- and tack-welded together to form the outer matrix assembly. The matrix tube bundles are themselves formed by tack-welding matrix tubes together. The tack welds used to form the matrix tube bundles start 1/2 in. from the front edge of the tubes and proceed, on 4-in. centers, along the entire length of the matrix tubes. The tack welds are placed on both exposed sides of the matrix tube bundle.

The sequence of construction of the outer matrix assembly is as follows: The matrix tube bundles are first tack-welded together to form the three separate parts of each half of each outer matrix assembly, the two side parts forming the vertical and slanting octagonal sides and the center 10-tube part forming the horizontal side. The tack welds are on the exposed edges of the matrix tube bundles. The same tack-weld pattern is used as was used to form the matrix tube bundles. The matrix tube bundles in each separate part of the outer matrix assembly are then spot-welded together. The spot welds (3/16-in. welds) start $1\frac{1}{2}$ in. from the front face of the matrix tubes and proceed in pairs on 2-in. centers for the full length of the matrix tubes. The three separate parts are tack- and spot-welded together to form the complete outer matrix assembly as shown in Fig. 15.

The outer matrix assembly has the same outer dimension as a 15 x 15 array of matrix tubes. Most of the tubes making up the outer matrix assembly are 48 in. long, though some of the tubes are shorter as shown in Fig. 15, to give room for the air-cooling ducts. The ducts are shown in a side view of the outer matrix assembly in Fig. 16. The ducts are also shown in a rear view of the outer matrix assembly in Fig. 17.

The outer ball-mount brackets mounted on the outer barrel are shown in Fig. 16. There are five ball-mount brackets on each vertical side of the outer matrix assembly. The brackets begin about $3\frac{1}{2}$ in. from the front edge of the outer matrix assembly and are spaced about 8 in. apart. The rear bracket is $36\frac{1}{2}$ in. back from the front edge of the outer matrix assembly. Since the matrix in the inner matrix assembly is in the front 36 in., the major portion of the weight supported by the ball-mount brackets will be in the front 36 in., and the ball-mount brackets are concentrated in this length. Special inserts are provided in the triangular tubes in the lower half of the outer matrix assembly to provide additional support for the lower ball-mount mounting pads.

The outer matrix assembly of each VTRZ half-zone has a thickness of only two matrix tubes immediately over the central cavity. To ensure adequate stiffness and strength in the support of loads above the central cavity, an additional welded matrix tube array, 10 tubes high and 19 tubes wide for the first five rows and 15 tubes wide for the next five rows, referred to as the central zone bridge, is placed over the outer matrix assembly of each VTRZ half-zone. The central zone bridge is shown in Figs. 7 and 18.

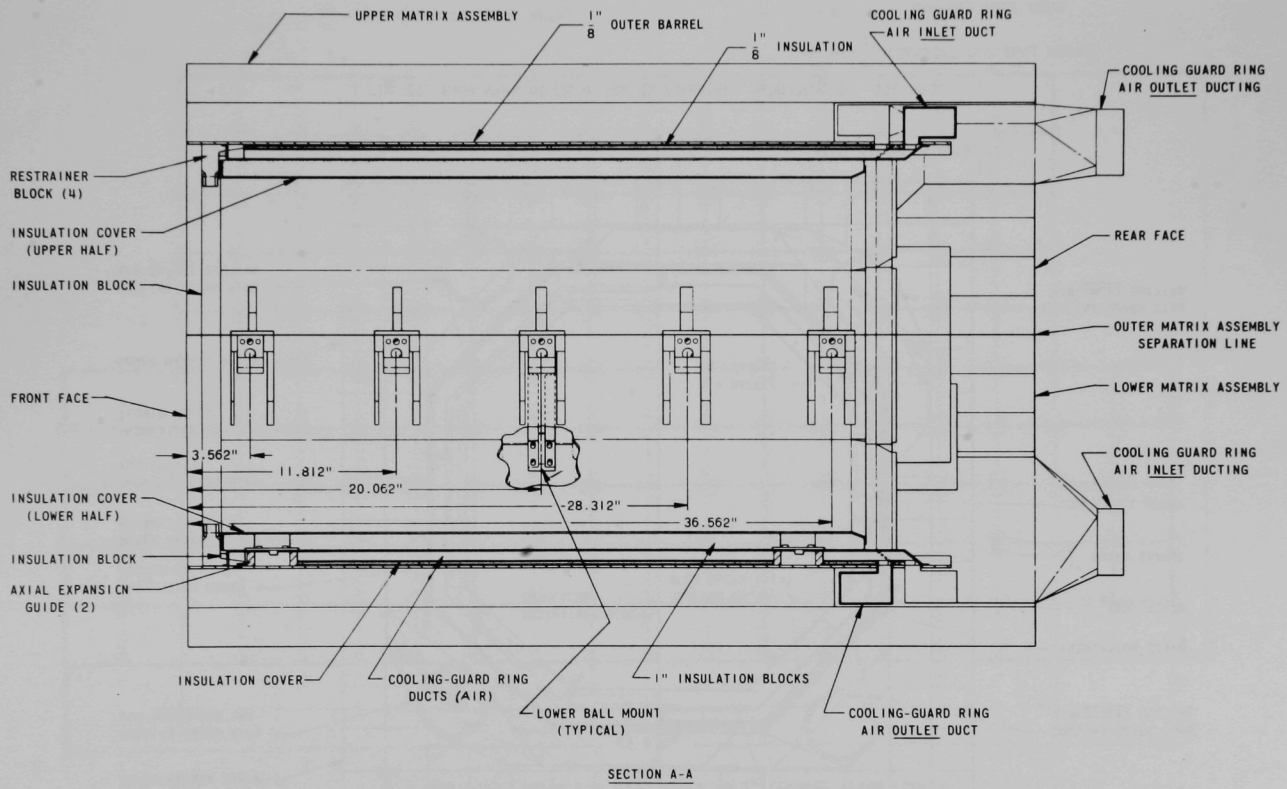

Fig. 16. Side View of Outer Matrix Assembly. ANL Neg. No. 116-428.

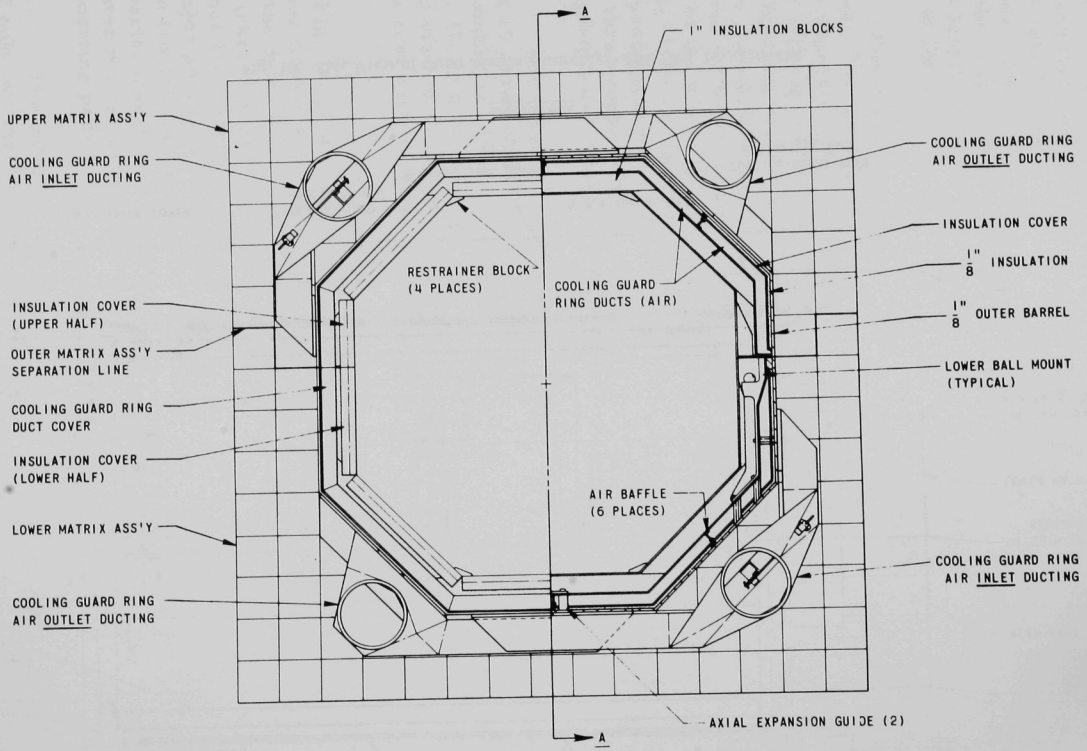

Fig. 17. Rear View of Outer Matrix Assembly. ANL Neg. No. 116-427.

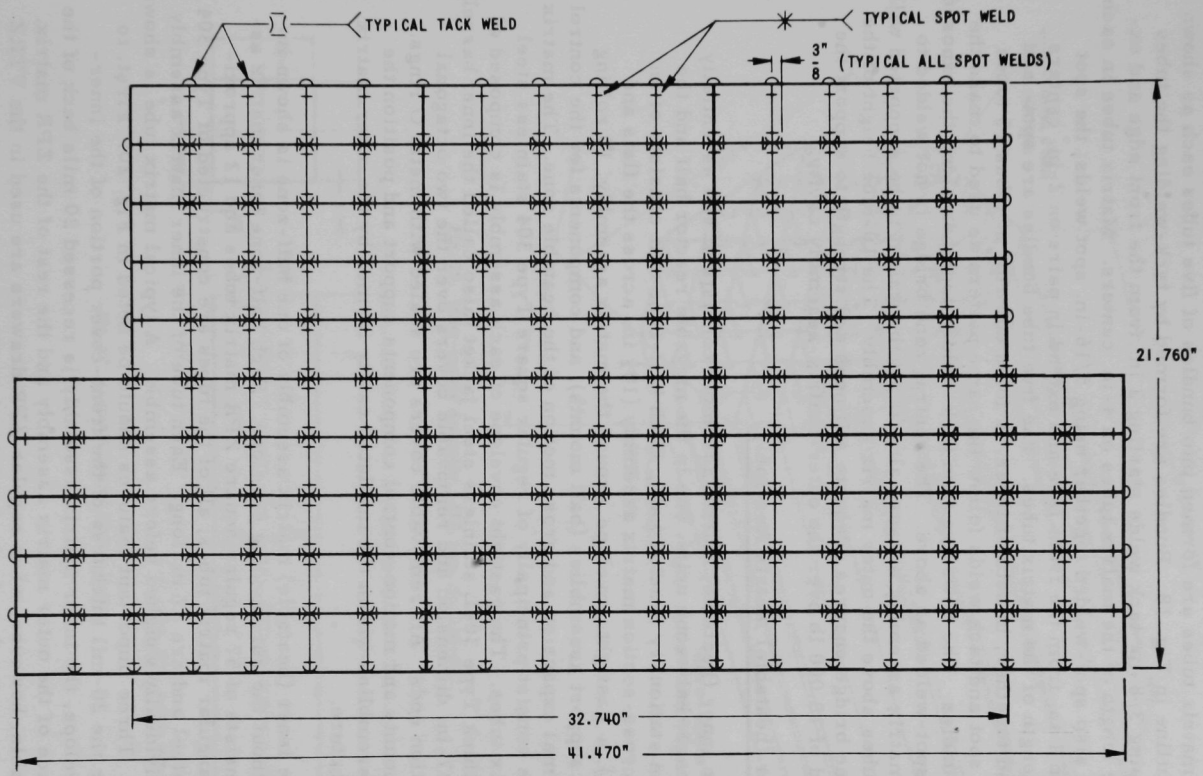

KEY
— SPOT WELD, 3/16" DIA. SPOT WELDS ON 2" CENTERS ALONG LENGTH
⌒ TACK WELD, 3/8" LONG GTAW WELD ON 4" CENTERS ALONG LENGTH
—o— PLUG WELD, 1/8" DIA. PINS ON 4" CENTERS ALONG LENGTH

Fig. 18. Central Zone Bridge

The central zone bridge is made from regular 48-in.-long ZPR matrix tubes. Individual matrix tubes are formed into bundles of five tubes each as shown in heavy outline in Fig. 18. Bundles are formed by tack-welding the tubes together using 3/8-in. tack welds starting 2 in. from the front edge and extending the length of the matrix tubes on 4-in. centers. Matrix tubes in each bundle are also spot-welded together using 3/16-in. spot welds; the spot welds begin 1 in. from the front face and extend in pairs on 2-in. centers along the length of the matrix tubes. The five tube bundles are spot- and tack-welded together, in sets of three, to form one row of tubes 15 tubes long. The spot and tack welds follow the same pattern as used to make the five tube bundles. The rows are then tack-welded together along the exposed sides and spot-welded as above. The central zone bridge is not welded to the outer matrix assembly because almost all the weight to be supported will be in the tubes above the outer matrix assembly. The 10-tube height of the central zone bridge ensures adequate stiffness and strength to support the design load of 18,000 lb over the outer-matrix-assembly cavity.

4.5.3 Inner (heatable) Matrix Assembly

The inner (heatable) matrix assembly consists of two essentially mirror-image, half-zone units, one in the movable reactor half and the other in the stationary reactor half. Each half-zone unit consists of an octagonal cross-section matrix assembly ($19\frac{1}{2}$ in. across the flats and 37 in. long), a gastight envelope around the matrix assembly, 10 rolling structural support assemblies (ball mounts), and components for the control of the thermal expansion and gross motion of the heatable zone. The matrix assemblies consist principally of regular square Type 304 stainless steel ZPR matrix tubes. The gastight envelope of each assembly is composed of a 1/8-in.-thick Type 304L stainless steel jacket (also called the inner barrel) along the 37-in. dimension and removable covers over the two octagonal cross-section ends. All removable covers are sealed with metal O rings. The ball mounts and motion-control components support and position the heatable assemblies within the insulated cavity formed by the outer matrix bridge structure.

The inner (heatable) matrix assembly of one half-zone is shown in Fig. 19 without the surrounding envelope. Each half-zone inner matrix assembly consists of 57 regular square ZPR matrix tubes and 12 approximately triangular matrix tubes; all of the tubes are constructed of Type 304 stainless steel and are 37 in. long. Each tube of the inner matrix assembly will be individually weighed before assembly. A typical matrix tube is shown in Fig. 20. Three important features should be noted in Fig. 20: First, to provide for the 20-mil thickness of the front-cover portion of the inner-matrix envelope, the inner matrix assembly is recessed 20 mils back of the front surface of the outer matrix assembly and the rest of the ZPR matrix. It is desirable, however, when regular ZPR drawers are used in the VTRZ (at room temperature), to have the ends of the drawers line up with the rest

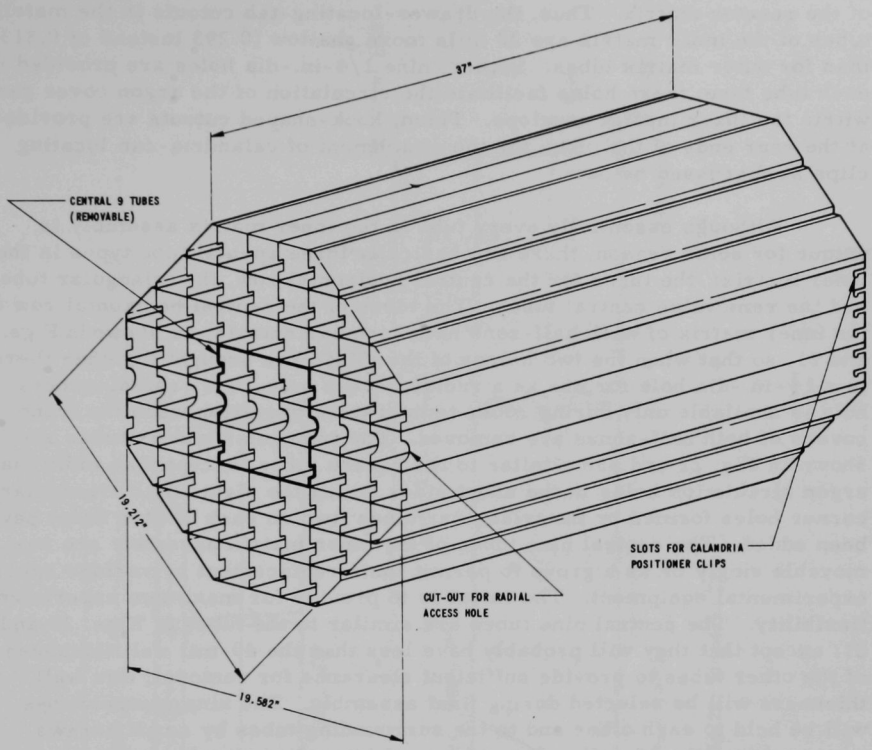

Fig. 19. Inner-matrix Assembly. ANL Neg. No. 116-426.

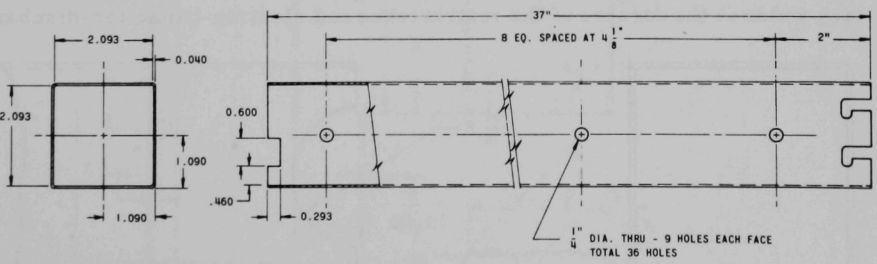

Fig. 20. Typical Square Matrix Tube

of the reactor matrix. Thus, the drawer-locating-tab cutouts in the matrix tubes of the inner matrix are 20 mils more shallow (0.293 instead of 0.313) than for outer matrix tubes. Second, nine 1/4-in.-dia holes are provided in each tube face; these holes facilitate the circulation of the argon cover gas within the inner matrix envelope. Third, hook-shaped cutouts are provided at the rear ends of the tubes for the attachment of calandria-can locating clips as discussed below.

Although essentially every tube in the inner matrix assembly is unique for some reason, there are basically three special tube types in the inner matrix: the tubes for the central horizontal row, the triangular tubes, and the removable central tubes. The tubes of the central horizontal row of the inner matrix of each half-zone have circular cutouts, as shown in Figs. 19 and 21, so that when the two halves of the VTRZ are brought together there is a $1\frac{3}{8}$-in.-dia hole for use as a radial-access hole. This radial-access hole is available only during room-temperature operation when the front covers of both half-zones are removed. The triangular matrix tubes are shown in Fig. 22 and are similar to the square tubes, except that additional argon circulation holes in the short sides facing the eight small triangular corner holes formed by the triangular tubes (two on each of four flats) have been added. The central nine tubes of the inner matrix assembly are removable singly or as a group to permit their replacement by various special experimental equipment. The intent is to provide for maximum experimental flexibility. The central nine tubes are similar to the tubes of Figs. 20 and 21, except that they will probably have less than the 40-mil wall thickness of the other tubes to provide sufficient clearance for removal; this wall thickness will be selected during final assembly. The nine central tubes will be held to each other and to the surrounding tubes by small screws recessed into the 40-mil walls and tapped into adjacent tube walls.

The matrix tubes of each half-zone inner matrix assembly are fastened together by a combination of GTAW (inert-gas shielded tungsten arc weld) tack welds at the corners of the matrix tubes and electric-capacitor-discharge

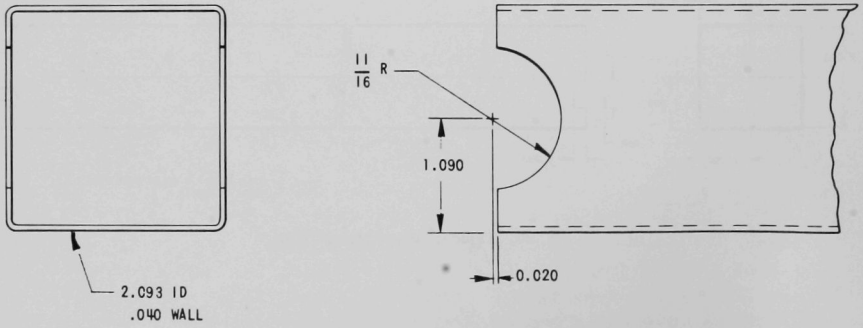

Fig. 21. Cutout for Radial Access Hole

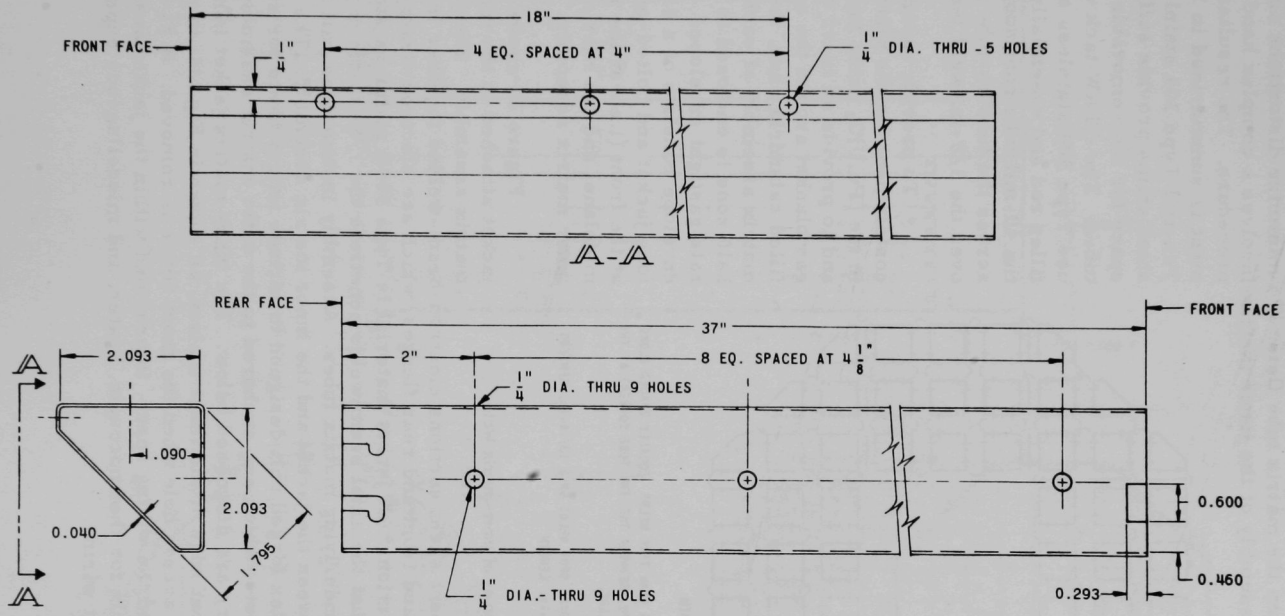

Fig. 22. Triangular Tubes

spot welds between the matrix tube flats. To minimize distortions and maximize strength, assembly of the inner matrix involves a complex hand-fitting procedure. The resultant weldment is summarized in Fig. 23. Ten-mil Type 304 stainless steel shims provide sufficient space for the removable central tubes. The GTAW tack welds use Type 304 stainless steel filler rod and essentially make the 40-mil tube continuous across the tube-to-tube gap over the 3/8-in. weld lengths.

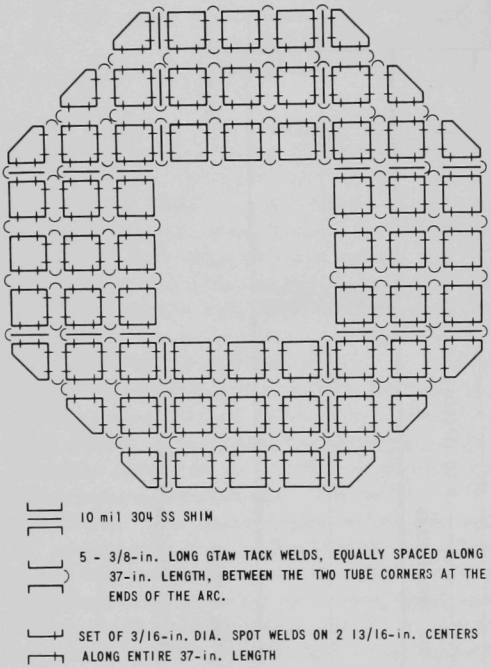

Fig. 23. Summary of Inner-matrix Weld

To provide secondary containment for the plutonium in the $(Pu,U)O_2$ oxide fuel rods and to provide an inert cover-gas blanket around the sodium-filled calandria cans, the inner matrix assembly of each VTRZ half-zone is enclosed in a separate gastight envelope. The envelope consists of a 42-in.-long jacket and bolted-on covers at the front (i.e., at the reactor midplane) and the rear of the inner matrix assembly.

Figure 24 shows the jacket attached to the inner matrix assembly. The jacket consists of two bent sheet sections electron-beam-welded together in the 42-in. direction and front and rear flanges, which are electron-beam-welded onto the sheet section. All jacket material is Type 304L stainless steel. Note in Fig. 24 that the axial seam welds penetrate the 1/8-in.-thick jacket and pick up the underlying matrix tubes. Assembly instructions call for a very tight fit between the jacket and the inner matrix assembly. The front flange is a complex forged unit designed to include four pockets for scram-restrainer brackets, which are anchored to the outer matrix assembly; the scram restrainers are discussed below. The inner matrix jacket is recessed in back of the front edge of the inner matrix, as shown in Fig. 24, to permit use of the radial access hole when the front cover is removed. A $5\frac{1}{2}$-in.-deep space, called the wiring space, is provided within the jacket at the rear of the inner matrix for thermocouple, heater, and miscellaneous experimental equipment wiring.

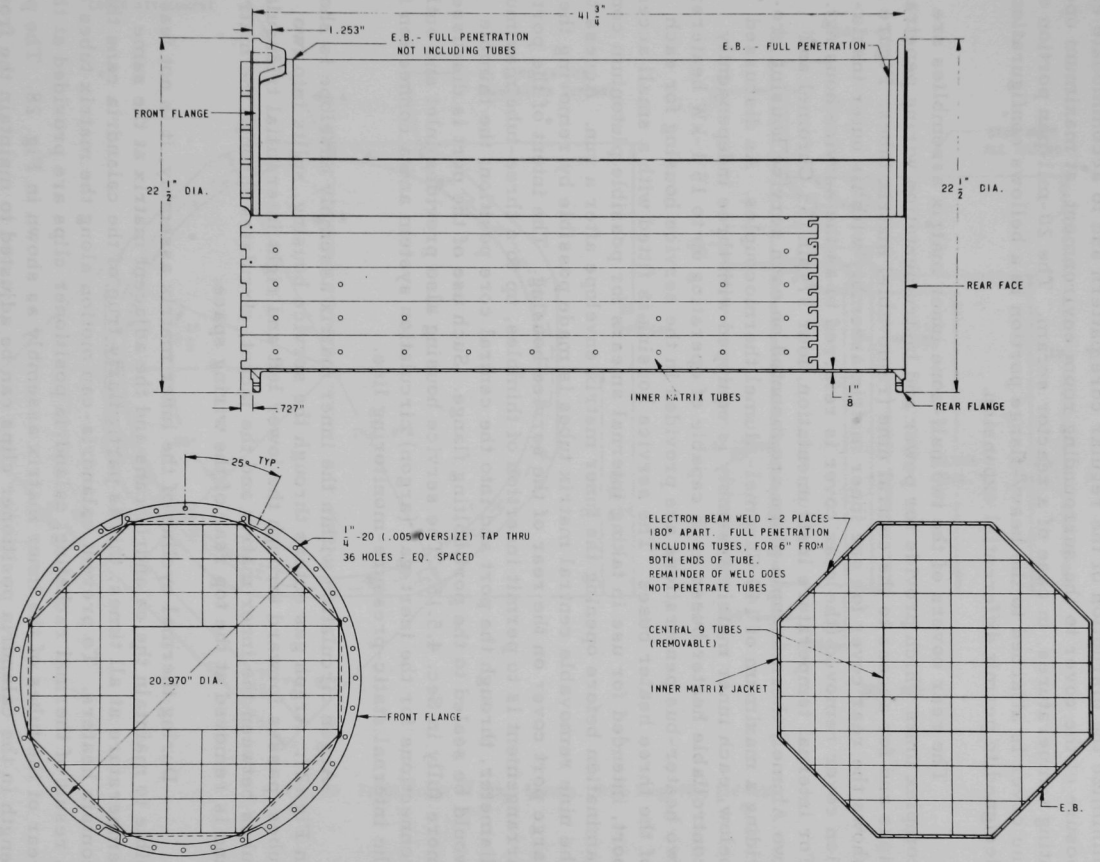

Fig. 24. Inner-matrix Jacket

The standard front-cover design is shown in Fig. 25; special versions of this cover are discussed in Sec. 4.5.15. This cover has been designed to minimize the disruption of the regular core pattern and to accommodate exposure of the cover to the surrounding room environment, at maximum operating temperatures, in case of a reactor scram. The 20-mil-pan portion of the cover is attached to the heavy-flange portion in a bellows configuration designed to permit differential expansion.

The rear covers of the two half-zone inner matrix assemblies are complex units which provide for power and instrumentation wiring penetrations and for access to the central nine (removable) matrix tubes. Figure 26 shows the rear cover for one inner matrix assembly with its outer insulation cover removed (the rear cover is referred to as the service housing). For internal temperature instrumentation, four 37-pin (35 Chromel and two Alumel) thermocouple plugs are mounted on each service housing providing a maximum of 140 Chromel-Alumel thermocouples. As discussed below, each inner matrix assembly is equipped with three independently controllable heater buses each capable of operating up to 15 1-kW heaters; two heater-bus penetrations are provided in the service housing for each of the three heater buses. The service housing is fitted with a small access port, intended for use in taking internal smears for possible plutonium contamination before opening the inner matrix envelope after a run. Access to the nine removable central matrix tubes is made possible by removing the large port cover on the rear of the service housing. The intent of the port arrangement is to permit insertion of thimbles, up to a three-tube maximum diameter, through the port and into the central core position; the thimble would be sealed to the port bolting flange. Such use of the port is discussed more fully in Sec. 4.5.15. The service housing also provides inlet and outlet connections for the inert-gas (argon) circulation system and a connection for the internal static-pressure-monitoring line.

Argon circulation within the inner matrix assembly envelope is shown in Fig. 27. Argon gas enters through the service housing, splits into two tubes, passes forward through the lower left and right interstitial triangular tubes between the inner matrix and the jacket, circulates through the matrix, and is removed at the top rear of the wiring space.

During thermal cycling of the inner matrix assembly, it is not feasible to maintain the calandria cans and the adjacent matrix at the same temperature at all times; this is particularly true of the calandria cans that contain heaters. To prevent calandria-can motion along the matrix tubes as a result of thermal racheting, calandria positioner clips are provided at the rear of the tubes of the inner matrix assembly as shown in Fig. 28. The pin length in the calandria positioner clips can be adjusted to maintain the front calandria can 20 mils behind the reactor midplane (i.e., at the front edge of the inner matrix) or to maintain the front calandria can at the reactor midplane. The latter position would be used during room-temperature operation,

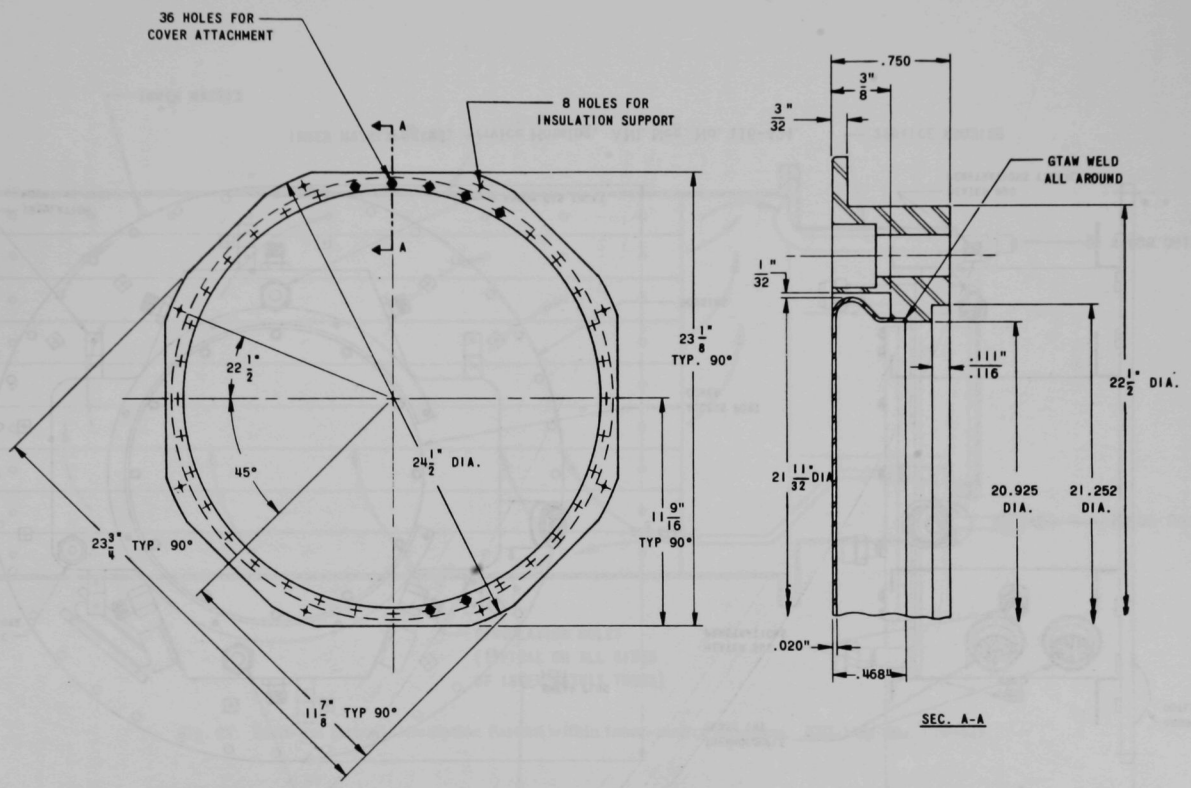

Fig. 25. Front Cover of Inner Matrix. ANL Neg. No. 116-425.

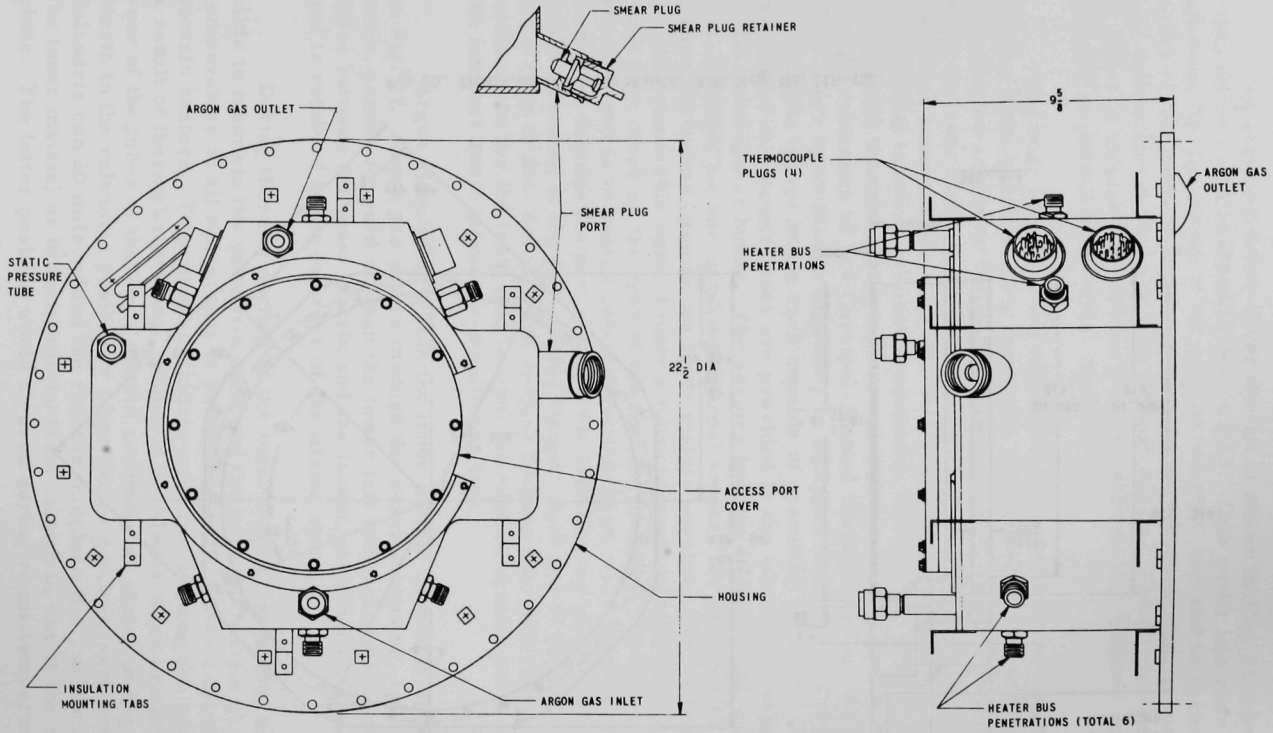

Fig. 26. Service Housing. ANL Neg. No. 116-424.

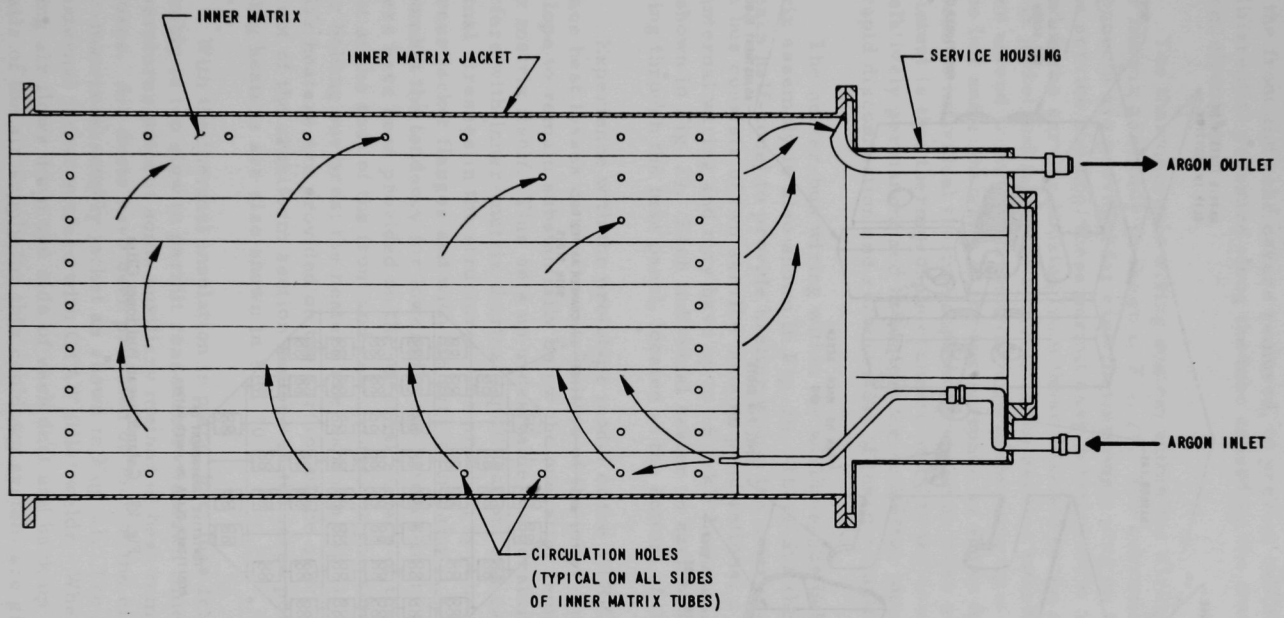

Fig. 27. Inert-gas (argon) Circulation Pattern within Inner-matrix Envelope. ANL Neg. No. 116-423.

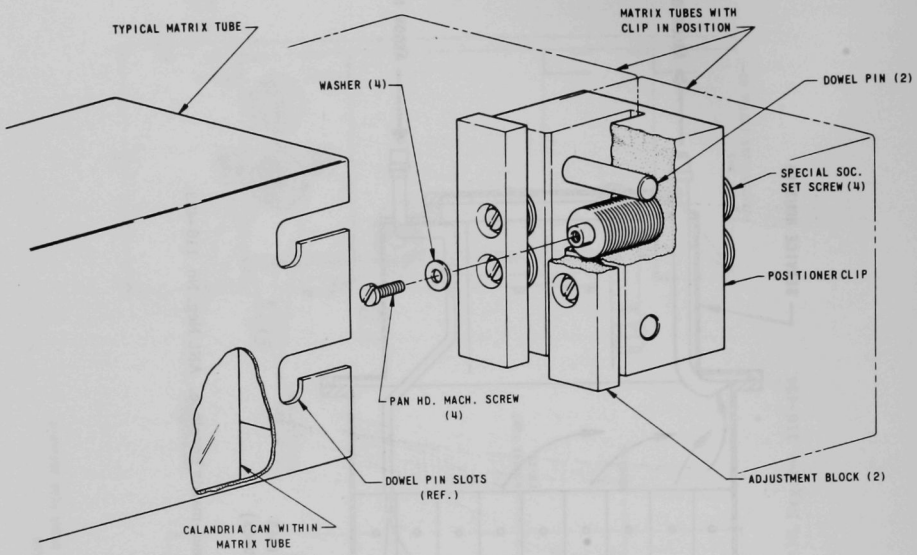

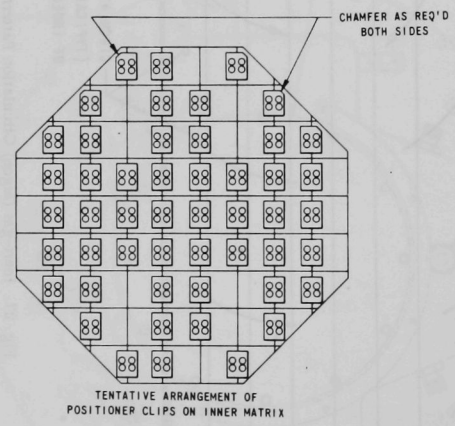

Fig. 28. Calandria-can Positioner Clips

with the front and rear covers removed, to prevent calandria motion due to the differential pressure along the tube caused by the matrix air-cooling system circulation.

The thermocouple wiring system within the wiring space behind the inner matrix assembly is shown in Fig. 29. For convenience, screw-plug disconnects are provided for each thermocouple plug on the inside surface of the service housing; these permit easy disconnection of components attached to the service housing from those attached to the inside of the inner matrix jacket and facilitate removal of the service housing. Thermocouple cables extend from the disconnect plugs to thermocouple connector blocks on the left and right walls of the wiring space as shown in Fig. 29. Connections to individual thermocouples are made at these connector blocks. The intent is that thermocouple connections up to the connector block would be relatively permanent and in cables; the connector blocks are designed for rapid disconnection and reconnection of thermocouples.

The heater-bus wiring within the wiring space behind the inner matrix assembly is also shown in Fig. 29. There are three heater buses (on each half-zone) to provide heating within the inner matrix assembly. Each bus consists of two service housing penetrations, a fuse-panel sector, and internal wiring and may have up to 15 1-kW heaters. These components are shown in Fig. 29. Each individual heater on each heater bus has one leg passing through the fuse panel, located at the bottom of the wiring space.

Experience with the prototype model of the VTRZ has indicated that surface heat losses cause the extremities of the inner-matrix-assembly envelope to remain substantially below the operating temperature of the inner matrix itself. This sets up undesirable temperature gradients, which interfere with inner-matrix thermal equilibration, and causes undesirable thermal stresses in the structure. The problem is principally with the front and rear jacket flanges and with the service housing (i.e., the rear cover). To combat the tendency for lowered temperatures in the flanges, tubular heaters have been provided on the external surface of the inner-matrix jacket at the root of the front and rear flanges on the sides opposite to the cover bolting surfaces; the heaters are shown in Fig. 30. In addition, two tubular heaters are provided on the surface of the service housing: one at the root of the cruciform section and one on the large port. The service-housing heaters are also shown in Fig. 30.

With the thermal insulation in place, heat loss from the inner matrix assembly is too slow to permit reasonable cooldown times from operating temperatures without some auxiliary method of heat removal for cooldown purposes. Air ducts have been provided on four of the eight surfaces of the inner-matrix-assembly jacket as shown in Fig. 31. The ducts are sealed to the external jacket surface with GTAW fillet welds. When activated, the cooling air flows down one side of each duct and back up the opposite side. (Details of the air supply for this cooldown system are given in Sec. 4.5.6.)

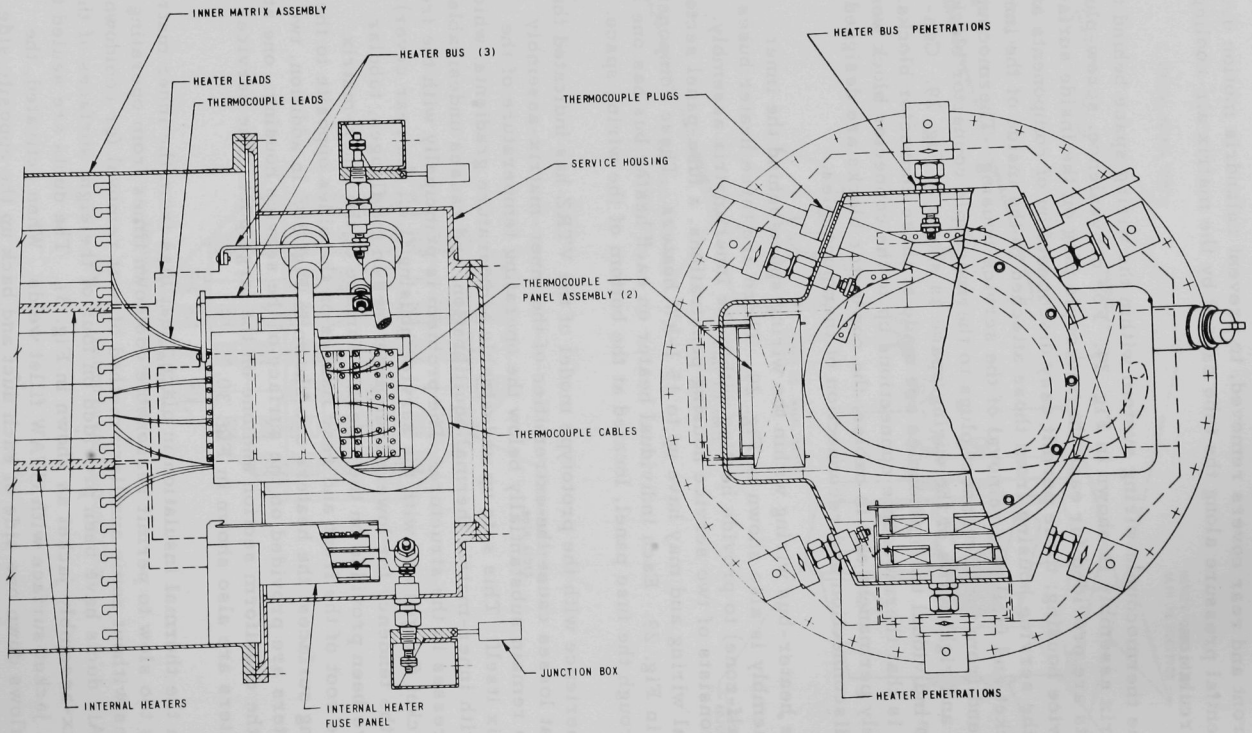

Fig. 29. Thermocouple and Heater-bus Wiring within Wiring Space

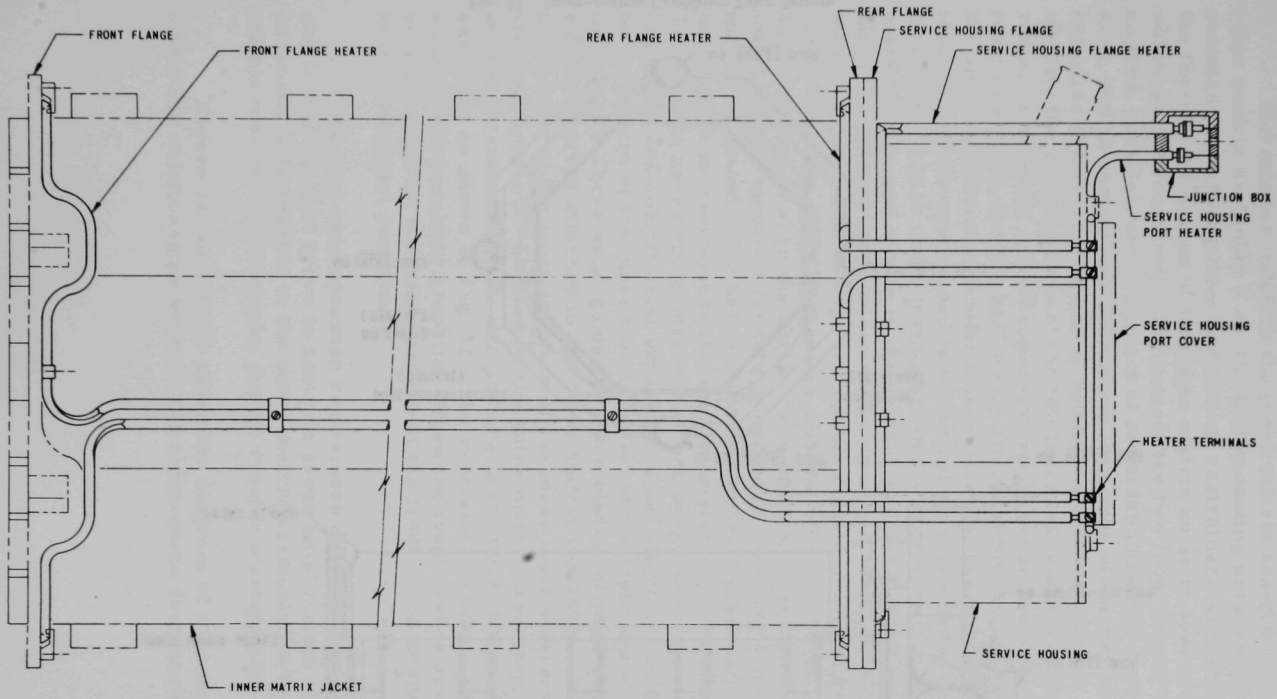

Fig. 30. Inner-matrix Flange and Service-housing Heaters

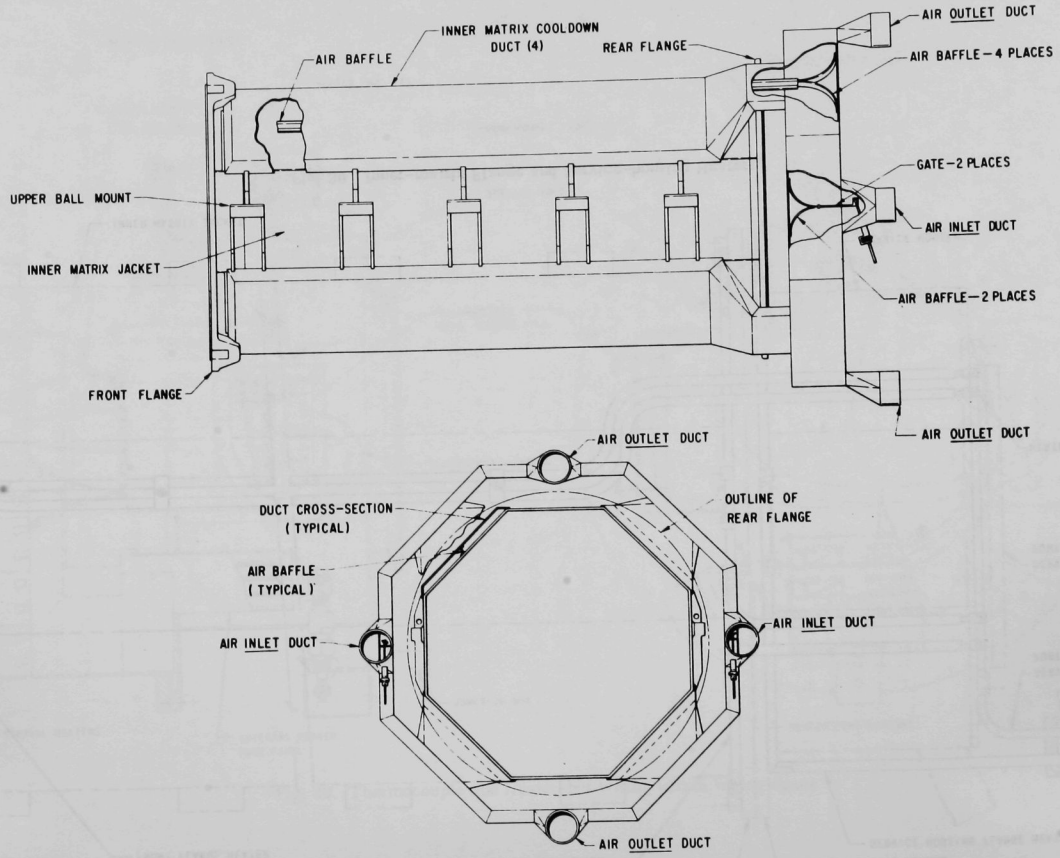

Fig. 31. Inner-matrix Cooldown Duct System

The manner in which the inner matrix assembly is mounted on the outer matrix assembly (i.e., the ball-mounting arrangement) and the associated expansion guides and motion restrainers are intended to control the thermal expansion of the inner matrix so as to approach the ideal in which, as the inner matrix is heated, the two front covers (which are aligned, parallel, and in contact at room temperature) remain aligned, parallel, and in contact and the central long axes of the two inner matrix assemblies (which are aligned at room temperature) remain aligned. That is, ideally, the center points of the two inner-matrix front covers would always remain stationary and all expansion would occur radially and axially away from this point, the two half-zones always remaining aligned. Except for the small effects of nonuniform inner-matrix-assembly temperatures, this ideal is closely approached in the actual mounting arrangement. The structural load of each inner matrix assembly is transmitted to the associated outer matrix, and thence to the reactor bed, through 10 ball mounts arranged along the horizontal midplane of the inner matrix assembly. The ball-mount locations are shown in Fig. 32, and the details of the upper and lower ball-mount brackets, the insert plates, and the balls are shown in Fig. 33. The ball mounting is near the horizontal midplane of the inner matrix so that there is little tendency for this midplane to move vertically when the inner matrix is heated. The ball mounts fix the horizontal midplane in position, but provide no restraint to thermal expansion or gross motion in this plane. To restrain gross horizontal motion and at the same time maintain axial alignment and permit axial expansion, axial alignment guides are attached to the bottom of the inner matrix jacket at the front and at the rear as shown in Fig. 32. These axial guides are thin blades, aligned axially, fitting into rolling fixtures attached to the outer matrix assembly. To provide axial positioning of the front surfaces of the inner matrix assemblies, four restrainer brackets, mounted on the outer matrix assembly, span across the insulation annulus and fit into pockets in the front flange of the inner matrix assembly as shown in Fig. 32. The restrainer brackets are thermally insulated with pyrolytic graphite. When the front covers are installed, the restrainers control the axial position of the front cover so that the front surface is in the correct position.

The four axial-position restrainers described in the last paragraph and in Fig. 32 also serve to restrain gross axial motion of the inner matrix assembly with respect to the outer matrix assembly during rapid outer-matrix motion--for example, during reactor startups and scrams.

Figure 34, an overall assembly diagram of the inner matrix complex, shows the relationships between the components described in this section.

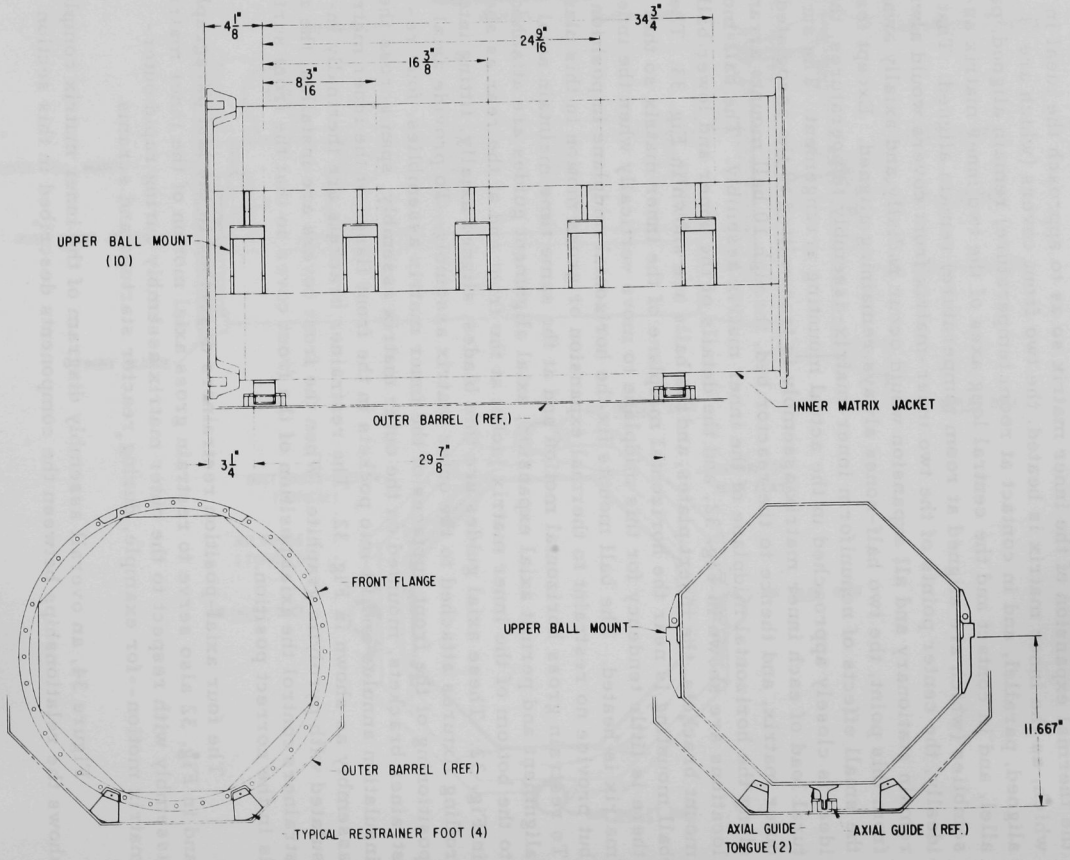

Fig. 32. Inner-matrix Jacket, Ball Mount, Axial Guides, and Motion-restrainer Positions

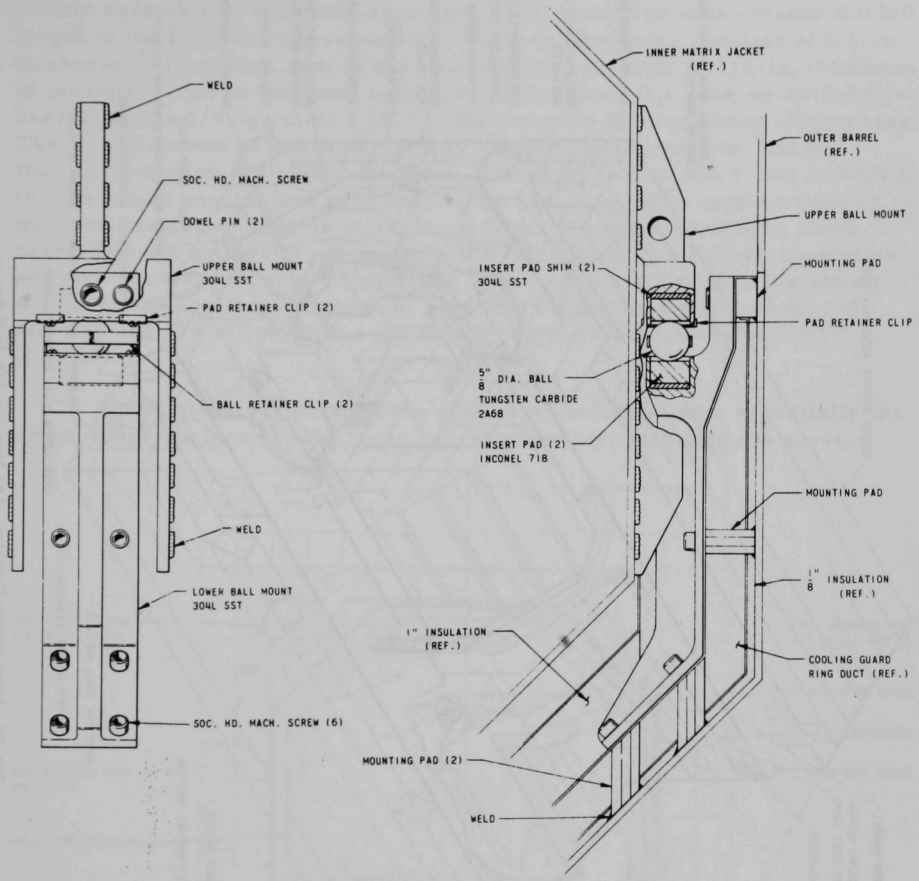

Fig. 33. Ball Mount. ANL Neg. No. 116-422.

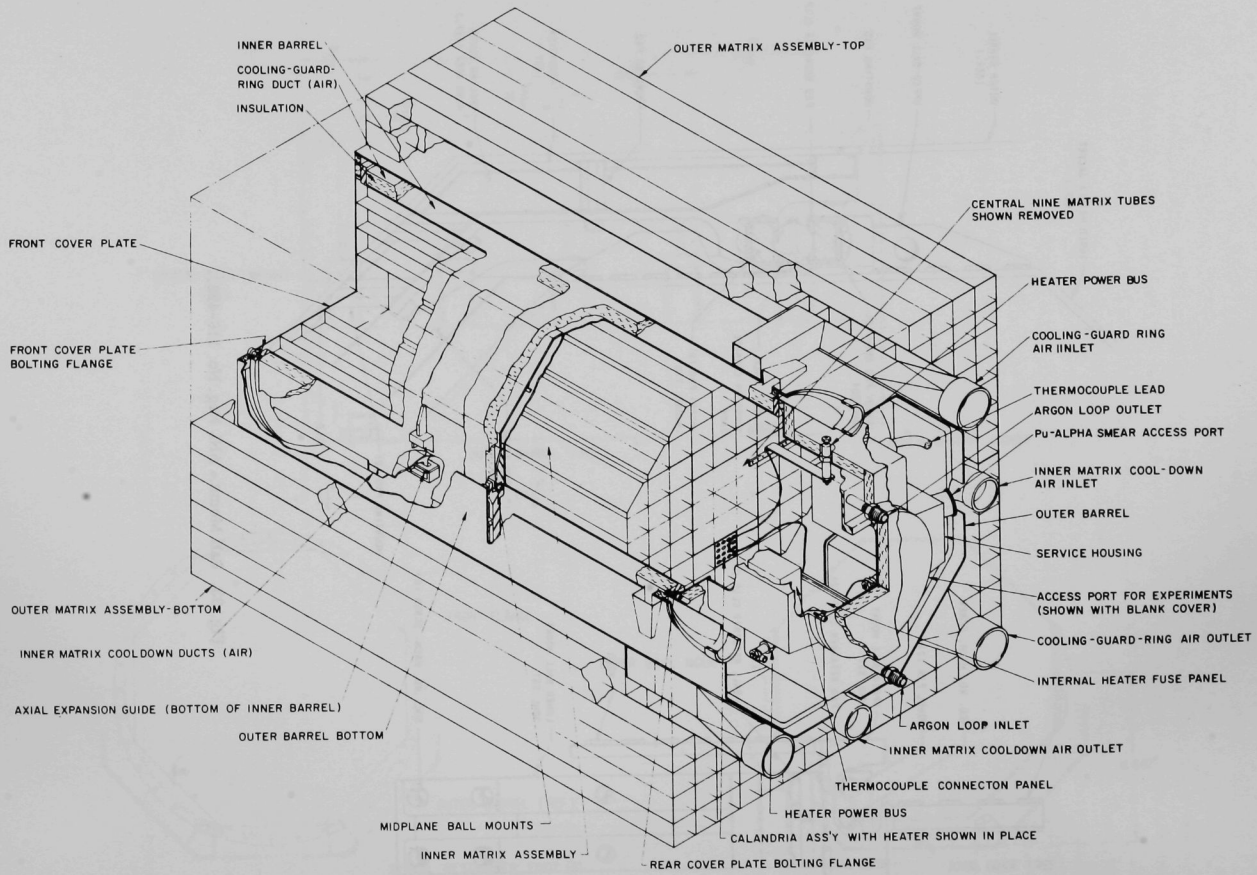

Fig. 34. Inner-matrix Complex. ANL Neg. No. 113-1527 Rev. 1.

4.5.4 Insulation-annulus Components

An approximately 2-in.-thick annular insulation zone is provided in the VTRZ design between the inner (heatable) barrel assembly and the outer matrix assembly of each half-zone unit. The insulation zone extends the full length of the inner barrel assembly. The 2-in. thickness consists of a 1-in. thickness of insulation next to the inner barrel assembly, a 1/8-in. thickness of insulation next to the outer matrix assembly liner (i.e., the so-called outer barrel), and a 3/4-in.-thick CGR duct between the two insulation thicknesses. The 10 ball-mount assemblies, the two axial guide assemblies, and the four axial-motion restrainer brackets, discussed in Sec. 4.5.3, are located in the insulation annulus and span across the 2-in. gap. The configuration of the 2-in. insulation annulus is shown in Figs. 35 and 36, where the inner barrel assembly is removed and only the ball mount, axial guide, insulation, and duct components actually attached to the outer matrix liner are shown. All the insulation is a commercial refractory-fiber insulation, about 50% alumina and 50% silica, with a maximum service temperature of 2300°F (1260°C).

In the elevated-temperature operating configurations, essentially the entire outer surface of each inner barrel assembly, including the service

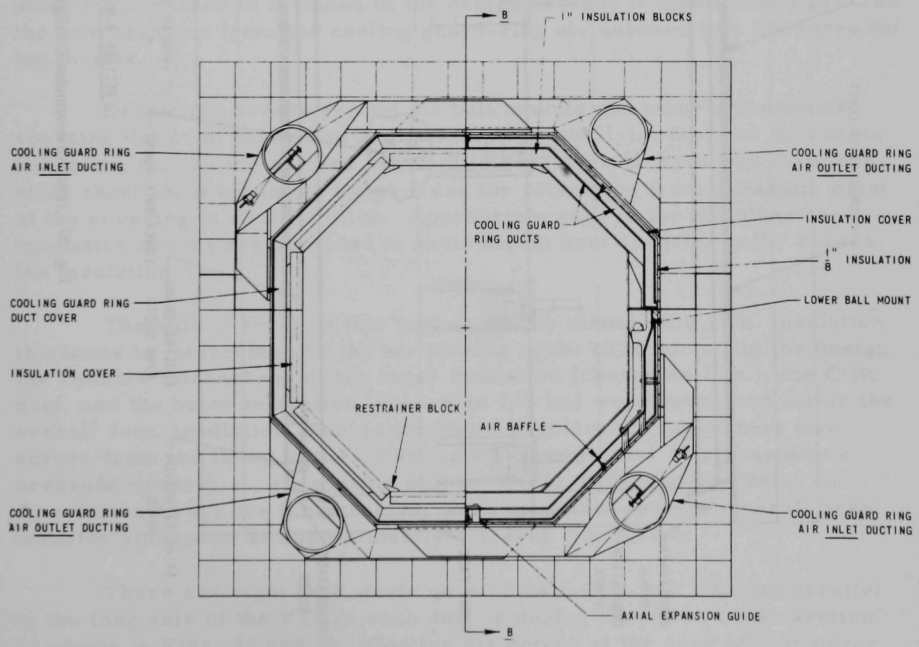

Fig. 35. Insulation-annulus Configuration, Rear View

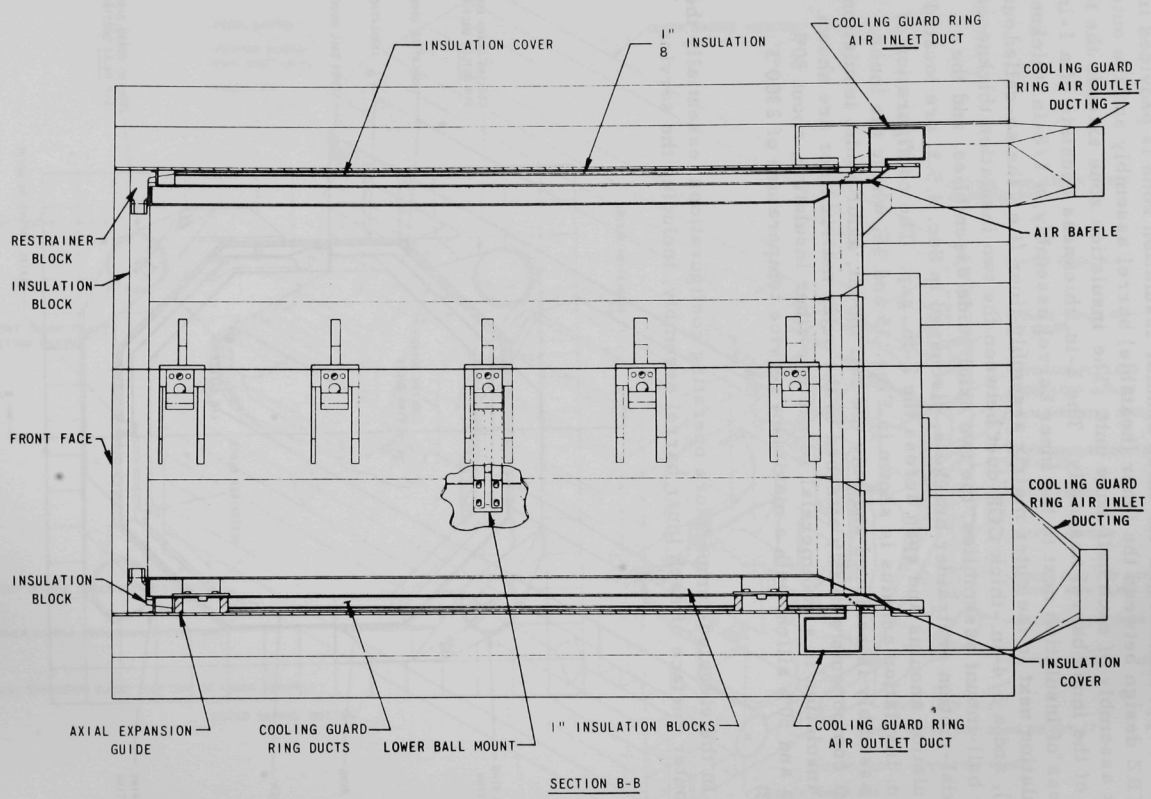

Fig. 36. Insulation-annulus Configuration, Side View

housing (rear cover), is covered with a 1-in. thickness of insulation; only the mating front surfaces of the inner-barrel-assembly front covers are not insulated. Although there is little direct metal-to-metal contact between components of the heatable inner barrel assembly and components of the nominally room-temperature outer matrix assembly, the insulation thickness is of necessity locally reduced (and in some places eliminated) in the vicinity of the ball mounts, axial guides, axial motion restrainers, and front- and rear-cover bolting flanges. Unavoidably, some heat is transferred from the inner matrix assembly to the outer matrix assembly through these insulation gaps, which must be removed by gross air cooling of the outer matrix assembly, as discussed in Sec. 4.5.6.

The 1-in. insulation thickness was chosen as a compromise between competing requirements--i.e., the requirement to minimize the thickness and mass of the material in the insulation annulus, on the one hand, and the requirement to minimize radial heat transfer on the other. One inch is a reasonable compromise, from the physics viewpoint, and gives radial heat losses consistent with desired radial temperature profiles in the inner matrix region; these considerations are discussed further in Sec. 5.2.6.

The 1/8-in. insulation thickness between the CGR ducts and the outer matrix liner is included in the design because it significantly reduces the heat transfer from the cooling guard-ring air outward into the surrounding matrix.

Except for breaks around the ball mounts and other components spanning the 2-in. insulation gap, all the 1/8- and 1-in. thermal insulation (including that on the service housing) is covered with Type 304 stainless steel sheet for mechanical support and for protection from abrasion; most of the covering is 10 mils thick. Appropriate gaps in the stainless steel insulation covers are provided to avoid direct heat-transfer paths across the insulation.

The bulk of the heat that leaks radially through the 1-in. insulation thickness is intercepted by the air flowing in the CGR ducts. In the design, the relative thicknesses of the inner insulation (chosen as 1 in.), the CGR duct, and the outer insulation (chosen as 1/8 in.) were optimized within the overall 2-in. insulation annulus thickness to minimize radial heat flow across from the inner to the outer matrix assemblies. For reasonable pressure drops (i.e., reasonable blower sizes), CGR air-flow rate, and therefore average air temperature, were optimized from an overall heat-transfer standpoint at approximately a 3/4-in. duct height.

There are eight CGR ducts on each half-zone unit running parallel to the long axis of the VTRZ; each duct is dogleg shaped in cross section as shown in Figs. 35 and 36. Cooling air enters at the rear of four of the ducts, alternating around the circumference, and flows forward along the

insulation. Near the front flange, the air reverses direction by flowing into adjacent return ducts and exhausts into external ducting near the rear flange. Details of the CGR airflow pattern are given in Sec. 4.5.6. The CGR ducts are completely sealed so that there is no air leakage into the insulation annulus. This is an important feature; air leakage from the CGR and inner-matrix cooldown air systems into the insulation annulus in the VTRZ prototype resulted in undesirable temperature gradients near the outer surface of the inner matrix assembly, but did not compromise system integrity.

The detailed design of the CGR duct system, has been arranged to effectively intercept radial heat leakage through the annulus at the points at which penetrations occur in the insulation as well as over the wide, undisturbed insulated areas. As may be seen in Figs. 35 and 36, the CGR ducts pass between the lower ball-mount brackets and the outer matrix liner to which they are attached. The lower web portion of these brackets is fastened to the CGR duct wall; the upper, central, and two lower supports, which attach the lower ball-mount brackets to the outer matrix liner, act as cooling fins in the air duct. It is expected that this arrangement will effectively remove heat leaking through the ball-mount assemblies. In a similar manner, the axial guide assemblies are arranged so that the leakage heat path from the guide fin, attached to the inner barrel assembly, through the rollers to the guide base, attached to the outer matrix liner, forces the heat flow through portions of guide assemblies that are essentially fins in the cooling-guard airflow. The rear portions of the base of each of the four axial-motion-restrainer brackets are within the CGR ducts, at their forward-most ends of the ducts, in the region in which the airflow is reversing direction as it changes from entering to exit ducts. Air-deflection fins are placed within the CGR ducts to direct the air against the bases of the restrainer brackets to more effectively cool them.

As mentioned in connection with the necessity for sealed CGR and inner-matrix cooldown air-system ducts, it is important to avoid extraneous cooling of the inner barrel assembly by leakage airflow over its surface. Because it is not feasible to seal the rear end of the insulation annulus of each VTRZ half-zone between the inner and outer matrix assemblies, it was foreseen that there was a potential leakage air-cooling problem from the gross matrix air-cooling system to be used in conjunction with the VTRZ. The gross matrix air-cooling system was designed to remove plutonium-alpha decay heat from plate-type core assemblies by circulation of cooling air directly through the matrix tubes around the inserted fuel drawers. This air system consists of blowers, filters, and large air-distribution plenums behind the movable and stationary reactor halves of the ZPR facilities. (The system is described in more detail in Sec. 4.5.6.) It is intended that this gross matrix air system be used with the VTRZ to cool the matrix regions outside of the outer matrix liner to remove decay heat from the plutonium fuel that may be there and also to remove whatever leakage heat penetrates the

insulation annulus. The problem with respect to extraneous leakage air cooling of the inner barrel assembly occurs because the rear of the insulation annulus is directly exposed to the gross matrix air-cooling plenum behind the reactor half and the air-pressure head necessary to force air through the matrix tubes also tends to force air axially through the insulation annulus. To protect against this induced-leakage airflow, an outer-matrix-assembly to rear-mounting-plate skirt will be designed to isolate the insulation annulus from the reactor-cooling-system pressure head.

4.5.5 Argon Loop System

4.5.5.1 Design of Overall Argon Loop System

The function of the argon loop system, shown schematically in Fig. 37 and as a simplified line drawing in Fig. 38, purges the air out of both inner-matrix-assembly half-zones, before heated operation, replacing it with and maintaining a pressure-controlled argon cover gas free of oxygen and water vapor. The purpose of the cover gas is twofold: First, it prevents significant burning of sodium within the enclosed zone in the event of a sodium leak from a calandria can. Second, the argon loop provides the site for most of the VTRZ component failure monitors described in Sec. 4.5.9. These component failure monitors, together with other loop monitors and controls, are located in the control-rod mounting-plate areas or at the "Dri-Train station" just east of the stationary half of ZPR-6. It is assumed for this discussion that the VTRZ will be installed in ZPR-6, although it may also be installed in ZPR-9. Both half-zones will be operated at a pressure of approximately -1 in. of water, with respect to cell pressure, during heated operation to ensure retention of contamination from a plutonium rod failure within the inner-matrix-assembly envelopes or, in the event of a concurrent leak in the inner-matrix-assembly envelope, within the reactor-matrix air-cooling system. The decision to operate at approximately -1 in. of water is a compromise between a desire to limit in-leakage of oxygen and water vapor by raising the half-zone pressure, a desire to ensure plutonium confinement by lowering the half-zone pressure, and a desire to limit mechanical yielding of the front cover plate by maintaining the half-zones at close to cell pressure. The analyses and testing of these three factors are discussed in Secs. 8.5, 8.4, and 6.5.

The gas flow rate through each half-zone is set at approximately 1 cfm (STP), providing a fresh gas blanket by flushing out the 2.5 ft^3 half-zone gas space every 2.5 min. The decision to operate at this flow rate is a compromise between a desire to minimize the time required to detect component failures (e.g., pin failure with subsequent plutonium-alpha contamination), a desire to maximize half-zone purification rates by increasing flow, and a desire to minimize system pressure drops by limiting flow. The analyses and tests relevant to the determination of these flow levels are discussed in Secs. 7.1, 8.5, and 8.4.

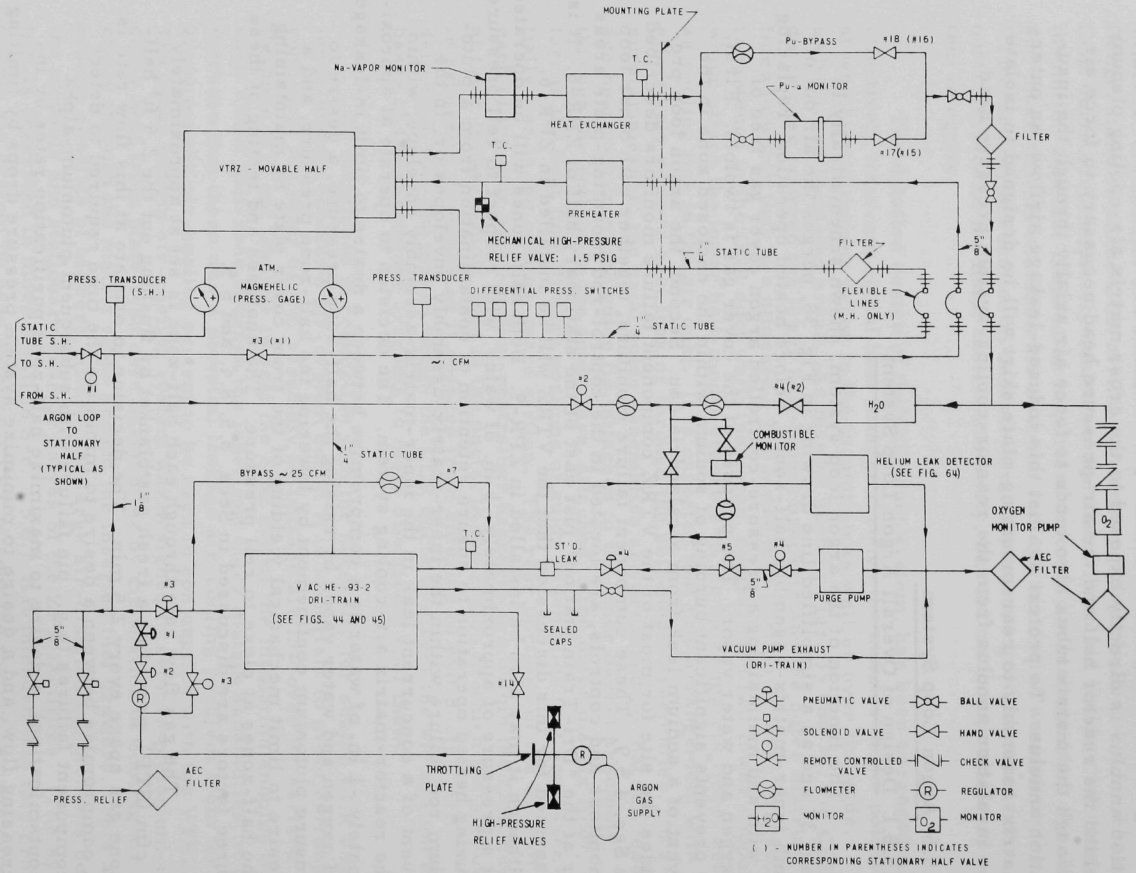

Fig. 37. Schematic of Argon Loop System

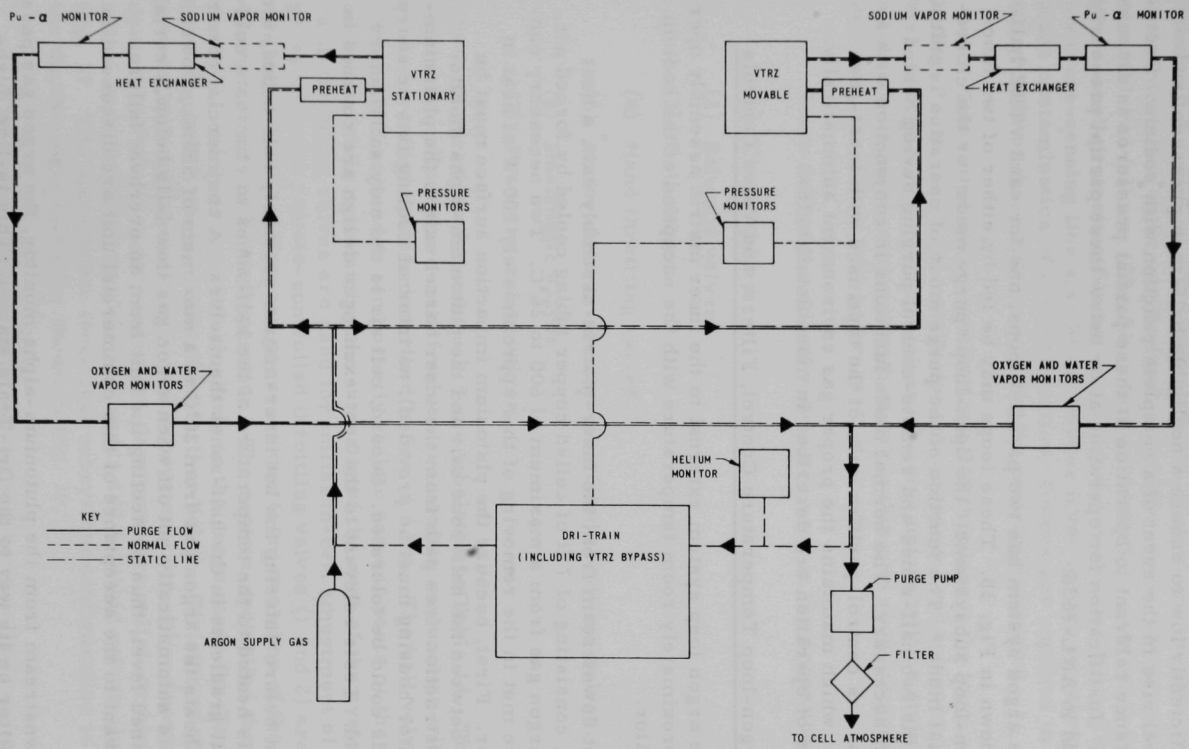

Fig. 38. "Purge" and "Normal" Mode Schematic of VTRZ Argon Loop System

The oxygen and water-vapor partial pressure in both half-zones will be kept sufficiently low to ensure a negligible half-zone pressure (and temperature) rise in the event of a complete reaction with sodium. Prototype experience relevant to operation at these partial pressures is discussed in Sec. 8.5. Justification for operating at or below these partial pressures can be found in ANL-7638.

The argon system has two parallel loops, one for each VTRZ half-zone, as shown in Fig. 38. These loops may be fed by either of two functional argon-loop subsystems: the open-loop "purge mode" or the closed-loop "normal mode." The function of the purge mode of operation is initial purging of the two half-zones and remote-control purging during heated operation if necessary. The normal mode functions in conjunction with a commercial gas control-purifier unit, of the type used with inert-gas gloveboxes, which maintains the proper gas environment automatically. Both modes of operation are described in more detail below.

4.5.5.2 Argon-loop Temperature Control, Filters, and Valve Controls

The argon loop system external to the inner matrix assembly operates at approximately room temperature with the exception of the sodium vapor monitor.

Just downstream from the inner-matrix-assembly exit, a heat exchanger, consisting of 7 ft of coiled copper tubing cooled by forced air, cools the argon gas from a maximum of 600 to 26°C. Two necessary constraints are met in the removing of this approximately 200 W of heat in this manner. First, because the plutonium impaction surface must be minimized between the half-zone exit and the plutonium-alpha monitor (i.e., an obstruction-free path from the inner barrel exit to the plutonium-alpha monitor housing must be provided), no internal cooling fins or sharp tubing bends could be tolerated. Second, cell air is the only satisfactory cooling fluid. Tests relevant to the heat-exchanger design are covered in Sec. 7.1.

Just before entering the hot inner-matrix-assembly half-zones, the argon gas is heated to the temperature of the half-zones to eliminate cold-gas thermal gradients in the half-zones themselves. A commercial electric air heater heats the argon gas from 20°C to a maximum of 550°C. Power to the heater is automatically cut off when argon gas flow falls below a certain predetermined level, thus protecting the unit from an overheat failure. Tests relevant to the acceptance of this commercial unit are discussed in Sec. 7.1.

Downstream from the plutonium-alpha monitor, the argon gas passes through a filter on its way to the Dri-Train station. This in-line, high-efficiency, small-volume filter unit is made by Mine Safety Appliance Company.

It uses a convoluted fiber glass filter paper, which filters out particles down to 0.3 μ with an efficiency of 99.9%. It protects the Dri-Train station instrumentation and controls from plutonium-alpha contamination in case of a fuel-rod failure. The filter is not intended for personnel protection. (Personnel-protection filters are discussed in Sec. 4.5.5.4.) The half-zone pressure-sensing line also has a similar filter in-line to prevent plutonium-alpha contamination of instrumentation. Unions are supplied in the pipes on either side of these filters to facilitate cartridge changing.

Other pipe unions will be installed throughout the loop, as indicated in Fig. 37, to facilitate installation, maintenance, and temporary disassembly. In high-temperature sections, the pipe unions will be stainless steel, ultrahigh-vacuum couplings with metal packing; in room-temperature sections, the unions will be brass, O-ring type.

Seven different kinds of valves are used in the argon loop system:

(1) Check valves.

(2) Solenoid valves.

(3) Ball valves.

(4) Hand throttling valves.

(5) Motor-driven, remote-controlled throttling valves.

(6) Pneumatic valves.

(7) Pressure-relief valves.

The configurations for valves 1-6 are tabulated in Table 14. The check, solenoid, and pressure-relief valves are used in conjunction with the high-pressure relief system described in Sec. 4.5.5.6. The ball valves are on-off type valves used to temporarily isolate various parts of the system for servicing while maintaining the integrity of the rest of the system. The hand-throttling valves are used for initial in-cell adjustment of flows and pressures; the remote-controlled throttling valves (1 and 2) are used for fine adjustments of flow and pressure due to mismatches of the half-zones during heatup and heated operation. The remote-controlled throttling valves (3 and 4) are used exclusively in the purge mode for flows and pressure regulation and are described further below. Division of the argon loop system into appropriate functional subsystems for either "normal mode" operation, "purge mode" operation, low-pressure relief, or high-pressure relief is accomplished by the pneumatic and solenoid valves shown in Fig. 37. The appropriate functional subsystem configuration is achieved by the digital-logic circuitry shown in Fig. 39.

Two high-pressure relief valves will be installed immediately downstream from the high-pressure regulator. The high-pressure relief valves

TABLE 14. Argon-loop-system Valve Configurations

(Does not include Dri-Train Unit valves)

Valve Type[a]	Valve No.[a]	Operation Mode: Purge	Normal	Low-pressure Relief	High-pressure Relief	Comments
Pneumatic	1	O	C	O	C	Normally C.
	2	C	C	O	C	Normally C.
	3	C	O	C	C	Normally O.
	4	C	O	C	C	Normally O.
	5	O	C	C	C	Normally C.
Solenoid	1	C	C	C	O	Normally O.
	2	C	C	C	O	Normally O.
Check	1	C	C	C	O	Cracks at <1 in. of water.
	2	C	C	C	O	Cracks at <1 in. of water.
	3	O	O	O	O	Safety feature of O_2 monitor.
	4	O	O	O	O	Safety feature of O_2 monitor.
Remote-control Throttling	1	T-B	T-B	U	U	Mechanical stops and/or limit switches prevent complete closing.
	2	T-B	T-B	U	U	
	3	T	NIU	NIU	NIU	Closed before purging starts.
	4	T	NIU	NIU	NIU	
Hand Throttling						Before switching from cell control to Control Room control, all these valves will be locked in position. Valve No. 7 will be initially throttled in order to generate enough pressure head to drive the loop.
Main Line	1	T-B initial / U-remote	U	U	U	
	2	T-B initial / U-remote	U	U	U	
	3	T-B initial / U-remote	U	U	U	
	4	T-B initial / U-remote	U	U	U	
Combustibles Monitoring	5	T-initial / U-remote	U	U	U	
VTRZ Bypass	7	T-initial / U-remote	U	U	U	

[a]Reference: Fig. 37.

Note: O = Open; B = Balancing; C = Closed; NIU = Not in use; T = Throttling; U = Unchanged. The ball valves will be locked open (with the exception of the regeneration-line ball valve, which will be locked closed). Hand-throttling valves 8, 9, 10, and 11 will be locked closed.

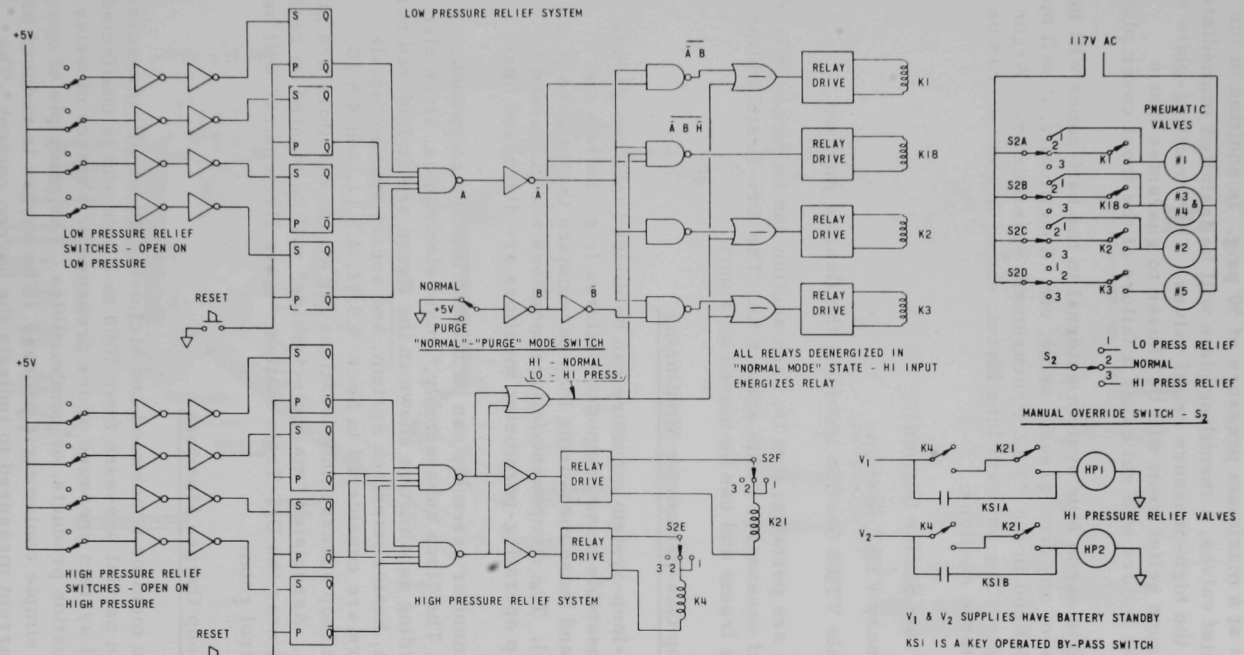

VALVE POSITION TABLE				
VALVE	LO P.	PURGE	NORMAL	HI P.
1 NC	O	O	C	C
2 NC	O	C	C	C
3 NO	C	C	O	C
4 NO	C	C	O	C
5 NC	C	O	C	C
HP1 NO	C	C	C	O
HP2 NO	C	C	C	O

Fig. 39. Pneumatic-valve Digital-logic Circuitry

will be set to open at a maximum pressure of 50 psig. In addition to the high-pressure relief valves, a throttling plate will be installed immediately downstream from the high-pressure relief valves. The throttling-plate size and the high-pressure relief limit will be chosen to guarantee that a pressure-regulator failure will not cause a failure of the front cover plate.

The complete argon loop system external to the half-zones will be leak-tight and free of any dirt, grease, oxide, etc. Specifically, it will meet the requirement defined in the VTRZ Procurement Specifications, Argon Loop System Section. The physical loop layout, shown in Fig. 40, can be broken down into three sections:

(1) Dri-Train Station Section.

(2) Stationary VTRZ Section.

(3) Movable VTRZ Section including the flexible junction.

All three sections are portable; that is, each section can be removed from the reactor cell, if necessary, within about 8 hr. The Dri-Train station will be on a single frame and can be moved as a unit.

4.5.5.3 Argon-loop Gas-parameter Monitoring

The argon-loop-system monitors can be divided into two groups: those measuring heatable-zone component failures (e.g., helium and plutonium-alpha) and those measuring loop parameters themselves (e.g., flow and pressure). The component-failure monitors are discussed in Sec. 4.5.9; the loop operating-parameter monitors are discussed here.

A typical monitor assembly can be divided into the components shown in Fig. 41. The "loop subassembly," main electronics, slave electronics, and recording capabilities shown in the figure are considered here. The alarm system, heater interlock system, and scram system for all applicable monitors are considered in Secs. 4.5.12, 4.5.11, and 4.5.10, respectively. The loop subassembly locations for all the monitors are given in Figs. 37 and 40. Associated "main electronics" will be located on racks in the reactor cell near the Dri-Train station; "slave electronics" will be located in the control room.

4.5.5.3.1 Argon-loop Oxygen Monitors

The oxygen monitor (Lockwood and McLorie, Model GP) measures equilibrium oxygen partial pressure from 1000 to 1 ppm and is unaffected by changes in total system pressure or the presence or absence of water vapor, CO_2, combustion products, or combustibles. The principle of operation is based on a simple coulometric process. The oxygen is reduced and the electrolysis current measured to indicate the oxygen content. The sample gas passes through a porous silver electrode immersed in a liquid electrolyte, and complete oxygen reduction occurs in the pores of the electrode.

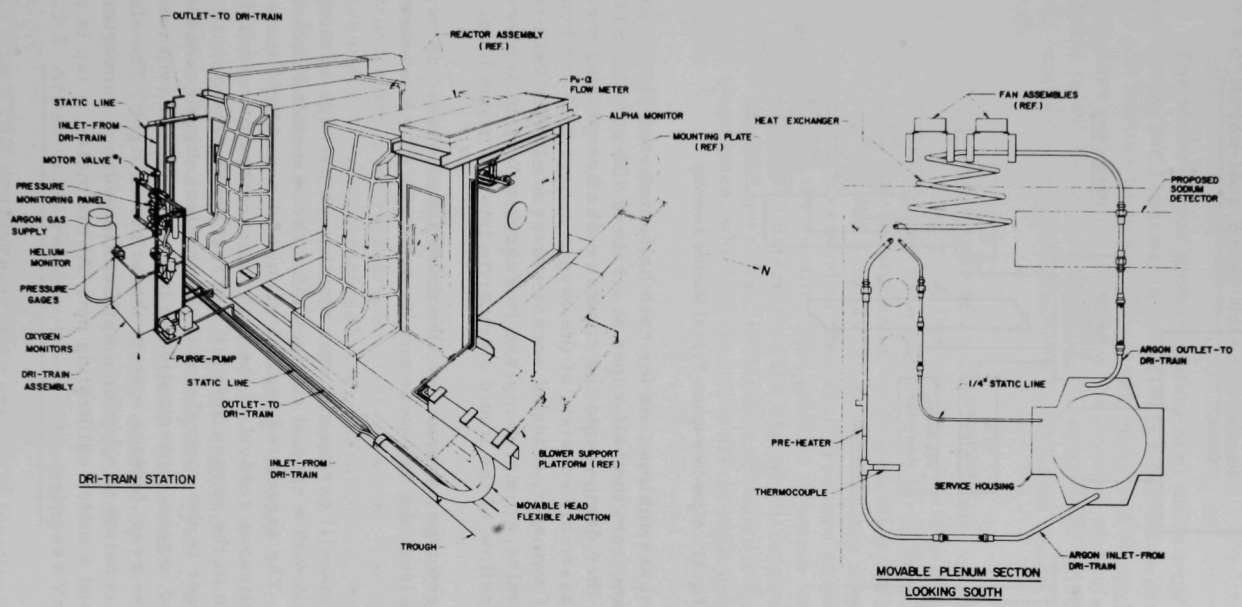

Fig. 40. Simplified Argon Loop System

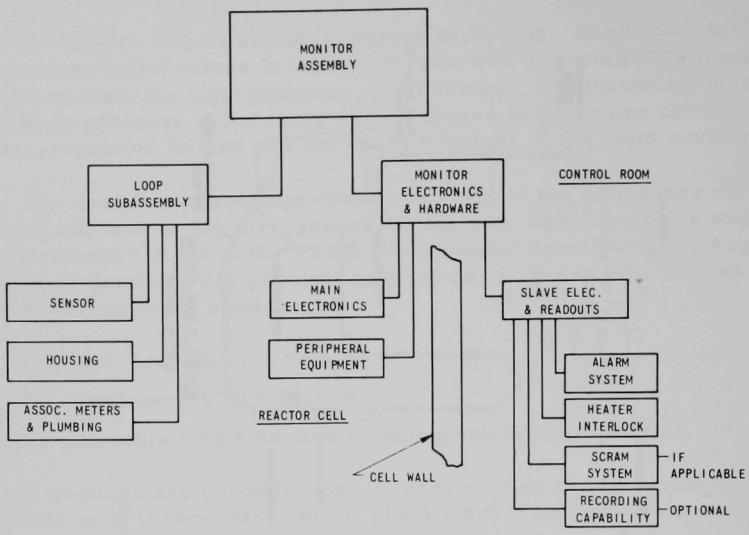

Fig. 41. Argon-loop-system Typical Monitor Assembly

Two loop subassemblies, one for each half-zone, sample the argon loop gas downstream from the half-zones at a rate of 100 cc/min (STP). The sample gas is then dumped into the reactor cell after passing through a filter. Each subassembly consists of the oxygen sensor cell and housing, a glass-tube-type flowmeter, external access valves for meter calibration, a flow-adjustment valve, a meter pump, and two check valves in series to protect against backflow of the liquid electrolyte into the argon loop.

Based on prototype experiments, the delay time between an oxygen injection upstream from the half-zone and its detection 45 ft downstream is 1 min.

The main (in-cell) oxygen-monitor electronics package is simply the commercial unit with a special connector for the associated control-room electronics. The associated control-room unit consists of the slave meter giving a continuous readout of the oxygen concentration and lights indicating power on to the oxygen monitor, correct range on the main electronics, ac power to the control-room electronics, oxygen concentration in alarm range, and oxygen concentration in heater-interlock trip condition. All these lights have reset buttons, except the ac power light. The slave-meter electronics consists of a buffer amplifier (impedance converter), a 0-100-μA meter, and a meter calibrating pot. At the meter, a tap is provided for a 0-10-mV recorder.

4.5.5.3.2 Argon-loop Water-vapor Monitors

The water-vapor monitor (aluminum oxide hygrometer, Model 1000, Panametrics, Inc.) measures water-vapor partial pressure from 20,000 ppmv (parts per million by volume) to 0.002 ppmv and is unaffected by ambient temperature and pressure changes, flow rates, materials of construction (external to the sensor), and piping configuration. Also, the sensor is completely unaffected by the presence of petroleum gases, hydrogen, and carbon dioxide.

The sensor consists of an aluminum strip, which is anodized to provide a porous oxide layer. A thin coating of gold is evaporated over this structure. The aluminum base and the gold layer form the two electrodes of what is essentially an aluminum oxide capacitor. Water vapor is rapidly transported through the gold layer and equilibrates on the pore walls in a manner functionally related to the vapor pressure of water in the atmosphere surrounding the sensor. The number of water molecules adsorbed on the oxide structure determines the electrical conductivity of the pore wall. Each value of pore-wall resistance provides a distinct value of electrical impedance, which in turn is a direct measure of the water-vapor pressure.

Two loop subassemblies, one for each half-zone, sense the main-line gas downstream from the half-zones. Each subassembly consists of a water-vapor sensor and its "tee-coupling" housing.

As with the oxygen monitor, mentioned earlier, the delay time between an air leak entering the loop and the detection of water vapor is about 1 min.

The main (in-cell) water-vapor-monitor electronics package is the commercial unit with a special connector for the associated control-room electronics and a shorted-probe selector switch. The latter alteration of the commercial unit guarantees meter operation with the single probe no matter what the switch position. The associated control-room unit consists of the slave meter giving a continuous readout of the water-vapor concentration and lights indicating correct range on main electronics, ac power to control-room electronics, water-vapor concentration in alarm range, and water-vapor concentration in heater-interlock trip condition. All these lights have reset buttons, except the ac power light. The slave-meter electronics consists of a buffer amplifier (impedance converter with gain of 10), a 0-100-μA meter, and a meter-calibrating potentiometer. At the meter, a tap is provided for a 0-10-mV recorder.

4.5.5.3.3 Argon-loop Pressure-sensing Monitors

The VTRZ pressure-sensing system is identical for both half-zones. Each pressure-sensing monitor assembly is located at the Dri-Train station

and consists of a pressure-sensing line which is run to a tap at the rear of the half-zone, a pressure transducer (potentiometer-type, infinite-resolution pressure transducer, Model 6000, CIC, Inc.), five differential-pressure switches, and a differential-pressure gauge (Magnehelic, Model 2320, Dwyer Mfg. Co., Inc.). The transducer provides continuous argon-pressure readout in the control room and provides a site for various abnormal-condition set points. These abnormal-pressure set points, together with the five differential-pressure switch set points, signal trips for the reactor-scram system, heater-interlock system, and alarm system (discussed in Secs. 4.5.10, 4.5.11, and 4.5.12, respectively) and for the high- and low-pressure relief systems. The control-room pressure readout meters are part of the pressure-control-unit front panel discussed below. The electronics circuitry for this meter consists of a buffer amplifier (impedance converter), a trim pot, and a 0-100-μA meter. During leak checking of the argon loop, initial purging, and normal operation startup, the in-cell differential-pressure gauge provides readout for the half-zone pressures.

All diaphragms in the pressure-sensing system are isolated from atmosphere by a throttling plate so that in the case of a diaphragm rupture any pressure drop to atmosphere occurs across the throttling plate and not in the pressure-sensing area. Tests have shown that throttling plates with five 13-mil holes can prevent significant pressure drops in the pressure-sensing area without slowing the response of the pressure switches to anticipated pressure changes.

4.5.5.3.4 Argon-loop Flow Monitors

There are eight flow monitors in the argon loop system: two monitors, 0-380 cc/min for the oxygen monitor assemblies; two monitors, 0-1.7 cfm for the plutonium-alpha monitor assemblies; two monitors, 0-1.7 cfm for half-zone flow monitoring; one monitor, 0-47 cfm for VTRZ bypass flow monitoring; and one monitor, 0-2 cfh for the combustibles monitor assembly. Control-room monitoring of flows is accomplished via the reactor-cell closed-circuit T.V. system. In addition, the half-zone flow meters have circuits that sense flow drops of 75 and 25% of the normal 1 cfm. These two conditions are read out in the control room as part of the alarm and heater-interlock systems.

4.5.5.3.5 Argon-loop Combustibles Monitor

The combustibles monitor is a Thermox Probe sensitive to both oxygen and combustibles. The principle of operation is that oxygen, charged as negative ions, can migrate through a specially defected ceramic-oxide solid electrolyte in response to a gradient in oxygen partial pressure. When conductive electrodes are located on opposite sides of this solid electrolyte and connected through an external circuit, a difference in oxygen partial

pressure in the two sides produces an emf. To facilitate oxygen migration, the electrochemical cell is heated to 758°C at which temperature combustibles quickly combine with any oxygen present and reduce the apparent oxygen concentration. With low levels of oxygen concentration characteristic of the inert gas within the VTRZ, the emf generated in the electrochemical cell becomes quite sensitive to ppm levels of combustibles. With the known oxygen level as determined by the Lockwood and McLorie oxygen monitors, which are not affected by combustibles, the combustibles level for low levels of combustibles can be determined quantitatively.

A single combustible subassembly samples the argon gas downstream from the half zones at 1 cfh (STP). The subassembly consists of the electrochemical cell and housing, a glass-tube-type flowmeter, external access valves for meter calibration, a flow-adjustment valve, and two tube unions for maintenance accessibility.

The main (in-cell) combustibles-monitor electronics package is the commercial unit with a special connector for the associated control-room electronics. The associated control-room unit consists of the slave meter giving a continuous readout of the emf in the electrochemical cell and lights indicating power on to the electrochemical cell, correct range on the main electronics, ac power to the control-room electronics, and combustibles concentration in alarm range. All these lights have reset buttons, except the ac power light. The slave-meter electronics consists of a buffer amplifier (impedance converter), a 0-100-μA meter, and a meter-calibrating potentiometer. At the meter, a tape is provided for a 0-10-mV recorder.

4.5.5.3.6 Argon-gas Temperature Monitors

The argon-loop-system thermocouples monitor argon-gas temperatures at the following locations:

(1) Preheater exit--both half-zones.

(2) VTRZ heat-exchanger exit for both half-zones.

(3) Dri-Train entrance.

(4) Dri-Train heat-exchanger No. 1 exit.

(5) Dri-Train heat-exchanger No. 2 exit.

Thermocouples at locations 2, 4, and 5 check for heat-exchanger effectiveness and possible cooling-air-fan failure; the thermocouple at location 1 checks operation of the preheaters. The remaining thermocouple checks that the Dri-Train entrance temperature conforms to the Dri-Train operation specifications. A representative temperature sensor (Thermocouple Products Co., Inc.) and housing are shown in Fig. 42. In the control room, panels containing six meters continuously display the heat-exchanger

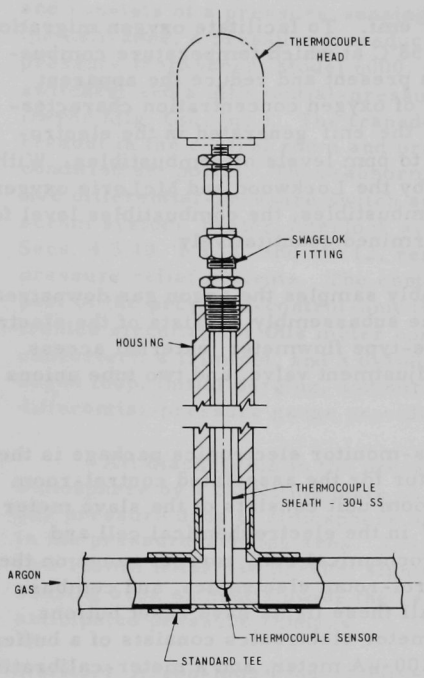

Fig. 42. Typical Thermocouple Sensor and Housing

and preheater temperatures. The Dri-Train entrance temperature is not monitored in the control room. A thermocouple bridge is used for in-cell temperature checks.

Analyses and tests relevant to the selection of the various monitors and to the design of the monitor assemblies are covered in Secs. 7.1 and 8.5. Detailed assembly specifications can be found in the VTRZ Procurement Specification, Inert Gas Loop Section (ANL Specification No. ANL-IGL-RP).

4.5.5.4 Argon-loop Purge-mode Operation

The purge mode of the argon-loop operation has the function of flushing relatively large quantities of an unwanted gas from the heatable half-zones in a short period of time and replacing them with a high-purity argon-gas blanket. In the purge mode, the argon loop is open, taking argon gas from a supply tank and dumping the mixture of argon gas and unwanted gas into the reactor cell. The chief purpose is to purge air out of both heatable half-zones before heatup until a level of purity is reached where the normal mode of argon-loop operation can take over without excessively loading the purifiers. However, the purge mode can be used at any time during operation, if it is felt to be necessary, since it is designed to be operated from the control room as well as from the reactor cell. Examples of situations other than startup warranting purge-mode operation are:

(1) A failure in the normal mode, e.g., pump failure, rendering the loop monitors useless and terminating half-zone purification.

(2) Outgassing of large amounts of oxygen or other contaminants from the matrix tubes, calandria cans, wiring, etc. Rather than loading down the normal-mode purification system, these contaminants could be flushed out by purging.

To maintain a purge flow between 1 and 2 cfm per half-zone and, at the same time, maintain half-zonestatic pressures of 0.0 ± 1.0 in. of water, the system must be arranged to have both a positive pressure upstream

from the half-zones and a negative pressure (relative to reactor-cell pressure) downstream from the half-zones. The positive pressure is supplied by the argon-gas supply cylinder; the negative pressure is supplied by the purge pump. The flow and VTRZ pressure are adjusted using two throttling valves (motor-driven valves Nos. 3 and 4 of Fig. 37); one on either side of the half-zones. If a mismatch in pressure occurs between the movable and stationary half-zones, two balancing valves (motor-driven valves Nos. 1 and 2 of Fig. 37) can be used to rebalance the pressures. Ordinarily, the purge is started by switching to "purge mode" on the control-room argon-flow-system front panel. This automatically sets the correct pneumatic valve configuration for the purge mode (given in Table 14), turns on the purge pump, and turns off the automatic control function on the Dri-Train unit. Next, the two purge-throttling valves are cracked open, allowing argon gas to flow from the gas cylinder, through both half-zones, and to the purge pump and filter. The flow is brought up to ~1.5 cfm while maintaining half-zone pressures in the range of 0.0 ± 1.0 in. of water. A typical startup purge, based on prototype experience, lasts about 45 min before the oxygen and water vapor level is such that the Dri-Train purifier can efficiently take over. Further purging experience is detailed in Secs. 7.1 and 8.5.

The monitoring and pressure-relief functions associated with the argon loop system are operational in the purge mode, except the helium monitor and its associated alarm and heater interlock trips.

All purged gases are filtered before being dumped into the cell. The filter is a high-efficiency AEC-type filter with inorganic media, asbestos separators, and fire-retardant plywood frame. The 8 x 8 x $3\frac{1}{6}$-in. filter is inserted in a special housing as shown in Fig. 43.

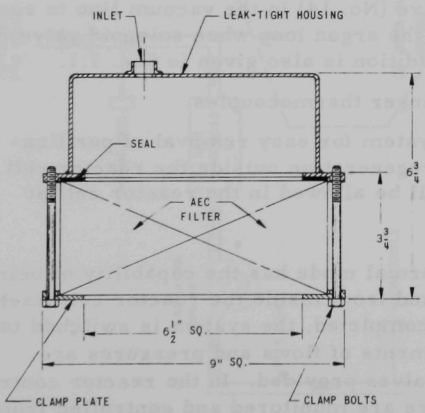

Fig. 43. AEC Filter and Housing. ANL Neg. No. 116-2601.

4.5.5.5 Argon-loop Normal-mode Operation

The normal mode of the argon-loop operation automatically maintains the proper gas environment in the inner matrix assemblies. Specifically, this closed-loop mode maintains prescribed argon-gas purity, half-zone pressures, and half-zone flow rates during all VTRZ experiments. The unit that performs the above three functions is called the "Dri-Train" (a somewhat modified version of Vacuum/Atmosphere's Model He-193-2). Two sealed rotron pumps generate the necessary pressure head for loop flow; two purifiers (used one at a time or together in parallel)

continually remove oxygen and water vapor from the loop gas. A "Photohelic" pressure gauge, connected to the VTRZ movable half-zone, controls the pressure in that half-zone by adding argon gas when the pressure drops and removing gas, through a vacuum pump, when the pressure rises. The stationary half-zone pressure is controlled indirectly by the same system. Any pressure mismatch between the two halves can be corrected either manually or automatically by throttling either or both of the two motor-driven balancing valves in the stationary half-loop. Details of the pressure-control system are given below. Since the Dri-Train unit operates most effectively with a gas flow of ~30 cfm, a "VTRZ Bypass" system removes most of the flow at the Dri-Train exit and returns it directly to the main loop at the Dri-Train entrance. All the Dri-Train flow passes through this bypass during the purge mode, high-pressure relief, and low-pressure relief.

The modified Dri-Train flow schematic is shown in Figs. 44 and 45. The modifications to the commercial VAC-He-193-2 unit are as follows:

(1) Addition of another rotron pump in series with the original in order to develop the necessary pressure head.

(2) Substitution of an air-cooled pump heat exchanger for the original water-cooled pump heat exchanger.

(3) Addition of a second air-cooled pump heat exchanger.

(4) Addition of a throttling valve (No. 13) in the argon supply line to reduce the amount of gas added to the argon loop when solenoid valve J is open. Justification for this valve addition is given in Sec. 7.1.3.

(5) Addition of a throttling valve (No. 14) in the vacuum line to reduce the amount of gas removed from the argon loop when solenoid valve K is open. Justification for this valve addition is also given in Sec. 7.1.

(6) Addition of two heat-exchanger thermocouples.

(7) Redesign of purification system for easy removal of purification system from Dri-Train to allow regeneration outside the reactor cell. No hydrogen-containing gas bottles will be allowed in the reactor cell at any time.

As with the purge mode, the normal mode has the capability of being operated both from the control room and from inside the reactor cell itself. After initial in-cell purging has been completed, the system is switched to the normal mode and balancing adjustments of flows and pressures are made if necessary by using the hand valves provided. In the reactor control room, the argon-loop flow and pressure are monitored and controlled from the Argon Flow System front panel shown in Fig. 46. In addition to displaying the high-pressure relief, low-pressure relief, scram, heater-interlock, and alarm lights indicating flow and/or pressure abnormalities, the top panel shows the configuration of all the pneumatic, solenoid, and motor-driven

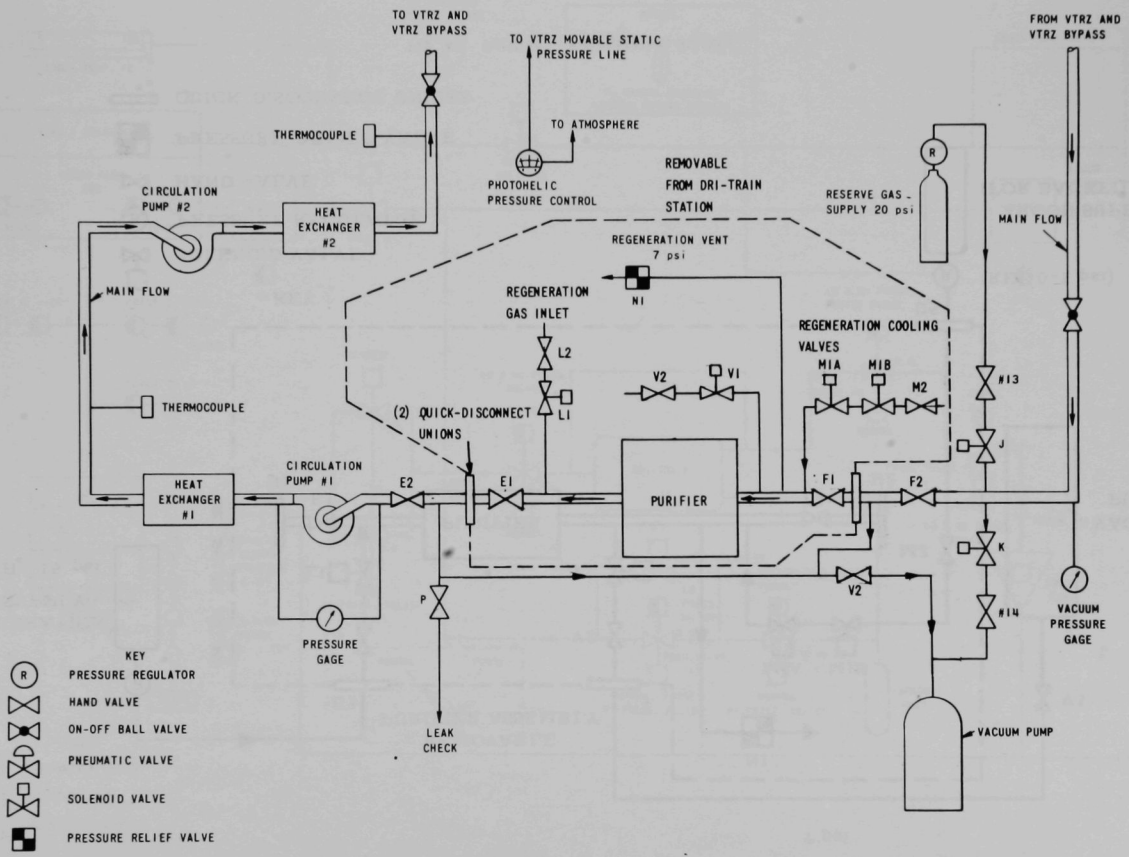

Fig. 44. VAC Dri-Train with VTRZ Modifications

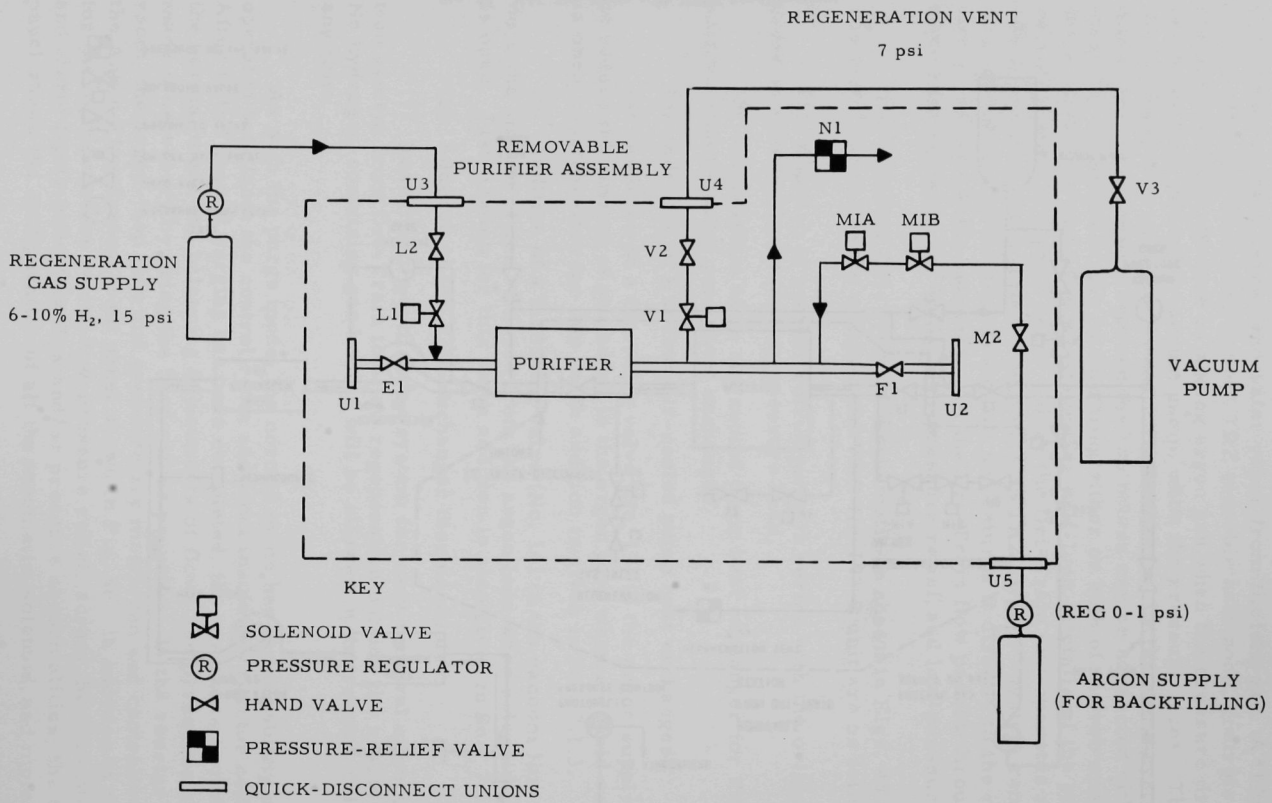

Fig. 45. Purifier in Regeneration Station

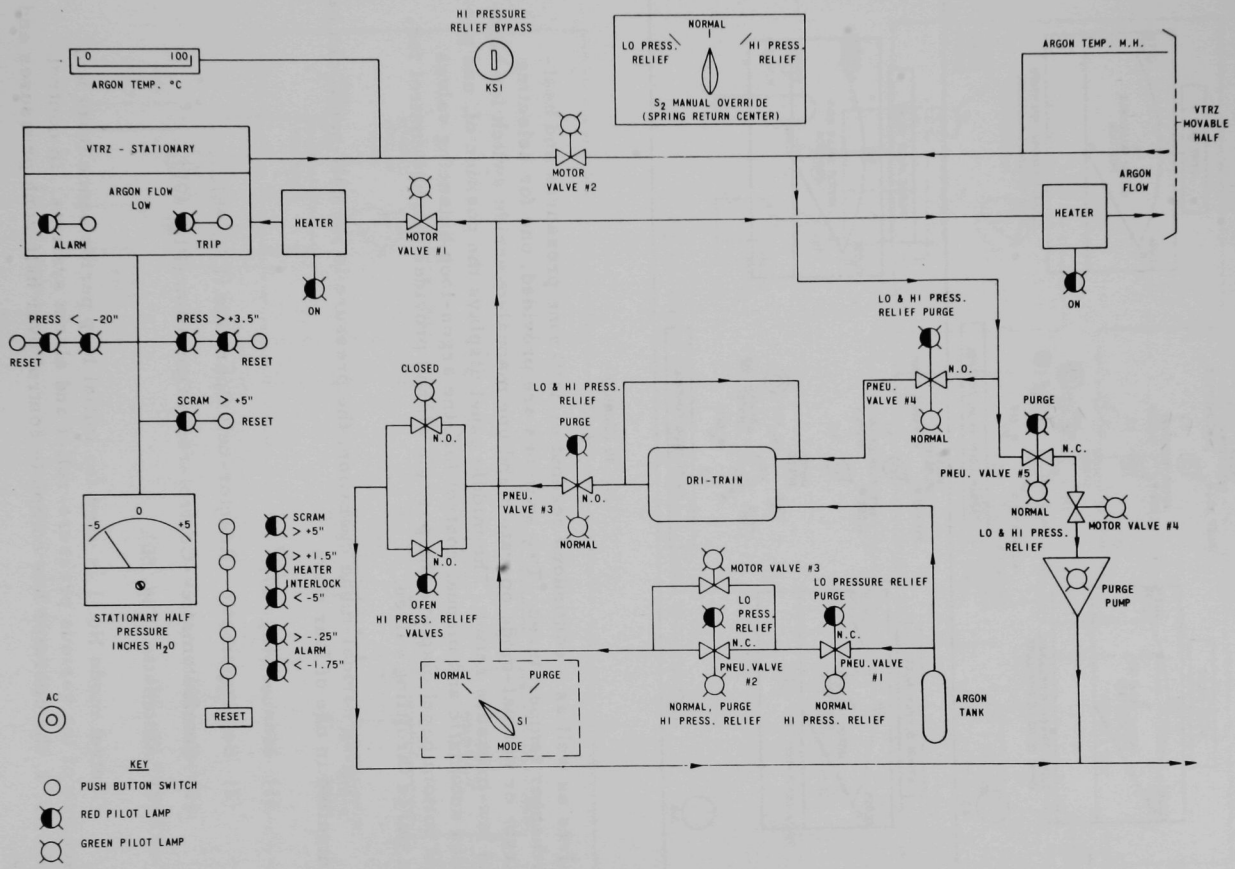

Fig. 46. Front Panels--Flow and Pressure Control

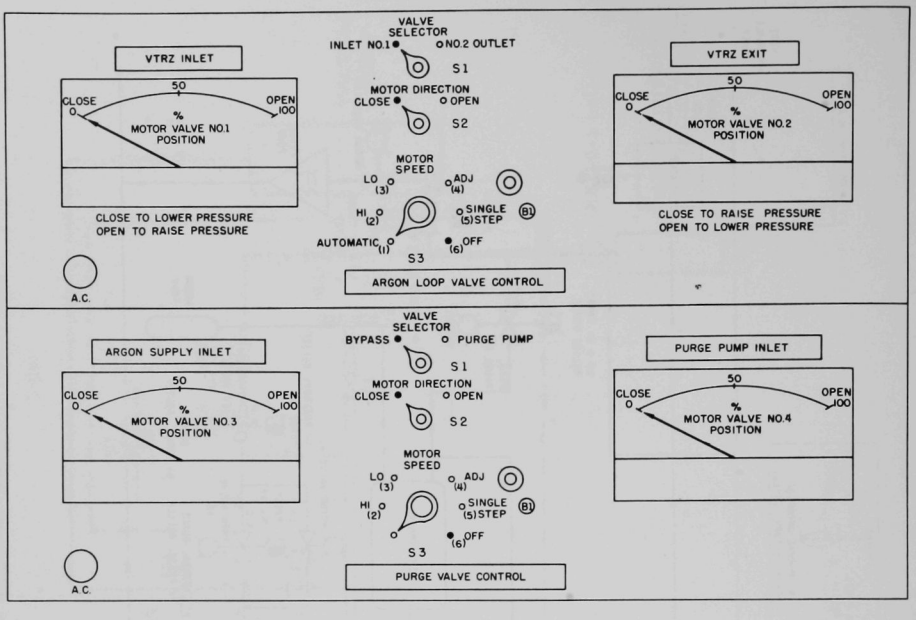

Fig. 46 (Contd.)

valves as well as a continuous readout of half-zone pressures and heat-exchanger temperatures. Two switches are provided, one for selecting purge- or normal-mode operation and one manual-override switch for high- and low-pressure relief. The middle panel displays the position of, and provides automatic and manual control for, the argon-loop balancing valves. The bottom panel displays the position of, and provides manual control for, the purge throttling valves.

During normal-mode operation, the pressure in the half-zones can be controlled in one of four ways:

(1) Manual (Fig. 47).

(2) Semiautomatic--Reactor-cell Operation (Fig. 48).

(3) Semiautomatic--Control-room Operation (Fig. 49).

(4) Automatic (Fig. 50).

Control mode No. 1 is used for initial loop performance tests and checkouts of the various pressure-relief and alarm systems. In control mode No. 1, the operator has complete control over half-zone pressures and flow.

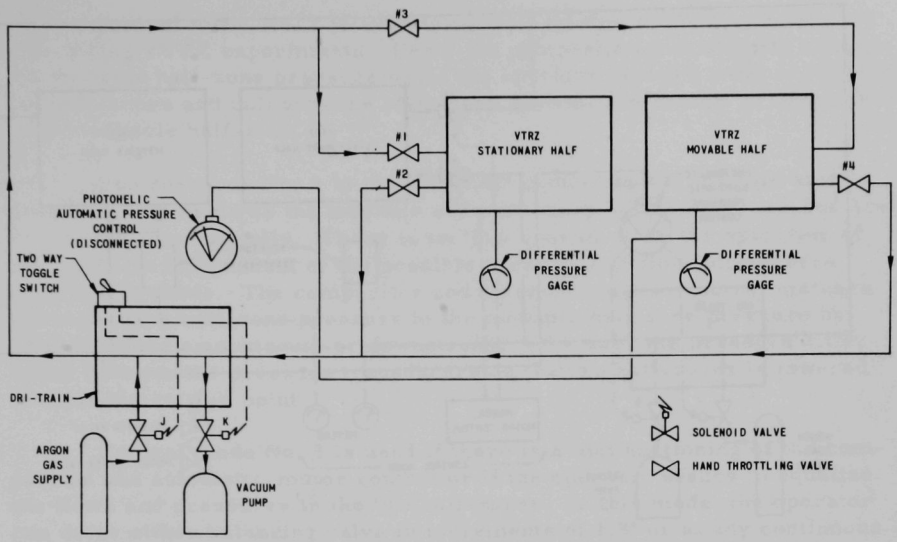

Fig. 47. Manual Normal-mode Pressure Control in Reactor Cell

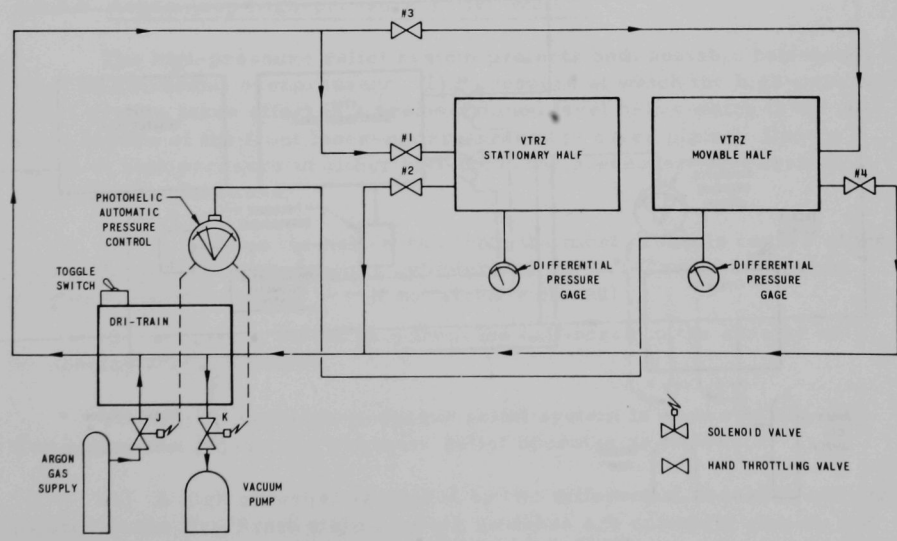

Fig. 48. Semiautomatic Normal-mode Pressure Control in Reactor Cell

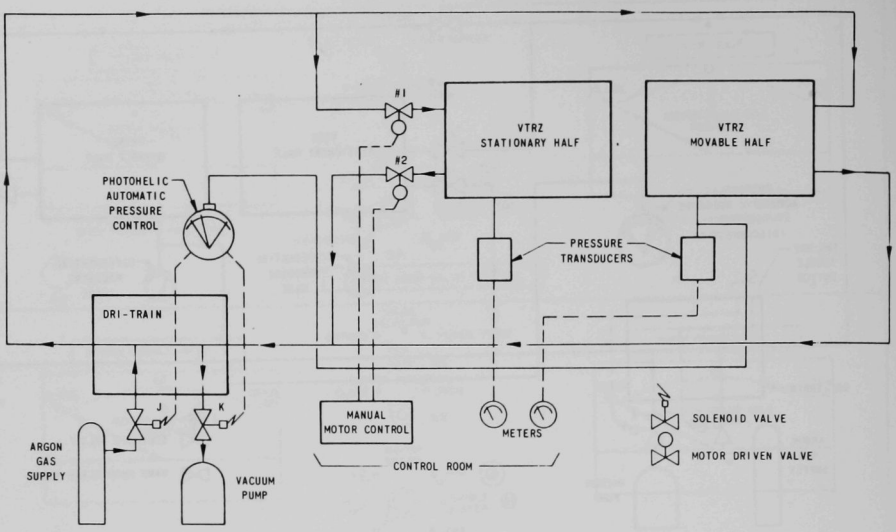

Fig. 49. Semiautomatic Normal-mode Pressure Control in Control Room

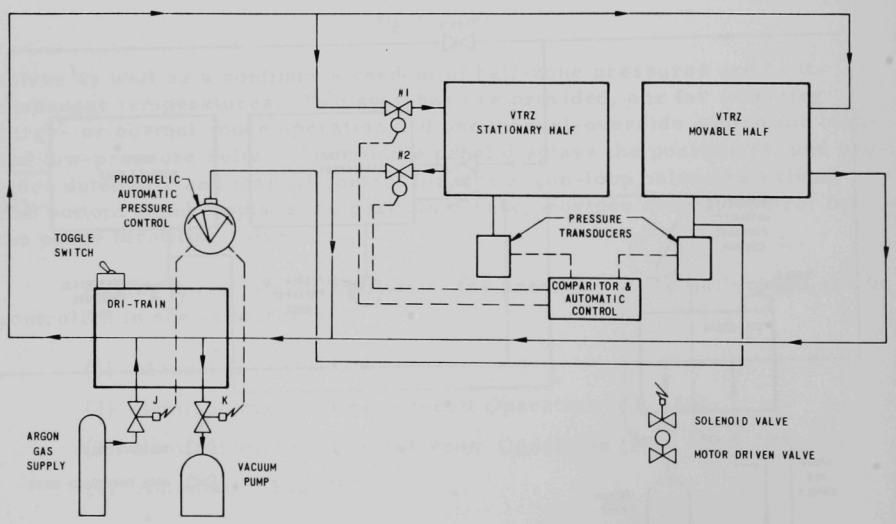

Fig. 50. Automatic Normal-mode Pressure Control

Control mode No. 2 is used for initial startup of the argon loop system during VTRZ experiments. Here, the photohelic automatically controls the movable half-zone pressure while the operator sets the level of flows in the half-zones and balances the stationary half-zone pressure to match that of the movable half-zone.

Control mode No. 4 is the "normal" control mode. No operator is needed in this mode as the movable and stationary half-zone pressures are controlled automatically. There is no flow control since the operation of the VTRZ is independent of the possible variations in flow encountered once in this mode. The comparitor and automatic-motor control matches the stationary half-zone pressure to the movable half-zone pressure by driving either an upstream or downstream valve until the pressure differential between the pressure transducers on the two half-zones is lowered to a predetermined point.

Control mode No. 3 is used if there is a malfunctioning of the comparitor and automatic-motor control or if the operator wishes to equalize the flows and pressures in the two half-zones. In this mode, the operator can drive either balancing valve in increments of 1.8° or at any continuous speed up to 100 rpm. The pressure-balancing controls are shown in Fig. 46.

4.5.5.6 Argon-loop High-pressure Relief System

The high-pressure relief system protects both heatable half-zones from an accidental overpressure. The pressure at which the high-pressure relief system takes effect is a predetermined level below which there will be no failure of the front inner-matrix-assembly cover plates. Upon a signal of high pressure in either half-zone, the pressure relief system performs two functions:

(1) It isolates the half-zones from the most probable causes of the high pressure (the argon supply cylinder and the Dri-Train blowers) by closing pneumatic valves 1-4 (if not already closed).

(2) It opens a direct path from the half-zones to the reactor cell by opening solenoid valves.

The argon-loop high-pressure relief system is shown in Fig. 51. For a given half-zone, the pressure relief operates as follows:

(1) A high pressure is sensed by two differential pressure switches located at the Dri-Train station. Both switches are normally closed, and the opening of either switch deenergizes both normally open solenoid valves.

(2) The half-zone high pressure is relieved by opening the loop at point A to reactor cell pressure. Gas flows from the half-zone, through the

piping and valves shown, into an AEC-type high-efficiency filter. Check valves prohibit back flow of air into the loop. The argon loop remains in the high-pressure relief condition until reset manually.

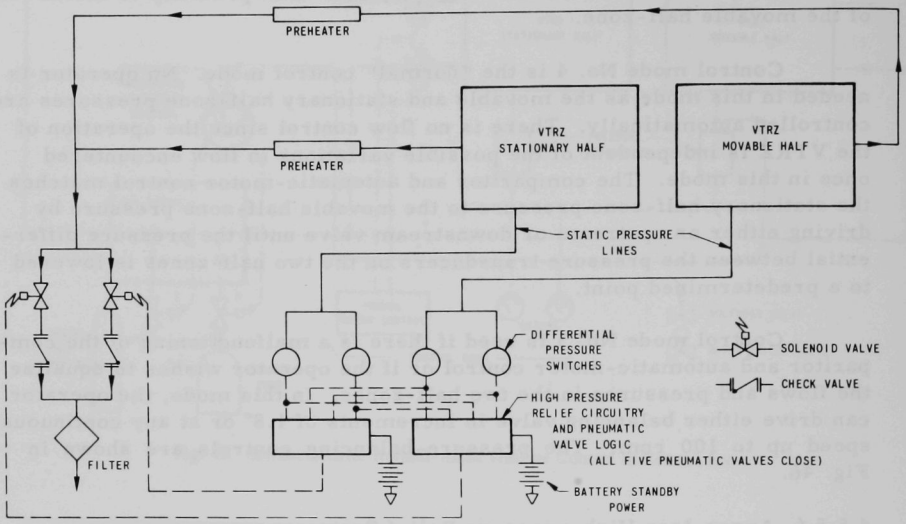

Fig. 51. High-pressure Relief System

The relief system is completely redundant, except for common piping. In the event of a power failure, batteries supply the system power until normal power has been restored or the reactor emergency power system takes effect.

This system is monitored on the VTRZ Argon Flow System front panel shown in Fig. 46. There are separate lights for each pressure switch and a complete layout of valve configurations. A manual override switch is provided for use at the discretion of the operator.

The circuitry logic has been designed so that high-pressure relief overrides all other systems. For example, if one half-zone had a pressure low enough to signal for low-pressure relief while the other half-zone had a pressure high enough to signal for high-pressure relief, the high-pressure relief would override.

There are several reasons why the high-pressure relief piping is tapped off of point A at the Dri-Train station (see Fig. 51) rather than directly off the rear of the half-zones. First, space in the shroud area behind the zones is at a premium, but it is readily available at the Dri-Train station. Second, the design would have to incorporate two more solenoid valves,

two more check valves, and two more filter housings, all adding loop costs. Third, during normal operation, point A is at a higher pressure (about 20 in. of water), than the half-zone. About +3.5 in. of water will trigger high-pressure relief at the half-zone. Therefore, the initial pressure drop upon activating high-pressure relief is greater if the pressure relief is tapped at point A rather than at the half-zones. Fourth, the check valves have a cracking pressure of +1 in. of water and therefore need the additional pressure head provided at point A. Fifth, since all valves between the half-zones and point A have mechanical limit points so they cannot close, the line from point A to either half-zone cannot be closed.

As a backup to the above-mentioned high-pressure relief system, each half-zone contains a mechanical high-pressure relief valve, with a cracking pressure of approximately 42 in. of water (1.5 psig). As shown in Fig. 37, the relief valve for each half-zone is located in the argon-loop piping between the service housing and the preheater. In the extremely unlikely event of a high-pressure relief-system failure, these relief valves protect the VTRZ assemblies from serious overpressure damage and associated hazards by relieving the pressures and dumping the overpressure gas into the reactor plenum areas. Gases entering the plenum areas are filtered by the reactor cooling system before recombining with the reactor-cell atmosphere.

4.5.5.7 Argon-loop Low-pressure Relief System

The low-pressure relief system protects both heatable half-zones from an underpressure. The pressure at which the low-pressure relief system takes effect is a predetermined level above which there is no yielding of the front cover plates. The difference between the low-pressure relief pressure and operating pressure is considerably larger than for the high-pressure relief because of the support given to the front cover by the inner-barrel matrix. Upon a signal of low pressure in either half-zone, the low-pressure relief system performs two functions:

(1) It isolates the half-zones from the only two possible causes of low pressure (the Dri-Train vacuum pump and the purge pump) by closing pneumatic valves 3-5 (if not already closed).

(2) It opens pneumatic valves 1 and 2 to allow the argon supply gas to backfill the zone(s) at low pressure.

The argon-loop low-pressure relief system is shown in Fig. 52. For a given half-zone, the pressure relief operates in the following manner:

(1) A low pressure is sensed by two differential switches located at the Dri-Train station. Both switches are normally closed, and the opening of either switch actuates pneumatic valve logic, which in turn opens valves 1 and 2 while closing the pneumatic isolation valves.

(2) The half-zone low pressure is relieved by backfilling from the argon supply cylinder. A low-pressure regulator drops the supply-line pressure from 20 psi to about 3 in. of water. This 3-in. (relative to cell pressure) pressure head allows a gradual backfill and a final system pressure that is less than that which would actuate the high-pressure relief. The argon loop remains in the low-pressure relief condition until reset manually.

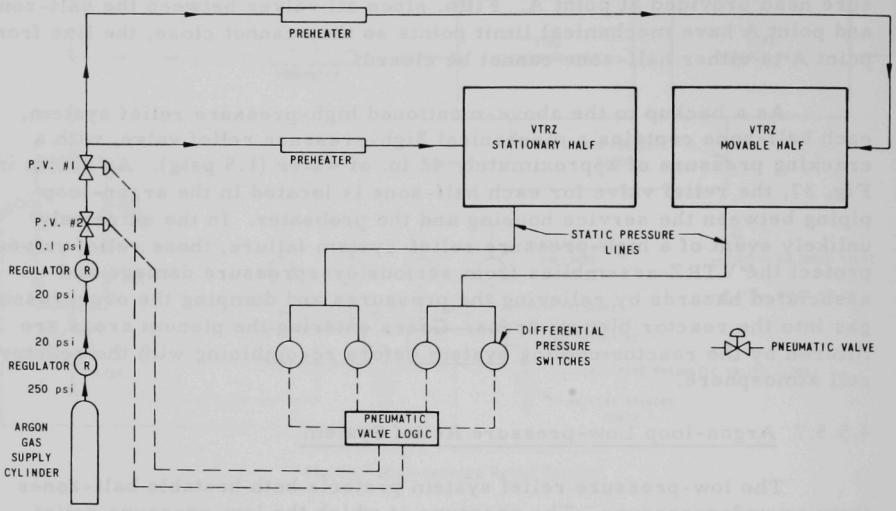

Fig. 52. Low-pressure Relief System

As with the high-pressure relief, the low-pressure relief system is monitored on the VTRZ Argon Flow System front panel shown in Fig. 46. There are separate lights for each pressure switch and the complete layout of valve configurations. A manual override switch is provided for use at the discretion of the operator.

4.5.6 Air-cooling Systems

Five completely independent air-cooling systems are associated with the VTRZ: a cooling guard-ring (CGR) for each half-zone, an inner-matrix cooldown (IMCD) for each half-zone, and the existing ZPR-6 reactor-matrix cooling system. Each air system includes a blower, flow controls, flow monitors, and a ducting system. These air systems are shown schematically in Figs. 53-55.

A pair of blowers that supply cooling air for the CGR and IMCD systems for each VTRZ half-zone are located on a small shelf at the rear edge

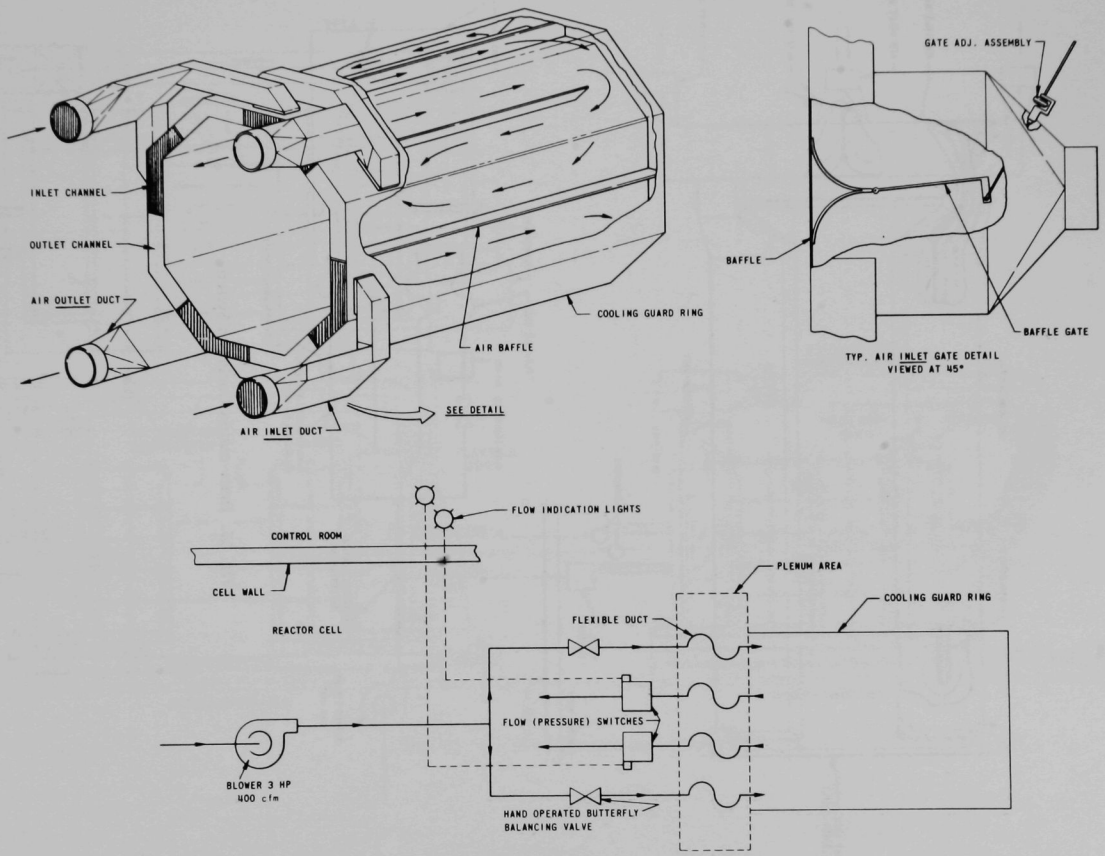

Fig. 53. Cooling Guard-ring (CGR) System. ANL Neg. No. 116-421.

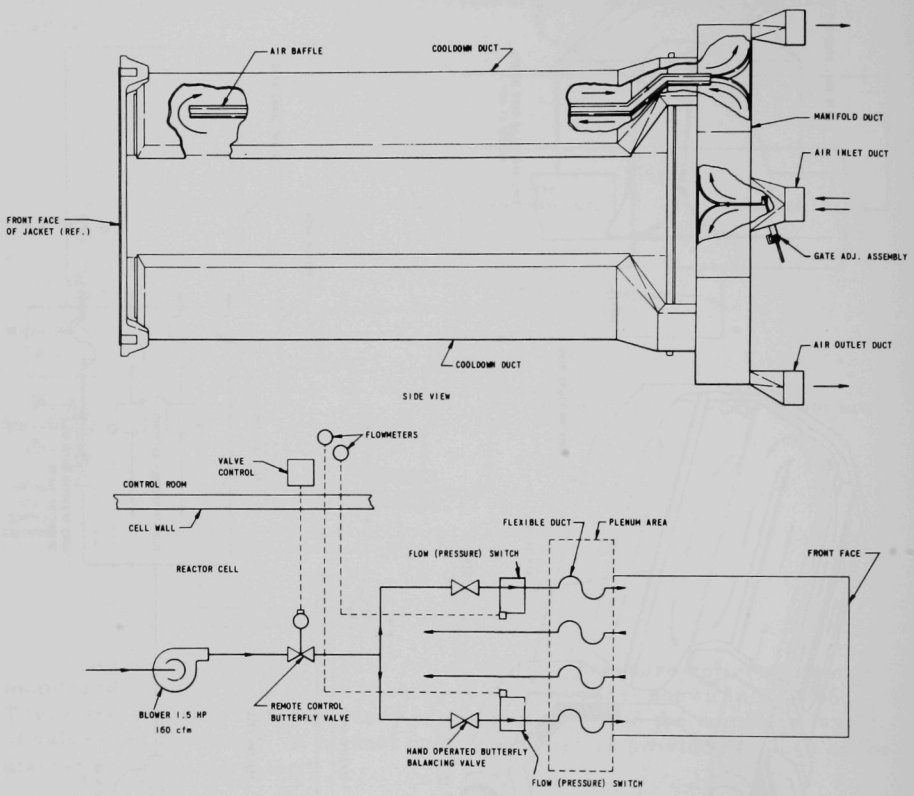

Fig. 54. Inner-matrix Cooldown System

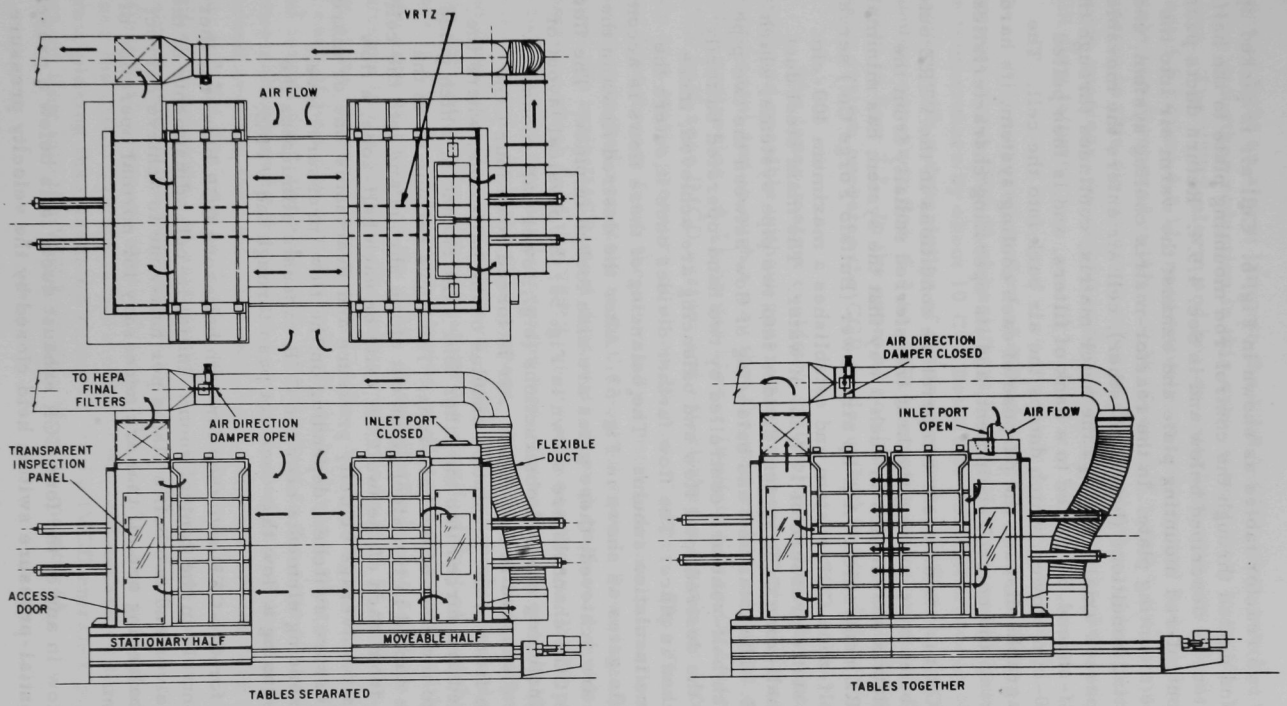

Fig. 55. Outer-matrix Cooling System

of each of the two reactor tables as shown in Fig. 6. Cell air is picked up at this point and ducted through the control-rod mounting plate to the half-zone duct system as described below and in Sec. 4.5.4. Return ducts pass through the control-rod mounting plate and exhaust the warm air into the cell behind the mounting plate. In the reactor-matrix cooling system, under normal operating conditions (halves together), cell air enters the movable half-shroud, passes axially through the outer matrix, continues through the stationary half-shroud, is ducted to a bank of filters, and is then pulled through a 5000-cfm blower, which dumps the air back into the cell. The following paragraphs discuss the purpose of each cooling system, its hardware, monitoring and control equipment, and its operating characteristics.

The CGR maintains room-temperature conditions in the VTRZ outer matrix assemblies by removing the heat transferred radially from the VTRZ inner matrix assemblies in such a way that the system has minimal effects on VTRZ neutronics. A 3-hp air blower (Buffalo Forge Co.) serves each VTRZ half-zone CGR system and establishes a maximum 400-cfm flow rate at a static pressure of 17.6 in. of water. The main steel duct work of each half-zone CGR system divides into two pipe systems, which feed the VTRZ. The total flow and balancing of flow between the two pipe systems of each half-zone are controlled by two hand-operated butterfly valves. After the desired total flow and balancing are achieved, these valves are locked in place. The flow further divides once it enters the VTRZ half-zone insulation annulus. The balancing of these flows is accomplished by baffle gates as shown in Fig. 53. After the desired flows in the CGR channels are achieved, these gates are also locked in place. The flow patterns in the CGR channels are shown in Fig. 53; the physical layout of the channels, including channel obstructions (e.g., lower ball-mount brackets), are discussed in Sec. 4.5.4. Air is forced down four CGR channels to the front of the insulation annulus of the half-zone, where the flow is reversed and forced into the other four CGR channels, which guide the flow back to the rear of the half-zone. The flows recombine in the shroud and are ducted in two steel pipes out of the shroud and into the cell. Just upstream from each of the two CGR exits on each half-zone, a flow element senses the average velocity pressure and deactuates one or more differential-pressure switches, depending on the flow (pressure) level. Placing these sensing elements near the CGR exhausts eliminates the possibility of sensing a flow that does not pass through the VTRZ.

Except for ON-OFF switches for both half-zone CGR blowers, there are no CGR controls in the control room. Initial in-cell adjustments of the two butterfly valves and two baffle plates per half-zone to achieve correct total flow and balancing are all that are necessary for normal operation of the CGR system.

If the flow in any of the four CGR exhaust ducts falls below a preset level, a differential-pressure switch, held closed by the velocity pressure,

opens to light an alarm lamp on the VTRZ-CGR front panel in the control room. A further reduction in this exhaust duct flow trips the VTRZ heater power. The VTRZ alarm and heater-interlock systems are described in Secs. 4.5.12 and 4.5.11, respectively; the alarm and heater-interlock trip levels are discussed in ANL-7638 (Secs. 3.2.3 and 3.2.2, respectively). In addition to this direct monitoring of CGR operation, outer-matrix thermocouple readings (described in Sec. 4.5.8) provide a backup indication of CGR flow failure.

At an operating flow of 400 cfm (STP), each of the two CGR loops removes about 1800 W of heat from each half-zone, which raises the cooling-air temperature by about 10 C°. Details of the heat transfer of the system, together with a description of the temperature profile across the insulation annulus, appear in Sec. 5.2.6. CGR prototype experience and flow analyses appear in Sec. 7.2. In the event of an electric power failure, the emergency power system operates the CGR as described in Sec. 4.5.7.

The inner-matrix cooldown system cools down the inner matrix as rapidly as possible without generating excessive thermal stresses in the inner barrel and in such a way that the system has minimual effects on VTRZ neutronics. A $1\frac{1}{2}$-hp gas blower (Buffalo Forge Co.) serves each VTRZ half-zone IMCD system and establishes a maximum 160-cfm flow rate at a static pressure of about 20.2 in. of water. This flow is controlled just downstream from the blower by a motor-driven butterfly valve, which can be operated remotely from the control room. Downstream from this valve, the main IMCD steel duct work of each half-zone divides into two pipe systems, which feed the VTRZ. Flow between the two IMCD pipe systems is balanced by two hand-operated butterfly valves on each half-zone, similar to the ones used on the CGR system. After the desired maximum total flow and flow balancing are achieved, these valves are also locked in place. The flow further divides once it enters the manifold duct of each half-zone, as seen in Fig. 55. This flow division is adjusted by a baffle with an adjustable gate similar to that of the CGR. It too can be locked in place. The flow patterns in the annulus channels are shown in Fig. 54, and the physical layout of the channels is discussed in Sec. 4.5.3. Air is forced down one side of each of four ducts to the front of the half-zone, where the flow is reversed and forced down the other side of each duct to the rear of the half-zone. The flows recombine in the shroud and are ducted in two steel pipes out of the shroud and into the cell. The IMCD air exiting from the VTRZ can be very hot, and for this reason the exit air is deflected toward the ceiling of the cell as it exhausts. In each of the two entrance pipes for the IMCD, a flow element senses the average velocity pressure and actuates one or more differential-pressure switches depending on the flow (pressure) level. Since the IMCD system is monitored to prevent excessive flow during cooldown, placing these sensing elements in the IMCD entrance pipes ensures that all flow into the VTRZ cooling ducts is monitored.

In addition to ON-OFF switches for both half-zone IMCD blowers, the control-room IMCD chassis contains the drive controls for the two motor-driven butterfly valves. The valve motors have a continuously variable drive speed and also can be driven in a single-step mode with increments of 1.8° (50 steps from full open to closed). After in-cell adjustments of the balancing valves and baffle gates are made, these two remote-controlled valves provide all necessary IMCD control.

The IMCD monitoring scheme can be divided into two sections: valve-position monitoring and IMCD exhaust-flow monitoring. The exhaust-flow monitoring section is similar to the CGR system, with four exceptions:

(1) If the flow in any of the four IMCD exhaust ducts rises above a preset level, a differential-pressure switch, normally closed, is forced open by the increased velocity pressure, lighting alarm lamps, etc.

(2) This flow-trip preset level is adjustable in the control room and varied during a cooldown.

(3) The IMCD flows are only on the alarm system because the heaters are turned off during cooldown.

(4) Finite-step flow meters are provided for each exhaust flow.

The valve-position monitors are meters sensing the change in resistance of potentiometers located on the motor-drive linkages. The inner-matrix thermocouple readings (described in Sec. 4.5.8) provide a check on performance and guide the operator in making flow adjustments.

Details of VTRZ IMCD heat-transfer characteristics during cool-down appear in Sec. 5.2.7. Inner-matrix cooldown prototype experience and flow analysis appear in Sec. 7.3. Electric power for the IMCD air blowers is not on the reactor emergency system.

The outer-matrix air-cooling (OMAC) system is the reactor cooling system described in Ref. 2. In addition to its primary function of stabilizing the temperatures of and removing the heat from a plutonium-loaded core, the OMAC system is used with the VTRZ to remove the small amount of heat that leaks through the insulation and CGR system from the inner matrix assembly to the outer matrix assembly. Its primary function is to stabilize outer-matrix temperatures rather than to remove large quantities of heat. As discussed in Sec. 4.5.4, in certain areas in the insulation annulus the thickness of the insulation is significantly reduced. These areas provide a heat-transfer path to the outer matrix and would cause undesirable local temperature rises if the OMAC system was not functioning.

The OMAC system, shown in Fig. 55, has two modes of operation. During normal operation, air is pulled through both reactor halves, entering

the movable half and exiting through the stationary half. The air is then ducted up to a bank of HEPA filters, through the blower, and dumped back into the cell. When the halves are separated, air is drawn into the halves at the exposed faces, out the shrouds, into the ducts, and through the filters. Since the system is under negative pressure (relative to the cell) in both modes, all the air passing through the VTRZ outer matrix assembly is eventually filtered before being dumped back into the cell. With the VTRZ in place, the OMAC system functions exactly as described in Ref. 2. A typical flow per matrix tube in the operating OMAC system is 4 cfm with a 24-in. water-pressure drop. All the matrix tubes of the VTRZ outer matrix assembly are identical to the normal ZPR-6 and -9 tubes, except for the 12 triangular tubes on the diagonal flats of the outer barrel. The triangular tubes contain special orifice plates to control OMAC flow through them.

4.5.7 Electrical Power System

The VTRZ electrical power system modifies and extends the existing ZPR reactor-cell electrical-distribution system to provide all necessary electrical power and control equipment for in-cell VTRZ components, i.e., for the cooling guard-ring (CGR) and inner-matrix cooldown (IMCD) systems, the internal and external inner-matrix-assembly heaters, the inert-gas loop system, and in-cell instrumentation. Figure 56 (with Fig. 57) is a schematic of the electrical power system; Fig. 58 shows the location of the major components of the system in the ZPR-6 cell. (Installation in ZPR-9 would be similar.) Procurement of the VTRZ electrical power equipment is governed by the Electrical Power Section specification mentioned in Sec. 1.2.c(2).

The inner-matrix cooldown-system blowers are supplied, from the existing in-cell 480-V three-phase bus. This power bus is not connected to the reactor emergency power system. Electrical power loss to the cool-down air blowers, even during cooldowns and for long time periods, would be inconvenient but not dangerous.

Although heat transfer radially through the insulation annulus is slow, even with the CGR airflow off, operability of the CGR system during extended normal power-supply outages is considered desirable. Therefore, the CGR blowers are connected to the reactor emergency-power-system 208-V three-phase bus, which is automatically switched to the steam-driven generator in the basement when the normal power supply fails. Note that time-delay (3-55 sec) relays are connected between the CGR blowers and the 208-V emergency bus. These delays are needed to avoid the very high starting load on the emergency bus during the first few seconds after the power is transferred to the steam-driven generator; an interruption of a few seconds (or even a few hours) is not important for the CGR system.

Mechanically-latched start-stop switches for both the CGR and IMCD systems are located remotely on the VTRZ control panel in the

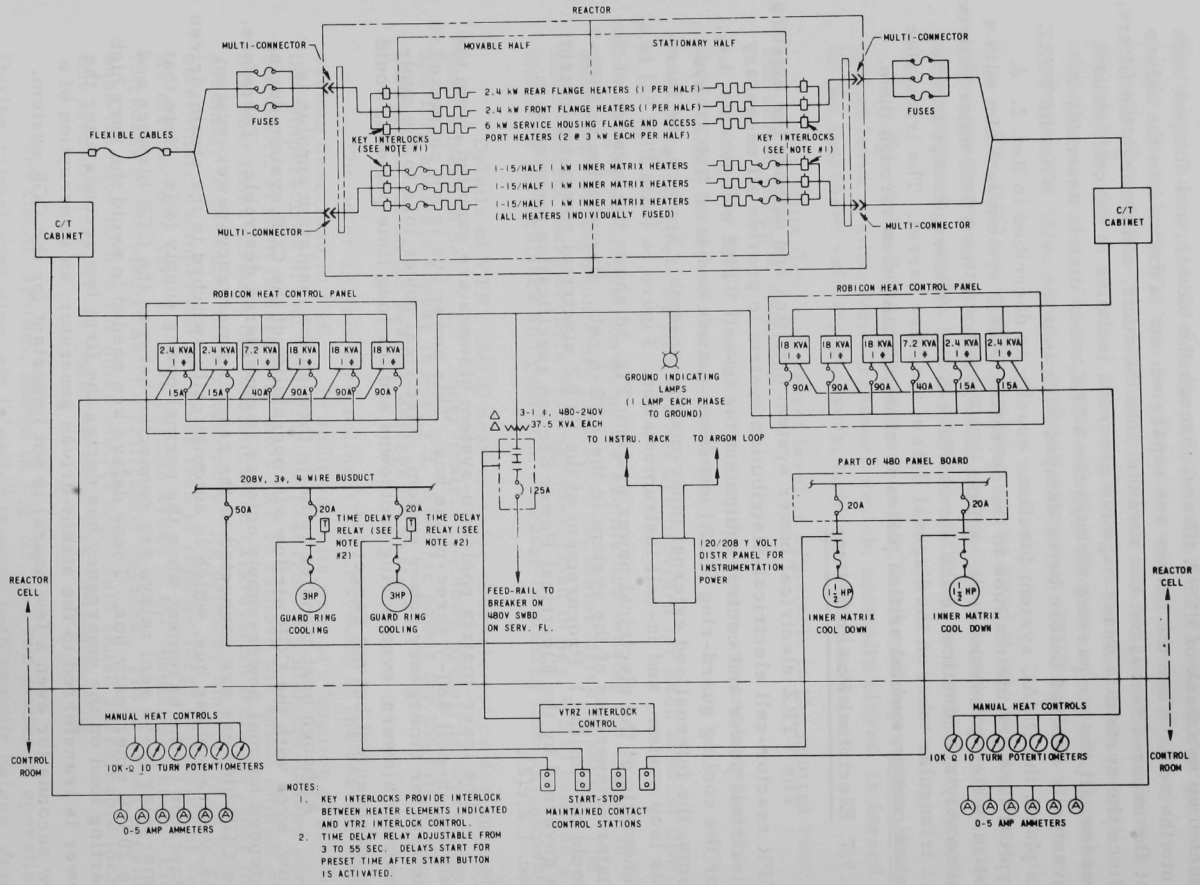

Fig. 56. Schematic of VTRZ Electrical Power System

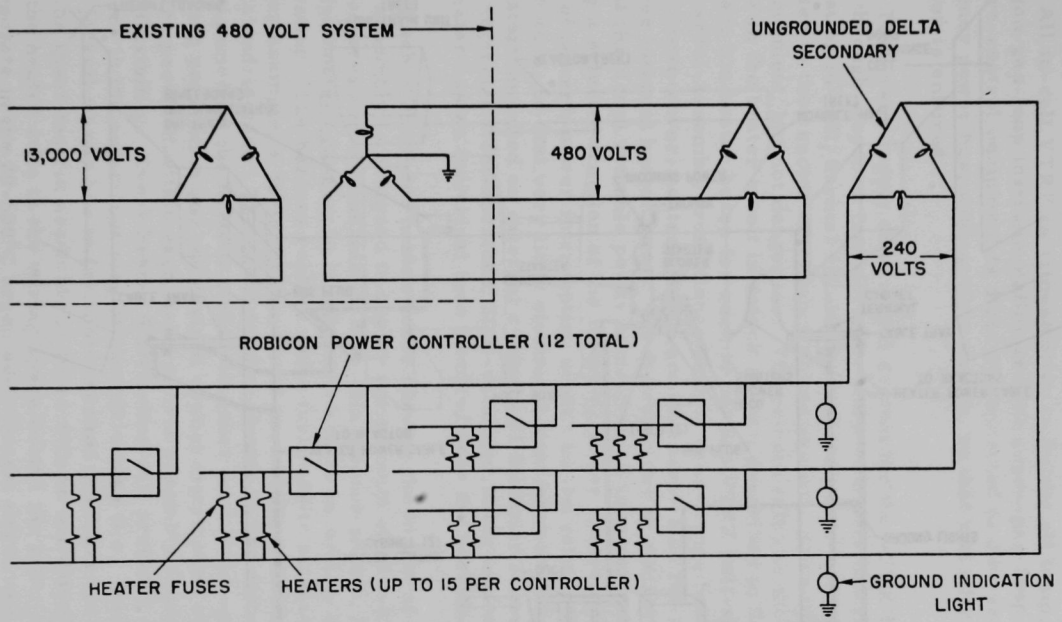

Fig. 57. Detail--Electrical Power-distribution System for VTRZ Inner-matrix-assembly Heaters

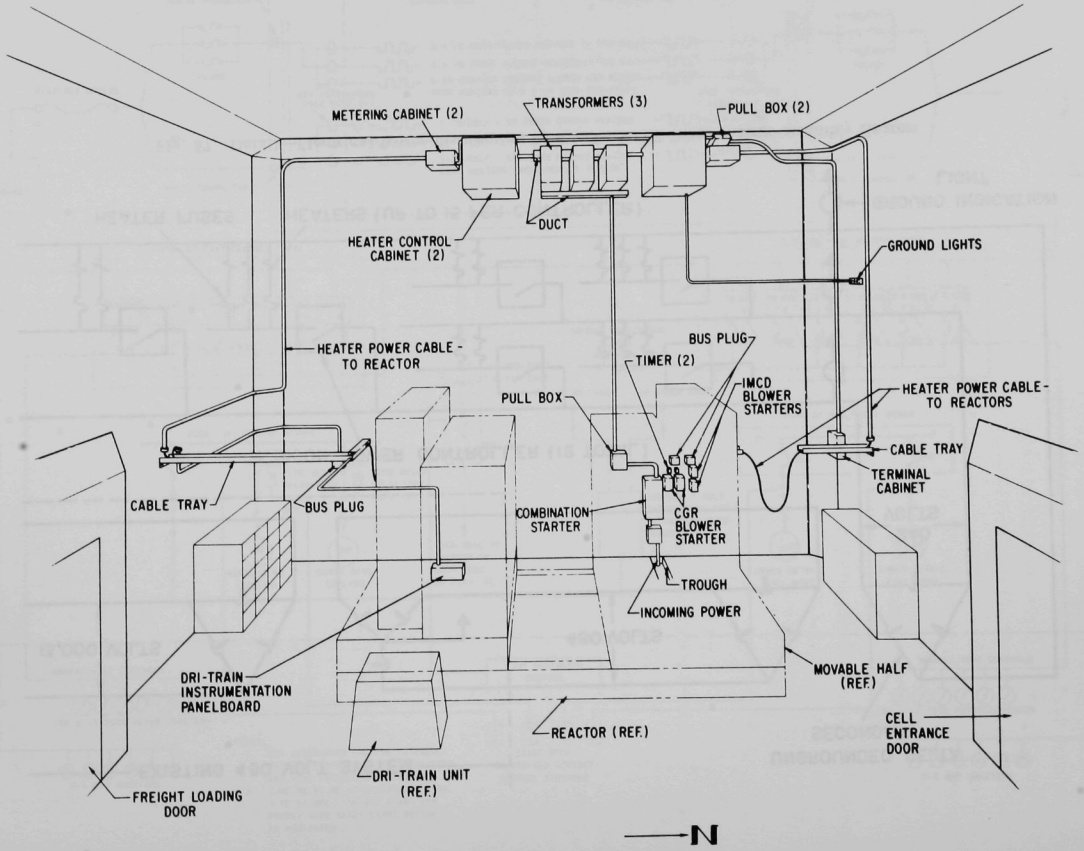

Fig. 58. Installation of VTRZ Electrical System in ZPR-6 Cell

reactor control room. Once in the start position, these switches remain in that position and cause the blowers to start again after a power loss as soon as the power is restored or transferred to the emergency bus.

All in-cell VTRZ instrumentation including all temperature, airflow, and argon-gas-loop instrumentation and the argon-gas-loop circulation and pressure-control equipment is directly connected to the reactor 208-V emergency power bus, without time delays, so that virtually uninterrupted operation is ensured.

The power supply and control system for the VTRZ heaters is connected through stepdown transformers and a remotely controlled relay to the existing in-cell, normal 480-V three-phase power bus; this bus is not connected to the reactor emergency power system. Loss of heater power is inconvenient, but not dangerous. The remote relay is the central control element in the heater cutoff interlock system described in Sec. 4.5.11. There are six heater buses for each of the two VTRZ half-zones: the inner-barrel-assembly front-flange heater, rear-flange heater, service-housing (rear-cover) heaters (there are two heaters on the service housing), and three internal heater buses. Each heater bus is controlled by a commercial (Robicon) variable power controller. These controllers operate by passing a selected fraction of the incoming power cycles (to produce rapid pulses of power); power interruption occurs as the voltage wave passes through zero, so that very little electrical interference should be generated. The heaters mounted on external surfaces of the inner barrel assembly are commercial steel-sheathed, MgO-insulated, Nichrome wire heaters; each heater has an individual fuse mounted near the service housing.

Each of the three heater buses serving the inside of each inner barrel assembly is designed to supply a maximum of 15 1-kW heaters. These heaters are commercial 3/8-in.-dia Inconel-sheath, MgO-insulated, cartridge heaters ranging in length from 6 to 36 in. and up to a maximum 1-kW rating. The heaters replace oxide fuel rods in selected calandria cans; for example, a 36-in. heater would pass along a matrix tube through three calandria cans. The exact number, power rating distribution, and bus assignment of the heaters within the inner matrix depend on the experiment being performed and the desired spatial distribution of heating; three buses are provided within each inner matrix assembly to permit maximum heating flexibility. Every heater distribution will probably include a ring of heaters in the outermost ring of calandria cans (i.e., next to the inner-matrix jacket) on one bus to facilitate thermal equilibration. Each heater within the inner matrix assembly is fitted with an individual fuse mounted within the heated zone in the wiring space behind the inner matrix. These fuses operate in the 20-600°C argon environment and have a 6.3 ± 0.3-A fusing current (1.5 ± 0.07 kW) regardless of fuse temperature or history; the fuses are described in detail in Sec. 8.1. Fusing within the hot zone is necessary because of the large number of individual heaters needed, the

practical limit on the number of service-housing penetrations, and the impracticality of protecting against individual heater failures by fusing an entire bus external to the hot zone. Current limitation to 6.3 A is adequate to protect the calandria cans and the fuel rods.

The cartridge heaters are constructed of a series of 1- to 3-in. spiral Nichrome heater sections connected in parallel to a pair of power leads that pass down the center of the heater assembly. Failure modes in these heaters are unknown; the only failure that has ever occurred (even at full power and hanging free in air) throughout the prototype testing work has been lead-wire breakage during heater disconnections.

As shown in Fig. 56, potentiometer controls and current monitors for each heater bus are provided on the VTRZ control panel located in the reactor control room.

The only part of the electrical power system to be routinely handled by the VTRZ operating crew will be the connections to the 12 heater buses, six on each half-zone. These connections are located on the outside of the service housing and, for the six cartridge-heater buses, within the wiring spaces behind the heatable matrices. The maximum operating voltage of each bus is 240 V ac. Protection against electrical shocks to personnel will be handled primarily by administrative controls, particularly operating checklists. However, two safety precautions have been taken in the electrical system design: First, the entire heater power system beyond the 480-240-V transformers is connected as an ungrounded-delta system and is electrically isolated from the grounded reactor assembly. (The secondary side of the 480-V transformer is a grounded-Y connection.) This limits the electrical shock to a person standing on the reactor bed and accidently touching one leg of the three-phase 240-V system to the capacitive-coupling current in the 240-V phase to ground. Ground lights are mounted on the north wall of the reactor cell. There are three lights, and they are all on if the delta-connected system is ungrounded. One of the lights goes out if the corresponding phase becomes grounded. Second, the plenum doors providing access to the heater bus connections at the service housing are locked. The VTRZ control-panel interlock key must be removed and the remote relay thereby opened to gain access to the plenum-door key. The padlock key must be inserted in the heater interlock chassis of the VTRZ control panel to permit closure of the remote relay and the acquisition of heater power. The padlock system is not foolproof, but is intended as a precautionary step. The design of the VTRZ heater power system has been reviewed and approved by an electrical safety engineer from the ANL Industrial Health and Safety Division. In particular, the 240-V system was not considered by the safety engineer to be appreciably more hazardous than a 120-V system. Significantly lower voltages have been ruled out by the required cable and service-housing penetration bus sizes and by the unavailability of commercial heaters of sufficient power rating.

4.5.8 Temperature Instrumentation

The purpose of the VTRZ temperature-instrumentation system is twofold: First, it measures and records radial and axial temperature profiles needed for the control of VTRZ heating and cooling and for the analysis of VTRZ experiments. Second, it signals the occurrence of various abnormal conditions in the heating, cooling, and argon loop systems. The temperature instrumentation provided for the VTRZ is described in this section. The description is divided into the following paragraphs:

4.5.8.1 Thermocouples and Their Locations

4.5.8.1.1 Inner Matrix

4.5.8.1.2 Outer Matrix and Insulation Annulus

4.5.8.1.3 Cooling Guard-ring and Inner-matrix Cooldown Air Systems

4.5.8.2 Readout and Recording System

The temperature instrumentation for the argon loop external to the inner barrels is described in Sec. 4.5.5.3.6. The scram, heater-interlock, and alarm systems associated with VTRZ temperature monitoring are described in Secs. 4.5.10, 4.5.11, and 4.5.12, respectively. Safety considerations and temperature trip levels are discussed in Secs. 3.2.1-3.2.3 of ANL-7638. The relation of inner-matrix temperature monitoring to calandria-can overheat detection is detailed in Sec. 8.2.

4.5.8.1 Thermocouples and Their Locations

4.5.8.1.1 Inner Matrix

The principal inner-matrix thermocouples have Chromel-Alumel sensing elements packed in a high-purity magnesium oxide insulation and are sheathed in 20-mil-OD Type 304 stainless steel or Inconel 600 tubes. The wire connecting these thermocouples to the thermocouple reference junction is Chromel-Alumel thermocouple wire, insulated with glass braid. The VTRZ service housing provides feedthroughs to accommodate up to 136 thermocouple wires, which sets the limit of inner-matrix locations that can be monitored at one time. Of these 136 thermocouple locations (per half-zone), 66 are fixed in order to meet the calandria-can overheat-detection requirements. Briefly, the calandria-can overheat-detection requirement is that every inner-matrix calandria can containing a cartridge heater must be in direct contact with, or directly adjacent to (separated only by a matrix tube thickness), a thermocouple. Figure 59 shows a thermocouple location scheme that meets the above requirements for one echelon of calandria cans, independent of cartridge-heater position. This scheme is repeated for the number of calandria-can echelons in a VTRZ half-zone. In the standard VTRZ loading, there are three calandria-can echelons in the

36-in. axial length of each inner barrel. Since the calandria cans heat uniformly along their length, it is unimportant just where the thermocouples are located along their 12-in. length. The locations for the remaining 70 of the total of 136 thermocouples are completely arbitrary (within the limits of practicability) and are determined by the nature of the experiment taking place. Normally, however, an effort will be made to provide a redundancy for the calandria-can overheat requirement. Without this redundancy, the operator would have to shut down if any one of the 66 thermocouples failed. For example, with a "complete-redundancy" pattern as shown in Fig. 60, there is a backup thermocouple for each of the basic 66; the operator would be forced to shut down only if two adjacent thermocouples failed, thus leaving a calandria can unmonitored. For the matrix tubes marked with triangles in Fig. 60, there would have to be a three-adjacent-thermocouple failure in order to lose monitoring. In addition to providing a complete redundancy, the thermocouple distribution shown in Fig. 60 provides a detailed inner-matrix axial-cross-section temperature profile including 45 thermocouples per half-zone that show the effects of the IMCD and CGR on the inner-matrix jacket temperatures. If this scheme were used, there would be 10 uncommitted thermocouples per half-zone that could be used as seen fit by the experimenter.

When a calandria can is pushed to one side of the matrix tube, a (nominally) 50-mil gap is created between the can and the tube, providing

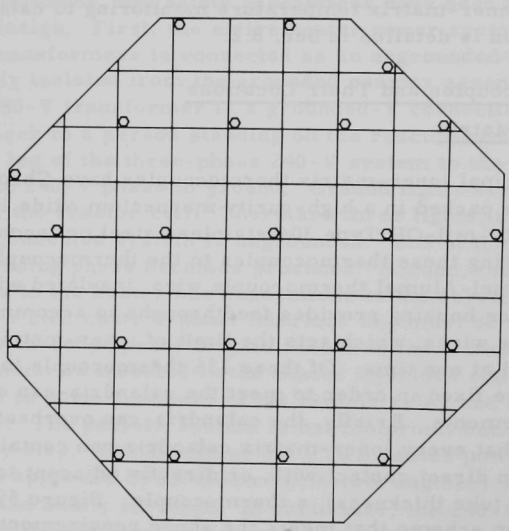

TOTAL PER AXIAL CROSS-SECTION = 22
TOTAL PER HALF-ZONE = 66

Fig. 59. Thermocouple Location Scheme for Calandria-can Overheat Requirement

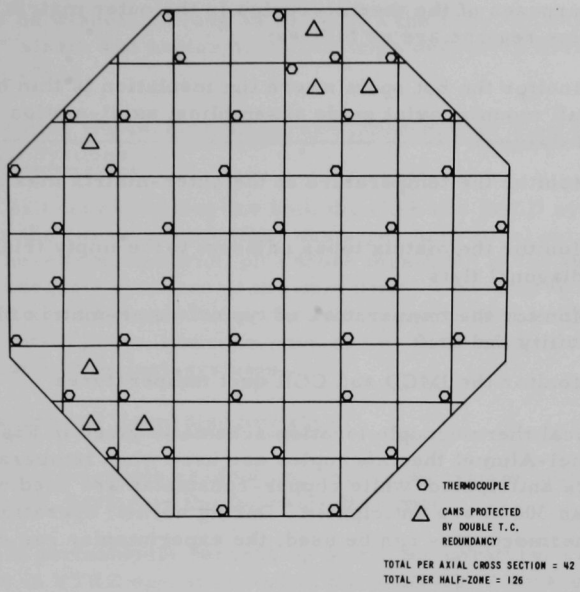

Fig. 60. Thermocouple Location Scheme with "Complete Redundancy"

ample room for thermocouple installation. A special insert is provided to guarantee good thermal contact between the thermocouple, the matrix tube, and the calandria can.

The thermocouple wire is run from the thermocouple to a connector block located in the wiring space of the inner matrix assembly, then through the service housing feedthroughs, and finally to the master thermocouple reference junction located in a rack beside the Dri-Train station. The inner-barrel thermocouple wiring is discussed further in Sec. 4.5.3 and shown in Fig. 29.

4.5.8.1.2 Outer Matrix and Insulation Annulus

There will be two operational phases to the monitoring of temperatures in the outer-matrix and insulation-annulus regions: The first phase will be in-cell monitoring as part of the initial VTRZ checkout. The second will be the normal operational monitoring from the control room during routine VTRZ operation. The number and location of thermocouples for the checkout phase are very flexible and are dictated by the demands of the checkout. For the normal operation phase, the thermocouples are limited to 44 of which a maximum of 20 can be Chromel-Alumel (high temperature). These limitations are determined by the capacity of the thermocouple scanner and multipoint recorders described in Sec. 4.5.8.2.

The purposes of the thermocouples in the outer matrix and the insulation annulus regions are as follows:

(1) Monitor the hot spots where the insulation is thin or nonexistent (i.e., at the ball mounts, axial guide assemblies, axial-motion restrainer brackets, and flanges).

(2) Monitor the temperature at the outer-matrix maximum-stress points.

(3) Monitor the matrix tubes adjacent to the empty triangular-matrix tubes on the diagonal flats.

(4) Monitor the temperature of typical outer-matrix tubes, and check for stability and drift.

(5) Monitor the IMCD and CGR duct temperatures.

A typical thermocouple location scheme is given in Fig. 61. Normally, Chromel-Alumel thermocouples are used when temperatures greater than 100°C are anticipated, while copper-constantan are used when temperatures less than 300°C are anticipated. During normal operation, when only 44 of these thermocouples can be used, the experimenter can choose any

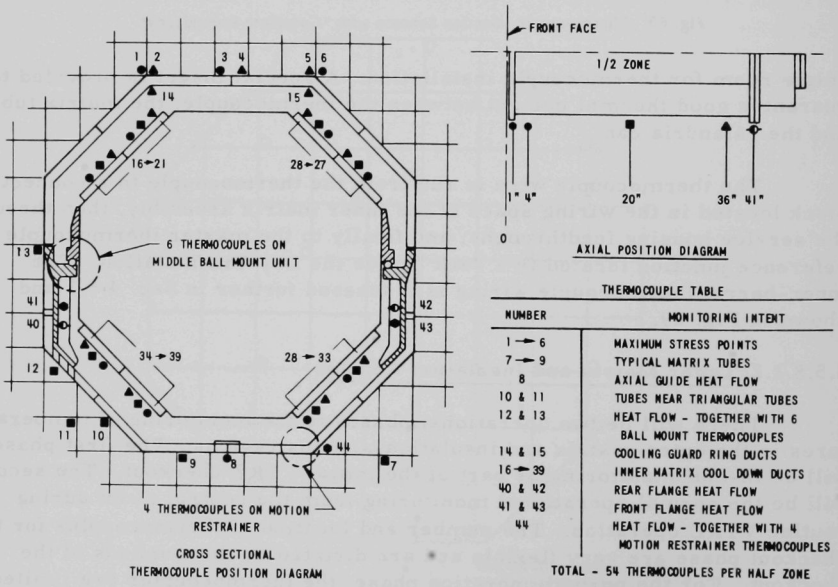

Fig. 61. Typical Thermocouple Location Scheme for Insulation Annulus and Outer Matrix

combination he wishes, as long as he fulfills the requirements of the "Cold Zone" alarm and heater-interlock trips defined in Secs. 3.2.2 and 3.2.3 of ANL-7638.

4.5.8.1.3 Cooling Guard-ring (CGR) and Inner-matrix Cooldown (IMCD) Air Systems

The exit temperatures for both the CGR and IMCD systems are measured in the exhaust ducts (four ducts per half-zone) outside the shrouds. These temperatures, plus those measured in the insulation annulus, are an adequate measure of the operating temperatures of these two systems. The exit temperatures can be monitored both in the reactor cell and in the control room; however, they are not part of the control-room alarm or heater-interlock systems.

4.5.8.2 Readout and Recording System

The thermocouple readout and recording system, shown schematically in Fig. 62, performs the following functions:

(1) It permanently records up to 372 temperatures as a function of time for use in VTRZ operation and in the analysis of experiments (300 are typed on the printer, and 72 are recorded on the three 24-point, strip-chart recorders).

(2) It trips the alarm system if temperatures are sufficiently abnormal.

(3) It trips the heater-interlock system if temperatures are sufficiently abnormal.

(4) It signals a failure of any of the 372 thermocouples monitored.

(5) It provides readout of 72 temperatures on multipoint recorders, and provides virtually instant readout of any of 300 temperatures in preassigned sequences on the printer-scanner system.

Each reactor half is assigned 200 thermocouples, 150 of which are reserved for the hot zone. The thermocouple extension wires are run from the service-housing feedthroughs and from the reactor locations external to the inner barrel to terminal boxes mounted in or on the reactor plenum of each half-zone. The terminal strips and input and output connectors in the terminal boxes are compatible with the thermocouples used. The thermocouple wires from each reactor half-zone terminal box are run in 24-conductor thermocouple extension cables to the main thermocouple junction box mounted next to the reactor in a relay rack.

All the terminal strips and input and output connectors in the main junction box are made of thermocouple materials. In the main junction box,

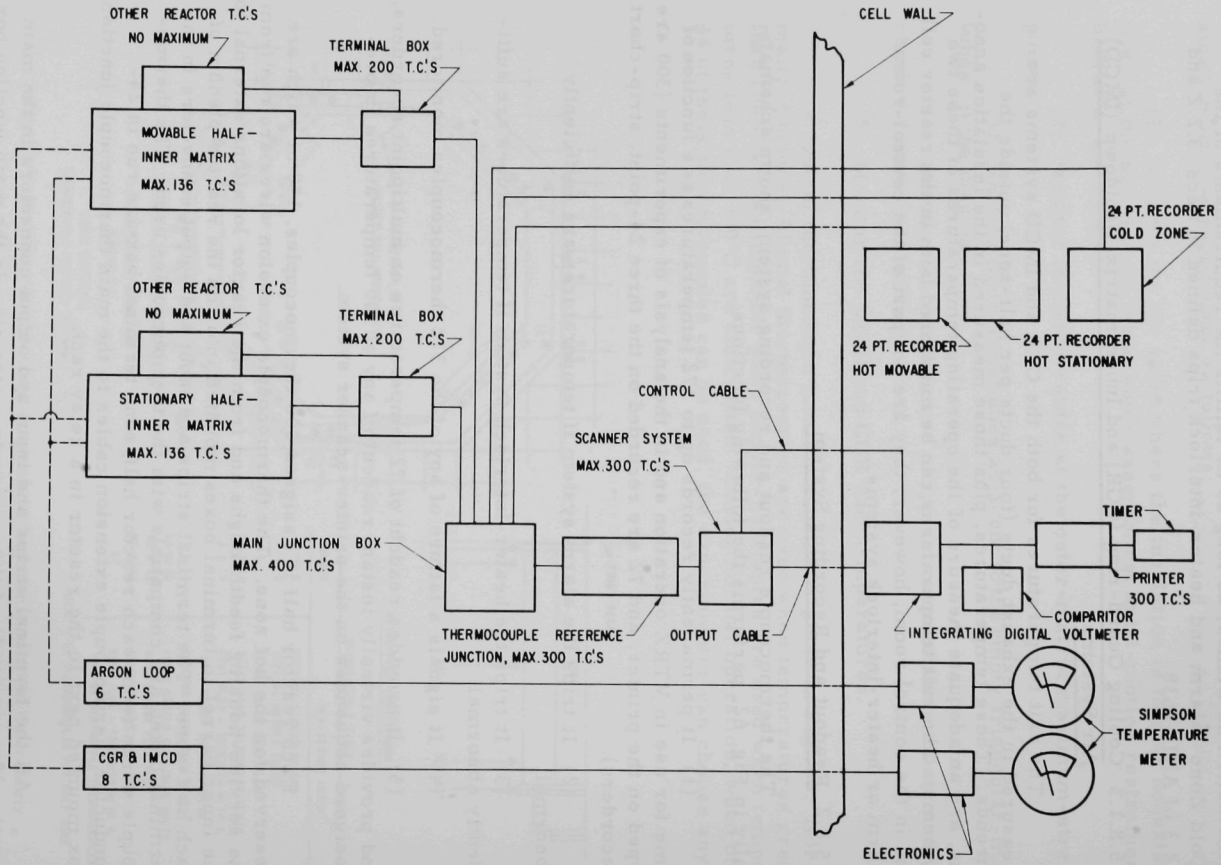

Fig. 62. VTRZ Temperature Instrumentation

300 of the 400 thermocouples are selected for monitoring by the scanner-printer system. The only constraint on the choice of thermocouples for the scanner-printer system is that those thermocouples required for the heater-interlock and alarm systems must be included. The scanner system will accept both Chromel-Alumel and copper-constantan thermocouples. In the main junction box, 72 of the 400 thermocouples are selected for monitoring by the multipoint recorders.

There are two constraints on the selection of the thermocouples for the multipoint recorders: First, a given multipoint recorder will not accept both Chromel-Alumel and copper-constantan thermocouples, and therefore these types cannot be mixed. Second, as with the scanner-printer system, the choice of thermocouples for the multipoint recorders must conform to the requirements of the heater-interlock and alarm systems.

The scanner-printer system is made up of a thermocouple reference junction, a scanning system, an integrating digital voltmeter, a printer, a temperature comparitor, and a timer. The thermocouple reference junction establishes a reference temperature and permits the conversion from thermocouple wire to copper wire without introducing temperature errors. The scanning system, made up of a master scanner containing 100 channels and a slave scanner containing 200 channels, scans 300 thermocouples in about 1 min, according to a preselected sequence. The scanning-system circuitry is set up so that it will be read 0°C for an open thermocouple. The output of the scanning system passes through an integrating digital voltmeter (analog-to-digital converter) and then to a high-speed printer, which can be started and stopped at the discretion of the operator. The printer also prints the time signaled from the timer and the individual thermocouple identification. A digital comparitor signals the heater-interlock and alarm systems if abnormal temperatures are present.

The multipoint recorders are fed directly by thermocouple extension wire from the main junction box. The recorders are the chief readout system for the VTRZ operator. Normally, there will be one recorder assigned to monitor temperatures in each heatable half-zone and one assigned to monitor "cold-zone" temperatures. The alarm and heater-interlock trips associated with these recorders are described in Secs. 4.5.11 and 4.5.12, respectively. All three multipoint recorders are of the down-scale burnout type; i.e., they read 0°C for open thermocouples.

The CGR and IMCD thermocouples are wired directly to two Simpson temperature meters in the control room, one for each system. Manual switches permit readout of any of the four exhaust temperatures desired.

The independent temperature-sensing channels associated with the VTRZ scram system are described in Sec. 4.5.10.

4.5.9 Component Failure Monitors

The key to safe operation of the VTRZ is the maintenance of the integrity of the calandria cans and fuel rods. Most of the VTRZ equipment discussed elsewhere in this report is designed to protect the integrity of these components. However, as a backup, a system of monitors has been developed to signal a failure of either component or an overheat condition that could lead to a failure of either component. A helium monitor and a plutonium-alpha monitor have been developed to detect fuel-rod failures by sensing increased levels of helium gas (from the fuel-rod fill gas) and plutonium-alpha content, respectively, in the argon cover gas downstream from the half-zones. A sodium monitor has been developed to detect a calandria-can failure by sensing an electrical short produced by the accumulation of liquid sodium at the bottom of the inner-matrix-assembly wiring space. The inner-matrix-assembly temperature-monitoring system is designed to detect any abnormal heating in time for the proper action to be taken before a thermally induced can or rod failure can take place. The temperature-monitoring system is described in Secs. 8.2 and 4.5.8.1.1. The plutonium-alpha, helium, and sodium monitors are discussed below.

The plutonium-alpha monitor detects plutonium particles in the argon blanket gas as it exits from the inner barrel and thereby signals a fuel-rod failure. The plutonium-alpha monitor is not used when there are no $(Pu,U)O_2$ fuel rods in the VTRZ. The heater-interlock trip-point setting for plutonium-alpha contamination in the closed argon loop is determined by the number of counts corresponding to 1000 RCG-hr (i.e., 2×10^{-9} μCi-hr/cm^3); the alarm set point is set for just half that amount. The theoretical sensitivity of the plutonium-alpha detector is such that counts corresponding to 10 RCG-hr (i.e., 2×10^{-11} μCi-hr/cm^3); can be distinguished from background. Theory of operation, analyses of the monitor sensitivity, and prototype testing relevant to the monitor performance are covered in Sec. 8.4.2. Monitor-system hardware and electronics are discussed here.

Figure 63 shows the plutonium-alpha-monitor-piping with a detail of the sensing unit and a block diagram of the monitor electronics. The loop subassembly design is a compromise between conflicting operational criteria; the pressure drop across the subassembly must be kept to a minimum, and the particle attenuation on the filter must be kept to a maximum. In the design, only one-fourth of the argon flow passes through the filters; the remaining gas flows in the bypass line. This division of flow generates a tolerable pressure drop (about 14 in. of water) while reducing the overall efficiency of the detecting system by only a factor of four. The main-line valves and unions are arranged to allow removal of the monitor housing for filter changes and/or monitor calibration with minimal air contamination of the argon loop. The housing itself has a quick-disconnect clamp for rapid access to the filter area.

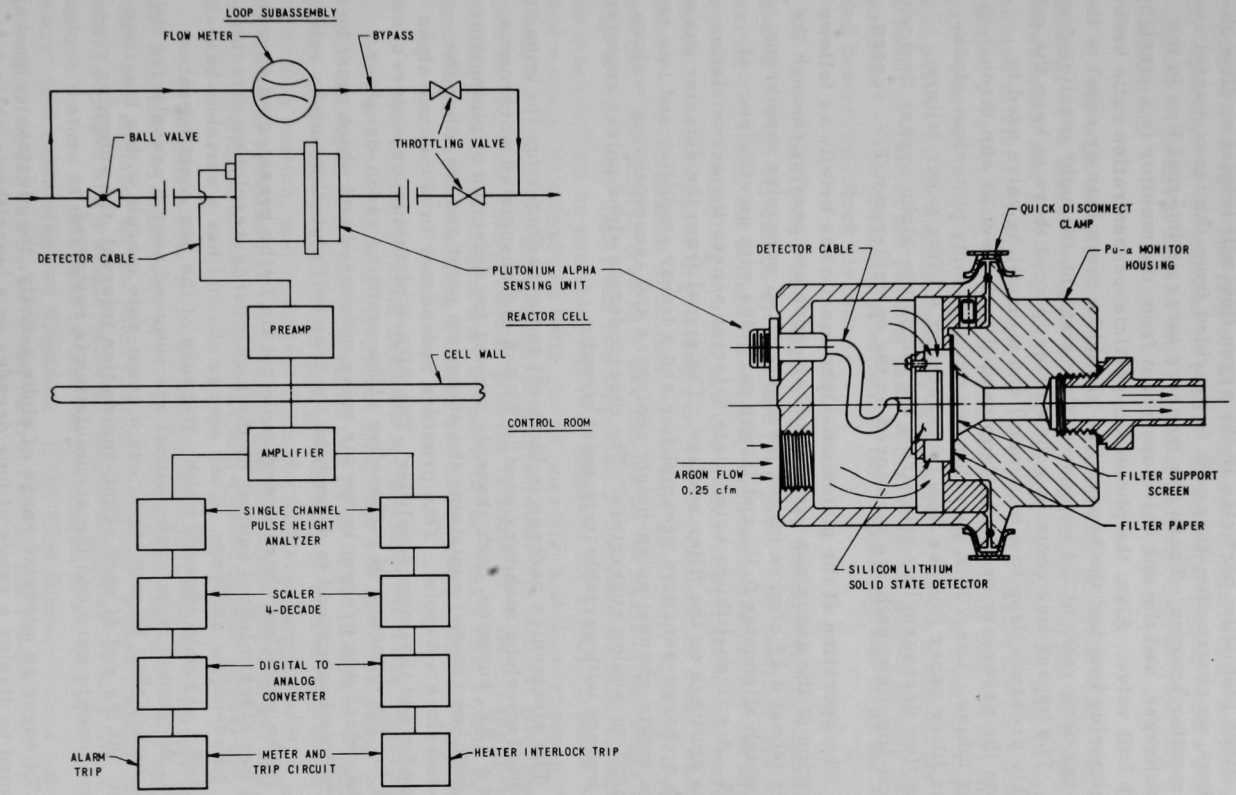

Fig. 63. Plutonium-alpha Monitor (with detail of sensor)

Since plutonium particles in the argon flow will impact on flow obstructions, an obstruction-free path is provided from the inner-barrel exit to the monitor housing. There are no sharp turns or internal fins in the heat exchanger, and the one valve upstream from the monitor is a straight-through ball valve. Also, the plutonium-particle-concentration ratio between the monitoring line and the bypass line should be more than or equal to the argon-gas-flow ratio of 1:3 because of the "straight-through" monitor-line piping. The bypass line contains a flowmeter (placed there to keep the subassembly pressure drop to a minimum) and a throttling valve used to generate the necessary pressure drop needed to drive 0.25 cfm through the monitor tubing. The VTRZ operator can detect a dirty plutonium-alpha-monitor filter paper (bypass flow increases) or a filter paper failure (bypass flow decreases) by comparing the plutonium-alpha bypass flow with the main-line flow; both are monitored on the control-room T.V. screen.

The operation of the plutonium-alpha monitor is briefly as follows: The portion of the argon gas exiting the half-zone and passing through the monitor (about 0.25 cfm) is forced through a 1.2-μ pore-size membrane filter, which attenuates 0.3 μ and larger particles with an efficiency of 99.942%. A silicon-lithium solid-state detector senses the accumulation of alpha emitters on the filter surface. The signal from the detector passes through a charge-sensitive preamplifier and a linear amplifier and into two parallel single-channel pulse-height analyzers and accompanying scalers and digital-to-analog converters. The discriminated alpha pulses register on two meters with variable-trip-point circuits.

The electronics package is identical to the packages for the impactor-type plutonium-alpha monitors used in ZPR-6 and associated workrooms. For the VTRZ, however, both channels are set for detection of plutonium-alpha, with one channel containing the alarm set point and the other the heater-interlock set-point. This provides redundancy in plutonium-alpha detection beyond the linear amplifier. The ZPR-6 plutonium impactors use one channel for the detection of radioactive alpha-emitting radon-daughter products, which are present in the air being monitored and which must be subtracted as background to determine the true cell plutonium-alpha activity.

Alpha particles whose energies do not lie in the preselected energy channel are discriminated against by the high-energy-resolution detector and the pulse-height analyzer. Each energy channel has a variable-base-line setting and a variable channel width. Because of the low counting rates involved, the counts from each channel are summed over a preselected time interval rather than attempting to use a count-rate circuit with a longtime constant. At the end of each count-summation interval, the summing circuits are reset to zero and the accumulation is restarted.

To cover an adequate range of alpha activity, the electronics package is designed to display a range of four decades on a logarithmic scale from

counts of 1 to 10^4. The trip circuit is operated by a voltage proportional to the logarithm of the number of counts. If the total logged counts over the summation interval exceed the trip-level setting, the relevant trip circuit is actuated.

As with the plutonium-alpha monitor, the purpose of the helium monitor is to detect fuel-rod failure. In each fuel rod, the void space between the fuel pellets and the rod cladding is backfilled with an argon-helium mixture during fabrication. If a rod fails during operation, nominally 0.2 cc (STP) of helium is released and is mixed with the argon cover gas. The helium is then flushed out of the inner barrel with the argon gas and passes by the helium-monitor-gas sampler, which continuously sniffs a small portion of the passing gas. A mass-spectrometer helium detector responds to the presence of helium in the sample gas and trips the alarm and heater-interlock circuits.

The basic flow and electronic circuits for the helium monitor, shown in Fig. 64, can be divided into four parts: the sampling system, the vacuum system, the helium mass-spectrometer detector, and the electronics system. The sampling system has two modes of operation: the normal mode, which samples argon loop gas, and the calibration mode, which introduces a known amount of helium for system-sensitivity and trip-level checks. The sniffer leak rate was chosen on the basis of prototype test experience (Sec. 8.4.1) and is a compromise between a desire to sample as much helium as possible, and thus increase the signal-to-noise ratio, and a desire to sample as little gas as possible, and thus increase the overall vacuum system and mass-spectrometer operational efficiency. The sniffer leak rate presently planned is about 10^{-4} std cc/sec (helium), although some adjustment may be made in the final VTRZ setup. All valves associated with the helium monitor are bellows-type high-vacuum valves.

The vacuum system designed for use with the mass spectrometer includes a 150-liter/sec air-cooled NRC HSA 150 diffusion pump, a 36-hr liquid-nitrogen cold trap with automatic filler, a 21-liter/sec Welch fore-pump, and bellows-sealed O-ring-type valves. A throttling plate in the cold-trap section, just upstream from the diffusion pump, permits greater diffusion of sampled gas to the mass spectrometer and thus greater sensitivity. Justification for insertion of this throttling plate appears in Sec. 8.4.1.

The mass-spectrometer helium detector, Norton Company NRC 925-20, has a basic sensitivity of 1×10^{-11} std cc/sec (helium). The spectrometer tube contains an ion source, an ion collector, a preamplifier, a discharge gauge, and a single external magnet for all necessary fields. A unique feature of this tube is that the ion source is an inexpensive "throw-away" unit containing two filaments. If the first filament burns out, the second filament can be switched on from either the reactor cell or the control room.

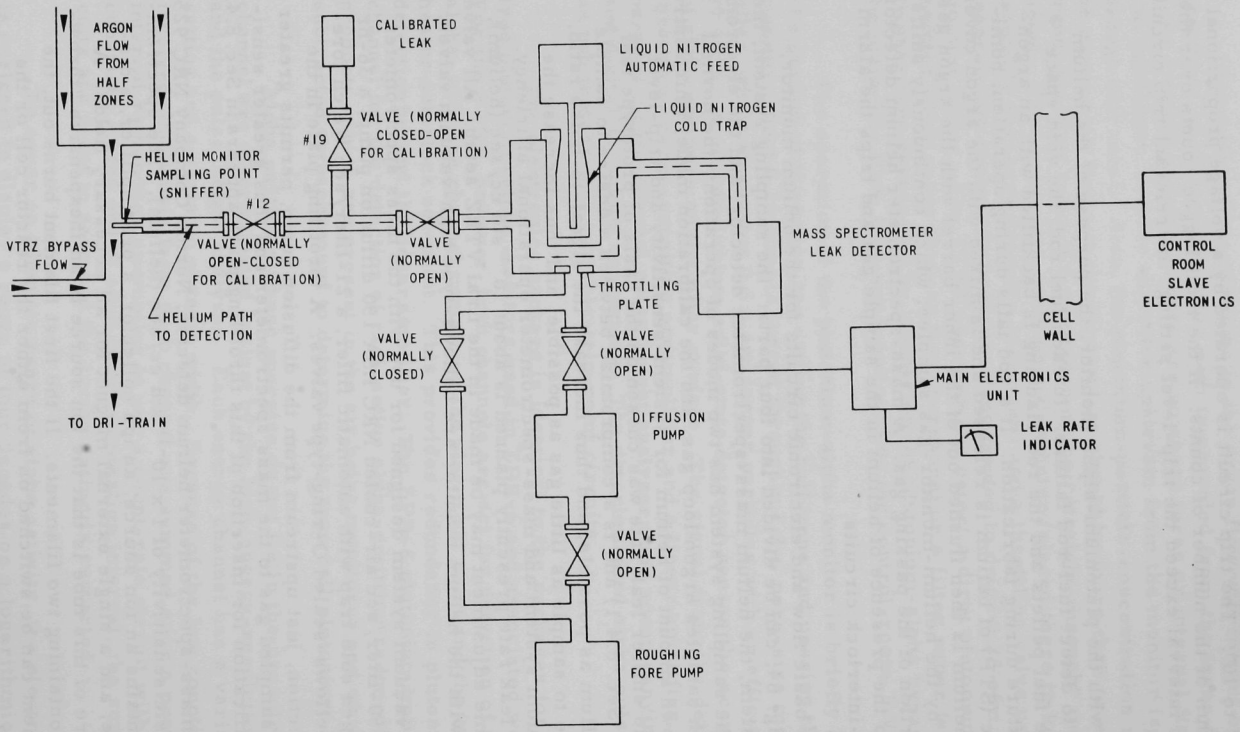

Fig. 64. Helium Monitor Assembly

The electronics system for the helium monitor consists of the NRC-925-20 mass-spectrometer electronics located in the reactor cell and the control-room slave electronics designed by ANL. The mass-spectrometer electronics unit supplies all power, amplification, and control circuitry to the spectrometer tube. Tuning controls are behind locked panels. The Norton mass-spectrometer "leak-rate" meter, pressure meter, and emission-current meter are duplicated in the control room. The operator can select filaments and energize them as he wishes from the control room.

A detailed description of the helium detection theory, the operating specifications and conditions, and prototype experience appears in Sec. 8.4.1. The alarm and heater-interlock trips are discussed in Secs. 4.5.12 and 4.5.11, respectively.

The sodium monitor is designed to detect gross sodium leakage from the calandria cans by allowing the liquid sodium to short out a specially designed electrical grid located at the bottom of the wiring space of each inner-matrix-assembly half-zone. Integrity of the grid circuit is constantly monitored by a continuity circuit. Four thermocouple feedthrough pins per half-zone are reserved for the necessary electrical connections to the external circuitry.

Each sodium monitor contains two circuits (A and B), electrically isolated from each other during normal operation. Circuit A shorts to circuit B across the circuit grid plates if liquid sodium accumulates between the grid plates. Each circuit contains a constant-current source (nominally 10 mA), lead wires to and from a shorting grid, a shorting grid (located in the inner-barrel wiring space), and a resistance to ground, which completes the circuit and across which voltages are measured. Each circuit also contains a bucking-voltage source, which is connected to the voltage measuring point through a large resistance. Circuits A and B are of opposite polarity, one voltage measuring +8 V (circuit A) and the other measuring -8 V (circuit B) during normal operation. The circuits are so designed that:

(1) A discontinuity in circuit A will register as -1 V and light a discontinuity alarm light.

(2) A discontinuity in circuit B will register as +1 V and light a discontinuity alarm light.

(3) A spurious short in circuit A lead wires will register at +10 V and light a spurious-short light.

(4) A spurious short in circuit B lead wires will register as -10 V and light a spurious-short light.

(5) A liquid-sodium-induced short from circuit-A grid to circuit-B grid will drop both circuit voltages to zero, light the appropriate lamps, and open the heater-interlock circuit.

(6) A bucking-voltage-source power failure will make the discontinuity monitoring inoperative, but will not affect the sodium-short monitoring.

4.5.10 VTRZ-ZPR Reactor-scram System

If the inner-matrix-assembly temperature or pressure rises significantly after the heater power is cut off, the VTRZ is considered to be in an uncontrolled operating condition and an automatic reactor scram should be initiated. Thus, VTRZ high-temperature and high-pressure reactor-scram trips have been added to the regular ZPR scram conditions.

The VTRZ reactor-scram system comprises 10 independent channels of which six (three per half-zone) respond to high temperatures and four (two per half-zone) respond to high pressures. The corresponding 10 relay interlocks, together with the abnormal ZPR condition interlocks comprise the VTRZ-ZPR scram chain. An opening of the scram chain simultaneously cuts power to the boron-rod magnets, driving the boron rods into the core, and cuts power to the fueled-rod magnets, driving the fueled rods out of the core. As a redundancy to the above actions, opening of the scram chain also opens the control power chain, which, in turn, actuates a boron-rod scram and a fueled-rod scram and initiates table separation.

Figure 65 is a simplified circuit diagram (showing eight of the 10 channels). The primary VTRZ inner-matrix-assembly high-pressure scram channel for each half-zone is composed of a static pressure-sensing line, a differential-pressure switch, and associated electronics. The redundant high-pressure scram channel for each half-zone comprises a static pressure-sensing line, a pressure transducer, and associated electronics. For high-temperature scrams in either half-zone, the primary channel includes a sensing thermocouple, a sensing amplifier, and scram trip circuitry. The two redundant high-temperature channels per half-zone have circuits identical to the primary channel. There is no coupling between the high-temperature scram circuitry and the VTRZ temperature monitoring system, specifically the scanners and the multipoint recorders.

An identical temperature scram system (95°C) is now used on both ZPR-6 and -9. The scram circuitry is outlined in Table 15. All the scram relays are normally energized, all pressure switches are normally closed, and, where necessary, other electronic circuits are in fail-safe configurations. In the event of a scram, all the abnormal-condition lamps remain on and relays remain deenergized until the abnormal condition is corrected and the relays manually reset. If the positive portion (+15 V) of the scram-trip-circuit power supply for a given chassis fails, all the corresponding alarm, heater-interlock, and scram lamps for that chassis light. If the negative portion (-15 V) of the scram trip circuit power supply fails, a

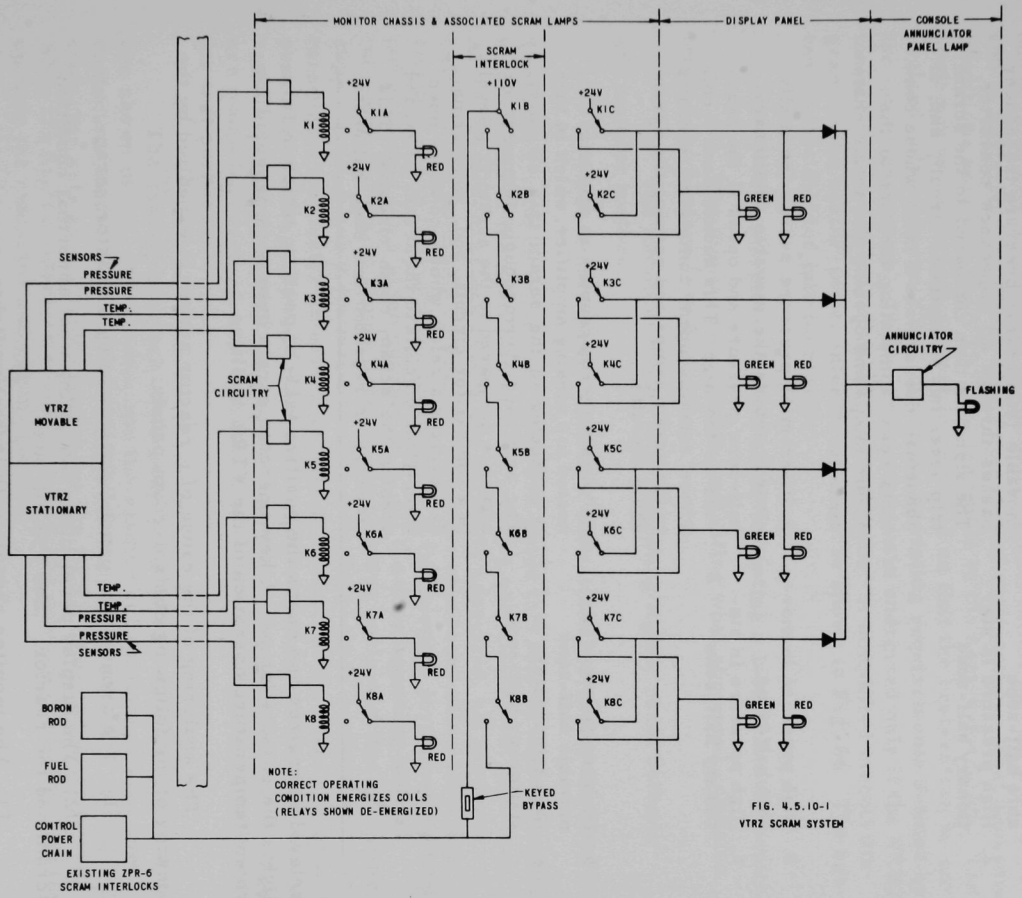

Fig. 65. VTRZ Scram System

TABLE 15. VTRZ Scram Conditions and Circuitry

Scram Condition	Scram Circuitry
1. High pressure in movable half-zone 2. High pressure in stationary half-zone	A continuous electrical signal from the movable (stationary) pressure transducer passes through an impedance converter. The signal is then compared to the scram trip level in a comparitor circuit, and, if abnormal, deenergizes a relay whose contacts open, completing circuits to the scram lamps and opening the scram chain circuits.
3. High pressure in movable half-zone 4. High pressure in stationary half-zone	A differential-pressure switch (normally closed) senses the movable (stationary) half-zone pressure and opens if the pressure is too high. This deenergizes a coil whose contacts open, completing circuits to the scram lamps and opening the scram chain circuits.
5. High temperature in movable half-zone 6. High temperature in stationary half-zone	A "scram thermocouple" is directly connected to a sensing amplifier, which in turn is connected to the scram trip circuitry. The amplified thermocouple temperature signal is compared to the scram trip level in a comparitor circuit, and, if abnormal, deenergizes a relay whose contacts open, completing circuits to the scram lamps and opening the scram chain circuits. This circuitry is repeated for each half-zone.

relay deenergizes and opens the positive (+15-V) portion, which in turn lights the chassis lamps. A key-operated scram bypass is provided for room-temperature operation of the VTRZ facility.

The analyzing of the cause of a reactor scram is expedited by the viewing of the following control-room panels:

(1) The annunciator panel light indicating a reactor scram.

(2) The display panel lights indicating what abnormal condition scrammed the reactor. (See Fig. 68 later).

(3) The monitor chassis with indicating lights, reset buttons, and monitor meters.

4.5.11 Heater-power-interlock System

Removal of all heater power by causing the opening, or preventing the closure, of the main circuit breaker that feeds all 12 VTRZ heater buses is an effective means of ensuring correct initial startup conditions and of mitigating the effect of any operational malfunction. Most abnormal conditions unique to the VTRZ are traceable to the heater operation. The heater-power interlock system is arranged so that the heaters can be energized only after the VTRZ meets the operating requirements defined by the interlock system. The heaters can remain energized only if the VTRZ maintains these required operating conditions. A simplified circuit diagram of the heater-power interlock system is shown in Fig. 66. The system can be divided into four parts:

(1) The annunciator panel light, indicating a loss of heater power.

(2) The display panel lights, indicating what abnormal condition tripped the heaters (see Fig. 68).

(3) The monitor chassis with indicating lights, reset buttons, and monitor meters.

(4) The heater-power interlock chain itself, including the contactor.

The heater-interlock trip conditions are listed in Table 16 together with a brief outline of the heater-interlock circuitry associated with each trip. All the heater-interlock relays are normally energized, all pressure switches are normally closed, and wherever necessary other electronic circuits are in fail-safe configurations. If the positive portion of the trip power supply for a given chassis fails, all the corresponding heater-interlock and alarm lamps light. If the negative portion of this trip power supply fails, a relay deenergizes and opens the positive portion, which in turn lights the heater-interlock and alarm lamps. In the event of a heater power trip, the appropriate abnormal-condition lamps remain on and relays remain deenergized until the abnormal condition is corrected and the relays are manually reset. A key-operated heater-interlock bypass is provided for test purposes.

The heater-interlock chain is made up of 25 relays (four of which are shown in Fig. 66), a cable into the reactor cell, and the heater power contactor (Model 712EDB combination starter with disconnect switch). The contactor acts as a circuit breaker for the VTRZ heater electric power. When the heater-interlock chain is broken, the contactor coil deenergizes, opening the contactor and cutting power.

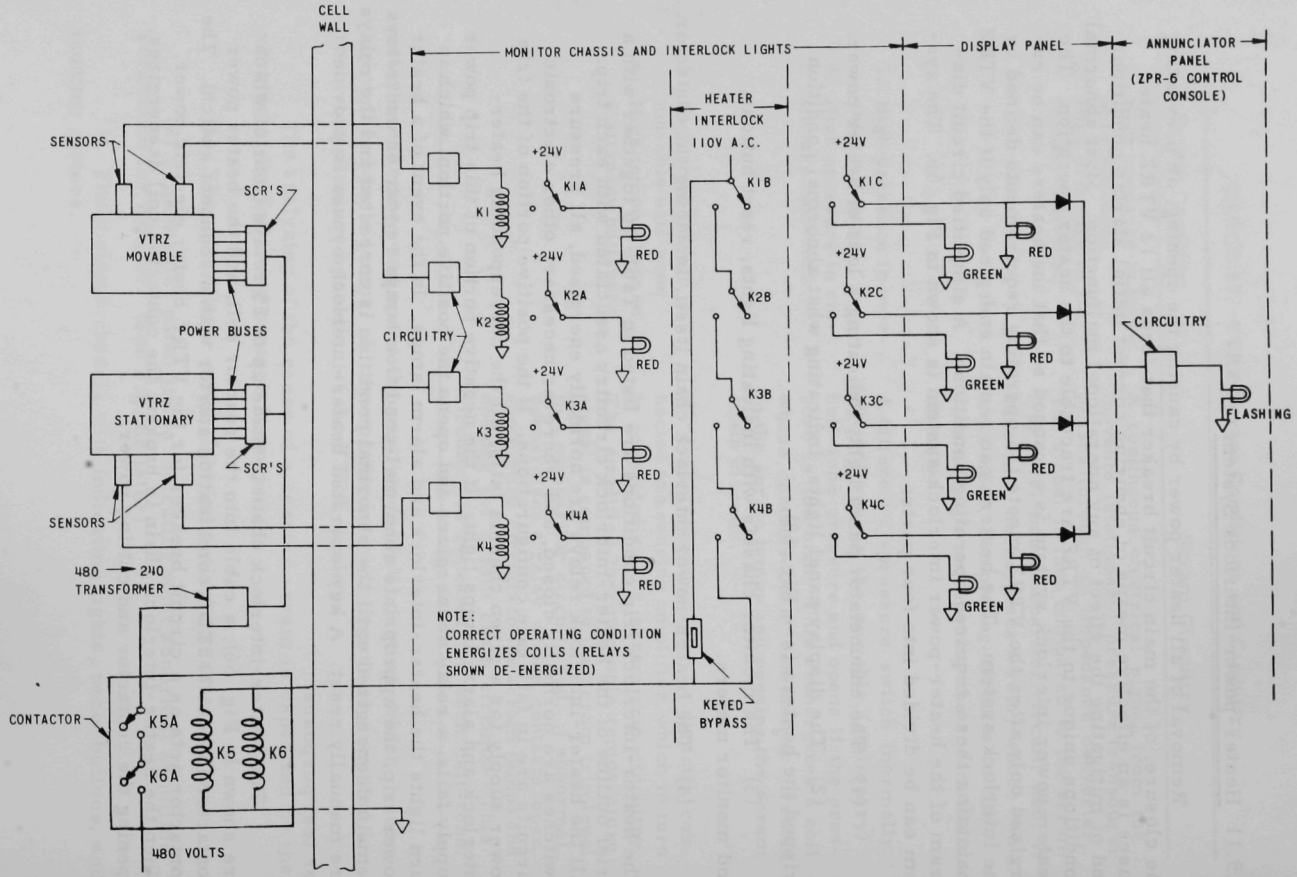

Fig. 66. Heater-power-interlock System (considering only four of the monitors)

TABLE 16. VTRZ Heater-interlock Conditions and Circuitry

Heater-interlock Condition	Heater-interlock Circuitry
1. High pressure in movable half-zone 2. Low pressure in movable half-zone 3. High pressure in stationary half-zone 4. Low pressure in stationary half-zone	A continuous signal from the pressure transducer passes through an impedance converter. The signal is then compared to the heater-interlock trip level in a comparator circuit, and, if abnormal, deenergizes a relay whose contacts open, completing circuits to lamps and opening the circuit in the interlock chain.
5. Low argon flow in movable half-zone 6. Low argon flow in stationary half-zone	The flowmeter float breaks a light-beam circuit to a photoresistor if the flow is low. This deenergizes a relay whose contacts open, completing circuits to lamps and opening the circuit in the interlock chain.
7. High oxygen content in movable half-zone 8. High oxygen content in stationary half-zone 9. High water-vapor content in movable half-zone 10. High water-vapor content in stationary half-zone 11. High helium content	A continuous oxygen-content signal passes through an impedance converter, is then compared to the heater-interlock trip level in a comparator circuit, and, if abnormal, deenergizes a relay whose contacts open, completing circuits to lamps and opening the circuit in the interlock chain.
12. Low flow in movable CGR exhaust No. 1 13. Low flow in movable CGR exhaust No. 2 14. Low flow in stationary CGR exhaust No. 1 15. Low flow in stationary CGR exhaust No. 2	A differential-pressure switch (normally closed) opens if the flow is too low. This deenergizes a relay whose contacts open, completing circuits to lamps and opening the circuit in the interlock chain.
16. High Pu-alpha content in movable half-zone 17. High Pu-alpha content in stationary half-zone	The trip circuit is operated by a voltage proportional to the logarithm of the number of Pu-alpha counts. If the total logged counts over the summation interval exceed the trip-level setting, the trip circuit is actuated by deenergizing a relay whose contacts open, completing circuits to lamps and opening the circuit in the interlock chain.
18. High temperature on movable multipoint recorder 19. High temperature on stationary multipoint recorder 20. High temperature on cold-zone multipoint recorder	A microswitch on the multipoint recorder cam opens on a preset high temperature, deenergizing a relay whose contacts open, completing circuits to lamps and opening the circuit in the interlock chain.
21. High temperature in scanner	For the scanner-printer system, temperature signals from the digital voltmeter are compared to the interlock trip level in a temperature-comparator circuit, and, if abnormal, deenergize a relay whose contacts open, completing circuits to the interlock lamps and opening the circuit in the interlock chain.
22. Movable bus cover open 23. Stationary bus cover open	Two "captive-key"-type switches in series must be closed to complete the interlock chain circuit. The keys can only be removed from the switches (in order to unlock the bus covers) if they are open.
24. Short in movable sodium monitor 25. Short in stationary sodium monitor	Upon shorting, the 8-V monitoring voltage drops to zero. This deenergizes a relay whose contacts open, completing circuits to lamps and opening the circuit in the interlock chain.
26. Helium filament off 27. Movable water-vapor-monitor range-switch position incorrect 28. Stationary water-vapor-monitor range-switch position incorrect 29. Movable oxygen-monitor range-switch position incorrect 30. Stationary oxygen-monitor range-switch position incorrect 31. Movable oxygen-monitor power off 32. Stationary oxygen-monitor power off	These ON-OFF conditions are not part of the actual heater-interlock chain. However, the coils for the oxygen, helium, water-vapor, heater-interlock-chain relays cannot be energized unless these requirements are met. Lights indicating that these seven conditions are met are part of the alarm system.

Table 17 lists the possible ranges of the heater-interlock set points. The actual set points and justification for them are given in Sec. 3.2.2 of ANL-7638. The heater-interlock setpoints are always indicative of a more serious condition than that indicated by an alarm (as discussed in Sec. 4.5.12); the alarm condition is always sensed first. The contactor has two independent relays with their contacts connected in series and their coils connected in parallel.

TABLE 17. VTRZ Heater-interlock Conditions and Ranges[a]

Heater-interlock Condition	Range
1. High pressure in movable half-zone 2. High pressure in stationary half-zone	0.0 to +2.0 in. of water
3. Low pressure in movable half-zone 4. Low pressure in stationary half-zone	-5.5 to -2.0 in. of water
5. Low argon flow in movable half-zone 6. Low argon flow in stationary half-zone	0.25-0.40 ft^3/min
7. High oxygen content in movable half-zone 8. High oxygen content in stationary half-zone	1-1000 ppm
9. High water-vapor content in movable half-zone 10. High water-vapor content in stationary half-zone	0.01-400 ppm
11. High helium content	Greater than half reference signal[b]
12. Low flow in movable CGR exhaust No. 1 13. Low flow in movable CGR exhaust No. 2 14. Low flow in stationary CGR exhaust No. 1 15. Low flow in stationary CGR exhaust No. 2	For each exhaust, 1200-3000 ft/min (80-200 ft^3/min)
16. High Pu-alpha content in movable half-zone 17. High Pu-alpha content in stationary half-zone	1-10,000 Pu-alpha counts; 0.1-99.9 min
18. High temperature on movable multipoint recorder	580-650°C
19. High temperature on stationary multipoint recorder	580-650°C
20. High temperature on cold-zone multipoint recorder	30-150°C
21. High temperature on scanner	580-650°C

[a]The ranges given reflect only the capabilities of the instrumentation used for each condition.

[b]Reference signal = helium monitor response obtained for a 0.2-cm^3 helium injection into the operating argon loop at 20°C.

4.5.12 Alarm System

A system of alarms designed to warn the operator of slightly abnormal conditions in the VTRZ is present in the reactor control room. The purpose of the alarm system is twofold: First, it alerts the operator to improperly operating monitors--for example, the incorrect "range" alarm on the water-vapor monitor or the thermocouple burnout alarms on the temperature monitors. Second, it warns of actual VTRZ malfunctions, which could conceivably lead to improper system operation and/or safety hazards, e.g., an inner-barrel leak with a resulting increase in oxygen and water vapor or a shorted calandria heater resulting in a local inner-barrel temperature rise. If a further deterioration of a given malfunction occurs,

the heater-interlock system described in Sec. 4.5.11 and (possibly) the VTRZ scram system described in Sec. 4.5.10 come into play.

To provide immediate recognition of a VTRZ alarm condition and, at the same time, a rapid analysis of the specific problem, all but one of the alarm conditions signals simultaneously at three different control-room locations as shown in Fig. 67. For a given alarm condition, the VTRZ alarm lamp on the ZPR control-room console annunciator panel lights directing the operator to the VTRZ display panel shown in Fig. 68. The display panel in turn directs him to the specific alarm condition displayed on a particular chassis. The one alarm condition not monitored in three locations is the loss of filament current in the helium monitor. However, loss of filament current deenergizes a relay that is part of the heater-interlock trip chain; this is discussed in more detail in Sec. 4.5.11. Table 18 lists all the alarm conditions and outlines the alarm circuitry.

All VTRZ monitors that have power supplies and/or range switches located in the reactor cell have corresponding "power-on" and "correct-range" alarms in the control room. All alarm relays are normally energized, all differential pressure switches normally closed, and other electronic circuits in fail-safe configurations whenever necessary. If the positive portion of the trip power supply for a given chassis fails, all the corresponding alarm and trip lamps light. If the negative portion of the trip power supply fails, a relay deenergizes and opens the positive portion, which in turn lights the lamps. For a given abnormal condition, all the corresponding alarm lamps remain on until the abnormal condition is corrected and the relay manually reset by the operator.

Table 19 lists the possible ranges of the alarm set points. The actual set points are listed in Sec. 3.2.3 of ANL-7638.

4.5.13 Room-temperature Operation of the Heatable Zone

During the comparison experiments between the plate- and rodded-fuel assemblies, there will be situations in which room-temperature operation of the VTRZ with plate or rodded fuel in the inner matrix assembly will be required. For the rodded fuel, either heatable (15% voided at 20°C) or unheatable (full at 20°C) calandria cans may be involved and heaters may or may not be distributed throughout the inner matrix.

With plate-fuel drawers in the VTRZ inner barrel assembly, no heating will be permitted. The only possible heat source in this case is the flange and service-housing heaters; these heaters will be disconnected whenever plate-fuel drawers are within the inner matrix. Operation with or without the front and rear (service-housing) inner-barrel covers is permitted with the plate fuel. If the plate fuel is plutonium, air cooling of the inner matrix region will be necessary to achieve thermal equilibrium with

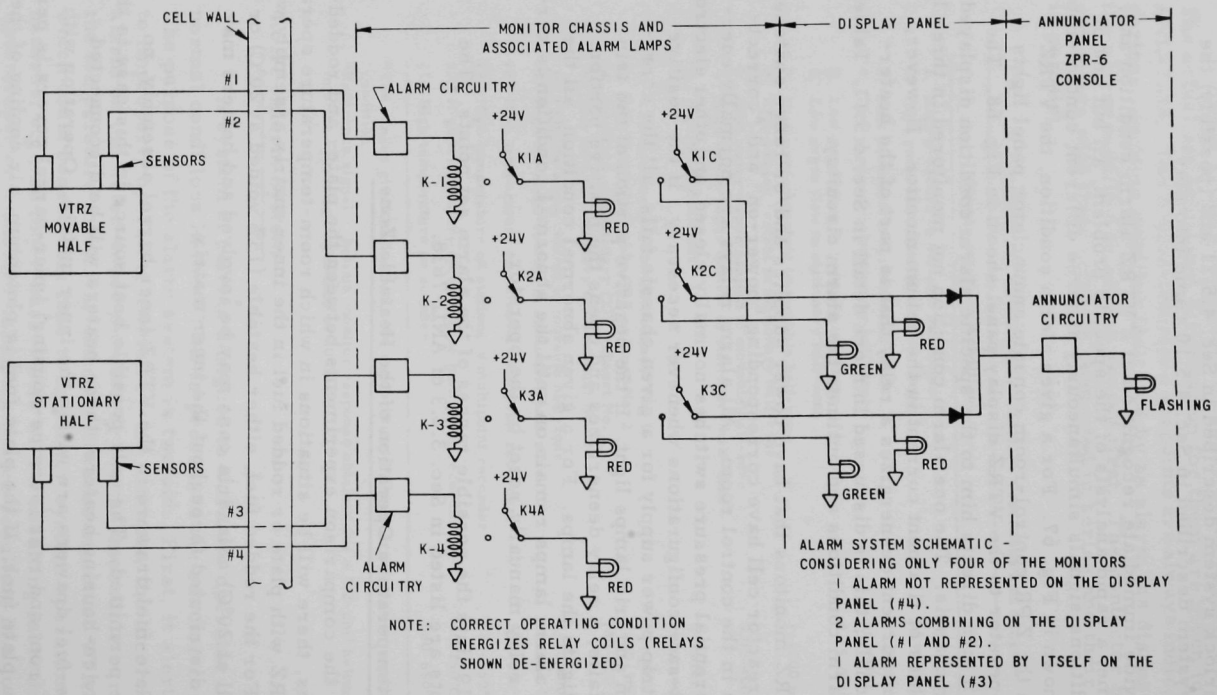

Fig. 67. VTRZ Alarm System

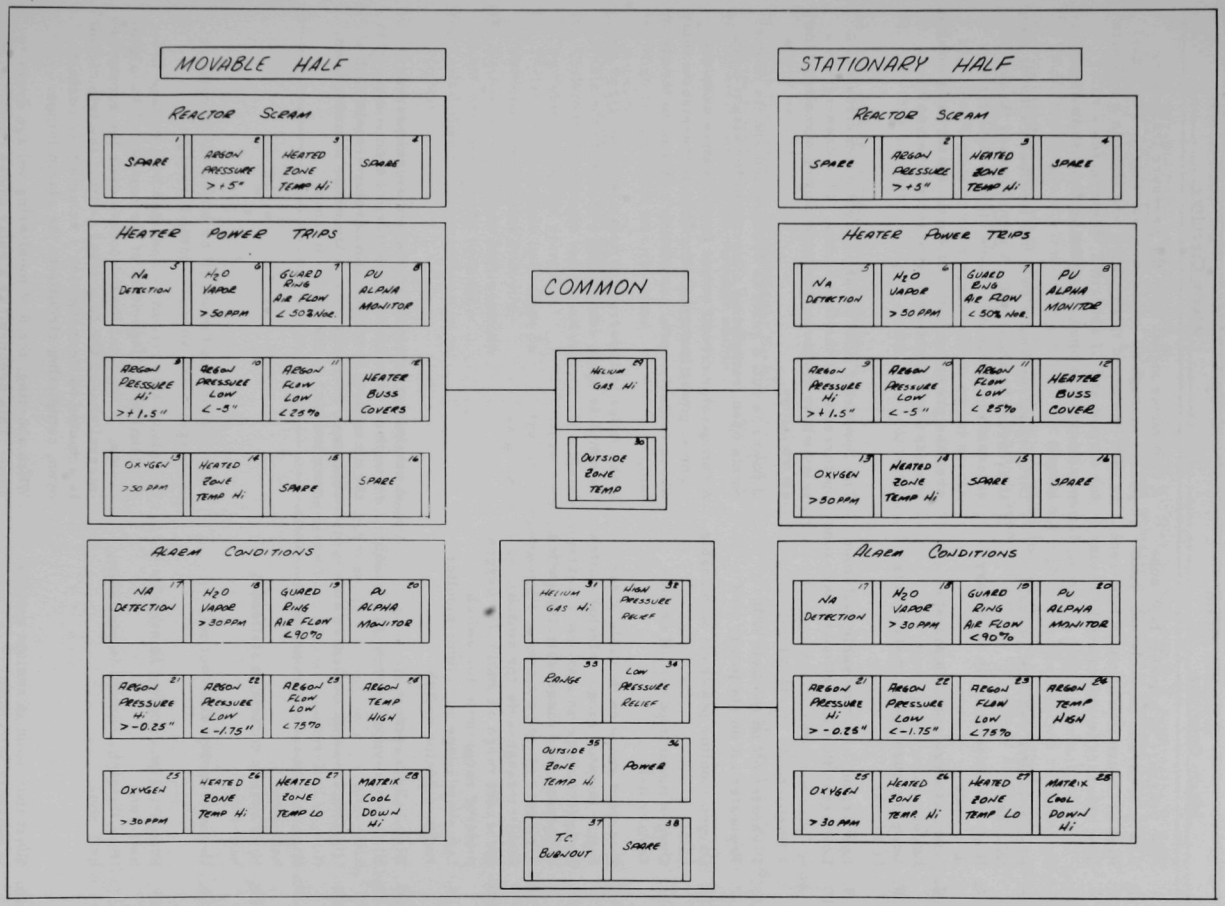

Fig. 68. VTRZ Display Panel

TABLE 18. VTRZ Alarm Conditions and Circuitry

Alarm Condition	Alarm Circuitry
1. High pressure in movable half-zone 2. Low pressure in movable half-zone 3. High pressure in stationary half-zone 4. Low pressure in stationary half-zone	A continuous signal from the pressure transducer passes through an impedance converter. The signal is then compared to an alarm trip level in a comparator circuit and, if abnormal, deenergizes a relay whose contacts open, completing circuits to alarm lamps.
5. High-pressure relief in movable half-zone 6. High-pressure relief in stationary half-zone 7. Low-pressure relief in movable half-zone 8. Low-pressure relief in stationary half-zone	Differential-pressure switches (normally closed) open if pressure is abnormal. A signal passes through the solenoid and pneumatic-valve digital-logic circuit. Alarm lamps on the Argon Flow System Panel light when the pressure switches open. Alarm lamps on the Display Panel light when appropriate valves open.
9. Low argon flow in movable half-zone 10. Low argon flow in stationary half-zone	The flowmeter float breaks a light-beam circuit to a photoresistor if the flow is low. This deenergizes a relay whose contacts open, completing circuits to the alarm lamps.
11. Preheater off on movable half 12. Preheater off on stationary half	If power is cut, a relay is deenergized and its contact points open, completing a circuit to the alarm lamp.
13. Oxygen monitor power off on movable half 14. Oxygen monitor power off on stationary half	A comparator circuit output goes negative when the monitor power is turned off. This deenergizes a relay whose contacts open, completing a circuit to the alarm lamp.
15. Incorrect range on movable water-vapor-monitor range-selector switch 16. Incorrect range on stationary water-vapor-monitor range-selector switch 17. Incorrect range on movable oxygen-monitor range-selector switch 18. Incorrect range on stationary oxygen-monitor range-selector switch 19. Incorrect range on helium-monitor range-selector switch	If the range is incorrect, a relay is deenergized and its contacts open, completing a circuit to the alarm lamp.
20. High helium content 21. High water-vapor content in movable half-zone 22. High water-vapor content in stationary half-zone 23. High oxygen content in movable half-zone 24. High oxygen content in stationary half-zone	A continuous foreign-gas-content signal passes through an impedance converter, is then compared to the alarm trip level in a comparator circuit, and, if abnormal, deenergizes a relay whose contacts open, completing circuits to alarm lamps.
25. Helium monitor filament off	If the filament is turned off or burns out, a relay is deenergized and an alarm lamp turned on.
26. High Pu-alpha content in movable half-zone 27. High Pu-alpha content in stationary half-zone	The alarm trip circuit is operated by a voltage proportional to the logarithm of the number of Pu-alpha counts. If the total logged counts over the summation interval exceed the trip-level setting, the trip circuit is actuated by deenergizing a relay whose contacts open, completing circuits to the alarm lamps.
28. Short indication in sodium monitor in movable half-zone 29. Short indication in sodium monitor in stationary half-zone	When shorting, the 8-V monitoring voltage drops to zero. This deenergizes a relay whose contacts open, completing circuits to the alarm lamps.

TABLE 18 (Contd.)

Alarm Condition	Alarm Circuitry
30. Loss-of-continuity indication in sodium monitor in movable half-zone 31. Loss-of-continuity indication in sodium monitor in stationary half-zone	If continuity is broken, the 8-V monitoring voltage reverses polarity and lights a discontinuity alarm lamp.
32. High flow in movable IMCD exhaust No. 1 33. High flow in movable IMCD exhaust No. 2 34. High flow in stationary IMCD exhaust No. 1 35. High flow in stationary IMCD exhaust No. 2	A differential-pressure switch (normally closed) opens if flow is too high. This deenergizes an intermediate relay, which in turn deenergizes another relay whose contacts open, completing circuits to alarm lamps.
36. Low flow in movable CGR exhaust No. 1 37. Low flow in movable CGR exhaust No. 2 38. Low flow in stationary CGR exhaust No. 1 39. Low flow in stationary CGR exhaust No. 2	A differential-pressure switch (normally closed) opens if flow is too low. This deenergizes a relay whose contacts open, completing circuits to alarm lamps.
40. High temperature on movable multipoint recorder 41. High temperature on stationary multipoint recorder 42. Low temperature on movable multipoint recorder 43. Low temperature on stationary multipoint recorder 44. High temperature on cold-zone recorder 45. High temperature on scanner	A microswitch on the multipoint recorder cam opens on a preset abnormal temperature, deenergizing a relay whose contacts open, completing circuits to the alarm lamps.
46. Failed-thermocouple indication on movable multipoint recorder 47. Failed-thermocouple indication on stationary multipoint recorder 48. Failed-thermocouple indication on cold-zone multipoint recorder 49. Failed-thermocouple indication on scanner	If a thermocouple fails, it gives an abnormal temperature reading of <5°C. Alarm circuitry is identical to that for abnormal temperature (with set point at 5°C) as given in 40-45 above.
50. High-combustibles-content indication on combustibles monitor 51. High-oxygen-content indication on combustibles monitor	A continuous foreign-gas-content signal passes through an impedance converter, is then compared to the alarm trip level in a comparator circuit, and, if normal, deenergizes a relay whose contacts open, completing circuits to alarm lamps.

TABLE 19. VTRZ Alarm Conditions and Ranges[a]

Alarm Condition	Range
1. High pressure in movable half-zone	-1 to +1 in. of water
2. Low pressure in movable half-zone	-2 to -1 in. of water
3. High pressure in stationary half-zone	-1 to +1 in. of water
4. Low pressure in stationary half-zone	-2 to -1 in. of water
5. High-pressure relief in movable half-zone	+1 to +4.5 in. of water
6. High-pressure relief in stationary half-zone	+1 to +4.5 in. of water
7. Low-pressure relief in movable half-zone	-40 to -8 in. of water
8. Low-pressure relief in stationary half-zone	-40 to -8 in. of water
9. Low argon flow in movable half-zone	0.75 to 1.0 ft^3/min
10. Low argon flow in stationary half-zone	0.75 to 1.0 ft^3/min
11. Preheater off on movable half	-
12. Preheater off on stationary half	-
13. Oxygen monitor power off on movable half	-
14. Oxygen monitor power off on stationary half	-
15. Incorrect range on movable water-vapor-monitor range-selector switch	-
16. Incorrect range on stationary water-vapor-monitor range-selector switch	-
17. Incorrect range on movable oxygen-monitor range-selector switch	-
18. Incorrect range on stationary oxygen-monitor range-selector switch	-
19. Incorrect range on helium-monitor range-selector switch	-
20. High helium content	Greater than 1/5 reference signal[b]
21. High water-vapor content in movable half-zone	0.01-400 ppm
22. High water-vapor content in stationary half-zone	0.01-400 ppm
23. High oxygen content in movable half-zone	1-1000 ppm
24. High oxygen content in stationary half-zone	1-1000 ppm
25. Helium monitor filament off	-
26. High Pu-alpha content in movable half-zone	1-10,000 Pu-alpha counts; 0.1-99.9 min
27. High Pu-alpha content in stationary half-zone	
28. Short indication in sodium monitor in movable half-zone	-
29. Short indication in sodium monitor in stationary half-zone	-
30. Loss-of-continuity indication in sodium monitor in movable half-zone	-
31. Loss-of-continuity indication in sodium monitor in stationary half-zone	-
32. High flow in movable IMCD exhaust No. 1	For each exhaust 20-80 ft^3/min
33. High flow in movable IMCD exhaust No. 2	
34. High flow in stationary IMCD exhaust No. 1	
35. High flow in stationary IMCD exhaust No. 2	
36. Low flow in movable CGR exhaust No. 1	For each exhaust 1200-3000 ft/min (80-200 ft^3/min)
37. Low flow in movable CGR exhaust No. 2	
38. Low flow in stationary CGR exhaust No. 1	
39. Low flow in stationary CGR exhaust No. 2	
40. High temperature on movable multipoint recorder	Less than 590°C
41. High temperature on stationary multipoint recorder	Less than 590°C
42. Low temperature on movable multipoint recorder	Variable
43. Low temperature on stationary multipoint recorder	Variable
44. High temperature on cold-zone recorder	30-100°C
45. High temperature on scanner	Less than 590°C
46. Failed-thermocouple indication on movable multipoint recorder	About 5°C
47. Failed-thermocouple indication on stationary multipoint recorder	About 5°C
48. Failed-thermocouple indication on cold-zone multipoint recorder	About 5°C
49. Failed-thermocouple indication on scanner	About 5°C
50. High-combustibles-content indication on combustibles monitor	Variable
51. High-oxygen-content indication on combustibles monitor	5-50,000 ppm

[a]The ranges given reflect only the capabilities of the instrumentation used for each condition.
[b]Reference signal = helium-monitor response obtained for a 0.2-cm^3 helium injection into the operating argon loop at 20°C.

the plutonium-alpha self-heating. This will require operation with the front and rear covers of both half-zones removed to permit the regular reactor-matrix air-cooling system to cool the inner matrix in the same manner as it cools the outer matrix.

The same considerations and operating configurations apply to the rodded-fuel assemblies used in room-temperature tests, except that the cartridge heaters may be installed in the calandria cans. Electrical connection of the cartridge heaters to the heater power supplies will not be permitted unless the front and rear covers are also installed and the inert-cover-gas blanket established.

4.5.14 Miscellaneous Auxiliary VTRZ Components

4.5.14.1 Control- and Safety-rod Mounting Plates

The drive units for the ZPR safety and control rods for each reactor half are mounted on a $1\frac{1}{4}$-in.-thick steel plate, called the control- and safety-rod (CSR) mounting plate. One CSR plate is mounted vertically at the rear of each reactor table parallel to the rear face of the reactor matrix and 28 in. behind it. In the present ZPR configuration, the CSR mounting plates form the rear wall of the reactor-matrix cooling-air plenum behind each reactor half-matrix; the CSR mounting plate is shown in Fig. 6.

Special CSR mounting plates are required with the VTRZ to provide penetrations for cooling guard-ring and inner-matrix cooldown air-cooling-system ducts, inert-gas-loop piping, electrical power leads, instrument leads, and experimental equipment and provide the normal control- and safety-rod-drive mounting holes. Secondarily, the design of the VTRZ CSR mounting plates permits use of the plates when the VTRZ was not installed. Use of the CSR mounting plate as a wall of the matrix air-circulation plenum requires all penetrations to be reasonably airtight. The CSR mounting plates operate at room temperature. Figure 69 shows the design of the VTRZ CSR mounting plates.

Duct and piping penetrations for the air and inert gas systems are shown in Fig. 69. The design of the air and inert-gas systems between the matrix and the mounting plate is discussed in Secs. 4.5.5 and 4.5.6. Inevitably, the presence of these ducts restricts the possible safety- and control-rod mounting locations. This restriction has been minimized by placing all penetrations, as much as possible, either where these rods cannot be mounted (as over the insulation annulus) or where it is not foreseen that they would be desired. Behind the mounting plates, all ducts are carried straight back beyond the rear of the control- and safety-rod drives before turning to avoid further interference with the rod drives. Relocation of rod drives will probably require demounting sections of the VTRZ ducting behind the mounting plate; this has been provided for in the design. When

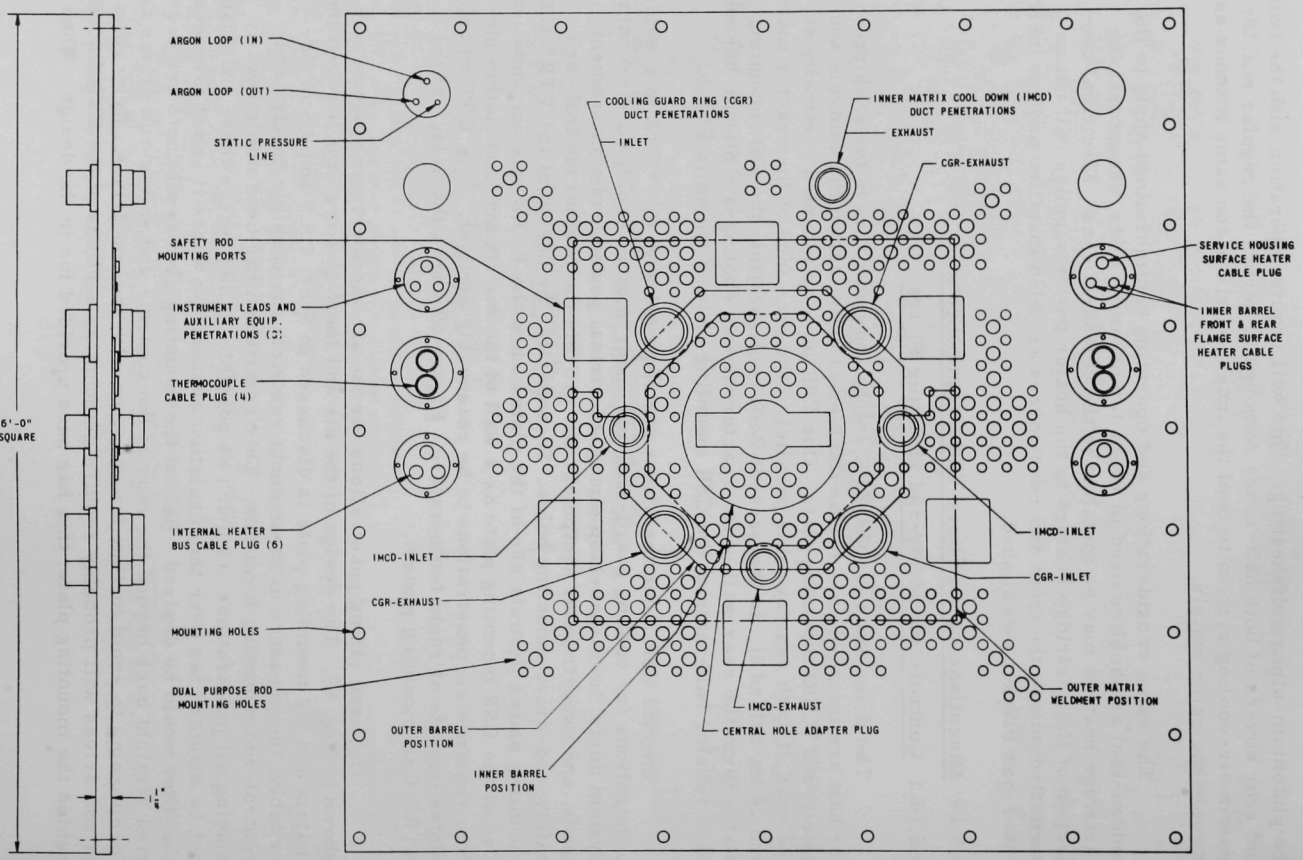

Fig. 69. VTRZ Dual-purpose Rod-mounting Plates

the VTRZ mounting plate is used without the VTRZ, the duct penetrations could be used for rod-mounting locations through the use of appropriate inserts.

The center of each VTRZ CSR mounting plate has a 14-in.-dia circular cutout to permit complete access for experimental equipment to the rear port on each inner-barrel-assembly half-zone service housing; the outer diameter of the bolting flange on the service housing port is $11\frac{1}{2}$ in., the port itself is 10 in. in diameter (permitting access to the central nine removable tubes). When this hole is not needed, it may be filled with the special insert plate shown in Fig. 69, which itself has a central 5-in.-dia experimental access hole and horizontal slot extensions to permit use of the ZPR-6 and -9 sample changer in the five central tubes of the central horizontal row.

Provision is made in the VTRZ CSR mounting plate for six safety-rod positions (the square cutouts). Numerous control-rod mounting locations are provided in the VTRZ CSR mounting plates. Additional control-rod positions will be added if they later prove to be needed.

Penetrations for the heater and instrument leads and also for the inert-gas-loop piping are shown in Fig. 69. These penetrations are placed at the outer extremities of the CSR plate so as to be as much out of the way as possible.

4.5.14.2 Reactor-knee Constraints

The design stress analysis and load testing of the outer-matrix bridge assembly has assumed firm horizontal support of the reactor matrix by the reactor knee assemblies. To ensure that the reactor knees do not move under any circumstances, and considering the uncertainty of the frictional resistance caused by the knee-to-table bolting, the VTRZ design has provided for special constraint assemblies on the knees to prevent horizontal motion. Assuming the 18,000-lb load limit over the inner-barrel-assembly cavity (see Table 5), not more than 13,000 lb of horizontal thrust can be applied to the reactor knees under static conditions, even under the most conservative assumptions. Actually, the horizontal thrust is estimated to be about 20% of that figure. To be very conservative, however, the knee-constraint design has been based on the earthquake criteria of Table 2 and the maximum permissible table load of 180,000 lb (this limit is taken from Ref. 2) shown in Table 6; i.e., 180,000 x 0.4 = 72,000 lb horizontal thrust against one knee acting alone without benefit of the knee-to-knee tie rods or horizontal friction from knee-to-table bolting. The knee constraint takes the form of a 48 x 16 x $1\frac{1}{2}$-in. mild steel plate bolted to the side of the table with four 3/4-10 high-strength bolts so as to overlap the base of the knee; the arrangement is shown in Fig. 70. Stress analysis of the constraint is given in Sec. 6.6.

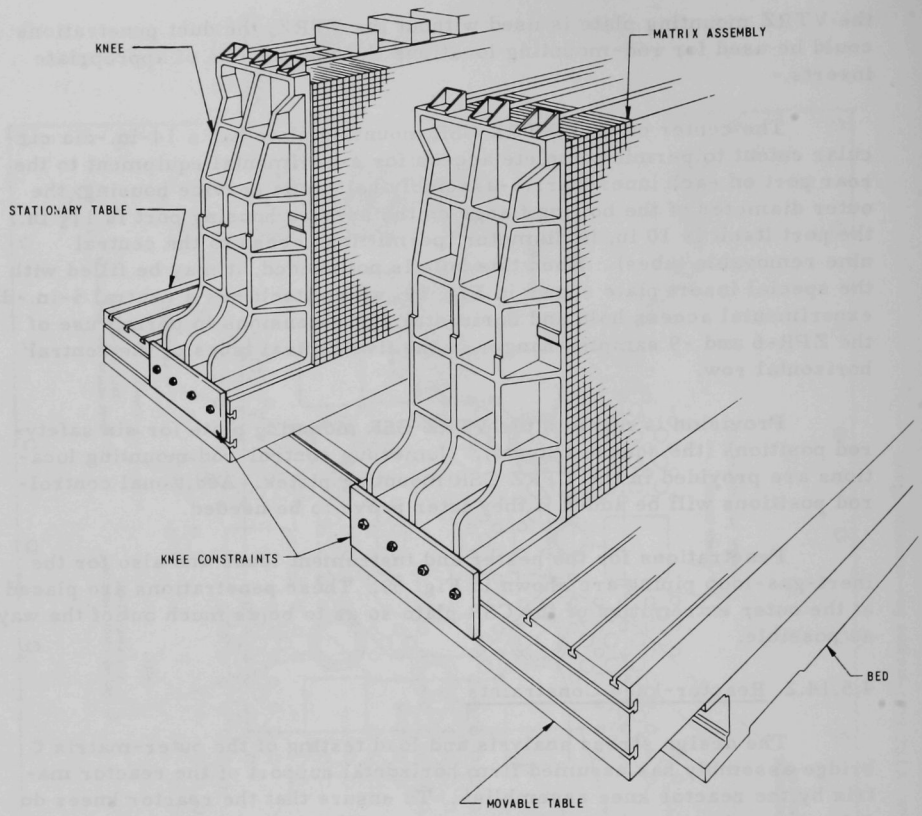

Fig. 70. Knee Constraint

4.5.14.3 Manually-mountable Front Insulation-support Covers

Under some operating circumstances, it will be convenient to have the inner matrix assemblies significantly above room temperature with the reactor halves separated. The design includes special front-cover manually-mountable insulation and support covers to be placed over the exposed inner-matrix-assembly front covers (between the reactor halves) in these operating circumstances. The covers serve three purposes: personnel burn protection, VTRZ insulation, and physical support for the thin (20-mil) front covers when positive internal pressures are applied to the inner matrix assembly for leak-test purposes.

The insulation and support covers are slightly larger than the front inner-matrix-assembly covers and basically consist of a 1/8-in.-thick stainless steel plate (against the front cover) backed by 1 in. of insulation.

4.5.15 Experimental Equipment

The VTRZ has been designed to permit the maximum operational flexibility for the performance of experiments consistent with the technical design criteria and with relevant safety considerations. The principal provisions made in the design for experimental flexibility are as follows:

(1) The front and rear covers over the heatable matrix of each half-zone are bolted on and easily removable. This permits complete access to the front and rear of every matrix tube.

(2) The central nine matrix tubes within each heatable half-zone are removable one-by-one, or as a group, to permit replacement by an instrument thimble or other special equipment.

(3) The rear cover (service housing) has a port and the control-rod mounting plate (behind the matrix) has a cutout which permit direct (straight-in) access to the central nine tube locations for the insertion of an instrument thimble or other equipment.

(4) The internal heating system of each heatable half-zone consists of many individual heaters (of several possible lengths), which can be flexibly located and which can be grouped into three independently supplied power groups to permit flexible zonal heating.

(5) Internal temperature monitoring is completely flexible as to location.

(6) There is no serious limitation on experimental equipment weight within the heatable zone.

(7) With the front cover removed (i.e., at room temperature), there is provision for use of the ZPR radial sample changer in the central horizontal row of tubes.

The principal considerations in the design of special experimental equipment for the VTRZ are the maintenance of the sealed inert-gas envelope and the avoidance of intolerable thermal stresses.

The design of special experimental equipment to be used with the VTRZ at elevated temperatures is not complete. The most significant portion of this equipment is that which will permit central-reactivity measurements on various samples of various sizes--for example, sodium-void measurements, Doppler measurements, and material worths. The design of this special equipment will be carried out within the design of the basic VTRZ components described in this report and within the operating limits specified in ANL-7638. The thimble and oscillator designs discussed in this section are intended only as illustrations of the type of equipment that can be used with the VTRZ. If any of the final designs include parts that connect between the reactor halves, provisions will be included for a breakaway feature to ensure that the reactor halves cannot be prevented from separating.

The thimble to be used for central-reactivity measurements must provide the following features:

(1) The interior of the thimble is to be thermally isolated from the heated zone of VTRZ. With the heated zone operating at 550°C, the interior walls of the thimble should not exceed 50°C (120°F) at any point.

(2) The thimble should have a minimal perturbing effect on the hot-zone temperature distribution and on the neutron spectrum. To this end, the following requirements have been established:

a. The rate of heat loss shall be less than 200 W per linear foot of thimble.

b. Significant amounts of light materials ($A < 20$) shall not be included in the design.

c. The total thickness of materials in the radial direction between the interior of the thimble and the adjacent fuel-diluent plates or calandria cans shall be less than 0.25 in. of Type 304 stainless steel, or its equivalent.

d. Neutron-streaming channels shall be held to a minimum.

(3) Identical straight-through thimbles are needed for both VTRZ half-zones, with provisions made for axial alignment.

(4) The thimbles are to be flush with the VTRZ front covers and open, with no protrusions extending across the reactor midplane.

(5) The maximum OD of the thimble shall be ≤6.5 in. (three drawer widths) to fit within the space provided by the removal of the nine central VTRZ matrix tubes.

(6) The thimble shall be located at the radial center of the VTRZ heated zone.

(7) Seals and bellows are required as necessary to maintain at all operating conditions the integrity of the sealed inert-gas-filled envelope in the VTRZ inner matrix assembly with the thimble installed.

(8) The thimble must support internal moving loads of 25 lb/ft.

(9) The principal material of construction shall be Type 304, 304L, or 316 stainless steel, which dictates a maximum operating temperature of 600°C.

(10) The thimble design should be such as to minimize installation and removal time.

(11) With the thimble installed, the VTRZ design criteria (see Chapter 2) must not be compromised. Where applicable, the thimble shall meet these VTRZ design criteria.

The thimble is to be fabricated from three concentric, thin-walled, stainless steel tubes. To minimize the radial heat-transfer rate across the thimble walls, the outer annulus formed by this three-tube arrangement will be evacuated and its facing surfaces will be polished and coated with a thin layer of gold. Air flowing through the inner annulus will provide the cooling required to maintain the central cavity, in which reactivity measurements are to be made, at room temperature. A fourth tube will support the thimble along the central axis of the heatable zone. To maintain the sealed inert-gas envelope in the VTRZ inner matrix assembly, one end of this support tube will be welded onto the 20-mil portion of a specially fabricated front cover and the other end sealed with a bellows to the rear-port bolting flange. Identical thimbles will be mounted in each reactor half with provisions for axial alignment. Access to the inside of the thimble is from behind the control-rod mounting plate.

5. HEAT-TRANSFER ANALYSES AND TESTS

5.1 Room-temperature Operation of Calandria-can Assemblies with $(Pu,U)O_2$ Fuel Rods

5.1.1 Plutonium-alpha Self-heating

The alpha decay of the plutonium isotopes in the $(Pu,U)O_2$ fuel rods results in significant self-heating in the rods. This is the same situation as is present in the Pu-U-Mo fuel plates, and it is intended that the matrix air-cooling system, used to remove alpha-decay heat from the plutonium plates, will also be used to maintain near-room-temperature conditions within the inner barrel assembly during nominal room-temperature operation. To achieve matrix air cooling of the inner matrix, it is only necessary to leave the front and rear (service housing) covers off; this exposes the inner matrix to the air plenum behind each matrix.

Table 20 summarizes the calculated plutonium-alpha self-heating in the fuel rods.

TABLE 20. Calculated Pu-alpha Self-heating in $(Pu,U)O_2$ Fuel Rods

		11.5%-240 Fuel		High-240 Fuel	
Pu Isotope	Heat Generation, W/g	Nominal Isotope, g/g Pu	Heat Generation, W/g	Nominal Isotope, g/g Pu	Heat Generation, W/g
238	5.51×10^{-1}	0.0005	0.276×10^{-3}	0.0009	0.496×10^{-3}
239	1.87×10^{-3}	0.8640	1.616×10^{-3}	0.6730	1.259×10^{-3}
240	6.90×10^{-3}	0.1150	0.794×10^{-3}	0.2593	1.789×10^{-3}
241[a]	41.70×10^{-3}	0.0180	0.751×10^{-3}	0.0526	2.193×10^{-3}
242	7.83×10^{-5}	0.0025	-	0.0142	0.001×10^{-3}
			3.4×10^{-3}		5.7×10^{-3}

Rod Type	Nominal Weight of Pu per Rod, g	Alpha Heating, W/rod
15%	11.9	0.040
30%	23.7	0.080
High 240	14.4	0.082

[a]Includes ^{241}Am effect at 5 years.

5.1.2 Inner-matrix Air-cooling System

The design and operation of the matrix air-cooling system is discussed in Sec. IV.D of ANL-7442. The nominal operating parameters for this system are 5 ft^3/min airflow per tube at a total 18 in. H_2O pressure

drop across the two halves of the reactor (assuming two 33-in. drawers with cutdown ends). With the front and rear inner-barrel-assembly covers removed, matrix air cooling of fuel drawers containing plutonium plates or of calandria cans containing $(Pu,U)O_2$ will occur just as in the outer matrix in general.

The calandria can outer (square) dimension, 2.039 (+0.000, -0.005) in., has been chosen to closely match the airflow area available around the regular fuel drawers, i.e., about 0.23 in.^{2}, assuming a 2.093-in.-square inside dimension on the matrix tube. Thus, approximately the same head loss is to be expected for axial matrix air-cooling flow over calandria cans and fuel drawers of the same length.

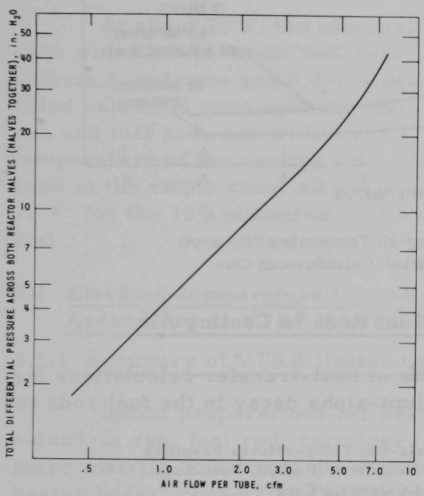

Fig. 71. Calculated Total Differential Pressure (halves closed) across Matrix for Three 12-in. Calandria Cans per Tube per Reactor Half (72-in. length); Matrix Cooling-air System

The calculated total head loss across the matrix with the halves closed, as a function of air flow rate, is plotted in Fig. 71 for three 12-in.-long, 2.038-in.-square, calandria cans per tube per reactor half, i.e., for a 72-in.-long calandria core. These calculations are based on experimental measurements of flow versus pressure drop with fuel drawers in the matrix tubes.

The temperature rise in the cooling air as it crosses the reactor matrix is a function of the flow rate per tube, the plutonium-alpha heating rate, and the pressure drop across the tube. Assuming 32 fuel rods per calandria can and three calandria cans per tube per reactor half, the alpha heating load is about 1.2 W per calandria for the 15% $(Pu,U)O_2$ rods and 2.4 W per calandria for the 30% and high-240 fuel rods. Figure 72 shows the calculated total temperature rise across the matrix (halves together) as a function of airflow rate per tube for three 12-in.-long, 2.038-in.-square calandria cans per tube per reactor half; the four central calandria cans are assumed to contain $(Pu,U)O_2$ fuel, and the outer two cans are assumed to contain depleted UO_2 fuel. The calculations of Fig. 72 account for frictional heating by the air as it passes through the tube and for the adiabatic-expansion cooling of the air as it expands through the tube. It is, in fact, true that the expansion cooling very nearly exactly balances the frictional heating in this system, so that the cooling-air temperature rise is essentially only a function of the plutonium-alpha heating rate.

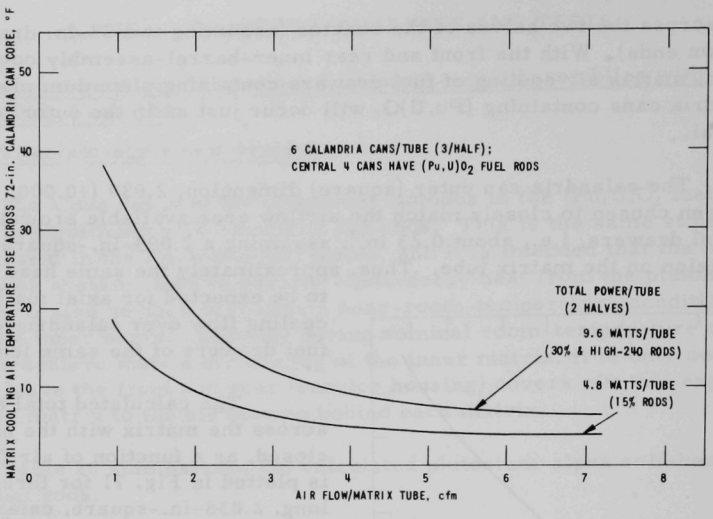

Fig. 72. Calculated Matrix Cooling-air Temperature Rise across 72-in.-long, $(Pu,U)O_2$-fueled, Calandria-can Core

5.1.3 Heat-transfer Analysis: Oxide Fuel Rods to Cooling Air

Table 21 summarizes the results of heat-transfer calculations for the flow of heat produced by the plutonium-alpha decay in the fuel rods to

TABLE 21. Calculations of Calandria-can Temperatures Resulting from Transfer of Pu-alpha Decay Heat from $(Pu,U)O_2$ Fuel Rods to Cooling Air Around Calandria Cans[a]

	Sodium-filled Calandria Cans		Empty Calandria Cans (air in can)	
	15% Pu Fuel, F°	30% Pu and High-240 Fuel, F°	15% Pu Fuel, F°	30% Pu and High-240 Fuel, F°
1. ΔT, average pellet temperature to pellet surface	<0.1	<0.1	<0.1	<0.1
2. ΔT, pellet surface to sodium side of calandria tubes (air to gap)	<0.1	0.1	<0.1	0.1
3. ΔT, average, from sodium side of calandria tubes to outer surface	<0.1	0.1	8.5	16.9
4. ΔT, calandria outer surface to cooling air	0.5	1.0	0.3	0.5
Total ΔT, pellet average to cooling air	0.5	1.2	8.8	17.5

[a]Assuming 32 6-in. $(Pu,U)O_2$ fuel rods per calandria.

the cooling air flowing between the calandria cans and the matrix tubes. Results of heat-transfer calculations for both sodium-filled and empty calandria cans containing 32 6-in. fuel rods of the 15% plutonium, 30% plutonium, or high-240 $(Pu,U)O_2$ fuel are included in the table. For the empty cans, the inside of each calandria can is assumed to be filled with air at 1 atm absolute pressure. In all cases, a 5-mil-thick radial air gap is assumed between the fuel-rod cladding and the calandria tubes. The calculations are consistently conservative. Fuel-rod cooling due to the fact that some cooling air flows between the oxide fuel rods and the calandria can tubes is ignored.

At about 70°F, the effective thermal conductivity, k, of the calandria cans with 32 6-in. oxide fuel rods in place is about 12 Btu/hr-ft-F° for the sodium-filled cans and 0.2-0.4 Btu/hr-ft-F° for the empty cans. The sodium-filled calandria cans operate essentially isothermally (i.e., all points in the can and fuel rods are within 1/4 F°), and the cans run about 1 F° above the temperature of the cooling air. This is not true for the empty cans. But even in the empty cans, all points in the can and fuel rods are within about 10 F° for the 15% plutonium fuel or comparable heat loads from the other fuel.

5.2 Elevated-temperature Operation of the Fuel-rod-loaded Calandria-can Assemblies in VTRZ Heatable Zone

5.2.1 Summary of VTRZ Heated Operation

Initial preparations for heated operation include placing the required calandria can, fuel rod, cartridge heater, and thermocouple arrays in the inner matrix; connecting the cartridge heaters, through fuses, to the desired heater buses; connecting the thermocouples; and sealing the inner matrix assembly by bolting on the front and rear covers of each half-zone. In the design-reference inner-matrix cartridge-heater array for each half-zone, shown in Fig. 73, all heaters are 36-in., 1-kW units (i.e., passing through three calandria cans axially), equally distributed throughout the inner matrix, and approximately equally distributed on the three heater buses serving the inside of each inner-matrix half-zone assembly. Figure 73 is only illustrative. Possible variations on the reference cartridge-heater array include:

1. The use of 6- and 12-in. 1-kW heaters, instead of 36-in. units.
2. Different spatial-heater distributions.
3. Use of one heater bus per half-zone for experimental purposes, and distribution of all general heaters on the remaining two buses.
4. Pattern of Fig. 74; this pattern removes heaters from the central portion of the zone and minimizes disruption of the rod-calandria pattern.

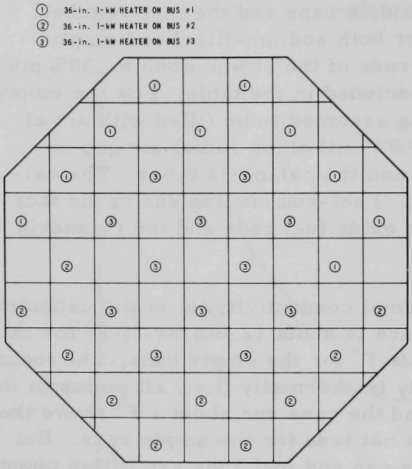

Fig. 73. Design-reference Inner-matrix Cartridge-heater Array

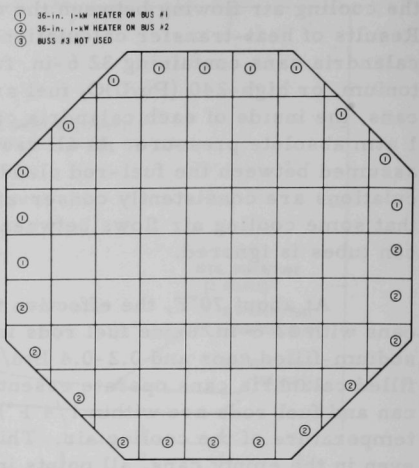

Fig. 74. Alternative Inner-matrix Cartridge-heater Array

The inner-matrix-assembly heating system is described in Sec. 4.5.7.

Final preparations for heating include the establishment of a high-purity argon atmosphere within the inner barrel assemblies, starting the CGR airflow, and moving the reactor halves together. The argon atmosphere is established by initial purging and is maintained by continual circulation (nominal 1 cfm per half-zone, which replaces the volume of gas in each half-zone once every $2\frac{1}{2}$ min) and purification as described in Sec. 4.5.5. The CGR airflow is nominally 100 cfm of air per half-zone face (as described in Sec. 4.5.6). Under normal conditions, VTRZ heatup occurs with the reactor halves together; this minimizes heatup and equilibration time and also minimizes distortion of the 20-mil front-cover pans. It is, however, possible to heat up with the reactor halves apart, and manually-mounted front insulation covers are provided for this purpose. By this technique, the insulation covers are removed and reactor halves brought together with the inner matrix assemblies hot. The reactor will not be critical during the bulk of the time for VTRZ heatup, except during some special experiments.

The total heat capacity of a fully loaded VTRZ half-zone with sodium-filled calandria cans is approximately 60 kWh between 20 and 550°C (about 20% less for empty cans). The power ratings of each of the three inner-matrix cartridge-heater buses per half-zone and of each individual cartridge heater (max 15 kW per bus, max 1 kW per heater) have been chosen to provide the capability of heatups in the range of 2 hr with flexible zonal heating;

for example, the array of Fig. 73 is capable of an approximately 2-hr heatup with sodium-filled calandria cans, the array of Fig. 74 of an approximately $2\frac{1}{2}$- to 3-hr heatup. These heatup rates have been verified in the various full-scale prototype tests that have been carried out. As discussed in Sec. 5.2.2, the maximum heater power per calandria can is limited to 1000 W for the sodium-filled cans and 333 W for empty cans to protect the calandria tubes containing the heaters from excessively high temperatures.

Experience with the VTRZ prototype has indicated that the front- and rear-bolting flange areas and, particularly, the entire rear cover (service housing) tend to seriously lag the temperature of the inner matrix during heatup and remain low at equilibrium if leakage heat from the cartridge heaters is depended upon for their heating. This is due to the proportionally larger surface-heat losses from these portions of the inner matrix assembly and, for the rear cover (service housing), the high thermal resistance of the heat path around the wiring space (behind the matrix) to the rear cover. These temperature lags cause undesirable thermal stresses. To offset these effects, special independently controllable heaters have been placed on the inner-matrix-assembly outer surface just behind the front and rear flanges and on the rear cover; the power rating of these heaters is based on prototype experience and calculations of heat losses. The surface heaters will be used routinely during inner-matrix-assembly heatup to maintain extremity temperatures within ±50°C of central temperatures.

Heatup is carried out until the central-heated-zone temperatures reach the desired level (max 600°C). At this point, the power input is progressively reduced until equilibrium is achieved. Because of surface-heat losses, a uniform distribution of heating throughout the inner matrix results in lower than average temperatures near the outer surfaces of the inner matrix. This tendency can be greatly reduced by maintaining equilibrium with a ring of heaters in the outermost calandria cans--for example, Bus #1 and #2 heaters in Figs. 73 and 74. At equilibrium, the flange and rear-cover-heater power levels are adjusted to match extremity temperatures to the inner matrix. The CGR is intended to be used at continuous full flow during all stages of heatup, equilibrium operation, and cooldown.

Inner-matrix cooldown is accomplished by turning off all inner-matrix heaters and running air through the inner-matrix cooldown-duct system. This cooldown system is capable of providing 40 cfm of air on each of four faces of the inner barrel assembly. Experience with the VTRZ prototype and rough calculations have indicated that unacceptable thermal stresses are produced in the inner matrix if the maximum center-to-radial-edge temperature difference is permitted to exceed about 150°C; minor buckling of the extreme front and rear 1-2 in. of the 37-in. matrix have been observed in tests in which the maximum center-to-edge temperatures reached 250°C during cooldown. To cool down at the maximum

rate consistent with the thermal-stress limitations, the cooldown procedure involves progressive adjustments in the flange and rear-cover extremity heaters and the cooldown air-system flow rate so as to remain in the range of 125-150 C° center-to-edge temperature differences. Within the 150 C° ΔT limit, cooldown from 550 to 100°C (sodium freezing) can be routinely accomplished in about 24 hr.

5.2.2 Heat Transfer within Calandria Cans

There are two important heat-transfer problems within the sodium-filled and empty calandria cans loaded with oxide fuel rods. First, for those cans containing heaters, there is the question of what limitations must be imposed on heater power to protect the heaters, the calandria tubes containing heaters, and the calandria cans in general from excessively high temperatures. The heaters have Inconel X sheaths and may be reliably operated to 2000-2100°F. The calandria-can tubes are Type 304L stainless steel and should not be subjected to temperatures exceeding 1700°F (assuming a pure argon atmosphere) in order to retain adequate strength and avoid excessive grain growth. In the sodium-filled cans, the calandria tube should not be permitted to exceed 1600°F to avoid local sodium-vapor pressures within the cans exceeding 1 atm absolute. Second, there is the question of the adequacy of heat transfer within the calandria can to permit transfer of heat from the heater to the rest of the can and to the can surface for transmission to adjacent cans.

At their maximum rated power, the 36-in., 1-kW cartridge heaters, which will be the most common type used, produce 333 W per calandria can. In some proposed special configurations, 12-in., 1-kW heaters will be used that are capable of inserting 1000 W into each calandria can. The heater fuses, primarily intended to protect sodium-filled calandria cans from overheat failures in case of heater high-power failures, are connected to limit the maximum power of any individual heater to 1500 W.

Table 22 summarizes the results of heat-transfer calculations on the sodium-filled and empty calandria cans assuming full loads of 32 6-in. oxide fuel rods in each can. The effective thermal conductivity of the sodium-filled and oxide-rod-loaded cans is approximately 12 Btu/hr-ft-F°, based on calculations and also on direct measurements on an array of prototype cans. For the empty (i.e., no sodium) calandria cans with 32 oxide fuel rods, the effective thermal conductivity (including radiation and conduction--there is no appreciable convection) varies from approximately 0.28 Btu/hr-ft-F° at a 70°F can temperature to about 0.79 Btu/hr-ft-F° at a 1000°F can temperature; these values are based on calculations assuming argon gas at 1 atm absolute within the empty cans. It is assumed in Table 22 that the heaters are separated from the calandria-can tube containing them by a 9-mil argon-gas-filled radial gap. The heater is assumed to be in one of the central four tubes, and the power produced by the heater is

assumed to be uniformly distributed along the 12-in. length of the can. Note that the reference temperature in Table 22 is the outer-can-surface (i.e., jacket) temperature. This is appropriate because the position of the thermocouple monitors the calandria can temperature.

TABLE 22. Operating Temperatures in Calandria Cans Containing Heaters

Temperature of Outer Surface of Calandria Can (i.e., jacket), °F	Heater Power per Calandria Can, W	Sodium-filled Can with 32 6-in. Rods		Empty Can with 32 6-in. Rods	
		Temperature of Calandria Tube Containing Heater, °F	Temperature of Heater Sheath Surface, °F	Temperature of Calandria Tube Containing Heater, °F	Temperature of Heater Sheath Surface, °F
70	333	100	640	1090	1350
	1000	150	1340	1730	2210
	1500	190	1680	-	-
500	333	530	930	1250	1470
	1000	580	1480	1800	2250
	1500	620	1800	-	-
1000	333	1030	1300	1490	1690
	1000	1080	1750	1830	2280
	1500	1120	2030	-	-

The results of Table 22 have led to the heater power restrictions and recommendations shown in Table 23. The limitation to 1000 W per can for the sodium-filled calandria cans has been verified as being sufficiently low by thermal-cycling tests on prototype and production calandria cans. Seven cans have each been cycled 90-600-90°C, with heating rates of 1000 W per can using typical cartridge heaters, in excess of 350 times, with only minor dimensional changes and without any can failures.

TABLE 23. Calandria-can-heater Power Restrictions and Recommendations

Calandria Can Type (with 32 6-in. oxide fuel rods)	Cartridge Heater Power Limit over 12-in. Can Length	
	Recommended Limit, W/can	Maximum, W/can
Sodium-filled can	333	1000
Empty (no sodium) can	150	333

The adequacy of the heat transfer within the calandria cans may be judged from Table 22 with reference to the difference between calandria-can-tube and outer (jacket)-surface temperatures. For reasonable heater power, the sodium-filled cans operate with the cans essentially isothermal. Temperature gradients within the empty cans are appreciable, and this fact must be considered in planning the heater distributions for VTRZ cores containing significant quantities of empty cans.

5.2.3 Heat Transfer between Calandria Cans

The calandria cans are nominally 12 in. long and 2.039 in. square outside. The matrix tubes into which they are inserted are nominally 2.093 in. square inside with 40-mil walls (Type 304 stainless steel). Thus, in the configuration for heated operation, there are two 27-mil argon-filled (1 atm) gaps and two 40-mil Type 304 stainless steel sheets between the side faces of two adjacent calandria cans. The conduction and radiation across the argon gaps control the calandria-to-calandria heat transfer; the intervening 80 mils of stainless steel has very little effect.

The heatable sodium-filled calandria cans are built with approximately 13% internal void at 20°C. To avoid internal gas-pressure buildup as the can is heated, the inside of the can is evacuated before it is sealed. This results in a slight inward deflection of the 2 x 12-in. sides of the can at 20°C under atmospheric pressure. As the can is heated, the sodium expands, and at approximately 550°C the sides are square; i.e., the can is nominally "full" at approximately 550°C. With further temperature increase, the sodium continues to expand, bulging the 2 x 12-in. faces outward until, at about 675°C, the centers of the four 2 x 12-in. calandria-can faces come into simultaneous contact with the inside surfaces of the matrix tube containing the can. Above 675°C, the calandria-can sides flatten out against the inside surfaces of the matrix tubes. High-temperature calandria-can failure is discussed in Sec. 6.2.2.

The inside volume of the empty (no sodium) calandria cans is vented to the inner-barrel-assembly argon cover gas through holes in the fill plugs. Thus, the empty cans remain nominally square at all temperatures.

The effective gap heat-transfer coefficient (h, Btu/hr-ft^2-F°) between adjacent calandria-can-jacket faces has been calculated and also directly measured in an experiment in which an approximately known thermal current was passed through an array of calandria cans and matrix tubes. The values of the heat-transfer coefficient are given in Table 24. For reference, the expected temperature differences required to transfer 100 W between adjacent 2 x 12-in. calandria-can faces through the argon-stainless-steel gap are also given in Table 24.

TABLE 24. Heat Transfer between Adjacent 2 x 12-in. Calandria-can Faces

Temperature, °F	Gap Heat-transfer Coefficient, h, Btu/hr-ft^2-F°	ΔT to Transfer 100 W (341 Btu/hr) between Adjacent 2 x 12-in. Calandria-can Faces, $\Delta T = \frac{q}{hA}$, F°
500	6	340
750	13	160
1000	22	90

5.2.4 Heat Capacities

A 3/8-in.-dia, 6-in.-long oxide fuel rod contains about 90.5 g of UO_2 or $(Pu,U)O_2$ and 12.3 g of stainless steel and has a heat capacity of about 0.51 W-min/C°, i.e., about 16.4 W-min/C° for all 32 pins in one calandria can.

A full-size (12-in.) sodium-filled heatable calandria can contains about 300 g of sodium and 1110 g of stainless steel and has a heat capacity of approximately 12.7 W-min/C°; the latent heat of fusion of sodium is about 568 W-min per calandria can. The total heat capacity per full-size (i.e., square-cross-section) sodium-filled calandria can in the heatable zone is approximately 33.4 W-min/C°, i.e., about 6.2 W-min/C° for the sodium, about 6.5 W-min/C° for the steel of the can, about 16.4 W-min/C° for the fuel rods and about 1.4 and 2.9 W-min/C°, respectively, for the stainless steel in the inner matrix assembly prorated per calandria can. Each heatable half-zone contains the equivalent of 193.5 full-size calandria cans, so that heatup from 20-550°C will require about 57 kWh per half-zone plus about 1.8 kWh per half-zone for the latent heat of fusion of sodium, assuming sodium-filled calandria cans are used. The total heat capacity per full-size empty calandria can (no sodium, but with 32 oxide rods) is 27.2 W-min/C° or 46.5 kWh per half-zone between 20 and 550°C.

These heat capacities have been verified in prototype heatup tests.

5.2.5 General Heatup

The general procedures for VTRZ heatup are discussed in Sec. 5.2.1. Results of calculations and prototype tests of VTRZ heatup characteristics are discussed here.

In the design-reference heater configuration of Fig. 73, 32 36-in., 1-kW (max) cartridge heaters per half-zone are distributed approximately uniformly among the 69 matrix-tube positions. Individual calandria cans with heaters have 333 W per can (max). Assuming fully loaded (32 oxide rods per calandria can) and sodium-filled calandria cans, the total heat capacity per half-zone of approximately 59 kWh will require a nominal 1-hr 50-min adiabatic heatup time, 20-550°C (70-1020°F), for the reference 32-heater array at full power.

Two-dimensional heat-transfer calculations have been performed for VTRZ heatup (70-1020°F) with the reference heater array of Fig. 73 operating at full power, i.e., 333 per can in the cans with heaters. The calandria cans were assumed to be sodium-filled and fully loaded with 32 oxide rods per can. The calculational model accounted for heat transfer within the calandria cans, the can-to-can argon gaps, the presence of the

inner-barrel cooldown ducts with stagnant air, and heat losses from the outer surfaces of the inner matrix assembly through the 1-in. insulation to the air flowing in the CGR ducts. The results of the calculations are summarized in Fig. 75.

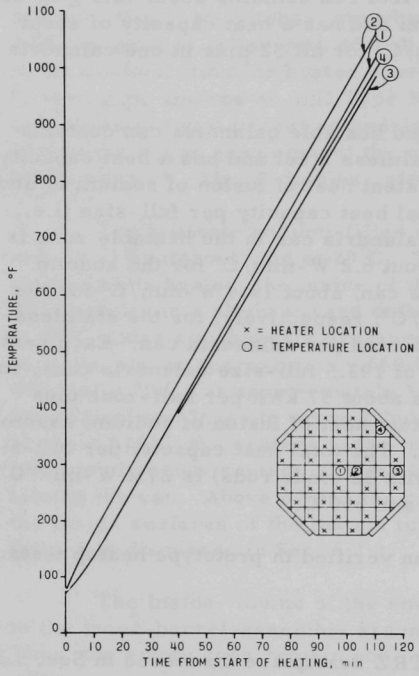

Fig. 75. Calculated VTRZ Heatup Pattern

The calculated heatup pattern of Fig. 75 has been confirmed in prototype heatup tests. Note, however, that the radial temperature gradient apparent in Fig. 75 is a result of the uniform distribution of heaters, operating at uniform power, which was the basis of the calculation. A much more uniform radial-temperature profile is obtainable by operating the outer ring of heaters at a higher power as described in Sec. 5.2.1; this has been repeatedly demonstrated in prototype tests.

5.2.6 Equilibrium Operation

After nominal operating temperatures are achieved, the heater power is reduced to zero for heaters in the central portion of the inner matrix and to a low equilibrium value for the outer ring of heaters. The general procedures are discussed in Sec. 5.2.1. This section discusses the rate of thermal equilibration, the equilibrium temperature distribution, and the equilibrium-heat-loss situation.

In the design-reference cartridge-heater-location pattern of Fig. 73, heaters are located in calandria cans in every other matrix tube in a checkerboard pattern. In heater distributions like the reference distribution, a typical heated calandria can is surrounded by four immediately adjacent unheated cans. The time constant for the decay of the temperature difference between the heated and unheated cans in an infinite checkerboard array, after the heating is cutoff, is a useful parameter of the rate of VTRZ inner-matrix equilibration and has been calculated for both sodium-filled and empty (no sodium) cans. Assuming 32 oxide rods per can and accounting for both the effects of the argon gap between cans and the internal thermal resistance of the cans themselves, the calculated relaxation time constant (1/e change) for the decay of the temperature difference between cans of higher and lower temperature in a checkerboard pattern at 1000°F is 2.2 min for the sodium-filled cans and 4.4 min for the empty (no sodium) cans.

Two-dimensional heat-transfer calculations of VTRZ equilibration at about 1060°F with sodium-filled calandria cans have been carried out and are summarized in Fig. 76 (note suppressed zero). These calculations have accounted for the effects of the internal thermal resistance of the oxide-rod-loaded calandria cans, the effects of the argon gap between cans, the presence of the stagnant inner-matrix cooldown ducts, and heat leakage through the insulation to the CGR. The heater distribution pattern assumed was the design reference pattern of Fig. 73, i.e., the checkerboard pattern. During heatup, 333 W per can with a heater was assumed. At the beginning of equilibration, all heaters were reduced to 21 W per can with a heater, i.e., from a total inner-matrix power of 32 kW during heatup to 2 kW during equilibration. Retaining 6.3% power uniformly in all heaters, rather than complete cutoff, causes the equilibrium condition to be established more slowly. Also, retaining 6.3% power uniformly in all heaters causes an equilibrium radial temperature gradient and an equilibrium temperature difference between heated and unheated cans. In routine VTRZ operation, heaters in the central portion of the inner matrix would be completely cut off and the outer ring of heaters used to maintain equilibrium.

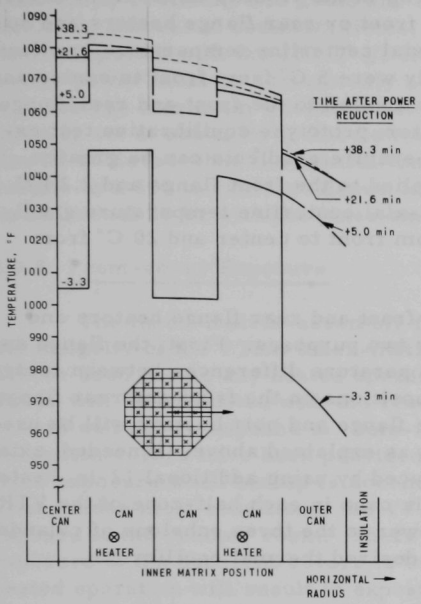

Fig. 76. VTRZ Equilibration from Uniform Power Reduction from 32 to 2 kW

The results of equilibration tests on the VTRZ prototype have generally confirmed the equilibration rates and radial temperature gradients shown in the calculations of Fig. 76. These tests have also confirmed the possibility of obtaining a more uniform inner-matrix temperature distribution by maintaining equilibrium with an outer ring of heaters.

The calculated heat loss from one inner-matrix-assembly half-zone is approximately 2000 W at an inner-matrix temperature of 550°C; this consists of 1800 W radially through the 1-in. insulation to the CGR and 200 W off the rear cover (service housing) through the 1-in. insulation to the matrix cooling-air plenum. Assuming the full total CGR flow of 400 cfm, the 1800 W of radial leakage causes an approximately 10 C° rise in CGR air temperature between inlet and outlet. These numbers have been generally confirmed in prototype tests.

The axial heat loss through the rear cover (service housing) results in an axial temperature drop between the center and the rear of the inner-matrix-assembly half-zone. Likewise, heat loss from the front-cover flange results in a slight axial temperature drop in the vicinity of the front cover. In prototype tests with no power to the front or rear flange heaters and no power to the access-port heater, the axial centerline temperature gradients for the prototype inner matrix assembly were 5 C° from front to center and 40 C° from rear to center. With power applied to the front and rear flange heaters as well as the access-port heater, prototype equilibration test experience has confirmed that axial temperature gradients can be greatly reduced or eliminated. With 500 W applied to the front flange and 2.2 kW applied to the rear-cover heaters, the axial centerline temperature gradients were reduced to less than 1 C° from front to center and 20 C° from rear to center.

In routine VTRZ operation, the front and rear flange heaters and the access-port heater will be used for two purposes. First, the flange and port heaters will be used to reduce temperature differences between central inner-matrix positions and extremity positions on the front and rear flanges, as described in Sec. 5.2.1. Second, the flange and port heaters will be used to reduce axial temperature gradients, as explained above. If needed, axial temperature gradients can also be reduced by using additional 12-in. heaters in any of the three echelons of calandria cans in each half-zone of the VTRZ inner matrix assembly. The heater power to the three echelons of calandria cans can then be varied to achieve the desired thermal equilibrium.

5.2.7 Cooldown

The inner-matrix cooldown system was originally designed to permit cooldown from 550°C to complete sodium freezing (100°C) in 10 hr. Sodium freezing is taken as the low-temperature criterion, because it is felt that an operator should be in continuous attendance whenever there is molten sodium in the VTRZ; below the sodium freezing point, cooldown could continue unattended. To accomplish the 10-hr cooldown, the system was designed for a total of 160 cfm maximum airflow per half-zone, based on the results of two-dimensional heat-transfer calculations.

It was subsequently determined in prototype tests that full inner-matrix cooldown airflow at high inner-matrix temperatures does in fact give the predicted cooldown rate, but also produces undesirable thermal stresses. These stresses arise from the center-to-edge temperature gradient, which can run as high as 300 C° with maximum airflow in the initial stages of cooldown, and result in local inner-matrix buckling. Although the observed buckling was not severe and confined to the extreme front and rear edges of the inner matrix, the distortion is definitely undesirable.

Rough thermal-stress calculations and trial cooldown runs in the VTRZ prototype have led to the establishment of a maximum permissible center-to-edge temperature gradient of 150 C° during cooldown. This is sufficiently restrictive to avoid any matrix distortion, but results in significantly increased cooldown times. To achieve the minimum cooldown time consistent with the 150 C° ΔT limit, cooldown airflow rate and flange heater power must be continuously adjusted during the cooldown process. In prototype maximum-cooldown rate tests, cooldown airflow has been initially set at about 5% of full flow and progressively increased until full flow is achieved when the central temperature drops to about 200°C. This results in a 550 to 100°C cooldown in about 22 hr and cooldown to 30°C in an additional 20 hr with the inner-matrix-assembly covers on.

5.2.8 Front-cover Exposure

The inner-matrix-assembly front covers are designed to maintain the integrity of the VTRZ inner-matrix-assembly inert-gas system and will be used during any heated operation. Most VTRZ heatups and cooldowns will be conducted with the reactor halves together so that the front covers will not be exposed to room-temperature air. Manually-mountable insulation covers have been provided for the front covers to protect them from exposure when heatup is accomplished with the reactor halves apart. Thus, under most conditions, the VTRZ front covers will not be directly exposed to the reactor room. There are, however, two situations in which exposure of the hot front covers is unavoidable: A reactor scram during heated operation will result in exposure of the hot front VTRZ covers. Also, if the VTRZ is heated with the halves apart, the front insulation covers will have to be removed and the covers exposed while the halves are coming together. This section discusses the thermal-stress situation resulting from the exposure of the hot VTRZ front covers.

The calculated heat loss from the front cover at 600°C is 8800 Btu/hr-ft^2 when the cover is exposed to room-temperature air. This heat loss will cause an appreciable drop in the temperature of the 20-mil-thick pan section of the front cover, but will not appreciably affect the temperature of the inner calandria. The exact drop in temperature of the front cover greatly depends upon internal pressure in the inner barrel (i.e., the degree to which the front cover is pulled into contact with the inner matrix) and the flatness of the front cover. If the contact between the front cover and the inner matrix is good over the entire front face, the calculated average temperature drop is about 30 C° at 600°C. If the front cover is warped or in other ways does not make good contact with the inner matrix, the temperature drop may be as great as about 150 C°. Since it is hard to ensure perfect flatness and good contact between the thin front cover and the inner-matrix edges, the expected temperature drop is 100-150 C°. The temperature may also differ by about 100 C° between points making good contact and points separated from the inner matrix, since conduction across the

face of the thin 20-mil front cover is relatively small. As discussed in Sec. 6.5.1, temperature gradients of about 100 C° will cause warpage of the front cover, but will not lead to failure.

The exposure of the front cover will not greatly affect the temperature of the inner matrix and calandria, because the heat-loss rate is small compared to the internal heat capacity of the inner matrix assembly and because the sodium-filled calandria cans are good conductors of heat. The 8800-Btu/hr-ft^2 heat-loss rate off the front cover will result in a uniform cooling of the inner matrix and calandria of less than 1 C°/min. Exposure of the front cover, therefore, will not cause fast changes in reactivity due to temperature effects.

The front flange through which the pan section of the front cover is attached to the inner matrix assembly will also drop in temperature when the front cover is exposed. The front flange will lose heat by conduction to the front-cover pan section and directly by radiation and convection from the exposed front surface. The calculated heat loss by conduction through the 20-mil front-cover face will be less than 2500 Btu/hr, whereas the heat loss due to radiation and convection off the exposed front-flange surface will be about 3000 Btu/hr. These heat losses can, however, be compensated for by the front-flange heater, a 2.4-kW (8000-Btu/hr) heater. During exposure of the front face, the temperature drop in the front flange can easily be kept to less than 50°C. The front flange can, therefore, be prevented from cooling enough to cause distortion of the inner matrix through the use of the flange heater during exposures of the front covers.

Tests of the front covers during heated exposure on the VTRZ prototype have generally confirmed the calculations. The prototype testing was conducted with an exact prototype of the final front-cover design. The final front-cover design has a radial bellows ring to permit expansion and contraction of the front cover face as shown in Fig. 25. It was originally hoped that, with a small negative pressure in the inner barrel, the front-cover contact with the inner matrix would be good enough to give only a 30 C° drop in the front-cover temperature when it was exposed. The prototype testing indicated, however, that good contact over the entire front-cover face is hard to achieve and the temperature drops recorded were in the range of 100-150 C°, as expected with poor contact. The larger temperature drop is acceptable, as explained in Sec. 6.5.1, because of the bellows design.

The prototype tests confirmed that the effect of exposure of the front cover on the inner matrix is minimal. Even thermocouples placed within 2 in. of the front cover in the inner matrix recorded essentially no temperature drop during exposure.

In the initial prototype tests, the front-flange temperature dropped about 100-150 C° during front-cover exposure. However, this was primarily due to the location of the front-flange heater in the prototype; the location was not the same as in the final design. That is, the prototype design had the front-flange heater on the front face of the flange so that when the insulation cover was removed the heater, as well as the front cover, was exposed to room air. Exposure of the flange heater, which operates at about 700°C, results in large heat losses from the heater and greatly changes the equilibrium power transfer from the heater to the flange. When the tests were repeated with insulation placed over the flange heater, so that only the front cover would be exposed, the front-flange temperature drop was reduced to less than 50 C°. In the final design, the flange heater is placed on the back side of the front flange so that it is not exposed to room air during exposure of the front face. The front of the flange will be exposed to room air; but as explained above, increases in the power to the flange heater will be able to compensate for heat losses from the front flange.

5.2.9 Air Cooling of Outer Matrix

Although the amount of heat leaking radially outward from the heated inner barrel assembly through the insulation annulus to the reactor fuel drawers in the outer matrix assembly is small, it is large enough to require continuous cooling if the stable temperatures needed for experiments are to be obtained in reasonable lengths of time. Heat leakage to the outer matrix assembly comes from components that penetrate the insulation annulus (the ball mounts, the scram restrainers, and the axial guides), thin areas in the insulation (principally over the front and rear flanges), and general heat flow from the CGR air through the 1/8-in.-thick insulation layer.

Table 25 lists the calculated leakage heat into the tubes of the outer matrix assembly immediately adjacent to the insulation annulus. The calculations were made on a very conservative basis and probably overestimate the leakage. Measurements of the leakage heat have been made in the VTRZ prototype and have shown significantly less leakage than calculated for the

TABLE 25. Calculated Heat Leakage from Inner Barrel to Outer Matrix at 550°C Operating Temperature

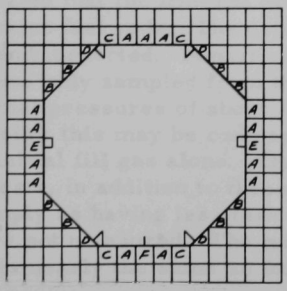

	Heat Leakage to Outer Matrix for Inner Matrix at 550° (watts per tube per half-zone)						
Tube Type	From CGR Air	From Ball Mounts	From Scram Restrainers	From Axial Guides	From Front Flange	From Rear Flange	Total
A	6	-	-	-	5	3	14
B	6	-	-	-	4	5	15
C	6	-	26	-	5	3	40
D	6	-	26	-	4	5	41
E	6	30	-	-	5	3	44
F	6	-	-	20	5	3	34

VTRZ prototype configuration. However, the amount of leakage heat is a sensitive function of the exact configuration of the insulation zone, and, since this is somewhat different for the prototype and the final design, the prototype results cannot be reliably extrapolated to the final design.

The worst case of Table 25 is for the tubes (Type E) that receive the leakage heat from the ball mounts (about 6 W per ball mount). Assuming a nominal $2\frac{1}{2}$-cfm matrix air-cooling flow in these channels, a 35 C° temperature rise across each half-zone (70 C° across the two halves together) would be predicted. Although this temperature rise would give a 90°C exit air temperature and come just within the temperature limit of Table 5 (95°C), it is considered undesirably high and will be lowered by increasing the matrix cooling-air flow per tube if tests on the final assembly show that heat leakages as high as calculated in Table 25 in fact exist. Increased matrix cooling-air flow will be obtained, if necessary, in the effected drawers (for example Type C, D, and E drawers of Table 25) by using special fuel drawers that are narrower than the standard drawers.

6. STRESS ANALYSES AND TESTS

6.1 Stress Analyses and Tests of the Oxide Fuel Rods

6.1.1 Fuel-rod Mechanical Characteristics

The physical characteristics of the UO_2 and $(Pu,U)O_2$ fuel rods are discussed in detail in Sec. 4.3; Fig. 12 shows the oxide rod assembly. The mechanical characteristics of the oxide rods that are important for the stress analysis are summarized below:

(1) The cladding tube, end plugs, and internal spacer are Type 304 stainless steel.

(2) The cladding tube of each rod is nominally 5.9 in. long and has a 0.377-in. OD and a 0.012-in. wall.

(3) The end-plug faces have 0.097-in.^{2} cross-sectional area.

(4) The tube-to-end-plug weld is an inert-gas-shielded tungsten electrode arc weld and produces a total shear area of at least 0.022 in.^{2} between the tube and the plug.

(5) The oxide pellets within the cladding are nominally 0.346 in. in diameter, and approximately 10 pellets are stacked to produce a nominal 5.72-in. stack length.

(6) The axial free length between the pellet stack and the end plugs, nominally 0.046 in., is taken up by a nominally 0.043-in.-thick spacer and 0.003 in. of gap.

(7) The internal spacers are in the form of a cup and are designed to collapse 10-15 mils under loads in the range of 20-30 lb.

(8) The internal gas volume of a fuel rod is nominally 0.027 in.^{3} and is filled with an argon-helium gas mixture of 1 atm abs at room temperature.

(9) The specifications for the oxide rods set a maximum acceptable internal rod pressure of 300 psig at 600°C. This includes the effects of any pellet outgassing as well as the effects of the initial gas fill.

Acceptance testing at ANL of the depleted and enriched-UO_2 fuel rods have indicated that the nominal dimensions given above are closely met in the production fuel rods. The entire inventory of the UO_2 fuel rods has been received and inspected. In particular, destructive burst tests at ANL on 30 rods randomly sampled from the UO_2 inventory have shown typical measured internal pressures of about 70 psig at 600°C (the maximum observed was 120 psig); this may be compared to the 44 psig pressure to be expected from the initial fill gas alone. The rod manufacturer has carried out about 60 burst tests, in addition to those carried out at ANL; all of these were reported simply as having less than 300 psig at 600°C, although the actual pressures were not measured. The manufacturing procedure for the $(Pu,U)O_2$ fuel rods is nearly the same as for the UO_2.

6.1.2 Fuel-rod Stress Analysis

The purposes of the stress analyses that have been carried out on the oxide fuel rods have been, first, to establish that, under normal operating conditions, the rods remain sealed and do not distort sufficiently to impair their use in the experiments planned and, second, to determine to what extent the rods remain sealed when subjected to accidental mechanical and thermal abuse. The results of stress analyses carried out for normal and accident operating conditions are summarized in the following sections.

6.1.2.1 Fuel-rod Stress Analysis under Normal Operating Conditions

The normal operating temperature range of the VTRZ is 20-650°C. As shown in Table 5, the VTRZ inner matrix assembly is designed to tolerate 30,000 hr at 600°C and 100 hr at 650°C without physical distortion sufficient to compromise its use. Assuming 45 1-kW heaters per half-zone (the maximum possible within the power-supply limits), the maximum VTRZ heatup rate to be normally encountered is about 8.5 C°/min (assuming calandria cans without sodium). At full cooldown airflow rate, the maximum cooldown rate possible for the VTRZ is about 2 C°/min. Thus, the oxide fuel rods will be exposed to the following normal operating conditions:

(1) Operating temperatures, 20-650°C; up to 30,000 hr at 600°C and up to 100 hr at 650°C.

(2) Maximum heating rate, 8.5 C°/min; maximum cooling rate 2 C°/min. (These are to be interpreted as cladding-surface temperature-change rates.)

Because of the internal axial gap between the oxide pellet stack and the cladding and because the rods are loaded at 0 psig at room temperature, there is no stress in the fuel rod at room temperature, except whatever is left over from the end-plug welding.

The linear expansion coefficient of stainless steel is greater than that of UO_2 or $(Pu,U)O_2$ so that, when the entire rod is at a uniform temperature, there is no contact between the pellet stack and the cladding and, therefore, no stress is produced in either the cladding or the pellets due to this cause. At uniform rod temperatures above 20°C, the important stress considerations are hoop and axial stresses in the clad tube and shear stress between the cladding tube and the end plugs produced by the internal gas pressure. Assuming the shear strength of the Type 304L stainless steel material to be half of the tensile strength and considering that the tube-to-end-plug shear area is more than twice that of the axial tube cross-sectional area, it may be concluded that, if the cladding is adequately strong for axial cladding-tube stress, it is also adequately strong for shear of the end-plug weld.

Even under very conservative assumptions, at least 3 mils of increased overall length is permissible over the lifetime of an individual oxide fuel rod; i.e., 0.05% axial creep is permissible. Under equally conservative assumptions, at least 3 mils of increase in the diameter of the fuel rod is permissible over its lifetime; i.e., 0.8% creep on the diameter is permissible.

At 600°C, it is conservative to assume a 300-psig internal pressure in the fuel rod (see Sec. 4.3). This produces a hoop stress of approximately 4400 psi and an axial stress of about 2200 psi in the tube. The maximum shear stress in the tube due to the combination of these stresses is about 1100 psi and does not significantly affect the creep rate. At 2200 psi and 600°C, the axial creep rate in the Type 304L stainless steel cladding tube will be less than 10^{-7}%/hr, i.e., less than 0.003% axial creep in 30,000 hr. At 4400 psi and 600°C, the creep rate on the diameter will be about 5 x 10^{-7}%/hr, i.e., less than 0.015% creep on the diameter in 30,000 hr. Both of these creep rates are acceptable.

At 650°C, the maximum internal pressure in the fuel rod is about 320 psig. This produces approximately 2350-psi axial stress and an axial creep rate of about 7 x 10^{-7}%/hr at 650°C, i.e., about 7 x 10^{-5}% axial creep in 100 hr. The 320-psig pressure produces about 4700 psi of hoop stress and a creep rate on the diameter of about 5 x 10^{-5}%/hr at 650°C, i.e., about 0.005% creep on the diameter in 100 hr. These creep rates are tolerable.

Therefore, assuming both 30,000 hr of operation of a fuel rod at 600°C and 100 hr operation at 650°C, the total predicted axial creep is about 0.003% (0.2 mil) and the total creep on the diameter is about 0.020% (0.1 mil). These total creep values are acceptable.

If a fuel rod is heated or cooled from the outer surface at an appreciable rate, a temperature difference that is set up between the cladding tube and the oxide pellet stack results in differential expansion. The possibility exists for a large axial tensile stress in the cladding tube if this differential expansion between the cladding and the oxide pellet stack causes the internal cladding length, less the spacer thickness, to become less than the length of the pellet stack at the temperature of interest.

The temperature coefficient of linear expansion for Type 304L stainless steel is greater than that for UO_2 or $(Pu,U)O_2$. Therefore, since the internal cladding length (less spacer) exceeds the pellet stack length at room temperature, there is no possibility of interference between the cladding and the pellet stack during a heatup, regardless of the heating rate.

There is a possibility of cladding-to-pellet-stack interference during rod cooldown. Since the internal gap between the internal cladding length (less spacer) and the oxide pellet stack becomes larger as the temperature

is increased and because the temperature difference between the cladding and the oxide pellet stack required to maintain a given cooldown rate increases as the temperature decreases, the worst situation for possible length interference exists at the lower end on the operating temperature range, i.e., near room temperature. Although it is impossible to maintain the maximum cooldown rate of 2 C°/min, even with maximum cooldown airflow, except at high temperature (where a high ΔT exists between the VTRZ and the cooldown air), assumption of a 2-C°/min rate gives a very conservative calculation. At approximately 20°C, a 2-C°/min cooldown rate requires a cladding-to-pellet-stack temperature difference of about 0.1 C°. This causes only a trivially small increase in the pellet-stack length over room temperature. Thus, there is no possibility of cladding-to-pellet-stack interference at 2-C°/min cooldown rates.

It may be concluded that under normal operating conditions there will be no significant fuel-rod distortions over the lifetime of the fuel rods.

6.1.2.2 Fuel-rod Stress Analysis under Accident Conditions

Two situations are considered here that are intended to be indicative of the limits of the conditions under which the fuel cladding will remain sealed. First, the highest uniform temperature the fuel rods will sustain without bursting is estimated. Second, the highest temperature difference that can be tolerated between cladding and oxide pellets is estimated.

If a uniform temperature is assumed throughout the fuel rod, the cladding bursting temperature is determined by the hoop stress in the cladding tube produced by the internal gas pressure. It is reasonable to assume, based on experience with UO_2 pellets at ANL and elsewhere, that all outgassing of the pellets occurs below 600°C; thus, the absolute internal rod pressure may be assumed to be proportional to absolute temperature above the reference value of 300 psig at 600°C. The assumption of 300 psig at 600°C is conservative (see Sec. 4.3). Table 26 summarizes the estimated rod-bursting temperatures taking the 100-hr and, alternatively, the 1000- or 10-hr rupture stresses as the criterion for bursting hoop stress. Table 26 gives the results of calculations assuming the fuel rod is heated alone and also assuming that the fuel rod is heated inside of a calandria-can tube. When the rod is heated alone, only the 12-mil cladding is available to absorb the bursting force. If the rod is in a calandria-can tube, the rod cladding can creep outward until contact is made with the calandria tube. In this case, both the 12-mil rod cladding and the 10.5-mil calandria tube are available to resist the bursting pressure. Even with the 10.5-mil calandria tube cross section added, hoop stress is still the determining factor in burst resistance. The bursting values of Table 26 are conservative in that they assume that the internal volume of the rod does not change as the tube expands under the high pressure. In fact, the internal volume would substantially increase as the rod expands and would reduce the internal

pressure and increase the bursting temperatures substantially over those given in Table 26. The minimum elongation to failure for Type 304L stainless steel at any temperature is 30%.

TABLE 26. Oxide Fuel-rod Bursting Temperatures

Case	Bursting Temperature, °C		
	1000-hr Rupture-stress Criterion	100-hr Rupture-stress Criterion	10-hr Rupture-stress Criterion
Fuel rod alone	750	840	~900
Fuel rod in calandria-can tube	830	890	~970

With the oxide pellets at 900°C, calculations indicated that the cladding tube can be instantaneously reduced to about 520°C before cladding-to-pellet-stack interference begins, to about 400°C with only crushing of the spacer occurring, and to 20°C with about 1% elongation of the cladding tube. With the oxide pellets at 600°C, the cladding tube can be instantaneously reduced to about 330°C before cladding-to-pellet-stack interference begins, to about 230°C within the built-in collapsibility of the spacer, and to 20°C with about 1/2% elongation of the cladding tube.

The fuel rods should remain sealed regardless of their thermal history if the maximum rod temperatures are limited to about 900°C.

6.1.3 Fuel-rod Operational Tests

Two operational tests have been carried out on the oxide fuel rods to directly test the results of the stress calculations as to the acceptable operating limits. First, the cladding tubes with welded-in end plugs from eight randomly selected production fuel rods were subjected to internal pressures from 100 psig to bursting at 600 and 800°C to determine the adequacy of the 300 psig at 600°C internal-pressure limit in reducing the rod deformation to negligible levels under normal operating conditions. Secondly, 180 randomly chosen typical production depleted UO_2 fuel rods have been cycled 90-600-90°C, in excess of 300 times, in six typical production sodium-filled calandria cans to test for any possible problems under actual VTRZ operating conditions.

Eight fuel rods were selected randomly from the inventory of 14,600 depleted-UO_2 fuel rods. The cladding tubes, end plugs, and end-plug-to-tube GTAW welds are considered typical of the entire inventory of depleted- and enriched-UO_2 and -$(Pu,U)O_2$ fuel rods because the tube and end-plug materials come from the same vacuum-melt material batches; the fabrication methods used for the 6-in. cladding tubes and end plugs are the same for all rods; and the welding equipment, welding parameters, and welding personnel will be the same for all rods. The selected rods were

sectioned, normal to the long axis, about 4 in. from one end and the pellets and internal spacer removed. The 4-in.-long section with one welded-in end plug was set up in a test rig, which was capable of independently controlling the temperature of the cladding and the internal cladding pressure. Each one of the eight samples was exposed to a single cladding temperature and internal pressure combination for 2 hr in a pure helium atmosphere and then cooled to room temperature and examined for distortion. The exposure of each sample is given in Table 27. No measurable dimensional changes (in excess of 0.1 mil) were observed in any of the samples, except the bursting pressure sample (No. 6). Sample No. 6 failed at 600°C and 3500 psig with a 0.38-in.-long longitudinal (i.e., axial) rupture beginning 0.38 in. from the end plug. The burst sample increased in diameter from 0.377 to 0.420 in. (11.4% elongation) before failure.

TABLE 27. Fuel-rod Exposure Tests for Various Temperature and Pressure Conditions

Sample No.	Cladding Temperature, °C	Internal Pressure, psig
1	600	100
2	600	200
3	600	300
4	600	400
5	600	500
6	600	Bursting pressure (3500)
7	800	200
8	800	400

To provide a final check on the design of the fuel rods and of the sodium-filled calandria cans, thermal-cycling tests were carried out on typical production fuel rods mounted in typical production calandria cans. Every effort was made to ensure that the test conditions were equal to, or more severe than, the operating conditions to be expected in the VTRZ. The 180 fuel rods tested were randomly selected from the inventory of 14,600 depleted-UO_2 fuel rods and are representative of all of the UO_2 and $(Pu,U)O_2$ rods in every respect; i.e., they are identical as to material, dimensions, and fabrication process. The calandria cans selected were the first six production sodium-filled cans and are completely representative of the entire inventory of calandria cans with respect to materials, dimensions, and fabrication process. Typical commercial 3/8-in.-dia cartridge heaters of the type to be used in the VTRZ were used in the tests.

The cycling tests were carried out from below the sodium freezing temperature to 600°C (i.e., 90-600-90°C on each cycle) to include whatever effects might be produced by repeated sodium freezing around the calandria-can tubes. The heatup rates were the maximum of which the heaters were

capable; 1 kW per calandria can was used. The environment of the tests was argon gas, but with 500 ppm oxygen rather than the 50 ppm as in the VTRZ, to enhance whatever effects might arise from surface oxidation.

The calandria-can tubes and the fuel rods were dimensionally inspected initially and at the end of 1, 50, 100, 150, 200, and 300 cycles. A special inspection was made at 154 cycles as discussed below. The first cycle had a 30-min heatup, 24-hr hold at 600°C, and a 4-hr cooldown; cycles 2-150 were $4\frac{1}{2}$-hr cycles; and cycles 151-300 were 2-hr cycles. Inspection of the calandria-can tubes used 7.5-in. fall-through gauges; the fuel rods were measured for diameter, with a micrometer, and for central runout. Initially, all calandria-can tubes passed 0.385-in.-dia, 7.5-in. fall-through gauges; all fuel rods had less than 0.378-in. OD with less than 1 mil of central runout.

After the first cycle, about half the calandria-can tubes would still accept the 0.385 x 7.5 fall-through gauges and about half had distorted so as to accept only smaller-diameter gauges. The average diametral reduction (measured by fall-through gauge diameter) of the tubes that had distorted was about $1\frac{1}{4}$ mils; the maximum reduction observed was 2.2 mils. The fuel rods did not change in diameter after the first cycle, but showed some increased bowing; the worst increase in bowing was 0.5 mil.

Some small increase in tube and rod bowing was observed at the 50- and 100-cycle inspections, but very little beyond that point. As the cycling progressed, some tubes increased and about an equal number decreased in total bowing. The worst cases observed were a (fall-through gauge) tube reduction from a diameter of 0.384 in. to about 0.381 in. and a rod-runout increase of 1 mil to a total of 2 mils. Taking the smallest tube and the rod with the largest bow (and assuming their bow is exactly opposite), there is still a 2-mil tube-to-rod diametral clearance. This is adequate. There were no observed interference fits between rods and calandria tubes at any time during the tests. The surface oxidation was minor, amounting to less than 0.5 mil on any surface. The thickness of the oxidation layer is included in the apparent bowing measurements reported here.

Just after the 150-cycle inspection of the calandria cans and fuel rods in the cycling tests, an accidental extreme overheat of the test cans and rods occurred at cycle 154 due to an operator error. The operator of the cycling test had accidentally disabled the automatic temperature-control system. The temperature-control system of the cycling test is much different than that for the VTRZ, and its failure does not indicate anything about the VTRZ system. The disabling of the cycling-test control system permitted the test calandria cans and fuel rods to rise to 750°C on cycle 154 before the operator noticed the problem and initiated a cooldown. The calandria cans and fuel rods were removed from the test rig as soon as room temperature was achieved, and a complete special inspection was made of

the calandria cans and fuel rods. Two of the calandria-can outer jackets remained bowed outward slightly after the cooldown. All the other calandria cans were unchanged from the 150-cycle inspection. None of the dimensions of the calandria-can tubes or fuel rods had changed significantly from the 150-cycle examination. The test calandria cans and fuel rods were reinstalled in the test rig, and the cycling tests were resumed at the 154-cycle point.

6.2 Stress Analyses and Tests of Calandria Cans

6.2.1 Mechanical Characteristics of Calandria Cans

The design and construction of the VTRZ calandria cans are discussed in detail in Sec. 4.4. Those mechanical characteristics of the cans that are important to the stress analyses discussed in subsequent sections are summarized here:

(1) All material is fully-annealed Type 304L vacuum-melt stainless steel.

(2) The headers, internal spacers, and jackets are nominally 19 mils thick; the tubes have a nominally 10.5-mil wall.

(3) The internal volume of a square-cross-section calandria can, nominally 11.71 in. between headers, is about 765 cm^3 inside the outer jacket at 20°C. About 404 cm^3 of internal volume is preempted by the calandria tubes, leaving about 361 cm^3 of free internal volume at 20°C.

(4) The maximum sodium loadings for the square-cross-section calandria cans are 301 g for the heatable (Type H) cans and 331 g for the unheatable (Type F) cans. At 20°C, the heatable cans are about 86% full and the unheatable cans about 95% full.

(5) The triangular calandria cans contain the same sodium loading per calandria tube but more internal free volume per tube than the square cans and therefore have greater void volumes than the square cans.

(6) The void volume within the sodium-containing calandria cans is evacuated before the cans are sealed.

(7) The internal free volume of the empty (i.e., no sodium) calandria cans is vented through a hole in the fill plug to the atmosphere of the VTRZ inner matrix assembly (air or argon).

(8) The heatable (Type H) calandria cans are designed to be nominally full (i.e., sides square and flat) at 550°C. Above 550°C, the jacket sides bulge outwards so that the centers of the four sides of the square cans will simultaneously touch the surrounding matrix tube about 675°C.

(9) Each end of the calandria can is fitted with a 19-mil Type 304L stainless steel cover plate secured by four nuts to studs spot-welded to the header. These covers are intended to keep the fuel rods from falling out of the calandria can during normal handling.

6.2.2 Stress Analyses of Calandria Cans

There are three important questions relating to calandria-can strength: First, are the stresses in the heatable cans (Type H) under normal 20-600°C operating conditions sufficiently low to avoid distortions large enough to compromise the use of the cans? Second, at what temperature will the heatable (Type H) cans release liquid sodium in an overheat accident? Third, at what temperature will the unheatable (Type F) calandria cans release liquid sodium if they are accidently loaded into a heated VTRZ configuration?

6.2.2.1 Normal Operation of Calandria Cans

Normal operating conditions include operation of the square and triangular heatable (Type H) and empty (Type V) calandria cans in the temperature range of 20-650°C. Operation beyond 600°C will not occur except as a result of an operational error. The actual number of cycles from 20 to 600 to 20°C will probably not exceed 100 over the lifetime of the VTRZ.

Except for indeterminate welding stresses, no significant forces act on the vented empty (Type V) cans at any time during normal operation. The sides remain nominally square and flat at all temperatures.

Sodium loading of the calandria cans is done at about 120°C. As the cans are cooled to room temperature, the sodium freezes at about 100°C and a small annular gap is probably formed around each calandria tube since the linear coefficient of expansion of sodium is less than that of stainless steel below the sodium freezing point. The exact width of the annular gap around the calandria tubes at room temperature is uncertain because of the general axial compression of the solidified sodium caused by the relatively faster contraction of the calandria jacket and tube length relative to the contraction of the sodium below 100°C.

Because of the lack of internal gas pressure in the sodium-containing calandria cans, the only cause of significant stresses in the cans in the temperature range of 20-650°C is the expansion of sodium relative to the calandria cans; above the melting point, sodium expands more rapidly with temperature than does stainless steel. The expansion of the sodium causes the can jacket faces to flex; in the worst case, at the jacket axial center of a square can, the centerline of the jacket faces flex from about 45 mils concave (due to atmospheric pressure) to about 24 mils convex. This flexing exceeds the yield stress of the stainless steel so that fatigue cracking is a

possibility. Rough calculations indicated that the can faces should be able to take in excess of 50,000 cycles of this magnitude, at room temperature, without cracking. Since the operating temperatures of the VTRZ are within the stress-relief range for Type 304 stainless steel, some of the effects of the fatigue cycling are probably mitigated during normal operation. As a backup on the fatigue calculations, a typical calandria-can jacket was fatigue-cycled in air at room temperature 75 mils concave to 75 mils convex; the specimen cracked at 21,000 cycles. There seems to be no problem with fatigue failure of the cans over any reasonable number of operating cycles. Calandria-can thermal-cycling tests are reported in Sec. 6.2.3.

The total weight of 32 6-in. fuel rods in a calandria can is about 3200 g or about 7 lb. Each of the four studs holding each calandria-can end cover (rod retainer) is required by the specifications to be capable of sustaining a 10-lb pull. The studs are arranged so that one stud is immediately adjacent to each calandria tube. Direct tests have shown that the covers will retain the rods under a 3-4-g jolt as when the edge of a loaded calandria can is struck on the edge of a table.

6.2.2.2 Overheat Conditions in Calandria Cans

As the temperature of a heatable (Type H) calandria can is raised above about 550°C and the temperature of an unheatable (Type F) can is raised above about 150°C, the square jacket sides bulge outward approaching a round cross section. The bulging starts at the axial center and moves progressively toward each end. The tendency for the jacket to become round is constrained by the presence of the matrix tube. Thus the expanding calandria can tends to fill the available volume within the matrix tube and, to the extent that the matrix tube walls are deflected, the available volume within the adjacent matrix tubes. The bulging can fills the matrix tube, beginning at the center of the can and progressing toward the ends as the can is heated.

Below about 900°C, the vapor pressure of the sodium is small and the calandria cans expand by yielding only enough to accommodate the internal volume of sodium within the yield stress of the jacket material. Above about 900°C, the sodium-vapor pressure rises rapidly to levels that cannot be contained by the diminished tensile strength of the Type 304L stainless steel.

If it is assumed that all the volume within the matrix tube containing the can and half the volume in the adjacent matrix tubes are available to accommodate the expansion of the overheated calandria can, then at 900°C, about 9.5 in. of the heatable can length and about 11 in. of the unheatable-can length (out of the total 11.7 in. of calandria-can length between the headers) will be expanded out against the matrix tube. Assuming reasonable ductility, probably neither the heatable nor unheatable can would fail up to 900°C. Direct calandria-can overheat tests, reported in Sec. 6.2.3, confirm this conclusion.

Above about 900°C, it is not possible to calculate accurately the course of calandria-can distortion and ultimate failure because of lack of strength data on Type 304L stainless steel in this range and the complexity of the header-to-jacket weld configuration. Rough calculations indicate that the rapidly rising sodium-vapor pressure will burst the cans, probably at the center of the header-to-jacket weld, somewhere in the range 950-1050°C, regardless of the calandria-can type. Calandria-can burst tests are described in Sec. 6.2.3.

6.2.3 Operational Testing of Calandria Cans

Two types of calandria-can testing have been carried out: first, thermal-cycling tests on heatable (Type H) cans within normal operating limits; second, overheat failure tests on heatable and unheatable sodium-filled cans.

A total of 17 heatable (Type H) calandria cans have been subjected to thermal-cycling tests at various times during the development and proof-testing of the calandria can design. Of the 17, 11 were prototype calandria cans produced with special tooling and stock materials, and the remaining six were production cans. The production cans were exactly typical of the entire inventory of cans in every way: material, tooling, welding, etc. The cycling tests carried out are summarized in Table 28. There were no calandria-can failures in the thermal-cycling tests nor any distortions large enough to significantly interfere with the use of the cans for the planned experiments. The cycling tests involving calandria cans HX01, HX03, HX04, HX06, HX07, and HX10 included an accidental overheat to 750°C, which caused only a small amount of distortion in the outer jacket of one can. The distortion was not significant operationally. Details on the 750°C accident are given in Sec. 6.1.3.

TABLE 28. Heatable (Type H) Calandria-can Thermal-cycling Tests

All tests were 90 to 600 to 90°C with 30-60-min heatup times (using approximately 1 kW per calandria can) and 2-4-hr cooldown times; about 10-min holds at 600°C

Heatable (Type H) Calandria Cans		Environment	No. of Cycles	Material in Calandria
Prototype cans:	No. 7	Argon	350	SS bars
	No. 8	Air	10	
	No. 10	Air	10	
	No. A4	Argon	10	
	No. A5	Argon	10	
	No. A6	Argon	10	
	No. A7	Argon	10	
	No. A8	Argon	10	
	No. A9	Argon	10	
	No. A10	Argon	10	
	No. 3	Argon	350	
Production cans:	No. HX01	Argon	350	Depleted-UO_2 fuel rods
	No. HX03	Argon	300	
	No. HX04	Argon	400	
	No. HX06	Argon	600	
	No. HX07	Argon	600	
	No. HX10	Argon	600	

Calandria-can overheat tests have been carried out on six heatable (Type H) and four unheatable (Type F) cans. All the tests except one have been carried out in matrix-assembly sections, with 2.037-in.-square steel bars in the tubes adjacent to the heated can, which very closely simulate the situation in the VTRZ matrix as to available volume for the expansion of the calandria can. All the tests were carried out in air. Two of the heatable and one of the unheatable calandria cans tested were prototype cans; the remaining cans were production cans exactly typical of the overall inventory as to materials, welding, tooling, etc. The results of the overheat tests are summarized in Table 29.

TABLE 29. Results of Calandria-can Overheat Tests

Prototype or Production Can	Can Type; H = Heatable F = Unheatable	Can No.	Can History	Test Setup	Temperature at Which Sodium Was Released, °C
Prototype	H	1	New can	In unconstrained matrix tube	1010
Prototype	H	2	New can	In matrix assembly typical of VTRZ	905[a]
Prototype	F	4	New can	In matrix assembly typical of VTRZ	>910
Production	F	FX12	New can	In matrix assembly typical of VTRZ	>960
Production	F	FX16	New can	In matrix assembly typical of VTRZ	>915
Production	F	FX18	New can	In matrix assembly typical of VTRZ	1035
Production	H	HX13	New can	In matrix assembly typical of VTRZ	>940
Production	H	HXR10	New can	In matrix assembly typical of VTRZ	925
Production	H	HXR07	New can	In matrix assembly typical of VTRZ	>930
Production	H	HX01	After 300 cycles[b]	In matrix assembly typical of VTRZ	>910
Production	H	HX04	After 400 cycles	In matrix assembly typical of VTRZ	935
Production	H	HX06	After 600 cycles	In matrix assembly typical of VTRZ	950

[a]Anomalous failure; see text.
[b]300 cycles, 90 to 600 to 90°C.

Several points should be made regarding the overheat test results of Table 29.

(1) The cans were heated in these tests with four independent 1-kW, 12-in. cartridge heaters per can of the type that will be used in the VTRZ. In almost every test run, one or more of these heaters failed below 900°C. Where the can exceeded 900°C but did not fail and enough of the heaters

failed to make it impossible to raise the temperature further, the test was not rerun and the highest temperature reached is given in Table 29 and marked by a greater-than sign (>). For example, prototype can Type F No. 4 did not fail up to 910°C, at which point all heaters had failed.

(2) Prototype can Type H No. 2 failed at an unusually low temperature due to the rupture of an accidental and unintentional weld between the fill plug and the underlying tube; i.e., the can was defective. A special X-ray examination step was added in the calandria-can production process to avoid this problem in the production cans.

(3) Prototype can Type H No. 1 was tested in an unsupported single matrix tube, which permitted bulging in excess of that which is possible in the regular VTRZ matrix assembly. This resulted in the relatively high bursting temperature.

6.3 The Inner Matrix Assembly

6.3.1 Stress Analysis

The design of the VTRZ Inner Matrix Assembly (i.e., the heatable zone) is discussed in detail in Sec. 4.5.3. This section summarizes the results of stress analyses of the inner matrix assembly mounted on the ball mounts, the inner-matrix-assembly gross axial motion restrainers, and the effect of a center-to-edge radial temperature gradient in the inner matrix assembly. Load-versus-deflection tests on the inner-matrix-assembly prototype are discussed in Sec. 6.3.3.

6.3.1.1 Stress Analysis of Inner Matrix Assembly Mounted on Ball Mounts

The combination of the 1/8-in.-thick jacket and the array of matrix tubes within it results in a very rigid box-like structure. From Tables 2 and 5 it is assumed that the load in the inner matrix, including the seismic load, totals 5500 lb and is uniformly distributed axially and radially.

In the direction transverse to its long (36-in.) axis, the inner matrix assembly may be considered as a simply-supported beam about 21 in. between the two sets of ball-mount supports with a height at the center of the span of about 19.5 in. and with an effective width of 37 in. (see Fig. 7). Because of the assumed uniform loading per matrix tube and the shape of the inner matrix (i.e., the octagonal shape), the beam is approximately of uniform strength across the span. Therefore, taking the conditions at the center of the span as typical, the beam may be considered as a beam of uniform cross section with a moment of inertia of about 1670 in.^{4} (including the jacket and the matrix, but excluding the front and rear flanges, the front and rear covers, and the central nine matrix tubes), a height of 19.5 in., a uniform load of about 395 lb/in., and an unsupported span of about 21 in. With this

assumption of an equivalent uniform beam, the calculated maximum outer-fiber tensile stress due to bending is about 110 psi and the central downward deflection much less than 1 mil.

In the direction of the long axis, the inner matrix assembly is essentially a uniform beam with an overall effective length of 37 in., a height of about 19.5 in., and a moment of inertia of about 850 in.^{4} (including the jacket and the matrix, but excluding the central nine tubes). Assuming the uniform 5500-lb load, the beam is loaded uniformly along its 37-in. length at about 150 lb/in. There are, in fact, five ball mounts uniformly distributed along each of the two sides of the inner barrel, which probably produce intermediate supports along the 37-in. length. For a conservative calculation, however, assume that the 37-in.-long inner barrel is simply supported only at the extreme ends. In this case, the maximum outer-fiber tensile stress due to bending is about 300 psi, and the maximum central deflection is about 0.2 mil.

These stresses and deflections are negligible at any temperature within the normal operating range.

6.3.1.2 Stress Analysis of Inner-matrix-assembly Axial Motion Restrainers

The axial motion restrainers serve two purposes: First, they control the axial position of the front cover face of each half-zone; second, they prevent gross axial motion of the inner matrix assembly as a result of rapid changes in reactor-table position as in reactor scrams, starting and stopping of the movable table, and earthquakes. Thus, the impact loads on the axial-motion-restrainer brackets may be axially forward or rearward. There are four motion-restrainer brackets on each half-zone. They are welded to the outer-matrix liner, near the front, and extend across the insulation space into pockets in the front flange. Figure 77 shows a motion-restrainer bracket.

The highest movable-table axial-motion speed occurs during a scram. To scope the problem, the scram speed of 30 in./min was taken as the criterion in the stress analysis for the motion restrainers. All friction in the ball mounts was ignored. Table acceleration time was ignored in the analysis. The stress analysis was carried out under the assumption that the inner matrix assembly will be moving at 30 in./min when the impact with the stationary outer matrix assembly occurs through the motion-restrainer brackets. This analysis also covers the case in which the outer matrix assembly is moving at 30 in./min and strikes the stationary inner matrix assembly through the motion restrainers (as in a scram).

As the inner matrix assembly is decelerated from 30 in./min to zero by the axial motion restrainers, there is an exchange of energy between the inner matrix assembly and the restrainer brackets; the kinetic energy of

the inner matrix assembly is absorbed into potential energy of the deflections of the brackets. The maximum deflection of the tips of the restrainer brackets can be obtained by equating the kinetic energy with the deflection energy of the bracket. The maximum fiber stress at the base of the bracket is then obtainable from the standard equations for a cantilever beam. Assuming a 5000-lb inner-matrix-assembly weight, the calculations predict a maximum restrainer deflection of about 1 mil, a maximum fiber stress in the base of the restrainer bracket due to bending of about 800 psi, and a maximum shear stress in the bracket-to-outer-barrel-liner weld of about 2500 psi. The restrainer brackets operate between a maximum of 650°C at the top of the bracket to about 40-50°C at the base. The calculated stresses are acceptable within the design limits of Tables 3 and 4.

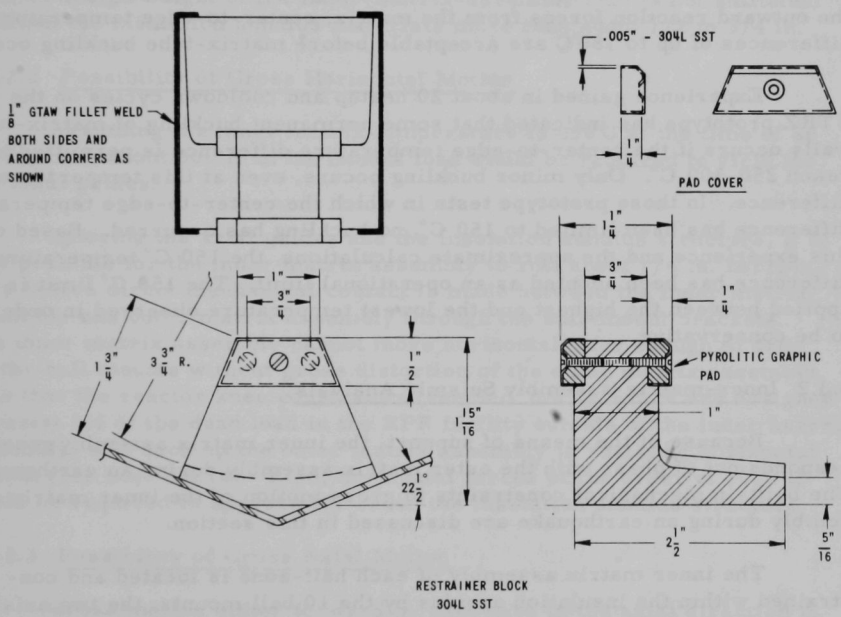

Fig. 77. Axial-motion-restrainer Bracket

There will be some tendency for the inner barrel to bounce off the restrainer brackets and restrike the brackets in the opposite direction. This is not considered serious. Axial-motion friction in the assembly should rapidly damp out the axial oscillation.

6.3.1.3 Thermal Stress in Inner Matrix Assembly due to a Center-to-Edge Temperature Gradient

If a radial temperature gradient is permitted to develop between the center of the inner matrix and the inner matrix jacket so that the jacket is

cooler than the matrix, the inner matrix is compressed by the jacket as it attempts to take on a smaller circumference. This thermal stress situation arises during inner-matrix cooldown because the heat is removed from the outer surface of the jacket.

Although yielding, and not simple buckling, of the matrix-tube walls is the real limiting factor in setting permissible center-to-edge temperature differences, rough thermal-stress calculations have been based on buckling of the matrix as the criterion. Very conservative calculations have been carried out that assume the entire inner matrix is isothermal and the jacket is at a cooler temperature (i.e., the radial temperature profile is flat with a step change at the matrix-jacket interface). The analysis indicates that, accounting for the elastic elongation of the jacket caused by the outward reaction forces from the matrix, center-to-edge temperature differences of up to 180°C are acceptable before matrix-tube buckling occurs.

Experience gained in about 20 heatup and cooldown cycles on the VTRZ prototype has indicated that some permanent buckling of matrix-tube walls occurs if the center-to-edge temperature difference is permitted to reach 250-300 C°. Only minor buckling occurs, even at this temperature difference. In those prototype tests in which the center-to-edge temperature difference has been limited to 150 C°, no buckling has occurred. Based on this experience and the approximate calculations, the 150 C° temperature difference has been adopted as an operational limit. The 150 C° limit is applied between the highest and the lowest temperature observed in order to be conservative.

6.3.2 Inner-matrix-assembly Seismic Analysis

Because of the means of support, the inner matrix assembly generally responds out of phase with the outer matrix assembly during an earthquake. The built-in mechanical constraints to gross motion of the inner matrix assembly during an earthquake are discussed in this section.

The inner matrix assembly of each half-zone is located and constrained within the insulation annulus by the 10 ball mounts, the two axial guides, the four axial-motion restrainers, and the insulation and CGR structure. Gross vertical motion is constrained by the ball mounts and the insulation annulus structure. Gross horizontal motion is constrained by the axial guides, the ball-mount brackets, and the insulation annulus structure. Gross axial motion is constrained by the axial motion restrainers, the axial guides, and the insulation annulus structure.

6.3.2.1 Possibility of Gross Vertical Motion

Calculated on the basis of the inner matrix jacket and matrix alone, the natural period of the inner matrix assembly is about 0.001 sec. With

the most pessimistic interpretation of the tests of the flexibility of the ball mount and outer matrix liner discussed in Sec. 6.3.3, the inner-matrix and ball-mount combination has a natural period of about 0.05 sec. In either case, the criteria of Table 2 apply and the appropriate vertical seismic design load is about 0.1 of the dead load within the design stress and about 0.2 within the yield stress. The criteria have been applied in the design of all VTRZ components and in the design of the inner-matrix and ball-mount components in particular.

Within the assumed earthquake conditions, it is clear that the ball mounts will not fail (see Sec. 6.4) so as to permit gross vertical motion. It is true, however, that even if the ball mounts were to fail completely, the 5000-lb design weight of the inner-matrix-assembly load is not sufficient to crush the insulation annulus materials more than about 1/2 to 3/4 in.

6.3.2.2 Possibility of Gross Horizontal Motion

Assuming the inner matrix temperature is 650°C at the time of an earthquake, about 300 lb of horizontal load would be required to yield the two axial guides.

Ignoring the axial guides and the insulation annulus structure, it is only possible for the inner matrix assembly to roll about 1/4 in. horizontally before direct mechanical contact is made between the inner matrix assembly and outer matrix assembly through the ball-mount brackets. The inner matrix assembly cannot move horizontally far enough to drop off the ball mounts without gross distortion of the outer matrix assembly. Note that the reactor knee constraints (see Sec. 6.6.4), which are designed to resist 0.4 of the dead load in the ZPR facility outside of the inner barrel assembly, will back up the outer matrix assembly in resisting horizontal motion (see Sec. 4.5.14). Also, horizontal forces of the order of 1000 lb would be required to appreciably crush the insulation annulus structure.

6.3.2.3 Possibility of Gross Axial Motion

Gross motion either forward or backward in the axial direction is constrained principally by the axial-motion restrainers (see Sec. 6.3.1.2). Assuming a temperature of 100°C at the base of the restrainer brackets, an axial force of more than 88,000 lb would be required to yield all four of the restrainer brackets. In addition, about 1000 lb applied axially would be required to yield the two axial guides and perhaps 200-300 lb to move the insulation annulus structure axially any appreciable distance.

Although arguments as to earthquake resistance are somewhat qualitative, no gross motion of the inner matrix assembly relative to the outer matrix will occur in any earthquake that can be reasonably foreseen.

6.3.3 Inner-matrix-assembly Prototype Load Tests

The flexibility of the upper and lower ball-mount brackets and, particularly, the flexibility of the connection of these brackets to the inner matrix assembly and the outer matrix liner are very difficult to calculate accurately. It is, however, important to know that these connections are not sufficiently flexible to permit excessive deflection of the inner barrel assembly under load or to cause a natural resonance period large enough to amplify earthquake acceleration spectra.

Load-versus-deflection tests carried out on the VTRZ prototype included a complete VTRZ half-zone assembly, i.e., inner matrix assembly, outer matrix assembly, and ball mounts. The tests were carried out at room temperature using depleted-uranium blocks inserted into the inner matrix. The front and rear covers were off during the test. To simulate the conditions in the ZPR assembly, the outer matrix was completely loaded with depleted-uranium blocks during the test. Although the test was not done in the regular reactor matrix, a jig structure was arranged around the outer matrix assembly to simulate the effect of the surrounding matrix tube bundles. Loading was varied from the empty matrix to 5500 lb in the matrix. The result of the test was a linear (no permanent set) downward deflection of the bottom center of the inner barrel assembly. At 5500 lb, the average deflection was about 28 mils; the front flange deflected downward about 38 mils, and the rear flange about 18 mils. Assuming that the deflections are inversely proportional to Young's modulus, the predicted deflections at 600°C would be about 15% larger--about 33 mils for the average.

The measured deflections are considered acceptable, but greater than ideal. To reduce these deflections in the final design, additional bracing has been added to the design of the ball mounts to reduce their flexibility. The axial distribution of the ball-mount locations has been changed to achieve a more equal front and rear deflection under load. Although the effect of the stiffening and relocation of the ball-mount brackets is not known accurately, the deflections in the final design will be less than those in the prototype.

6.4 Ball Mounts

6.4.1 Ball-mount Stress Analysis

6.4.1.1 Ball-mount Brackets

Each of the 10 ball mounts on each of the VTRZ half-zones has been designed to withstand a load of 2750 lb within the design stress limits of Sec. 3.3. The 2750-lb load per ball mount is based on the maximum load that could be applied to a single ball mount within the 5500-lb design load (5000 lb plus 10% seismic load; see Tables 2 and 5) of each inner-matrix half-zone assembly. Although there are 10 ball mounts (five per side) on each VTRZ half-zone, the most conservative assumption is that only three of them (two on one side and one on the other), the minimum number required

for static equilibrium, are actually in contact and taking load. Thus, one ball mount may be called on to carry half the 5500-lb load, i.e., 2750 lb.

The design of the lower ball-mount bracket shown in Fig. 78 reduces bending moments in the lower bracket by providing direct support in the vertical plane of the applied load. The designs of both the upper and lower ball-mount brackets are intended to provide very stiff support for the insert pad areas at the center of the brackets in order to reduce bending moments. This may be seen in Figs. 78 and 79.

A stress analysis of the upper ball-mount-bracket horizontal crosspiece (see Fig. 79) that supports the upper insert pad indicates that, for the design load of 2750 lb per ball mount, the maximum deflection of the crosspiece will be less than 0.1 mil. This will not cause any appreciable stresses in the insert pads. The load on the ball mounts will never be off the center of the crosspiece by more than 3/8 in. (3/8 in. is the maximum thermal expansion of the entire axial length of the VTRZ), so that with the central support the maximum stress in the crosspiece will not exceed 4000 psi. The stress level in the upper ball-mount crosspiece is, therefore, well within the design limit stresses given in Sec. 3.3 for Type 304L stainless steel up to 600°C.

The entire upper ball-mount bracket is made from a single piece of Type 304L stainless steel, so that welds are not needed to attach the vertical gussets to the horizontal crosspiece. This eliminates possible weld-stress concentrations if welds were used. A stress analysis of the bending-moment stresses induced in the vertical gussets indicates that even if the upper gusset is assumed to support the entire 2750-lb load, the maximum stress in the gusset will not exceed 4000 psi. If the upper and lower gussets are assumed to equally support the load, the maximum stress will be less than 1000 psi. These stress levels are well within the design stress limits.

Pickup holes are provided in each upper ball-mount bracket for lifting and removing the VTRZ inner matrix assembly from the outer matrix assembly. The calculated stress levels in the upper brackets will be less than 10,000 psi if at least two brackets per side (four per half-zone) are used in lifting the inner matrix assembly. Since the inner matrix assembly will always be removed at room temperature, the indicated stress levels are well within the design limit stresses for temperatures less than 100°F (see Sec. 3.3).

The upper ball-mount brackets are attached to the inner matrix jacket by 3/8-in.-long, 1/8-in.-deep fillet welds on 5/8-in. centers running along both sides of the upper gusset and the outside of the lower gussets, as shown in Fig. 79. The calculated tensile stresses in these welds due to bending moments are less than 3000 psi, and the calculated shear stresses are about 2500 psi. Both of these values are within the design stress limits for 600°C operation.

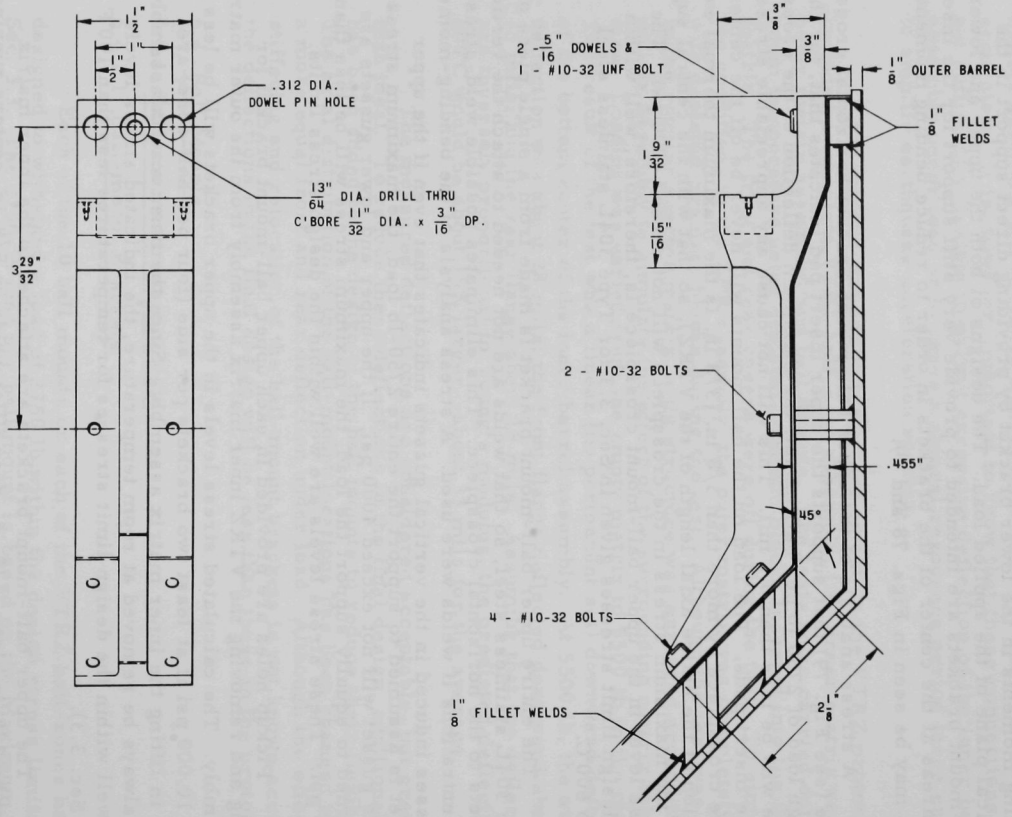

Fig. 78. Lower Ball-mount Bracket

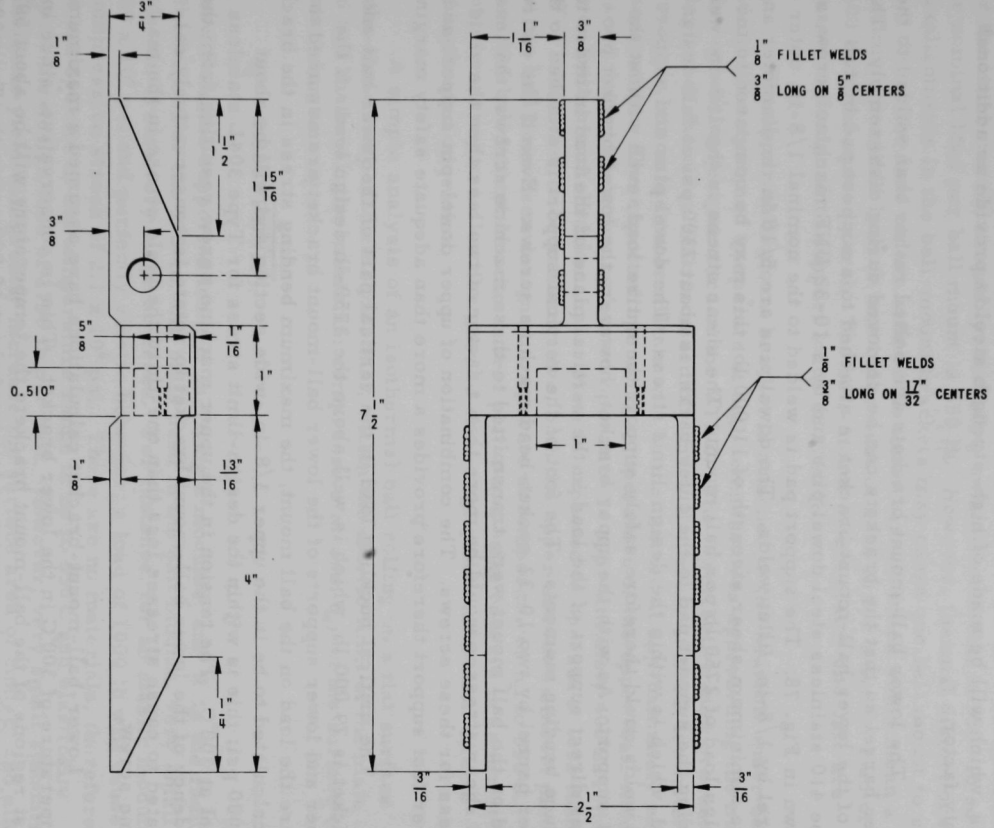

Fig. 79. Upper Ball-mount Bracket

The lower ball-mount bracket (Fig. 78) is attached to the outer matrix assembly and is designed to operate at temperatures near room temperature; operating temperatures on the lower bracket will certainly never exceed 300°C. The appropriate design stress limits, therefore, are those for Type 304L stainless steel below 300°C, except for the dowel pins and bolts, which will be made of high-strength steel to provide an additional safety factor.

The lower ball-mount brackets are bolted rather than welded to the outer barrel so that the brackets can be removed during disassembly. The top of the lower ball-mount bracket is attached to a support pad by two Type 410 stainless steel dowel pins and by a 10-32 UNF machine screw, as shown in Fig. 78. The support pad is welded to the nominal 1/8-in. outer barrel by 1/8-in. fillet welds. The dowel pins are 5/16 in. in diameter and have a minimum shear strength of 11,000 lb; this may be compared to the design load of 2750 lb per ball mount. The shear stress in the 1/8-in. welds holding the support pad to the outer barrel is about 7300 psi at full design load, which is within the design-limit stress. The dowel pins and support pad welds could therefore safely support the entire load, even without the foot support. As with the upper bracket, however, the lower bracket provides direct support of the load in the vertical plane of the load in order to reduce bending moments. The foot of the vertical support is attached to the outer barrel by two 10-32 socket-head machine screws. Even if the entire load on the ball mount were transmitted to these machine screws, the tensile and shear stresses would be more than a factor of two less than the yield stress for these screws. The combination of upper dowel-pin support and lower foot support therefore provides a more than adequate safety margin.

The critical buckling load in the vertical part of the lower ball-mount bracket is 79,000 lb, which is well above the 2750-lb design load. If the upper and lower supports of the lower ball-mount bracket are assumed to share the load on the ball mount, the maximum bending stress in the bracket is calculated to be in the upper 3/8-in.-wide section and will be about 10,000 psi; this is within the design-limit stress for Type 304L stainless steel at 300°C. The tension in the upper machine screw resulting from the tendency of the lower ball-mount bracket to rotate is conservatively calculated to cause stresses less than one-third the yield stress in the machine screw.

Lower-ball-mount-bracket calculations have assumed a maximum temperature of 300°C in the lower bracket. This is conservative, since in most regions of the ball-mount brackets the temperature will be about 50°C. Note that, with maximum stress levels of about 10,000 psi in the Type 304L stainless steel, it would take temperatures above 650°C to cause rupture in 1000 hr, so that even abnormally high temperatures in the lower brackets will not cause failure.

6.4.1.2 Ball-mount Insert Plates and Balls

The weight of the entire inner matrix assembly is supported by the 10 ball mounts. These ball mounts are the only vertical load-carrying connection between the inner and outer matrix assemblies. The design load for the inner matrix assembly, including seismic criteria, is 5500 lb so that the nominal load per ball mount is 550 lb. However, thermal distortions or misalignments in the ball-mount brackets may cause one ball mount to support the entire load on one side of the inner barrel, which would mean a maximum possible load on one ball mount of 2750 lb for a design load of 5500 lb in the inner barrel. The ball-mount insert plates and ball are therefore designed to support loads of 2750 lb.

The upper ball-mount bracket is attached to the heatable inner barrel and must be designed to operate at high temperatures approaching the maximum operating temperature of the VTRZ. The lower ball-mount bracket is attached to the outer matrix assembly and will operate at much lower temperatures, since the outer matrix will be maintained at approximately room temperature. The expected operating temperature of the upper-ball-mount-bracket insert plate during heated operation is approximately 400°C. The lower-ball-mount-bracket insert plate is expected to operate at less than 200°C. However, to be conservative, both the upper and lower insert plates and the ball have been designed to operate at temperatures up to 550°C. Since the ball-mount-bracket insert plates and balls operate in an air atmosphere, they are also designed to show negligible oxidization effects during heated operation.

A simple analysis of an isothermal ball rolling on a flat surface at the same temperature shows that, within the elastic limit of the plate and ball material, the maximum compressive stress, q_0, on the surface of contact is given by

$$q_0 = 0.388\sqrt[3]{PE^2/R^2},$$

where P is the supported load, E is Young's modulus, and R is the radius of the ball. For the 5/8-in.-dia balls used in the ball mounts, very small loads can create very large stresses. For instance, for an elastic modulus of 30×10^6 psi and perfectly elastic behavior, a load of 1000 lb will cause a compressive stress of 2.1×10^6 psi. There are no materials, therefore, that can operate in the temperature range of up to 550°C and elastically support the design load of 2750 lb per ball. However, very small amounts of inelastic yield will greatly increase the surface area of contact and allow the ball and plate to support the load without failure. Direct testing carried out as part of the VTRZ development program showed, in fact, that special machine-tool grades of tungsten carbide, titanium carbide, alumina (Al_2O_3), and silicon carbide could support the design load with very small inelastic yield. This is especially true of certain grades of tungsten and titanium carbides which supported loads in excess of 10,000 lb at 600°C without

failure in the tests. These materials, however, are very brittle, and failure will typically cause complete cracking of either the plate or the ball. Ductile materials such as steel will show much greater yielding under load than the very strong and hard carbides, but will not exhibit brittle failure. Ductile materials will simply continue to yield under load until the area of contact is large enough to support the load with stress less than the yield stress. Ductile materials therefore tend to exhibit inherently safer behavior under load.

Ductile materials such as stainless steel, while having excellent corrosion properties and exhibiting no brittle failure, are comparatively weak and give large amounts of yield. A large number of very strong super alloys were considered as possible materials for the insert plates and balls. Inconel 718 was chosen for testing on the basis of its excellent oxidization resistance and very high yield strength at elevated temperatures. Typically, Inconel 718 has a yield strength in excess of 150,000 psi at 600°C. No super alloys have significantly stronger yield strengths than Inconel 718 at 600°C.

No stress-analysis theory was found during the design of the VTRZ ball mounts to adequately describe the stresses in a rolling ball caught between two plates, carrying a vertical load, and subjected to a vertical temperature gradient. As a result, the ball-mount insert plates and balls were designed almost entirely on the basis of direct tests on various ball-mount configurations under conditions exceeding the actual VTRZ conditions in severity. The extensive ball-mount insert plate and ball testing carried out is described in Sec. 6.4.3 below. As described there, the ball-mount insert plate and ball combination shown by the tests to meet the load, rolling, temperature, and corrosion-resistance requirements was Inconel 718 plates and 5/8-in.-dia tungsten carbide balls.

6.4.2 Corrosion of Ball-mount Insert Plate and Ball Material

Since the ball-mount brackets are not in an inert atmosphere, the materials used in the brackets must have good oxidization resistance at elevated temperatures. The ball-mount brackets themselves are stainless steel and therefore exhibit very little oxidization. The various proposed insert plate and ball materials were specifically tested for oxidization resistance. The Inconel 718, alumina, and silicon carbide materials showed essentially no oxidization up to 600°C, even over very long time intervals. The tungsten and titanium carbides did show varying amounts of oxidization, depending upon material grade and temperature.

The oxidization tests were conducted in an open electric furnace with thermostatic control. Various sample sizes were placed in the furnace for periods between 10 and 72 hr with open exposure to the atmosphere. The test samples were weighed before and after heating to determine any weight gain or loss during heating in order to determine the oxidization rate. The samples could therefore be quantitatively rated in terms of weight change per unit surface area per hour.

As mentioned in Sec. 6.4.1.2, the insert plate material chosen for the final design was Inconel 718. For all temperatures tested up to 600°C, Inconel 718 showed no measurable oxidization and exhibited only very slight discoloration.

Tungsten and titanium carbides did exhibit measurable oxidization. The titanium carbides were appreciably better than the tungsten carbides in oxidization resistance at 600°C. The titanium carbide showed an oxidization rate gain of 5×10^{-6} g/cm^2-hr at 600°C in comparison with 5×10^{-3} g/cm^2-hr of tungsten carbide at 600°C. Nevertheless, tungsten carbide was chosen for the ball material on the basis of the load-test results discussed in Sec. 6.4.3 and the fact that the expected temperature range of the ball is 400°C or less. At 400°C the tungsten and titanium carbides have essentially the same oxidization rate, about 2×10^{-7} g/cm^2-hr, so that neither material is appreciably more oxidization-resistant than the other in the expected operating temperature range. Further, the oxidization rate of either material at 400°C is negligibly small, and both have sufficient oxidization resistance for the ball-mount application. Tungsten carbide was also chosen as the ball material because of its greater availability (especially in ball form).

The rolling-ball-mount tests and the prototype test experience, described in Sec. 6.4.3, confirmed that oxidization of the tungsten carbide balls and the Inconel 718 plates during heated operation is not a problem.

6.4.3 Ball-mount Tests

The preliminary ball-mount design used in the VTRZ prototype called for a total of 12 ball mounts to support the inner barrel. Each ball mount had high-density alumina (Al_2O_3) insert plates and a 1/2-in.-dia alumina ball. The preliminary design load for each ball was calculated on the basis of equal loading of each ball mount, giving a design load of about 320 lb per ball mount; the initial inner-barrel design weight was set at 3800 lb. A stress analysis of the preliminary ball-mount bracket design indicated adequate strength for the brackets under a design load of 320 lb per ball mount. In addition, the alumina plates and balls were tested at room temperature and found to have an ultimate strength of 1500-1800 lb per ball. This indicated an expected load capacity of 700 lb per ball at 600°C and a load capacity of about 1000 lb at the expected operating temperature of 400°C. The alumina plates were also known to be completely stable when heated to 600°C in an air atmosphere, so that no oxidization problems were expected.

The prototype VTRZ heatup tests confirmed many of the calculations made for the prototype design ball mounts. In particular, the calculated and measured temperature distributions in the ball mounts were in good agreement, and the expected maximum operating temperature of

about 400°C for the ball-mount insert materials was confirmed. The prototype tests also showed that oxidization of the alumina during operation was not a problem. The stainless steel portions of the ball-mount brackets also showed no sign of failure or yielding in the prototype VTRZ heatup tests, which included a 100-hr, 550°C heatup run. The prototype tests did uncover, however, misalignment and thermal-distortion problems leading to unequal loading of the ball mounts and resultant cracking of some of the alumina insert plates. The unequal loading of the ball mounts had not been considered in the preliminary design of the ball mounts. The prototype tests led to a reevaluation of the design load per ball mount, and the final design load was set at 2750 lb per ball mount. The 2750-lb load per ball mount is the maximum possible load on any one ball mount for a total design weight of 5500 lb in the inner barrel, since at least one ball mount per side must support the inner barrel no matter what thermal distortions or misalignments exist.

The alumina insert plates failed during the initial prototype testing. The failures could have been caused by one ball mount taking nearly half the prototype inner-barrel weight of 2500 lb during heatup, or could have occurred during handling of the barrel during insertion and removal. Whatever the cause, the failures proved that the original design load of 320 lb per ball mount was unrealistic. Later prototype tests were conducted with tungsten carbide balls and insert plates. The tungsten carbide balls and insert plates have shown no sign of failure in the later prototype testing.

Even though no tungsten carbide insert plates and balls failed in the VTRZ prototype testing, this testing was not considered adequate to provide a basis for the final ball-mount-insert material design. The prototype VTRZ inner matrix assembly, for example, weighs only about 2500 lb, which is the normal weight of a VTRZ half-zone but is less than half the desired design load of 5500 lb. Further, the exact load on each ball mount during prototype testing is not known, so there is no assurance that worst-case conditions have been encountered. For these reasons, a heatable ball-mount test rig was constructed to determine the best materials for the insert plates and balls. The test rig permits applying a load of up to 10,000 lb on a single ball, while at the same time heating the upper insert plate up to about 600°C and maintaining the lower plate at about 100°C. The test rig can therefore duplicate the worst-case conditions for the actual ball mounts in regards to load, insert-plate temperature, and temperature gradient across the ball. In addition, the ball-mount test rig can simulate the actual rolling of the ball between the insert plates by moving the lower platform supporting the lower insert plate.

The ball-mount test rig was used to test a large variety of possible combinations of insert-plate and ball material. Tungsten carbide and titanium carbide materials supported the largest loads with the least yield of any materials tested. In the static tests, loads of 10,000 lb could be supported

with total yield in the plates and ball of only about 2 mils. Inconel 718, a nickel-based super alloy, was also tested and shown to be able to support loads up to 10,000 lb, but with larger amounts of yield than the very hard and brittle carbides.

Rolling tests of the insert materials were also conducted to completely simulate the actual operating conditions. The tungsten carbide insert plates and balls were demonstrated to be able to support 5500 lb at 550°C through 50 rolling cycles in the same groove. However, if a tungsten carbide ball was rolled through a previous groove in an insert plate, at right angles to the groove, failure was observed at the design load of 2750 lb. The titanium carbide showed an even greater tendency to fail during rolling tests than tungsten carbide and was rejected in comparison to tungsten carbide. In the actual VTRZ, the ball can be expected to roll in virtually the same path in each heatup so that tungsten carbide does seem to be a suitable material for the insert-plate and ball material. However, tungsten carbide has the disadvantage that when failure occurs it typically means the complete fracture of either the insert plate or the ball. Further, the insert plates and balls would have to be changed each time the VTRZ was disassembled, or otherwise moved, in such a way as to change the position of the ball on the insert plates, i.e., change the groove.

Inconel 718 is a very strong nickel-based super alloy with excellent corrosion resistance and high-temperature yield strength. Test results from the ball-mount test rig showed that Inconel 718 can support loads of up to 10,000 lb with much less yield than other ductile materials such as steel. However, static tests of Inconel 718 showed that, for an Inconel 718 ball on Inconel 718 plates, significant flattening of the ball as well as grooving of the plates occurred at the design load of 2750 lb. This would lead to the possibility that the ball would be moved between the plates by sliding rather than rolling motion. For this reason, the use of a hard tungsten carbide ball between ductile Inconel 718 plates was considered the best potential combination for the final design.

Extensive rolling tests of a 5/8-in. tungsten carbide ball between Inconel 718 plates have demonstrated the adequacy of these materials for the final design. Tests have been conducted with loads of 2750 and 5500 lb on one ball and with the upper plate heated to 550°C and the lower plate maintained at about 100°C. The tests have confirmed that the tungsten carbide maintains its roundness, while the Inconel 718 deforms slightly (grooves) to support the load with greatly reduced stress relative to the tungsten carbide on tungsten carbide cases. Further, the tests have shown that sideways forces of less than 100 lb are enough to cause movement of the Inconel 718 plates relative to the tungsten carbide ball with a 2750-lb load. This sideways force is not appreciably greater than the force needed to cause movement of the tungsten carbide plate and ball, even though there is some yielding in the Inconel 718 plate.

The 5/8-in. tungsten carbide ball has been tested on Inconel 718 plates for more than 100 rolling cycles, and endurance tests have shown no failure during several weeks of heated operation at 2750-lb load. In addition, tests have also been conducted in which the ball has been rolled in many directions through previous grooves in the Inconel plates. No failure has been observed in either the Inconel plates or the tungsten carbide balls during any of the tests. The maximum depth of the groove in an Inconel plate after many rolling cycles with a 2750-lb load and a temperature of 550°C was about 6 mils. This means that the inner barrel should not drop more than 12 mils in operation due to grooving at the Inconel plates; this is an entirely acceptable amount and has been compensated for in the design of the ball-mount brackets.

No appreciable oxidization of the tungsten carbide ball has been observed during the rolling tests in which the upper plate was at 550°C. Since in actual operation the upper-plate temperature is expected to be about 400°C, no oxidization problems are expected. Further, there have been no signs of failure of the tungsten carbide ball due to thermal gradients through the ball. Tests in the ball-mount test rig have been conducted with a total gradient across the tungsten carbide ball of greater than 400°C, which is nearly twice the gradient expected in the actual operating configuration.

The results from the ball-mount test rig have indicated the suitability of the choice of Inconel 718 for the insert-plate material and tungsten carbide for the ball material. Testing is presently continuing to confirm these results for more rolling cycles and over longer periods of operation. However, the testing already conducted has been accomplished with greater pressures and temperatures than will be encountered in actual operation. Further, more than 100 rolling cycles with a 2750-lb load and an upper-plate temperature of 550°C have already been conducted. In addition to the periodic rolling cycles during heated operation, the ball-mount materials have been subjected to several thermal cycles (upper-plate temperature going from less than 100 to 550°C and back to less than 100°C), and the load has been continuously applied for more than 1000 hr of unheated operation and 500 hr of heated operation (upper-plate temperature of 550°C). Thus, the tests already made are adequate to confirm the ball-mount performance in actual operation.

6.5 Inner-matrix-assembly Cover Plates

6.5.1 Front Cover

The half-zone front cover plate of the inner matrix assembly is designed to maintain the integrity of the VTRZ inner-matrix argon cover-gas envelope with minimum perturbation of the neutron-flux spectrum in the center of the reactor. The thickness of 20 mils for the front-cover pan section was chosen as the best compromise between reasonable mechanical

strength and the minimum neutron-spectrum perturbation criterion. The front cover is not a structural member of the inner matrix assembly, and yielding of the front cover under unusual circumstances, such as a reactor scram during heated operation or internal overpressure, will not interfere with VTRZ operation. The front cover is, however, designed to have adequate strength to maintain the integrity of the inner-matrix-assembly cover gas under all operating conditions. If at any time, due to a series of abnormal operating conditions, yielding of the 20-mil-thick front-cover pan section becomes appreciable, the front-cover pan section will be replaced. The front cover is designed to permit rewelding a new 20-mil pan section into the front-cover flange without having to replace the front-cover flange. This makes replacing a distorted front cover a relatively simple and inexpensive operation.

6.5.1.1 Stress Analysis of Front Cover

With the reactor halves open, the front-cover plates are the weakest part of the inner matrix assembly with regard to internal overpressure. A stress analysis of the front-cover plate shows that yielding can be expected to occur at about +3.9 in. of water at 20°C and at about +2.1 in. of water at 600°C. The inner matrix assembly will have a pressure relief system set for a maximum of +3.5 in. of water pressure so that yielding in the front-cover plate may conceivably occur under unusual operating conditions. For pressures below +1 in. of water, the front-cover stresses will be within the design working stress for Type 304L stainless steel at 600°C, and, since the normal operating pressure limits are below +1 in. of water, yielding is not expected during normal operation. Actual failure of the front-cover plate will not occur until the pressure is several times the +3.5 in. of water limitation. In prototype testing of the front cover, overpressures of greater than +10 in. of water have been experienced without front-cover failure.

Negative internal pressures are not a problem as far as the front cover is concerned, due to the support given to the front cover by the matrix tubes and the calandria cans. A full internal vacuum can be supported by the front-cover plate without failure.

Exposure of the front cover during heated operation will cause stresses due to thermal gradients that result from heat losses off the front cover. The stresses in the front-cover plate due to gradients normal to the front-cover plate will be very small. For an estimated heat loss of 8800 Btu/hr-ft^2 from the front face at 600°C, the maximum stress in the front cover due to gradients normal to the front cover face will be less than 300 psi. Cooling of the front cover below the front-flange temperature, however, will cause appreciable strains in the front cover. For this reason the front cover was designed with an outer-ring bellows arrangement, as shown in Fig. 25, to help accommodate thermal shrinkage. Analysis indicates

that a temperature drop of about 60 C° in the front-cover temperature below the front-flange temperature may cause some yielding in the front cover. The expected temperature drop of the front-cover face below the front-flange temperature is very dependent upon internal pressure conditions and the initial flatness of the front-cover face and the inner-barrel-matrix edges, but it is expected that temperature drops of between 100 and 150 C° may be encountered if the heated inner-matrix-assembly front face is exposed to room air. Some yielding of the front cover is expected, therefore, during high-temperature exposure of the front cover. The thermal stresses will, however, be quickly relieved by small amounts of yielding, and the front cover will not fail.

There may also be some local yielding of the front cover caused by thermal gradients between the hot spots where the cover touches the inner-matrix tubes and the colder areas over the matrix-tube centers. Analysis shows that a small amount of yielding may occur, but that failure will not occur.

6.5.1.2 Test Results of Prototype Front Cover

Exposure tests of a prototype-front-cover plate during heated operation have been carried out on the prototype VTRZ assembly. Prototype-front-cover designs with and without the outer-bellows arrangement have been tested. The tests were carried out to simulate the front-cover exposure that will occur in the actual VTRZ during a reactor scram and in certain startup operations. In the exposure tests, the VTRZ inner matrix assembly was heated to 550°C and the front cover insulation removed to expose the front cover to room-temperature air. During the tests, temperatures were constantly monitored on the front-cover flange, at several points on the front-cover pan section, and in the matrix tubes at various distances behind the front cover.

The prototype tests confirmed the predictions that the front cover would maintain its integrity during exposure. The prototype-front-cover designs tested did not show any sign of failure after exposure. The cover designs did, however, show signs of yielding, and local warpages were fairly pronounced. This was expected from the analysis, since the tests indicated temperature drops between the front cover and the matrix tubes of up to 150 C°. The outer-ring bellows of the front-cover design used in the final VTRZ permitted enough flexibility that the front cover could easily be pushed back into a flat surface. This means that local warpage in the front cover will not compromise the ability of the reactor halves to come together during actual operation. Yielding in the front cover during operation therefore can be tolerated, and the front cover can be expected to maintain the integrity of the inner barrel during normal VTRZ operation.

The prototype tests also confirmed that the front-flange heater designed for the front-cover flange in the final VTRZ can maintain the temperature of the front flange at essentially the same temperature as the inner matrix tubes. This means that the inner matrix will not be warped by shrinkage of the heavy front flange during exposure of the front cover. The prototype tests indicated that failure of the front-flange heater would cause the front flange to drop about 100 C° in temperature below the inner matrix tubes, which would lead to slight buckling of the inner matrix array. However, the integrity of the system is still maintained even with front-flange heater failure.

6.5.2 Service Housing (rear inner-matrix-assembly half-zone cover)

6.5.2.1 Stress analysis of Service Housing (rear cover)

The rear cover plate and small access port comprising the service housing are made of 1/4-in.-thick Type 304 stainless steel and are much stronger than the front cover plate. Within the pressure limits of +3.5 to -20.0 in. of water set by the inert-gas pressure-control system, stresses due to pressure on the service housing are negligible. Further, the entire service housing is insulated from room air and is provided with a rear-cover flange heater and an access-port flange heater to ensure small thermal gradients in the service housing. Thermal stresses are therefore well within the design working limits.

6.5.2.2 Test Experience of Prototype Service Housing

The VTRZ prototype inner matrix assembly and service housing have been operated in the pressure range -40 to +10 in. of water with no signs of warpage or yielding of the service housing. Since the pressure limits for the actual VTRZ are to be between +3.5 and -20.0 in. of water, pressure stresses in the service housing do not seem to be a problem.

Prototype tests have also been conducted with no flange heaters on the rear cover or access port during heated operation. These tests gave gradients of more than 150 C° between points on the service housing and the inner matrix and caused warpage of the inner matrix array; yet no sign of yielding in the service housing was detected. The service housing can therefore be expected to maintain its integrity during all conceivable operations of the VTRZ.

6.6 Outer Matrix Assembly and Central Zone Bridge

6.6.1 Stress Analysis of Outer-matrix-assembly and Central-zone-bridge Combination

The outer-matrix and central-zone-bridge combination has been described in Sec. 4.5.2 and is pictured in Fig. 7. Basically, the outer matrix assembly is built of ZPR matrix tubes welded together to form an octagonal

cavity for placement of the inner matrix assembly. The central zone bridge is a welded ZPR matrix tube assembly, 10 tubes high by 19 tubes wide for the first five rows and 15 tubes wide for the next five rows, which is to be placed over the outer matrix assembly to provide added support for the load above the outer matrix assembly (see Fig. 18).

The stress analysis of the outer-matrix-assembly and central-zone-bridge combination described in this section is based on a beam-formula treatment of the entire structure (considered as a single unit) combined with a calculation of the distortion of the individual matrix tubes. The results of the stress analysis make clear two important facts about the structure:

(1) The limiting stresses in the structure are in the matrix-tube walls and not in the tube-to-tube welds.

(2) The deflection of the structure under load and the limiting stresses principally result from individual matrix-tube distortions and not from the response of the overall structure as a beam.

The basic analysis of the individual matrix-tube sections consisted of finding the relationship between the twisting moment at each corner of the matrix tube and the deflection of the top and bottom sides of the matrix tube relative to the side walls, under the assumption that the corner angles of the tubes remain fixed at 90°; i.e., the tubes distort from a square to a rhombus by distorting the walls, not the angles. With this relationship, the entire matrix array can then be replaced by a set of moments at each corner nodal point. The weldment array was then analyzed using elastic-deflection equations for each horizontal row of matrix tubes with moments at each corner nodal point. Each row was treated separately and the moments of each nodal point found in terms of the effective supported load at each nodal point. The deflections of each row at each nodal point were found in terms of the effective supported load at each point. The analyses of the individual horizontal matrix rows were tied together to form an analysis of the overall structure by requiring that each nodal point in a vertical column deflect the same amount and that the sum of the loads supported by each horizontal row equal the total applied load. The effect of the 1/8-in.-thick outer barrel was included in the calculations as essentially another horizontal row, but with moment-deflection properties based on simple beam formulas. The result of the calculational model is a set of simultaneous equations which were solved on a computer using a numerical matrix-inversion program.

The accuracy of this stress-analysis technique is justified in detail in Sec. 6.6.3, where it is compared with various load-deflection tests for the welded matrix tube assembly. The final results of the stress analysis indicate that, for a design load of 19,800 lb (this includes the seismic load factor; see Tables 2 and 5), the maximum stresses occur in the matrix-tube

walls and do not exceed 19,000 psi. The maximum indicated tube-to-tube weld stress is about 4000 psi. The maximum deflection under load occurs at the center of the outer-matrix weldment assembly and is less than 75 mils for the design load. The results are summarized in Fig. 80. The final predicted stress limits are within the stress-limit standards for Type 304 stainless steel as given in Sec. 3.3. The maximum shear stress anywhere in the structure is less than 1000 psi for the design load of 19,800 lb and is of negligible importance.

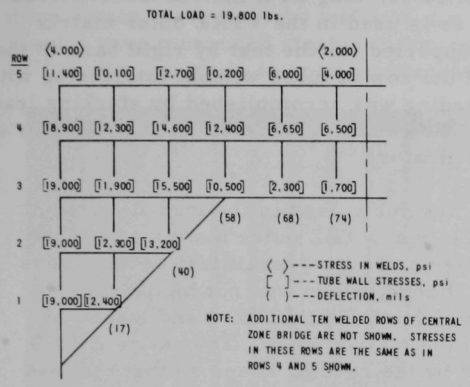

Fig. 80. Final Outer Weldment; Deflections and Stresses for Design Load of 19,800 lb

The question of possible buckling in the vertical sections of the outer matrix on either side of the octagonal central node in the outer matrix assembly was also considered in the analysis. Even assuming that the entire load on the outer matrix assembly is supported in the two-tube width of the vertical sections of the outer matrix assembly, it was found that the achievement of the critical buckling stress in the vertical sections of the outer matrix assembly on either side of the central hole requires a load in excess of 50,000 lb on each side. The maximum design load on the outer matrix assembly will apply less than 10,000 lb on each side, and part of the 10,000-lb load will in reality be supported by the two-tube-wide extensions of the central zone bridge beyond the outer matrix assembly. Therefore, buckling in the vertical sides of the outer matrix is not a problem.

6.6.2 Load Testing in VTRZ Prototype

Experimental load-versus-deflection measurements have been conducted on various matrix-tube structures to test the calculational models discussed in Sec. 6.6.1. The structures tested were (1) a single matrix-tube section, (2) a row of welded matrix tubes, and (3) the prototype outer-matrix weldment.

As a test of the basic load-deflection relationship for a single matrix tube, a 6-in.-long section of a matrix tube was welded to a rigid frame support on the top and bottom corners of one side and loaded on the opposite side. Both the resulting deflection versus load and the tube-wall strain versus load were measured. The strain measurements were made at the center of the tube on three different sides; two sides were in tension, and one in compression.

As a test of the predicted load-deflection relationship for a simple welded structure of matrix tubes, a single row of welded matrix tubes was tested. The row was constructed of 10-in.-long ZPR matrix tubes welded together in much the same pattern as is used in the VTRZ outer matrix assembly. The row of tubes was supported for the test by rigid bars in the two end tubes. The bars supported the row of tubes without interfering with their deflection under load. The loading was accomplished by stacking lead bricks on top of the welded tubes. The resulting deflections at the center of the row were measured with dial indicators.

The prototype outer matrix assembly used in the load-deflection testing is essentially identical to the final VTRZ outer matrix assembly shown in Fig. 7 and represents a very accurate overall test of the stress theory of the assembly. The central zone bridge was not included in the test. The prototype outer matrix was installed in ZPR-9 and loaded by placing depleted-uranium blocks in the matrix tubes. The entire ZPR-9 array was compressed horizontally by the reactor knees so that the load test was an exact duplication of the actual VTRZ loading conditions. Figure 81 shows the assembly mounted in ZPR-9, as viewed from behind, and also shows the dial indicators and strain gauges mounted for the tests. The dial indicators were supported from the reactor table. The prototype outer weldment was loaded to a maximum of 13,380 lb above the 11-matrix-tube-wide outer-matrix cavity. The loading was carried out in steps, and for each step the deflection at the center of the outer weldment bridge was measured along with the strain in the tack welds at the center of the outer weldment. An elastic modulus of 29×10^6 psi was assumed to convert all strain measurements to stress values.

6.6.3 Comparison of Calculated and Measured Outer-matrix-assembly Stress-load-deflection Values

The single-matrix-tube load tests were analyzed in the same manner as was used for the individual-matrix-tube distortion calculations outlined in Sec. 6.6.1. That is, the corner angles of the matrix tube are assumed to remain fixed while the sides of the matrix tube distort under load. The distortion of the tube walls causes moments at the corner nodal points that resist the load. The magnitude of the moment at each corner is easily given in terms of the slope of the horizontal-matrix-tube wall at the corner, and the entire matrix tube may therefore be represented by a single horizontal elastic member with known moments at its ends. This is the same analysis as used for the individual tube distortions in the outer-matrix analysis so that the calculated load-deflection values could be directly checked by comparison with the experimental results for the single loaded matrix tube. The measured total deflection of the matrix tube in mils, Δy, for a given load P in pounds was $\Delta y = 0.6P$. The calculated deflection-versus-load results were in the range $0.45P \leq \Delta y \leq 1.1P$, which bracket the experimental results. The calculational range of results comes from different analytical

treatments of the welds that were necessary to hold the matrix tube to the holding bracket in the test. These welds added an additional restraint on the slope of the matrix-tube walls. In any case, the calculations showed a maximum strain, ϵ, in the tube walls of $\epsilon = 10P \times 10^{-6}$ in./in. The measured results gave measured strains in the range $7.5P \times 10^{-6}$ in./in. $\leq \epsilon \leq 10.1P \times 10^{-6}$ in./in., which is in good agreement with the calculation.

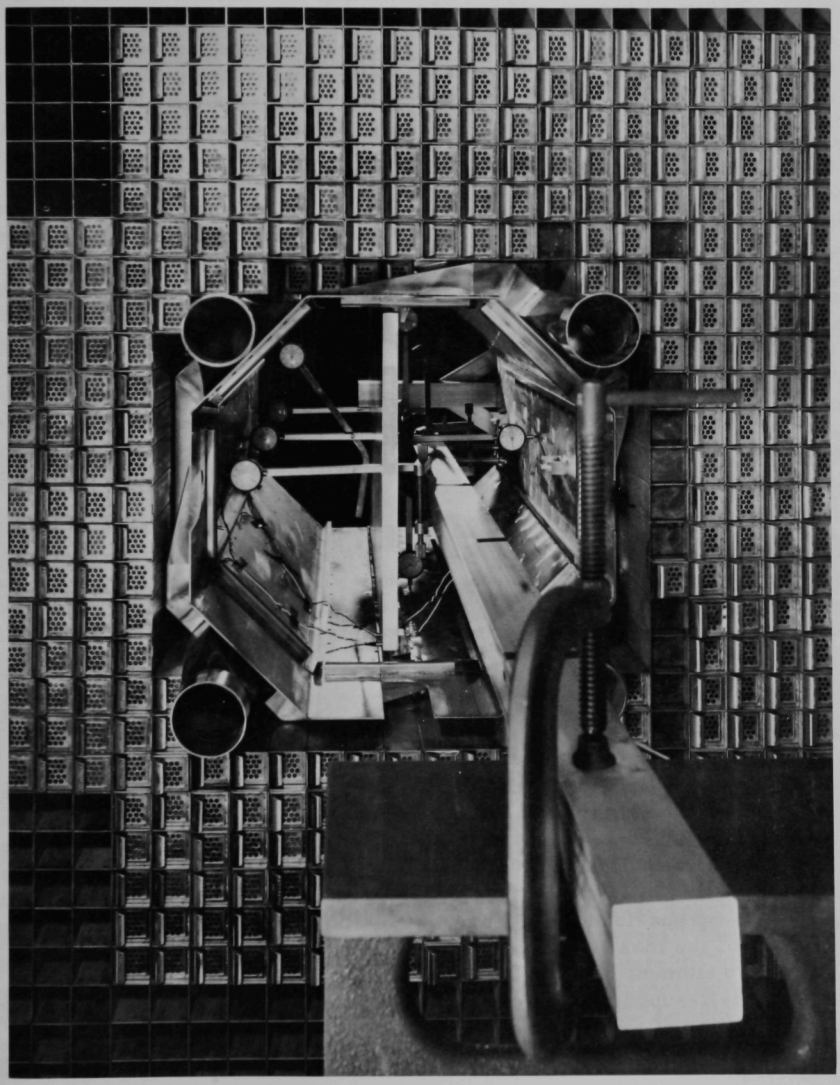

Fig. 81. Configuration for Prototype-outer-matrix Load Test. ANL Neg. No. 116-2601.

The experimental deflection-versus-load results for the single welded row of matrix tubes were also used to check the calculational model. The analysis treated individual tube distortions exactly as described above for the single matrix tube. In addition to these distortions, the loaded row of matrix tubes will distort as a single unit (i.e., as a simple beam), so that the calculated deflections were the summation of individual matrix-tube deflections and beam deflections of the unit as a whole as calculated from simple beam formulas. The calculated and experimental results are shown in Fig. 82. As can be seen in the figure, the initial part of the measured deflection-versus-load curve is in good agreement with the calculated results. The curvature of the measured deflection-versus-load curve for larger loads is not due to a nonlinear response of the matrix tube row, but rather to a binding of the rigid blocks used to load the structure that causes a reduction in the effective load. The calculated stresses in the single row of matrix tubes under the largest load exceeded the yield stress of stainless steel in the tube wall for tubes near the row ends, and, although strain measurements were not made, the row did show visible yielding in the tube walls in the tubes near the row ends. The calculational model therefore seems to adequately predict deflections and approximately predict stress in the single row of welded tubes.

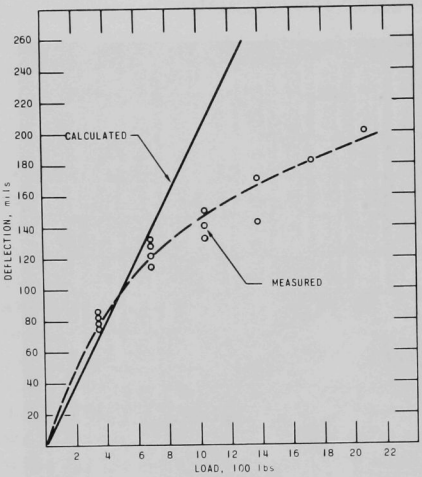

Fig. 82. Deflection vs Load in Single Row of Welded Matrix Tubes

The best test of the calculational model of the outer-matrix weldment is the comparison of experimental and calculated results for the load-deflection tests of the prototype outer weldment, since these tests were done in the exact configuration of the actual outer matrix assembly. The load tests on the prototype outer matrix have been described above. The calculated results were obtained with exactly the calculational model previously described. The final calculated and measured deflections versus load are plotted in Fig. 83. The initial slope of the calculated and measured deflection-versus-load curves are in excellent agreement. The nonlinear response of the measured load-deflection results is due to matrix tubes above the weldment binding, as the weldment distorts and thus becomes partially self-supporting. No attempt was made in the analysis to account for the binding of matrix tubes above the welded structure, since this is apt to be highly variable and ignoring the binding gives conservative stress estimates.

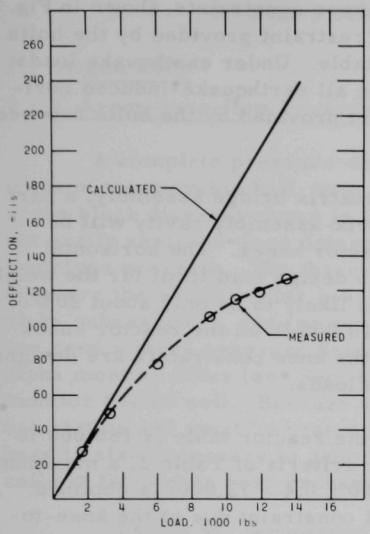

Fig. 83. Deflection vs Load in Prototype Outer Weldment

The calculations showed that the deflections measured in the prototype outer-weldment test were due almost entirely to individual tube distortions, rather than bending of the entire unit as a single beam. Therefore, a simple beam analysis alone cannot be used to adequately predict the deflection characteristics. A simple beam analysis can, however, predict the stresses in the tack welds, since these welds hold the unit together as a beam. The calculated weld stresses at the center of the outer weldment were in the range 6500-23,000 psi for the maximum load in the test of 13,380 lb. The lower estimate is based on treatment of the two slanted-tube sections on the slanting octagonal faces as rigid struts. The upper estimate resulted from neglecting any strut-like support. The measured center weld stress (strain gauge) was 18,000 psi, which is within the calculated range. The measured value was corrected for the reduction in effective load caused by the binding of the matrix tubes above the outer weldment in order to compare with calculation. A beam-formula calculation of the weld stresses assuming no strut support provides a reasonable and conservative way to calculate weld stresses, and this technique was used to determine the weld stresses in the analysis of the combined outer matrix assembly and central-zone-bridge structure.

A complete stress analysis combining individual tube distortions with a simple beam analysis was able to accurately predict the measurements made on the prototype outer weldment as well as on the single row of matrix tubes and the single matrix tube. The calculational model therefore appears entirely adequate to describe the actual outer matrix and central-zone-bridge assembly. Stress results using this analytical technique are described in Sec. 6.6.1.

6.6.4 Stress Analysis of the Reactor-knee Constraints

The ZPR-6 and -9 critical assemblies have large reactor knees to provide horizontal constraint for the reactor matrix tubes. The knees were designed to permit horizontal adjustment to accommodate different-size matrix-tube arrays. The knees are fastened to the reactor table by bolts, which fit into slots in the reactor table. The tops of the pair of reactor knees on each reactor half are fastened together with threaded tie bars, which can also be adjusted for different-size matrix-tube arrays. The VTRZ design assumes firm horizontal support of the reactor matrix, even

under earthquake conditions. The reactor-knee constraints, shown in Fig. 70, were designed to supplement the frictional restraint provided by the bolts fastening the reactor knees to the reactor table. Under earthquake loads, the constraints are designed to fully contain all earthquake-induced horizontal forces, even if the frictional restraint provided by the bolts between the knees and the table is ignored.

Because of the design of the outer-matrix bridge assembly, a part of the load applied to it over the inner-matrix-assembly cavity will be transmitted as a horizontal force to the reactor knees. The horizontal force, however, cannot exceed the 18,000-lb design load limit for the weight over the inner-matrix cavity and, in fact, is likely to be only about 20% of the 18,000-lb figure. A horizontal load of 18,000 lb on the reactor knees will cause very small stress levels, since the knee constraints are designed to contain much larger possible earthquake loads.

The maximum permissible load on the reactor table is 180,000 lb (see Table 6), so that, using the earthquake criteria of Table 2, a maximum horizontal seismic load of 72,000 lb (180,000 x 0.4 = 72,000) is obtained. Assuming that there would be no horizontal constraint due to the knee-to-knee tie rods, the full 72,000-lb load applied uniformly to the reactor knee considered as a cantilever beam results in a calculated maximum bending stress of less than 28,000 psi. The yield point of the Meehanite material that the reactor knees are made of is about 47,000 psi, so that yielding in the knees in bending will not occur. The reactor knees are bolted to the reactor table with sixteen 3/4-in. high-strength bolts. The maximum tensile stress in the bolts due to the bending moment in the knee caused by the assumed 72,000-lb load (the load tries to rotate the knee with respect to its base) is less than half the tensile strength of the 200,000-psi tensile-strength bolts to be used. The reactor knee constraints are 48 x 16 x $1\frac{1}{2}$-in. mild steel plates bolted to the side of the reactor table with four high-strength 3/4-10 bolts. The knee constrains overlap the base of the knee and prevent horizontal motion. The shear stress in the knee-constraint plate is only about 1000 psi with the assumed 72,000-lb seismic load. The maximum bending moment stress in the knee-constraint plate is about 16,500 psi, which is within the working stress for mild steel at room temperature. The steel plate is fastened to the reactor table by four high-strength 3/4-10 bolts. The indicated stress levels in the bolts will be less than 60,000 psi, well within the capabilities of high-strength bolts.

The knee constraints will hold the reactor matrix, and the VTRZ, on the reactor table during the design earthquake.

7. GAS-FLOW ANALYSES AND TESTS

7.1 Argon Loop

7.1.1 Argon-loop-flow Pressure-drop Analysis

A complete pressure-drop analysis, summarized in Table 30, was made of the movable half-zone argon loop section from Point A to Point B of the block diagram shown in Fig. 84. Those pressure-drop components not easily analyzed were determined experimentally as part of the VTRZ prototype program. The three largest contributors to the total pressure drop are the VTRZ heater heat-exchanger subassembly, the plutonium-alpha subassembly, and the combustibles-monitor subassembly. The latter two need a large pressure head to drive the argon gas through the plutonium-alpha monitor filter (see Sec. 8.4.2 for further details) and combustibles-monitor heated cell. Because argon gas has such poor heat-transfer characteristics and must be heated in a small section of tubing, a large pressure head is also necessary to generate the required turbulence over the heater coils in the heater heat-exchanger subassembly.

TABLE 30. Summary of Argon-loop Pressure-drop Analysis[a]

Component	Pressure Drop, in. of water		Comments
	VTRZ-hot	VTRZ-cold	
Tubing	3.3	3.3	90 ft of 5/8-in. tubing; 4 ft of $1\frac{3}{8}$-in. tubing
Fittings, couplings, and valves	1.3 0.4	1.3 0.4	Ref.: Handbook of Hydraulic Resistance, AEC-tr-6630
Pu-alpha subassembly	14.0	14.0	Experimentally determined
VTRZ heater heat-exchanger	22.6	7.0	Experimentally determined
VTRZ	2.0	0.7	Experimentally determined
Combustibles subassembly	6.7	6.7	Experimentally determined
Filter (clean)	1.4	1.4	Experimentally determined
Total	51.7	34.8	49% increase from cold to hot

[a]Flow is 1 cfm argon gas (STP) in 5/8-in. tube. Analysis is of movable-half section only. All calculated values are conservative; i.e., they are maximum pressure-drop values.

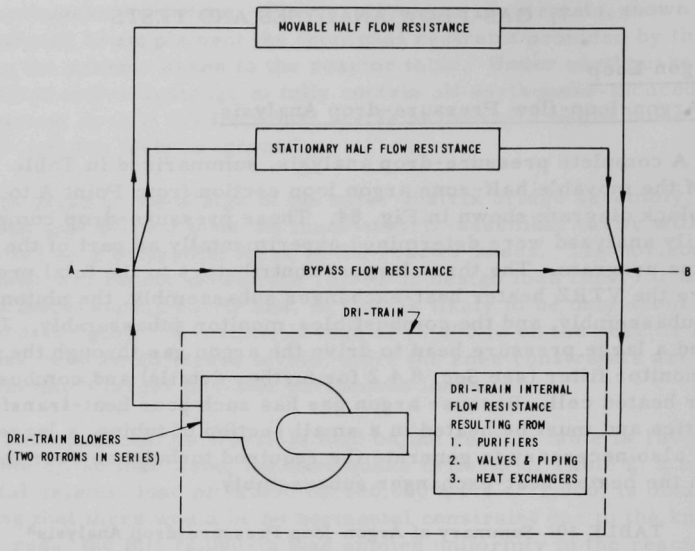

Fig. 84. Argon-loop Flow Resistance

Figure 84 shows that the total argon-system pressure drop is the sum of ΔP_{AB} and the pressure drop across the Dri-Train internal resistance. The resistance curves for this internal-flow impedance were experimentally determined and are shown in Fig. 85. At any given flow rate,

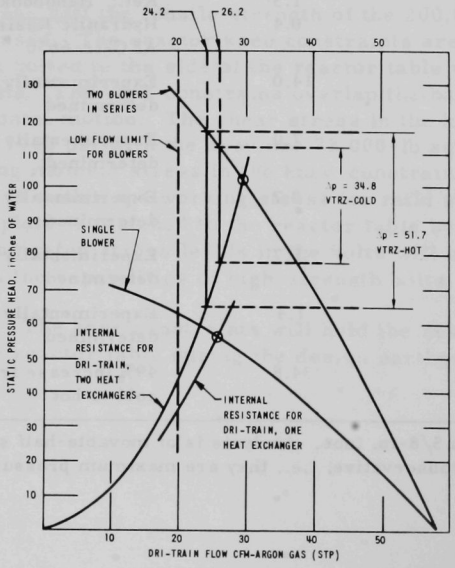

Fig. 85

VTRZ Dri-Train Blower Curves for Pressure-drop Analysis

the difference in static pressure between the Rotron blower curves and these internal-resistance curves gives the static pressure head available to the system from Point A to Point B. Two requirements must be met for satisfactory operation: First, the flow through the blowers must exceed 20 cfm. Second, there must be about 52 in. of water static-pressure head available to the external load. When the single Rotron blower characteristic is compared to the resistance curve for the Dri-Train with only one heat exchanger (one heat exchanger per blower), it is clear that only about 28 in. of static pressure are available at best. Thus, the one-blower Dri-Train unit (the commercial VAC-193-2-He unit) is inadequate, unless the flow rate of 1 cfm is lowered and/or the major contributors to the 51.7-in. ΔP are redesigned. Both alternatives are undesirable; therefore the Dri-Train was redesigned for two blowers in series (Fan Engineering, R. D. Madison, Ed., Buffalo Forge Company, pp. 287-289). An approximate characteristic curve for two Rotron Blowers in series is shown in Fig. 85 together with a new internal-resistance curve for the Dri-Train that includes the heat exchanger for the new blower. This scheme provides ample flow for the blowers and ample pressure head for the argon loop system. Each blower needs a heat exchanger because these blowers are sealed units and the pumped gas is also the motor-cooling gas.

There are two heatup schemes to ensure that in the heated configuration (550°C) the external pressure drop is about 50 in. of water and the flow in each VTRZ half-zone is about 1 cfm. The first scheme is to throttle a valve in each half-zone loop so that the cold ΔP is about 50 in. of water and then, as the system temperature rises, to open these valves slowly maintaining the 50 in. of water and 1 cfm. The other scheme is to set the cold half-zone flows high enough so that, when the half-zones are heated, the flows level off to 1 cfm. The chief advantage to the latter scheme is that no valves need be opened during heatup. The only question is whether the higher flow for the cold half-zones significantly alters the response of those monitors calibrated for operation at 1 cfm. Since the theoretical cold half-zone flow of 1.22 cfm (a value substantiated by prototype experience) only negligibly alters the response of those monitors, this latter scheme will be used during normal VTRZ heatups.

7.1.2 Analysis of High-pressure Relief System

The VTRZ high-pressure relief (HPR) system is designed to relieve slight overpressures of either half-zone by isolating the external source of high pressure and opening the halves to the reactor cell atmosphere. The system is described in Sec. 4.5.5. Figure 86 shows the maximum pressure drop of this system for the movable half-zone at 55°C. The largest contributors to this pressure drop are the check valves (for low flow) and the preheater (for large flow). That this system provides adequate pressure relief is shown in Table 31, which lists the causes of high pressure in the VTRZ together with the capabilities of the high-pressure relief system.

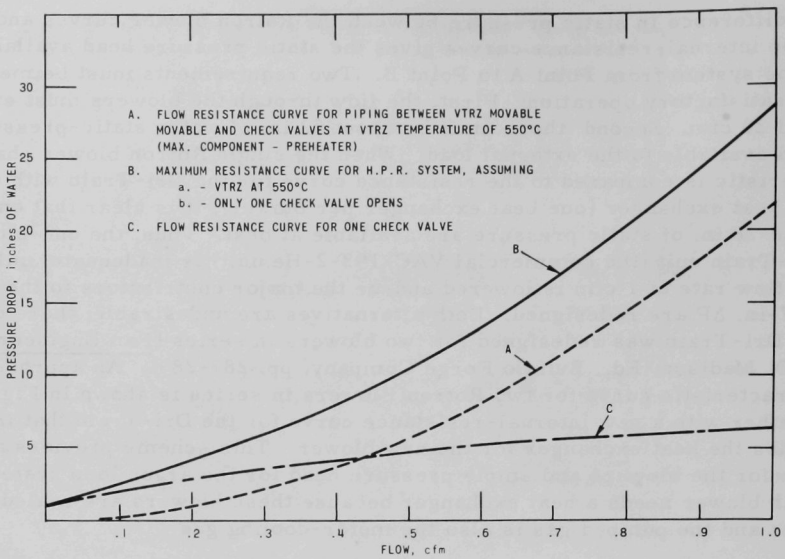

Fig. 86. Flow Resistance for High-pressure Relief System

TABLE 31. Capabilities of VTRZ High-pressure Relief System

Cause of High Pressure	Pressure Just before Trip, in. of water		Volume of Gas Which Must Be Removed, cu ft (STP)	Capability of HPR System	Heat Removed	Comments
	VTRZ	At HPR Valves				
Valve malfunctions and opens argon supply cylinder to VTRZ	+2.0	+20.0	0.06 total	0.3 ft^3/sec initially	At 550°C, 1 Btu	Assumed VTRZ Pressure reached 4 in. of water before supply cylinder was isolated.
Dri-Train vacuum pump fails to respond to pressure rise as VTRZ's are heated	+2.0	+20.0	0.04 ft^3/min until VTRZ temperature peak (heaters are turned off)	0.3 ft^3/sec initially. Leveling off to 0.06 ft^3/min.	At 550°C, 0.5 Btu in first minute	Assumed maximum temperature rise of 3 C°/min.
MCA results in 30 C° temperature rise in VTRZ	+45 at room temperature	+20.0	0.66 total at temperature	1.5 ft^3/min initially	0.5 Btu at room temperature	Assumed instant rise in VTRZ gas temperature (worst possible case).
	+15 at 550°C	+20.0	0.22 total at 550°C	0.84 ft^3/min initially	3 Btu initially	
Valve closes downstream from VTRZ	+2.0	+20.0	0.3 total (maximum possible)	0.3 ft^3/sec initially	4 Btu	Assumed pressure in VTRZ approaches 20 in. of water before HPR trip (worst possible case).

The calculations in Table 31 are conservative; i.e., they are scoping calculations which maximize the heat and gas volume to be removed and minimize the capability of the HPR system. A prototype simulation of the HPR system that excluded the check valve (and its corresponding pressure drop) demonstrated the effectiveness of the system in meeting the pressure-relief requirements.

The low-pressure relief (LPR) system, described in Sec. 4.5.5, is actuated when a half-zone pressure falls below -20 in. of water. If both half-zones are at -20 in. of water, the relief system must bleed in a maximum of 0.3 ft^3 of argon. The rate initially would be about 8 cfm and would approach zero as the VTRZ pressures were brought up to +3 in. of water.

7.1.3 Argon-loop Prototype Experience

The Dri-Train unit (including the VTRZ bypass loop) has been in operation for about 4000 hr as part of the argon-loop prototype program. In addition to using this unit in conjunction with the instrumentation testing (Chapter 8) and the VTRZ mechanical testing (Chapter 5) programs, extensive flow and pressure-control tests have been run. The results of the argon-loop prototype tests have led to modifications and additions to the commercial Dri-Train unit which are now incorporated in the final argon loop design.

In the prototype tests, the only major pressure-control problem encountered, during normal operation was an oscillation (at about 1 Hz) of VTRZ pressure due to a large feedback from the pressure-control system. This problem was solved by installing throttling valves in the argon-gas supply line and the argon-gas removal line (vacuum pump line). Thus, the total amount of gas added when the VTRZ pressure drops below the low-pressure-control set point and the total amount of gas removed when the VTRZ pressure rises above the high-pressure-control set point can be controlled so that no oscillations are present, but yet sufficient quantities of gas are added or subtracted to keep pace with the cooling or heating of the VTRZ. Typical photohelic-pressure monitor-control set points during prototype testing were -1.5 in. of water and -0.5 in. of water. Once proper pressure control is achieved in the argon loop, these two throttling valves will be locked in place.

The air-cooled copper coil that replaces the original water-cooled heat exchanger supplied with the Rotron blower has approximately the same pressure drop and cooling characteristics as the water cooler. Four small fans force room-temperature air over the coil and cool the blower exit gas the approximately 50 F° necessary for argon-loop operation. A thermocouple at the cooling-coil exit monitors the cooling effectiveness.

The VTRZ argon-loop heat exchangers (coolers) are similar in design to those used to cool the Rotron blowers. The prototype (cooler) heat exchanger was a coiled 7-ft length of 5/8-in. copper tubing. With no forced-air cooling, the coil cooled the argon gas exiting the VTRZ at 550°C and 1 cfm (STP) to 135°F; with forced air, it cooled the argon gas to 80°F.

The VTRZ preheater operated satisfactorily during about 100 hr of prototype testing. It is capable of heating room-temperature argon flowing at 1 cfm (STP) to 515°C by applying about 400 W of electric power.

The prototype testing of argon-loop instrumentation and of the Dri-Train purifier capabilities is described in Chapter 8.

About 20 complete VTRZ purges were completed as part of the prototype testing of the argon loop. The initial purging method of passing supply cylinder gas through the VTRZ and dumping it directly into the cell proved too slow (about 6 hr) if VTRZ pressures were limited to <+2.0 in. of water. If instead of dumping the purging gas directly into the cell, it is continuously pulled through a vacuum pump and then expelled, adequate purge flexibility as to flows and pressures is achieved. This method permits the use of high-pressure-drop needle valves, which have good throttling characteristics. Typically, a purge by this method will take about 40 min, each half-zone being flushed out the equivalent of 20 times. Several purges were completed with the VTRZ prototype hot, and no new problems in flow or pressure control were observed.

7.2 Cooling-guard-ring (CGR) System

The CGR pressure-drop analysis is summarized in Table 32. The assumption of a 400-cfm total flow rate conforms to the heat-transfer calculations for the insulation annulus, where the duct flow rate is assumed to be 100 cfm in each of the four ducts. The pressure drop (valves full open) of 12.4 in. of water is well within the capability of the CGR blower, whose characteristic curve is given in Fig. 87. Partial closing of the butterfly throttling valves easily provides the additional 5-in. pressure drop necessary to operate at 400 cfm. If desired, the CGR system can be operated anywhere from 460 to 250 cfm by opening or closing the CGR valves.

During the approximately 400 hr of CGR prototype operation, no blower or ductwork problems external to the VTRZ were encountered. The insulation annulus ductwork has been redesigned as described in Sec. 5.2.6 because it leaked and thereby created undesirable heat-transfer characteristics on the inner-matrix-jacket outer surface. In fact, the CGR leakage was so large (36%) that it lowered the accuracy of the pressure-drop and

TABLE 32. Summary of Cooling-guard-ring Pressure-drop Analysis

Duct Length, ft	Component	Flow, cfm	Velocity Pressure, in. of water	Pressure Drop, in. of water
6	6-in.-dia entrance duct	400	0.26	0.07
10	4-in.-dia entrance duct	200	0.33	0.24
~8	VTRZ duct work	100 per duct	Variable	9.53
	Valve (full open)	200	0.59	2.00
6	4-in.-dia exit duct	200	0.33	0.14
	Transitions, elbows, tees, etc.	200 and 400	Variable	0.40
	Total Pressure Drop	-	-	12.38

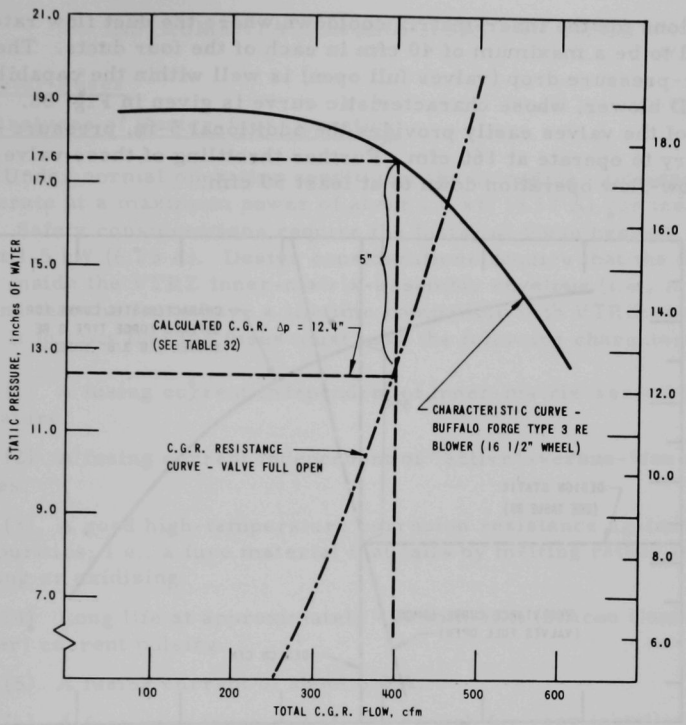

Fig. 87. Cooling-guard-ring Flow-pressure Curves

flow-rate data taken on the prototype. However, inlet duct flow measurements on the prototype showed no problem, with flow balancing and operation at 400 cfm.

7.3 Inner-matrix-cooldown (IMCD) System

The IMCD pressure-drop analysis is summarized in Table 33. The assumption of a 160-cfm total flow rate conforms to the heat-transfer

TABLE 33. Summary of Inner-matrix-cooldown Pressure-drop Analysis

Duct Length, ft	Component	Flow, cfm	Velocity Pressure, in. of water	Gas Temperature, °C	Pressure Drop, in. of water
6	4-in.-dia entrance duct	160	0.21	20	0.10
10	3-in.-dia entrance duct	80	0.16	20	0.20
6	3-in.-dia exit duct	133	0.26	220	0.17[a]
~8	VTRZ duct work	40 (STP)	Variable	Variable	12.80
	Balancing valve (full open)	80	0.10	20	0.32
	Throttling valve (full open)	160	0.40	20	1.28
	Transitions, elbows	80 and 160	Variable	20	0.60
	Total	-	-	-	15.47

[a]All values for the exit duct assume a maximum exhaust temperature of about 220°C.

calculations for the inner-matrix cooldown where the duct flow rate is assumed to be a maximum of 40 cfm in each of the four ducts. The 15.5 in. of water-pressure drop (valves full open) is well within the capability of the IMCD blower, whose characteristic curve is given in Fig. 88. Partial closing of the valves easily provides the additional 5-in. pressure drop necessary to operate at 160 cfm. Further throttling of these valves allows stable low-flow operation down to at least 50 cfm.

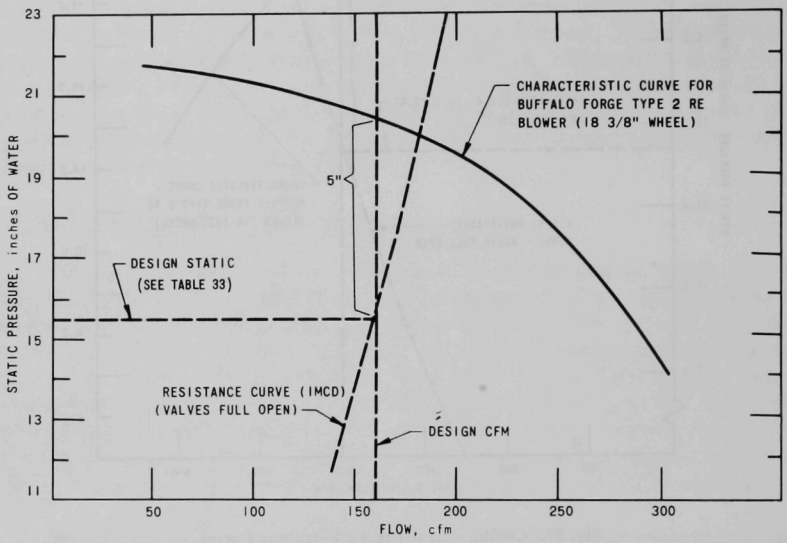

Fig. 88. Inner-matrix-cooldown Flow-pressure Curves

During the approximately 100 hr of IMCD prototype operation, no blower or ductwork problems external to the VTRZ were encountered. The inner-barrel ductwork has been redesigned as described in Sec. 5.2.7 because the prototype version leaked. As with the prototype CGR system, the IMCD system leaked badly enough (15% leakage) to compromise the pressure-drop and flow-rate data. However, as with the CGR, inlet-duct measurements showed no problem with flow balancing and operation in the range of flows desired.

8. INSTRUMENTATION ANALYSES AND TESTS

8.1 Heater Fuses

8.1.1 Analyses of Heater-fuse Operation

Under normal operating conditions, the calandria cartridge heaters will operate at a maximum power of about 1.0 kW (4.17 A) per individual heater. Safety considerations require the fusing of these heaters at a power of about 1.5 kW (6.25 A). Design considerations require that the fuses be located inside the VTRZ inner-matrix-assembly envelope (i.e., in the hot zone) and that the fuses have a lifetime compatible with VTRZ operating times. It follows that the fuses must have the following characteristics:

(1) A fusing current independent of inner-matrix-assembly ambient temperature.

(2) A fusing current independent of "active"-versus-"inactive" fuse lifetimes.

(3) A good high-temperature corrosion resistance against blanket gas impurities; i.e., a fuse material that fails by melting rather than by corroding or oxidizing.

(4) Long life at approximately 4 A with SCR (Silicon Control Rectifier) current pulsing.

(5) A fusing current of about 6.2 A.

(6) A fuse wire large and strong enough for easy installation.

The fusing (or melting) current for wire decreases as the wire's ability to transfer away heat decreases. Since this heat transfer decreases as the ambient temperature surrounding the wire increases, one would expect the fusing current of a given wire to be greater at room temperature than at 550°C. The following steady-state heat-balance equation considers the two principal modes of heat transfer from a fuse wire (heat conduction off both ends of the wire has been neglected):

$$\underbrace{I^2R}_{\substack{\text{Heat}\\\text{Source}}} = \underbrace{Ah(T_F - T_A)}_{\substack{\text{Convection}\\\text{Cooling}}} + \underbrace{A\epsilon\sigma(T_F^4 - T_A^4)}_{\substack{\text{Radiation}\\\text{Cooling}}},$$

where

I = current passing through wire just before melting (A),

R = wire resistance (ohms),

$A = \pi \ell d$,

d = wire diameter (in.),

ℓ = wire length (in.),

h = heat-transfer coefficient (W/in.^{2}-°F),

σ = Stefan-Boltzmann constant, 3.487×10^{-12} (W/in.^{2}-°R^4),

ϵ = emissivity,

T_F = fusing (melting) temperature of wire (°R),

and

T_A = ambient temperature (°R).

Clearly, the fusing current will be negligibly affected by changes in ambient temperature if the fusing temperature is sufficiently high.

For a 12.5-mil-dia, Type 302 stainless steel wire in a room-temperature argon environment, the fusing temperature is calculated to be about 3040°R. For the two inner-matrix-assembly extremes of ambient temperature [i.e., T_{A_1} = 1513°R (550°C) and T_{A_2} = 561°R (70°F)], the predicted fusing currents for this fuse differ by only 3.9%. The values for h and ϵ used in the calculations were h = 1 Btu/hr-ft^2-°F (2.04×10^{-3} W/in.^{2}-°F) and ϵ = 0.8. Thus, 12.5-mil-dia, Type 302 stainless steel wire appears to satisfy the first required fuse characteristic, the only fuse characteristic subject to quantitative analysis. This independence of ambient temperature is verified in the prototype fuse testing described in Sec. 8.1.2.

8.1.2 Prototype Tests of Heater Fuses

The fuse-prototype testing program is summarized in Table 34. A fuse consisting of a 1-in.-long, 12.5-mil-dia, Type 302 stainless steel wire

TABLE 34. Summary of Fuse Testing for VTRZ

Fuse: 1-in.-long, 12.5-mil, Type 302 stainless steel wire

Test Series No.	Fuse History	Mean Fusing Current, A	Standard Deviation, A	Highest Recorded, A	Lowest Recorded, A	Oven Type	Number of Fuses
1	Fuse at room temperature in argon or air (never heated)	6.3	± 0.2	6.6	6.0	None	14
2	Fuse at ~500°C in argon gas (zero lifetime)	6.1	± 0.2	6.5	5.8	Fuse-testing oven	10
3	Fuse at ~500°C in argon gas after various lifetime tests where fuses were operated at ~4 A	6.4	± 0.4	7.2	6.0	Fuse-testing oven	6
4	Fuse at ~500°C in argon gas after various lifetime tests where fuses were operated at 0 A	5.7	± 0.6	6.3	4.8	Fuse-testing oven	17
5	Fuse at ~350°C for 100 hr (fused at room temperature); current during 100 hr, ~4 A	6.6	± 0.06	6.7	6.6	VTRZ-prototype (using SCR's[a])	3
6	Fuse at ~350°C for 100 hr (fused at room temperature); current during 100 hr, ~0 A	6.6	± 0.06	6.7	6.6	VTRZ-prototype (using SCR's[a])	3

[a]Silicon-control-rectifier power supplies.

satisfied all the heater-fusing requirements mentioned above. The oven used in Series 2-4 tests is shown in Fig. 89 together with two different fuse racks used. The oven was heated electrically and was constantly purged with argon gas from a VAC-93 Dri-Train unit.

For the two inner-barrel extremes of ambient temperature (20 and 500°C), the fusing currents (6.3 and 6.1 A) differed by only 3.2% (as compared to the calculated 3.9%). This is much better than the lower-melting-point wires tested, such as copper, for which the difference was >30%.

A comparison of Series 1, 5, and 6 experiments shows no fusing dependence on "active" (with current) versus "inactive" (no current) lifetimes. However, the fusing current increases about 4.5% (from 6.3 to 6.6 A) after having been baked for 100 hr.

There was no evidence of corrosion of these stainless steel fuses in the Series 5 and 6 tests conducted in the VTRZ prototype itself. However, because of the relatively impure argon cover gas in the fuse testing oven, there was a marked deterioration in the fuses in the Series 4 tests. That the same deterioration did not occur in the Series 3 tests is not clear.

In all the lifetime tests (Series 3 and 5) there was never a fuse failure at an operating current of 4 A. The 12.5-mil wire proved strong and large enough for easy installation and replacement. Also, the fusing-current requirement of 6.2 A was met by these fuses that fuse at approximately:

(1) 6.3 A at room temperature.

(2) 6.1 A at 500°C at beginning of experiment.

(3) 6.4 A at 500°C at end of experiment.

(4) 6.6 A at end of experiment after having been cooled off to room temperature.

8.2 Calandria-can Overheat Detection

8.2.1 Analysis of Calandria-can Overheat Monitoring System

Basic protection against calandria-can overheat is provided by individual fuses for each calandria heater, as described in Secs. 4.5.7 and 8.1. The calandria heaters are nominally 1-kW heaters with one 36-in. heater provided for one row of three 12-in. calandria cans in a matrix tube in a typical case. Each heater is fused at a nominal 1.5 kW. There is never more than one heater per calandria can, so that no matter what the possible heater-failure mode may be, there can never be a greater power dump than 1.5 kW per 12-in. calandria can. The limiting of each calandria heater to 1.5 kW basically means that the calandria cans cannot be overheated

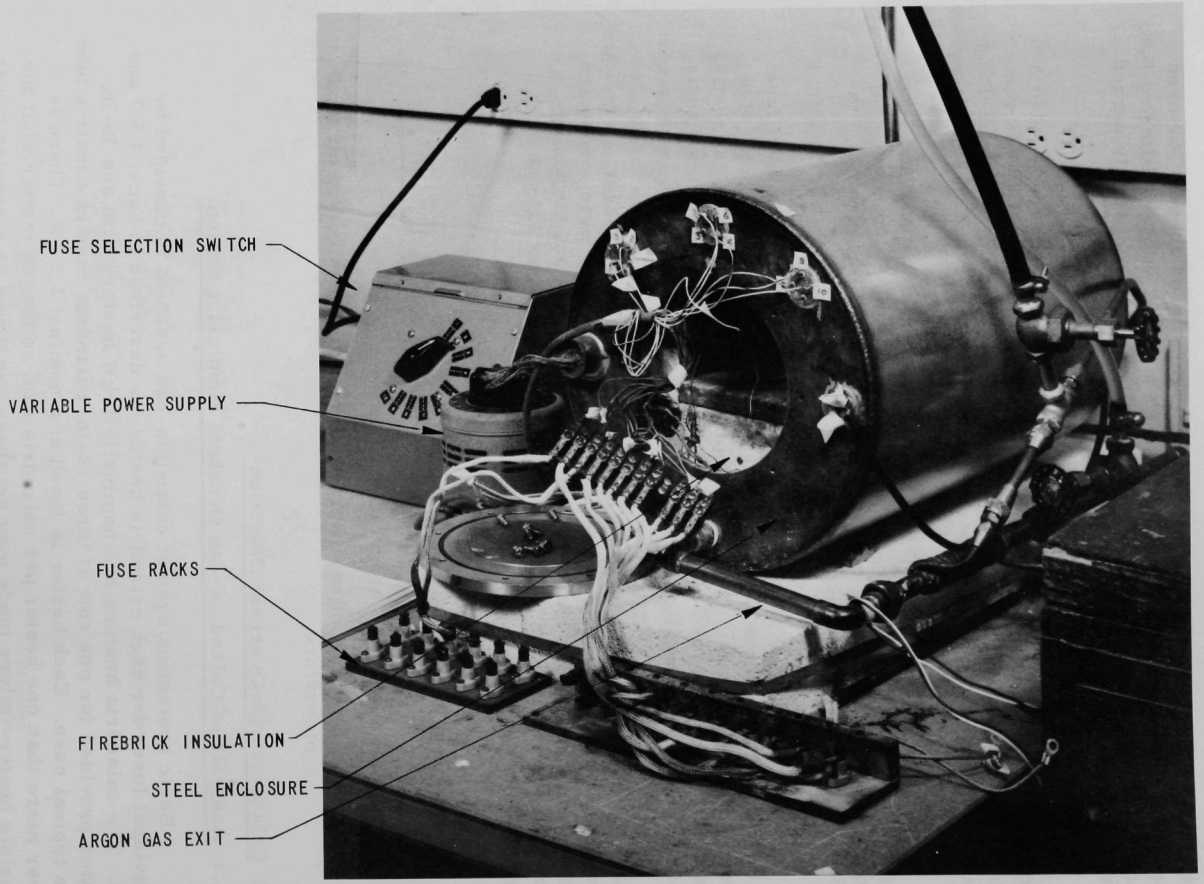

Fig. 89. Fuse-testing Oven

to failure fast enough to cause an appreciable hazard. Backup protection against overheat-induced calandria failure is provided by a thermocouple monitoring system designed to detect any calandria overheat before failure occurs.

A typical thermocouple layout for the overheat monitoring system is shown in Figs. 59 and 60. Basically, this thermocouple layout provides for at least one thermocouple immediately adjacent to each 12-in. calandria can containing a cartridge heater or separated from it by no more than the thickness of the matrix tubes. As described in greater detail in Sec. 4.5.8, the thermocouple layout of Fig. 59 also provides a backup set of thermocouples adjacent to each calandria can. The important consideration from the safety standpoint is that at least one operating thermocouple adjacent to every calandria can containing a cartridge heater must be monitored during all heated operation.

Two- and three-dimensional numerical heat-transfer analyses have been used to calculate the result of the worst-case calandria-heater failure accident. The worst-case accident is considered to be the case in which a full 1.5 kW is supplied to a single 12-in. calandria can. This case has been analyzed to see if the overheated calandria can can be detected before the calandria can fails. The analysis showed that, with the 1.5-kW heater limitation, heatup of the calandria can is relatively slow and the temperature rise is easily detected before the calandria can failure temperature is reached. Heat-transfer coefficients, particularly the gap conductivities between calandria can and matrix tube, used in the worst-case overheat calculations were chosen to make the heat-transfer analysis agree with the prototype overheat test results described in Sec. 8.2.2. The prototype overheat testing was conducted in a 3 x 3 array of 12-in.-long calandria cans. Calculations were used to extend the results of the tests to larger arrays and to include the effect of additional calandria cans abutting the test cans axially. As noted, before the results were extended to more complex problems, the heat-transfer coefficients were chosen to give good agreement between calculation and experiment in the 3 x 3 array.

The calculations of the calandria-can overheat accident showed that with 1.5 kW supplied to a single 12-in. calandria initially at 550°C, the calandria can will heat up to about 750°C in a relatively short time (about 10 min). Even assuming that the thermocouple monitoring the overheated calandria can is separated from the can by the thickness of a matrix tube, the calculations show that the thermocouple will see a temperature rise from 550 to 600°C (the heater-interlock trip point) in the 10-min period in which the overheated calandria can reaches 750°C. If the monitoring thermocouple is directly adjacent to the calandria can, it will, of course, reach the heater-interlock trip point sooner. Above 750°C, the heated calandria can swells and greatly increases the gap conductivities around the can so that the temperature rise is very slow beyond about 750°C. The calculations

indicate that it is impossible for a single malfunctioning heater at 1.5 kW to raise the general temperature of the VTRZ inner matrix sufficiently high to cause the overheated calandria can to reach the nominal failure temperature of 900°C. The calculations also indicate that the heated calandria can will never lead the monitoring thermocouple temperature by more than 150 C°, so that overheating of the calandria can will be easily detected by the 600°C heater-interlock trip before the calandria can reaches a temperature that could seriously damage it. The slow rate of the temperature rise in the overheated calandria can also means that there will be more than enough time to detect any overheating before serious damage occurs.

As indicated previously, heated operation of the VTRZ will not be permitted unless there is at least one thermocouple adjacent to each calandria can containing a cartridge heater (at least in the sense that only a matrix tube and not another calandria may separate the thermocouple from the calandria to be monitored). The calculations show, however, that an additional degree of redundant protection does exist in that the next nearest thermocouple to the overheated can (i.e., thermocouples separated from the overheated calandria can by one full calandria width) would be adequate to detect a calandria-can overheat before a temperature of 800°C is reached. The calculations also showed that none of the "next nearest" thermocouples lagged the peak temperature by more than 200°C, so that an overheat could easily be detected. In fact, heat transfer between adjacent calandria at elevated temperatures is so good that, before any overheated calandria can could reach 900°C, all the other calandria would be above 600°C, and the overheat would be detected by many thermocouples.

The calculated calandria-can overheat results were obtained from a two-dimensional calculation of a 5 x 5 array of calandria cans with an insulated boundary; axial gradients were not considered. As a check on the calculations, three-dimensional calculations were also made of a 3 x 3 array treating axial conduction explicitly. The results of the 5 x 5 two-dimensional calculations and the 3 x 3 three-dimensional calculations were nearly identical, which indicates that the results of a full three-dimensional calculation of the entire VTRZ array would not be much different than the results already obtained. The final rate of heatup of the overheating calandria would be somewhat less in the actual VTRZ than was calculated in the simplified cases, because the VTRZ does not have perfectly insulated boundaries as was assumed in the calculation. Further, the actual VTRZ is nearly a 9 x 9 array of calandria and thus contains a greater overall heat capacity than is used in the 3 x 3- or 5 x 5-array calculations. Thus, the calculations will show a faster heatup rate than would be seen in the actual VTRZ and should therefore be conservative.

The three-dimensional calculations did indicate that there is relatively poor axial conduction between the ends of adjacent calandria. However, within a single sodium-filled calandria can, there will be only very

small axial temperature gradients due to the large conductivity of the sodium in a calandria can. Thus, in a 36-in. row of three 12-in. calandria cans, each calandria can will be nearly uniform in temperature, but may have an appreciably different temperature from the next calandria can in the same row. For this reason, there will be three complete sets of thermocouples in each VTRZ half-zone, one for each axial echelon of the 12-in. calandria cans.

8.2.2 Prototype Testing of Calandria-can Overheat Monitoring System

Prototype tests of the calandria-can overheat monitoring system have been carried out in a special test rig. The tests were conducted to determine the thermal behavior of a calandria can in a situation simulating conditions in the VTRZ given a heat input of 1.5 kW to a single 12-in. calandria. The special test rig consisted of a 3 x 3 array of 12-in.-long calandria cans, with one or more heaters in each can, in a 3 x 3 section of welded matrix tubes. In the tests, the 3 x 3 array was surrounded by insulation and brought up to a uniform 550°C. The tests were conducted in an enclosed tank with an argon atmosphere to simulate actual VTRZ conditions. After temperature equilibrium was reached, the heater power to the central calandria was increased to 1.5 kW and the temperature history of each calandria was measured. Power to the central calandria can was supplied by four cartridge heaters placed in the central four fuel-rod tubes. The remaining calandria cans had one heater each; these were used to bring the entire array up to 550°C. Every fuel-rod tube not used for a heater was filled with a stainless steel rod to simulate the loaded calandria cans in the VTRZ. Thermocouples were placed in the center of each calandria to monitor the temperatures during the tests.

The special prototype tests indicated a rise in the central temperature of the center calandria to about 750°C in about 20 min with 1.5 kW supplied to the center calandria. With the center calandria at 750°C, the temperatures of all of the surrounding eight calandria cans were greater than 600°C. The indicated rate of rise of the center calandria temperature above 750° was less than the rate of rise of the temperatures of the surrounding calandria cans. That is, above 750°C, the temperature difference between the central calandria can and the surrounding calandria cans decreased with time; the maximum temperature difference between the center calandria can and the surrounding cans never exceeded about 150 C°.

The prototype-test results for the 3 x 3 array at an initial temperature of 550°C indicate that a single calandria can could not be appreciably overheated without detectable overheating of the adjacent calandria cans. The small size of the minimockup array would tend to give a larger temperature rise in surrounding calandria cans than would exist in a larger array, so that the results were extended by calculations to larger arrays as explained in Sec. 8.2.1. Note, however, that measuring the center temperature of the surrounding calandria cans in the tests is conservative,

since in the actual VTRZ, thermocouples will be adjacent to every can where the temperature will be closer to the maximum temperature in the overheated calandria can. In general, the test results and the calculational results both gave the same general conclusion; i.e., a calandria-can overheat could be easily detected before serious overheat damage occurs. The detection would be accomplished either by thermocouples adjacent to the overheating calandria can or by thermocouples in surrounding calandria.

Prototype-test results were also obtained for the case in which the entire array was initially at room temperature (22°C) and 1.5 kW was supplied to the center calandria can. In this case, the center calandria-can temperature reached 600°C fairly quickly (20 min) and then began to increase at a slower rate. The surrounding calandria cans lagged far behind in temperature during the first 20 min and were only up to about 100°C when the center calandria can was at 600°C. Beyond this point, however, the temperature of the center calandria can rose only very slowly and the temperature difference between center and surrounding calandria cans continually decreased with time. The overheating calandria can required more than 2 hr to reach 800°C in this case. By the time the central can reached 800°C, all the surrounding calandria cans were above 600°C. Again the test results indicated that a calandria-can overheat could easily be detected before the overheated can would be seriously damaged.

The special prototype-test results, besides providing direct experimental evidence of the detectability of an overheat, were used to provide a basis for extended calculational results. That is, as explained in Sec. 8.2.1, the temperature histories recorded in the well-defined test configuration were used to determine appropriate heat-transfer coefficients for use in the calculations.

8.2.3 Effect of Thermocouple Burnouts on System Operation

During heated operation, there must be at least one operating thermocouple for each 12-in. calandria can containing a cartridge heater. The thermocouple must be immediately adjacent to the calandria can or separated by no more than a matrix-tube-wall section. Operation depending upon temperature monitoring by secondary thermocouples (i.e., those separated by a full calandria-can width from the monitored calandria can) will not be permitted. The calculations and tests indicate that secondary thermocouples should be able to detect overheated calandria cans, but reliance on this result is not considered to provide an adequate safety margin.

To provide at least one thermocouple for each calandria can there will be typically about 66 thermocouples per half-zone, as is shown in the setup of Fig. 59. Failure of any of these 66 thermocouples will, however, necessitate turning off all heater power unless thermocouple redundancy is

provided. For this reason, a completely redundant set of thermocouples will be provided in the VTRZ in most operational configurations as shown for a typical case in Fig. 60. With the redundant set of thermocouples, failure of a single thermocouple will not compromise operation or safety in any way. It will, in fact, require simultaneous failure of two thermocouples monitoring the same calandria before heated operation will have to be terminated. This will greatly reduce the frequency of shutdown due to thermocouple failure. In no case will any number of thermocouple failures compromise safety, since heated operation will be terminated if there is not at least one thermocouple monitor for each calandria can.

8.3 Calandria-can Failure (Sodium Release) Monitor

The calandria-can failure monitor is basically a monitored electrical switch, which is normally open. The monitor is described in detail in Sec. 4.5.9. Liquid sodium falling on the switch grid located on the bottom of the wiring space of each VTRZ half-zone (i.e., behind the matrix) completes the switch circuit, which in turn energizes an alarm circuit and trips the heater interlock. Each leg of the switch grid is constantly monitored for continuity. This monitor is expected to detect only gross sodium leaks from calandria cans.

8.4 Fuel-rod Failure Monitors

8.4.1 Helium Fuel-rod Failure Monitor

The expected helium concentrations in the argon-loop system due to a fuel failure are considered in this section and compared to the theoretical mass-spectrometer leak-detector sensitivity.

The minimum, maximum, and nominal inside gas volumes of VTRZ fuel rods are 0.21, 0.60, and 0.40 cm^3, respectively. Since these rods must be filled with a gas that contains a minimum of 50 vol % helium, the minimum helium content per fuel rod is 0.10 cm^3 (STP). A nominal value for helium content per rod is set at 0.2 cm^3. If 0.10 cm^3 (STP) helium is homogeneously mixed in 6 ft^3 (the approximate total gas volume of the "normal-mode" argon-loop system) at room temperature, the resulting helium density is 10^{-10} g/cm^3; the resulting density is 0.6 part per million volume of helium in argon. Assuming no trapping of helium on the loop's internal surfaces, 0.6 ppmv represents the "smallest final helium concentration" that must be detected by the helium monitor system. Since the monitor "sniffer" samples loop gas at an approximate rate of 10^{-4} cm^3/sec, the helium flow into the monitor unit for this smallest concentration will be about 6×10^{-11} cm^3/sec. The basic sensitivity of the NRC-925-20 leak detector is 1×10^{-11} std. cm^3/sec; thus the leak detector should be able to detect 0.6 ppm helium if the argon present in the sample gas does not introduce a serious background problem. With the half-zones heated to 550°C,

the "effective volume" of the argon loop is reduced to about 3 ft^3, thus increasing the smallest final helium concentration to 1.2 ppm. It is difficult to calculate the initial helium concentrations, as they depend on the type of rod leak (slow leaks versus instantaneous burst), the location of the leak, the flushing patterns of the argon gas, and the rate at which the initial concentrations pass by the sampling point. Unless the rod is a slow leaker, the initial concentration should be appreciably larger than the final concentration, since the former has not been diluted by the Dri-Train and associated bypass gas. This has been borne out by prototype testing described below.

The purpose of the helium monitor prototype testing was to check helium detecting capabilities in as realistic a situation as possible. Specifically the following aspects were investigated:

(1) Detector sensitivity

a. As a function of quantity of helium introduced
b. As a function of half-zone temperature
c. As a function of vacuum pump throttling
d. As a function of sampling rate

(2) Detector response time

a. As a function of flow rate
b. As a function of length and diameter of the sniffer probe line
c. As a function of half-zone temperature

(3) Detector background noise

a. As a function of power supply filters
b. As a function of the spectrometer tube pressure

(4) Detector drift

a. Over long periods of time
b. As a function of liquid nitrogen level in the cold trap
c. After helium injections.

A helium injection port was installed in the prototype argon loop just upstream from the VTRZ prototype. About 45 ft (tube length) downstream from the prototype, a sampling port was installed that could accommodate various types of sniffer probes. Two different helium injection schemes were used: The first scheme used a calibrated hypodermic needle, with which it was possible to inject a known amount of helium through a rubber plug into the argon flow stream. The second scheme used a calibrated length of small-diameter flexible tubing, which was sealed until one end was connected to the injection port and opened to the argon flow stream. The first scheme simulated a rod "burst"; the second scheme simulated a slower rod leak. It was felt that an injection upstream from the VTRZ represented the worst rod leak from a detection standpoint; i.e., no inner-matrix rod leak would affect the monitor less than an upstream injection.

Since initial testing showed that the detector response was linear with respect to the amount of helium injected over the range of interest, a "nominal rod leak" injection of 0.2 cc was used for all the subsequent testing. This was about the lower limit of helium that could be effectively injected into the argon loop in the tests. It represents a final homogeneous mixture with the argon of about 2 ppm. The helium-monitor prototype testing is summarized in Table 35. The data show that detector sensitivity varied as follows:

(1) Sensitivity increases as the mass-spectrometer atom density increases (comparing injections 1, 4, and 7).

(2) Sensitivity decreases in most instances for second and third injections in a series (comparing injections 1 to 2 and 4 to 5).

(3) Sensitivity appears to be temperature-independent (comparing injections 10 and 11 to 12 and 13).

Since no helium will be released into the inner matrix assembly and argon loop system before a pin leak, those initial injections (No. 1, 4, 7, and 9) are more representative of the monitor response in the actual system. The best of these responses is clearly injection 1, where the mass-spectrometer vacuum was about 0.3 μ. Present plans call for a sniffer probe that has a leak rate similar to the Veeco No. 1.

TABLE 35. Summary of Helium-monitor Prototype Testing

Injection Number	Injection Series	Sniffer Used	Temperature at Injection, °C	Response to 0.2-cc (STP) Injection, mV	Background before Injection, mV	Delay Time from Injection to Detection	Vacuum in Mass Spectrometer, μ	Number of Prior Injections	Type of Injection
1	1	Veeco No. 1	20	>360	40	~2 min	~0.3	0	Slow leak
2	1	Veeco No. 1	160	45	85	~6 min	~0.3	1	Slow leak
3	1	Veeco No. 1	130	50	100	~5 min	~0.3	2	Slow leak
4	2	T.J.[a]	20	112	8	~10 min	~0.1	0	Slow leak
5	2	T.J.	550	26	25	~2 min	~0.1	1	Slow leak
6	2	T.J.	550	9	32	~2 min	~0.1	2	Slow leak
7	3	R.S.[b]	20	31	13	~2 min	<0.05	0	Burst
8	3	R.S.	20	17	6[c]	~2 min	<0.05	1	Burst
9	4	Veeco No. 2	20	6	0	55 sec	<0.05	0	Burst
10	4	Veeco No. 2	20	19	4	50 sec	<0.05	1	Burst
11	4	Veeco No. 2	20	3	13	3 min	<0.05	2	Burst
12	4	Veeco No. 2	200	9	6	45 sec	<0.05	3	Burst
13	4	Veeco No. 2	200	7	15	50 sec	<0.05	4	Burst

[a]T.J. Sniffer: Crimped copper sniffer that established a spectrometer vacuum of ~0.1μ.
[b]R.S. Sniffer: Crimped copper sniffer that established a spectrometer vacuum of <0.05μ.
[c]Background rezeroed for injection 8.

The sensitivity of the monitor is also dependent on the size of the throttling plate placed just upstream from the pumping system. A plate recommended by the manufacturer was installed before the tests summarized in Table 35. This plate increases the probability that a helium atom enters the mass spectrometer by decreasing the gas pumping efficiency--a tolerable deficiency since "pumpdowns" for this application are infrequent. The closing of the valve that is in series with this throttling plate has the same effect, except that it is nonreproducible.

The prototype testing of detector response times showed maximum times of about 6 min. These evidently depended on the injection rate rather than the helium transport time to the detector. No noticeable dependence on half-zone temperature or loop flow rates was noted. Of course, a large reduction in flow rate (nominally 1 cfm or 11 ft/sec) would increase the response time. It was noted that the larger-diameter and shorter-length sniffer probe line produced a faster detector response.

The detector background noise was the lowest for the No. 1 injection series (the series best representing the final monitor system). The tolerable variation of ±2 mV can be improved, if desired, by a judicial choice of filters and/or integrating circuits. Considerable decrease in background noise found in the other injection series was accomplished by using an input noise filter. There was no evidence that the background noise varied substantially with spectrometer tube pressure. However, it did increase as more sensitive detector meter scales were used.

Once helium was introduced into the system, it was difficult to distinguish detector drift from a decrease in the amount of helium present. During the series of tests, no large spurious change in the detector output level was noted, just after the filling of the liquid-nitrogen cold trap. No definitive dependence on half-zone temperature has been noted. For example, during the Series No. 2 tests, the detector output only increased from 23 to 25 mV during a 7-hr VTRZ heatup (20-550°C). Although more extensive tests measuring system drift are planned as part of the VTRZ preinstallation phase, no major problems with drift are anticipated.

After several helium injections, the loop helium density builds up and the millivolt response per injection decreases. To facilitate the helium monitor testing, attempts were made to purge the helium out of the loop using both argon and nitrogen gas. The results using argon purge were inconclusive. Results using nitrogen gas proved that nitrogen gas was more effective in flushing out helium.

In conclusion, the helium-monitor prototype testing has demonstrated that minimum helium releases (0.1 cc) can be adequately detected using the NRC-925-20 leak detector if the sniffer leak rate and spectrometer tube vacuum are maintained at values established by the Series-1 experiments. Drift, noise levels, and response times do not appear to compromise the effectiveness of this monitoring system.

8.4.2 Plutonium-alpha Fuel-rod Failure Monitor

8.4.2.1 Theory of Operation

The plutonium-alpha monitor response to a given inner-matrix-assembly PuO_2 contamination level is analyzed in this section. If

$n_i(t)$ ≡ the atom density (homogeneous dispersion) of the ith type nucleus at the inner-matrix-assembly gas exit,

V ≡ volumetric sampling rate of the plutonium-alpha monitor,

f_i^F ≡ average filter efficiency for the ith-type particle,

λ_i ≡ decay constant of the ith-type nucleus,

and

f_i^I ≡ average impaction loss (%) for the ith-type particle in traveling from the inner-matrix-assembly exit to the plutonium-alpha filter,

then

$$N_i(t) \equiv \int \left[\left(1 - f_i^I\right)\left(f_i^F\right) V n_i(t') - \lambda_i N_i(t')\right] dt',$$

where

$N_i(t)$ = number of atoms of the ith type seen by the detector crystal at time t, assuming negligible transport time from inner-matrix-assembly exit to monitor.

It follows that the total number of counts accumulated in the energy channel of interest for the ith-type particle is

$$C_T^i = \lambda_i f_i^c \int_{t_1}^{t_2} dt' \, N_i(t)$$

or

$$C_T^i = \lambda_i f_i^c \int_{t_1}^{t_2} dt' \int_0^{t'} dt \left[\left(1 - f_i^I\right) f_i^F V n_i(t) - \lambda_i N_i(t)\right], \qquad (1)$$

where

f_i^c ≡ counting efficiency for the ith-type disintegration in the channel of interest,

t_1 = accumulation initiation,

and

t_2 = accumulation termination.

If the following assumption is made:

$$n_i(t) = n_i^0 h(t) e^{-0.7t/T_0},$$

where

$$h(t) \equiv \begin{cases} 1 \text{ if } t \geq 0 \\ 0 \text{ if } t < 0 \end{cases},$$

and

$T_0 \equiv$ inner-barrel plutonium atom density half-life,

then

$\lambda_i N_i \rightarrow 0$ for the time scales of interest.

Equation 1 reduces to

$$C_T^i = \lambda_i f_i^c \left(1 - f_i^I\right) f_i^F V n_i^0 \{(T_0/0.7)(t_2 - t_1) + (T_0/0.7)^2[\exp(-0.7t_2/T_0) - \exp(-0.7t_1/T_0)]\}. \quad (2)$$

If the further assumption that $T_0 \rightarrow \infty$ is made, Eq. 2 reduces to

$$C_T = \sum_{\substack{\text{Pu} \\ \text{Isotopes}}} C_T^i$$

$$= \sum_{\substack{\text{Pu} \\ \text{Isotopes}}} \tfrac{1}{2} \lambda_i f_i^c \left(1 - f_i^I\right) f_i^F V n_i^0 (t_2^2 - t_1^2). \quad (3)$$

To determine a representative value for the plutonium-alpha monitor-count accumulation, C_T, assuming a ^{239}Pu-α disintegration rate at the inner-matrix-assembly exit corresponding to 1000 RCG, the following values were used:

$\lambda N^0 = 10^3 \times 2 \times 10^{-12}$ μCi/ml (RCG for ^{239}Pu soluble per 40-hr week)

$= 125.7$ disintegrations/min-ft^3,

$t_1 = 0$,

$f_c = 30\%$ (typical detector efficiency),

$f^F = 25\%$ (includes loss through monitor bypass),

$f^I = 5\%$ (estimate),

and

$V = 1$ cfm (STP).

Thus,

$$C_T = 9(t^2/2),\ t \text{ in minutes},$$
$$= 16{,}200 \text{ for } t = 60 \text{ min},$$
$$= 9100 \text{ for } t = 45 \text{ min},$$
$$= 4050 \text{ for } t = 30 \text{ min},$$

and

$$= 450 \text{ for } t = 10 \text{ min}.$$

If the time for count accumulation is set at 30 min, a final count of 40 would indicate 10 RCG. Since the accumulation of 40 counts in 30 min is well above the spurious count accumulation due to electronic noise, this scoping calculation indicates a monitor sensitivity two orders of magnitude greater than the heater-interlock trip level of 4050 (t = 30 min). There is no anticipation of radon or radon-daughter-product background since the argon-loop system is closed and uses ultrahigh-purity argon gas and since all the fuel and depleted pins are clad. Neutron background counts are not anticipated, since experience with the ZPR-6 impactor-type plutonium-alpha monitors, which have similar detectors and electronics, have shown no significant effect.

Equation 3 does not take into account the fact that the 2.5-ft^3 gas space in each inner barrel is constantly flushed by uncontaminated argon gas at a rate of 1 cfm (STP). Assuming that T_0 = 2.5 min and t_1 = 0, Eq. 2 reduces to

$$C_T = 9[3.57t - 12.74(1 - e^{-t/3.57})], \tag{4}$$

or

$$C_T = 1928 \text{ for } t = 60 \text{ min},$$
$$= 1446 \text{ for } t = 45 \text{ min},$$
$$= 964 \text{ for } t = 30 \text{ min},$$
$$= 213 \text{ for } t = 10 \text{ min}.$$

This much more conservative estimate of monitor-count accumulation still demonstrates adequate sensitivity (10 RCG results in 10 counts in 30 min).

These calculations have taken into account only plutonium rod failures that produce "airborne" plutonium concentration in the argon cover gas. If a rod failure would occur that did not produce sufficient plutonium aerosol to produce a corresponding monitor response, the failure would not

be detected until the inner matrix was unloaded. However, no monitor response would indicate sufficiently low plutonium-alpha background to permit safe disassembly and unloading procedures (described in Sec. 2.3.5 of ANL-7638).

In conclusion, the scoping calculations given above demonstrate the response of the plutonium-alpha monitor to a given inner-barrel plutonium contamination. Values for several of the parameters used in the calculations have been determined from experiments as part of the VTRZ prototype program. These experiments are described below.

8.4.2.2 Prototype-test Experience with Plutonium-alpha Monitor

The decision to pass only one-fourth of the inner-barrel exit flow through the plutonium-alpha detector is based on a compromise between minimizing the pressure drop across the monitor and maximizing the amount of plutonium deposited per unit time on the monitor filter. Using the 1.2-μ membrane filter in the plutonium-alpha monitor housing, the prototype tests showed that a 0.25-cfm flow of argon gas generated a pressure drop of 14.0 in. of water. A 0.8-μ filter generated excessive pressure drop at less than 0.25 cfm; a 5.0-μ filter did not appreciably lower the pressure drop at 0.25 cfm. A pressure-drop ceiling of 25 in. of water was placed on the plutonium-alpha monitor so that additional blowers would not have to be added to the argon-loop system. It remained to be demonstrated that the 1.2-μ filter effectively attenuates plutonium particles of the size to be encountered in the VTRZ.

The IHS Division of ANL performed a filter-efficiency test using a 1.2-μ filter enclosed in the plutonium-alpha monitor housing. The test was run using atmospheric dust particles and a Bausch and Lomb particle counter, which counted particles 0.3 μ and larger. With a flow rate of about 0.25 cfm, the count efficiency was found to be 99.942%. A further analysis of the dust particles used showed that 90% of them were in the size range of 0.3-0.5 μ. It was concluded that the 1.2-μ filter was virtually a 100% plutonium-particle attenuator. Since only one-fourth of the total flow passes through the filter, the effective attenuation of plutonium in the monitor is 25%, an amount which, as noted from the calculations of Sec. 8.4.2.1, seems adequate.

The counting efficiency, f_i^c, was determined from the electronically-similar impactor-type plutonium-alpha monitors used in ZPR-6. The impactors have a counting efficiency of about 10% within the relatively narrow counting channel necessitated by radon discrimination requirements. For the VTRZ, the energy channel will be wide enough to attain a 30% counting efficiency. The preinstallation phase of the VTRZ project will include a complete determination of counting efficiency versus channel width using a calibrated plutonium-alpha source.

A resolution check was performed on the silicon lithium-drifted detector using a PuAm-on-platinum-disk source, the result being a satisfactory full width at half-maximum value of 117 keV.

Although only negligible background is expected from radon and radon-daughter products during normal VTRZ operation, radon will be present in the loop gas during the initial phase of the startup purge. The extent of this potential background problem will be studied as part of the preinstallation phase. If initial purging does build up radon and radon-daughter-product-bearing dust particles on the detector, then, for future purgings, the monitor can be valved off until the purging is complete.

8.5 Monitoring of Argon Cover-gas Purity

The argon gas in the two VTRZ half-zones must be maintained at a high level of purity during normal operation of the VTRZ. Specifically, the oxygen and water-vapor contents must be less than 50 ppm. There are basically two reasons for these limits. First, an increase in oxygen and/or water vapor would indicate an inner-matrix-envelope seal failure. Second, the maintaining of low oxygen and water-vapor levels reduces the oxidation- and sodium-reaction potentials to negligible levels. This section reviews the capabilities of the Dri-Train purifier, analyzes the effect of argon-loop leak rates, and documents prototype experience using the oxygen and water-vapor monitors.

There are three important quantities to consider in the analysis of the argon-loop purification capabilities assuming a given half-zone leak rate:

(1) The total load of oxygen and water vapor the purifier is capable of handling while still maintaining a purifier exit purity of less than 30 ppm.

(2) The purifier cleanup rate.

(3) The inner-barrel flush-out rate.

As part of the VTRZ prestart checkout procedure, a no-flow leak check is made on the entire argon-loop half-zone system. The tentative maximum permissible leak rate for the system is defined as the leak rate that causes a drop in the system static pressure of 1 in. of water per hour when the system is at -10 in. of water. Such a leak in a half-zone operating at -1.0 in. of water will produce a maximum inleakage of air of 1 cc/min (3.2×10^{-5} cfm). Assuming that the argon gas entering the "leaking" half-zone contains no oxygen or water vapor, the gas exiting the half-zone will contain 32 x (% oxygen or water vapor in reactor cell air)/(argon flow in cfm) parts per million. For a flow of 1 cfm, the oxygen content in the half-zone exit gas is then 6.4 ppm and the water-vapor content (assuming a reactor-cell relative humidity of 10% at 70°F with a corresponding 0.3% water-vapor content) is 0.1 ppm. Clearly, the inner-barrel flush-out rate (1 cfm)

is more than adequate for the leak rates considered, if the Dri-Train purifier does its job of removing oxygen and water vapor from the argon gas.

The two half-zone flows combine and mix with the VTRZ bypass flow (of approximately 22 cfm) before entering the purifier. If the oxygen and water-vapor content of each half-zone is different, the oxygen and water-vapor concentrations entering the purifier will be altered accordingly. The detailed cleanup rate of the purifier is not known. However, it is efficient enough to maintain an exit purity of 1 ppm oxygen and 1 ppm water vapor until it approaches 50% of its total load limit. This load limit has not been reached in a controlled experiment (system in-leakage known for entire experiment). However, the manufacturer's specifications claim that the purifier lifetime for oxygen will be about 700 hr and the corresponding load limit 42,000 cc of air if the in-leakage rate is 1 cc/min. Comparable lifetimes and load limits for water vapor (10% relative humidity) are also claimed.

Since prototype testing has demonstrated that the tentative maximum permissible leak-rate requirement can be met by proper sealing of the half-zones, it is clear that the VTRZ purification system is more than adequate. If required, an even higher leak rate could be tolerated without compromising VTRZ operational flexibility.

Prototype experience has demonstrated the effectiveness of the purification system. For initial leak rates comparable to the tentative maximum tolerable leak rates, oxygen and water-vapor concentrations leveled off at 4 and 2 ppm, respectively, during normal-mode operation. The purge mode will bring both oxygen and water-vapor concentrations down to approximately 100 ppm in about 40 min. It takes another 10-20 min, after switching to the normal mode, for the purifier to bring the concentrations into the operating range ($<$50 ppm).

During prototype heatups, the water-vapor concentration would usually rise slightly due probably to moisture evaporating off the inner-matrix surfaces. The water-vapor monitor performed satisfactorily during its approximately eight months of prototype test operation. It was unaffected by the "bake-off" of inner-barrel combustibles, a phenomenon that was noted by the response of the combustibles monitor. Apparently these combustibles, which are in evidence only during heated operation of the prototype, are contained in dirt, fingerprint oils, etc., introduced into the inner matrix assembly during servicing. For the final VTRZ, great care will be taken to ensure a clean inner barrel and a clean external argon loop.

8.6 Inner-matrix-assembly Expansion Monitor

From room temperature to the heated configuration (20-550°C), the inner-barrel stainless steel expands about 9 mils/in. Since the VTRZ inner-barrel midplane is fixed (relative to the outer matrix), this expansion

has the accumulative effect of moving the VTRZ service housing back about 0.5 in. during heatup and, to a lesser extent, out radially from the VTRZ fixed axis. If the motion of any given point on the service housing is monitored, the heating-cooling cycle will produce a reproducible three-dimensional motion signature if the operation is normal. A mechanical failure of part of the inner-barrel support structure (for example, a cracked ball mount) would register an abnormal motion signature, which could be maximized by a judicial choice of monitoring points. The practicality of an expansion-motion-monitoring system is under study. Ideally, the monitoring system should be able to detect the three possible rotational motions as well as the three translational modes. However, space limitations will probably preclude such complete signatures. The two methods of monitoring suggested are (1) the sensing of the position of insulated metal-bar extensions to the service housing by a set of linear-motion potentiometers and (2) the direct sensing of points on the service housing by using optical techniques. An inner-barrel motion-monitoring system is considered optional and will be installed if it is felt both desirable and practical during the VTRZ installation phase.

9. NUCLEAR ANALYSES FOR TYPICAL VTRZ ASSEMBLIES

9.1 VTRZ Reference Assemblies

Nuclear analyses of typical VTRZ assemblies are described here for two reference assemblies: VTRZ-1 and VTRZ-2. Each assembly consists of radial annular regions surrounding the VTRZ. For VTRZ-1, these regions are an insulation region composed of stainless steel and insulation material, a buffer region of aluminum and U_3O_8, a driver region containing a high concentration of ^{235}U, and a depleted-uranium blanket. VTRZ-2 has an insulation region, a plutonium-fueled driver having approximately the same isotopic composition as the VTRZ, and a depleted-uranium blanket. The buffer and driver regions of both assemblies have an axial reflector of depleted uranium, and the VTRZ has an axial reflector containing depleted-UO_2 rods in place of fissile fuel rods. The detailed configuration of each region of each of the assemblies is summarized in Table 36. The sizes and homogenized compositions of these assemblies are given in Tables 37 and 38. The zone configuration of the assemblies is described in Figs. 90 and 91.

TABLE 36. Regional Cell Patterns in Reference Assemblies

Region	Cell Pattern
	VTRZ-1
VTRZ	$(Pu\text{-}U)O_2$ fuel pins in sodium-filled calandria cans. Plutonium is 15 wt % of the (Pu-U).
Insulation region	This region is a homogenization of Type 304 stainless steel inner- and outer-barrel components and insulation composed mainly of Al_2O_3 and Cr_2O_3.
Buffer region	Plate-form, ZPR drawer loading; 1/4 U_3O_8,[a] 1/4 Al, 1/4 U_3O_8, 1/8 Al, 1/4 U_3O_8, 1/8 Al, 1/4 U_3O_8, 1/4 Al, 1/4 U_3O_8.
Driver region	Plate-form, ZPR drawer loading; 1/8 C, 1/8 SS, 1/8 C, 1/8 enriched U, 1/8 SS, 1/8 C, 1/8 SS, 1/16 SS, 1/8 C, 1/16 SS, 1/8 SS, 1/8 C, 1/8 SS, 1/8 enriched U, 1/8 C, 1/8 SS, 1/8 C.
Radial reflector and axial reflector for buffer, driver, and radial reflector	2 x 2-in. depleted-uranium block in matrix tubes.
Axial VTRZ reflector	Depleted-UO_2 fuel pins in sodium-filled calandria cans.
	VTRZ-2
VTRZ	Same as VTRZ-1.
Insulation region	Same as VTRZ-1.
Driver region	Plate-form, ZPR drawer loading; 1/4 U_3O_8, 1/2 Na, 1/8 Fe_2O_3, 1/4 28 wt % Pu fuel (Pu-U-Mo alloy), 1/8 Fe_2O_3, 1/2 Na, 1/4 U_3O_8.
Radial reflector and axial reflector for driver region and radial reflector	Same as VTRZ-1.
Axial VTRZ reflector	Same as VTRZ-1.

[a]This means 1/4-in.-thick (by 2-in.-high by some length) U_3O_8 plate loaded vertically in the drawer.

TABLE 37. Reference Assembly VTRZ-1[a]

(VTRZ in ZPR-9 Assembly 19)

Region	Equivalent Outer Radius, cm	Homogenized Composition, 10^{20} atoms/cc												
		^{239}Pu	^{240}Pu	^{241}Pu	^{242}Pu	^{238}U	^{235}U	Fe	Ni	Cr	O	Al	Na	C
VTRZ	25.12	8.86	1.18	0.17	0.03	58.25	0.13	124.75	16.06	35.06	135.90		92.90	
Insulation	31.60							82.09	10.38	23.62	14.67	8.05		
Buffer	38.24					82.59	0.17	70.10	7.93	20.00	217.32	187.08		
Driver	49.99					3.25	45.53	288.19	35.36	81.96				303.31
Reflector[b]	79.99					399.30	0.81	43.32	5.40	11.40				
VTRZ axial reflector[c]						69.64	0.15	141.00	12.87	29.06	146.30		90.91	

[a]All regions are 122 cm high.
[b]Radial reflector and 30-cm-thick (each end) axial reflector for buffer, driver, and radial reflector.
[c]30-cm-thick (each end) axial reflector for VTRZ; insulation has no reflector.

TABLE 38. Reference Assembly VTRZ-2[a]

(VTRZ in ZPR-6 Assembly 7)

Region	Equivalent Outer Radius, cm	Homogenized Composition, 10^{20} atoms/cc												
		^{239}Pu	^{240}Pu	^{241}Pu	^{242}Pu	^{238}U	^{235}U	Fe	Ni	Cr	O	Mo	Al	Na
VTRZ	25.12	8.86	1.18	0.17	0.03	58.75	0.13	124.75	16.06	35.06	135.90			92.90
Insulation	31.60							82.09	10.38	23.62	14.67		8.05	
Driver	101.46	8.90	1.18	0.21	0.02	58.14	0.13	138.00	12.49	28.21	146.80	2.26		90.91
Reflector[b]	131.46					399.30	0.81	43.32	5.40	11.40				
VTRZ axial reflector[c]						69.64	0.15	141.00	12.87	29.06	146.80			90.91

[a]All regions are 152.4 cm high.
[b]Radial reflector and 30-cm-thick (each end) axial reflector for ZPPR-3 core.
[c]14.8-cm-thick (each end) axial reflector for VTRZ; insulation has no reflector.

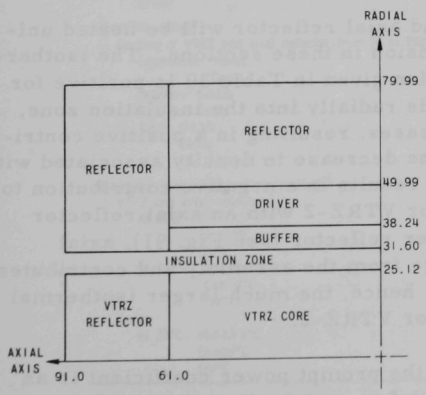

Fig. 90. Zonal Configuration for VTRZ-1 (dimensions in cm)

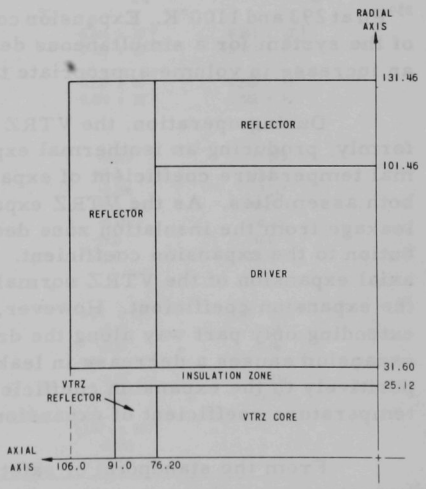

Fig. 91. Zonal Configuration for VTRZ-2 (dimensions in cm)

The nuclear characteristics of the two reference assemblies are considered to be illustrative of the type of assembly in which the VTRZ will be used during the study of dilute liquid-sodium-cooled fast breeder reactors.

9.2 Operational Characteristics of Reference VTRZ Assemblies

Extensive calculations have been performed to describe the operational parameters of the reference assemblies. For the bulk of these computations, the one-dimensional multigroup diffusion code, MACH1,[7] was used. Where diffusion theory was inadequate, as in the description of the effect of insulation zone distortion in criticality, the two-dimensional multigroup S_n transport code, SNARG-2D,[8] was used. The cross sections used in these calculations were generated from ENDF/B data by the MC^2 code[9] and corrected for unit-cell heterogeneity effects. Twenty-two-group cross-section sets were used in the diffusion calculations and six-group sets with an S_n order of six were used in the transport calculations. The criticality parameters and reactivity coefficients computed for the two reference assemblies are listed in Table 39.

Standard techniques were applied to determine control- and safety-rod worths and reactivity coefficients. The worth of a rod was computed as the change in k of the system for an appropriate change in ^{10}B density (^{10}B rod) or fuel density (fuel rod) in the annular control region. The ^{10}B worths were adjusted to account for self-shielding effects within a boron blade. Doppler coefficients were derived from perturbation calculations involving the use of Doppler differences in the cross section of ^{235}U, ^{238}U, and ^{239}Pu at 293 and 1100°K. Expansion coefficients were computed as the change in k of the system for a simultaneous decrease in density of zonal material and an increase in volume appropriate to an expansion over a temperature range.

During operation, the VTRZ and axial reflector will be heated uniformly, producing an isothermal expansion in these sections. The isothermal temperature coefficient of expansion given in Table 39 is positive for both assemblies. As the VTRZ expands radially into the insulation zone, leakage from the insulation zone decreases, resulting in a positive contribution to the expansion coefficient. The decrease in density associated with axial expansion of the VTRZ normally results in a negative contribution to the expansion coefficient. However, for VTRZ-2 with an axial reflector extending only part way along the driver reflector (see Fig. 91), axial expansion causes a decrease in leakage from the assembly and contributes positively to the expansion coefficient; hence, the much larger isothermal temperature coefficient of expansion for VTRZ-2.

From the standpoint of safety, the prompt power coefficient is an important operating parameter. It is the sum of the Doppler coefficient in all core zones and the coefficient of expansion for fuel in the driver. Table 39 gives the coefficient at 20 and 550°C for each assembly. All coefficients are negative and are less at 550°C, due to the smaller Doppler coefficient at this temperature.

TABLE 39. Criticality Parameters and Reactivity Coefficients for Reference Assemblies

Parameter	VTRZ-1	VTRZ-2
Fissile mass (^{239}Pu + ^{241}Pu) in VTRZ, kg	86.7	108.3
Fissile mass (^{239}Pu + ^{241}Pu or ^{235}U) in driver, kg	705.9	1608.5
Total fissile critical mass, kg	792.6	1716.8
Prompt-neutron lifetime, ℓ, sec	4.22×10^{-7}	6.02×10^{-7}
Effective total delayed-neutron fraction, β_{eff}	6.06×10^{-3}	3.18×10^{-3}
Ih/(%Δk/k)	509	1030
Fuel-rod worth in driver region, %Δk/k	0.202	0.024
^{10}B rod worth in driver region, %Δk/k	0.192	0.190
Isothermal temperature coefficient of expansion, (%Δk/k)/°C		
VTRZ and axial reflector	$+3.8 \times 10^{-5}$	$+1.42 \times 10^{-4}$
Buffer	$+1.05 \times 10^{-4}$	-
Coefficient of expansion, driver fuel only heated, (%Δk/k)/°C	-5.59×10^{-4}	-5.06×10^{-4}
Doppler coefficient, C, T(dk/dT) = C, %Δk/k		
VTRZ ^{239}Pu	+0.022	+0.012
VTRZ ^{238}U	-0.206	-0.183
VTRZ axial reflector ^{238}U	-0.011	-0.002
Buffer ^{238}U	-0.147	-
Driver ^{235}U	+0.076	+0.003
Driver ^{238}U	-0.008	-0.871
Driver ^{239}Pu	-	+0.098
Doppler coefficient, C/T, (%Δk/k)/°C		
At 20°C		
VTRZ (^{239}Pu + ^{238}U)	-0.628×10^{-3}	-0.584×10^{-3}
VTRZ axial reflector (^{238}U)	-0.375×10^{-4}	-0.068×10^{-4}
Buffer (^{238}U)	-0.502×10^{-3}	-
Driver (^{235}U + ^{238}U + ^{239}Pu)	$+0.232 \times 10^{-3}$	-0.263×10^{-2}
At 550°C		
VTRZ (^{239}Pu + ^{238}U)	-0.224×10^{-3}	-0.208×10^{-3}
VTRZ axial reflector (^{238}U)	-0.134×10^{-4}	-0.024×10^{-4}
Buffer (^{238}U)	-0.179×10^{-3}	-
Driver (^{235}U + ^{238}U + ^{239}Pu)	$+0.825 \times 10^{-4}$	-0.938×10^{-3}
Prompt power coefficient,[a] (%Δk/k)/°C		
At 20°C		
VTRZ and axial reflector	-0.666×10^{-3}	-0.591×10^{-3}
Driver	-0.327×10^{-3}	-0.314×10^{-3}
At 555°C		
VTRZ and axial reflector	-0.237×10^{-3}	-0.210×10^{-3}
Driver	-0.476×10^{-3}	-1.444×10^{-3}
Reactivity defect[b]		
Heating of VTRZ and axial reflector from 20 to 550°C		
Expansion: %Δk/k	+0.020	+0.075
Cents	+3.3	+23.6
Doppler: %Δk/k	-0.196	-0.177
Cents	-32.3	-55.6
Total: %Δk/k	-0.176	-0.102
Cents	-29.0	-32.0
Ih	-86.0	-105.0
Net isothermal coefficient of reactivity[c]		
VTRZ and axial reflector		
At 20°C: (%Δk/k)/°C	-6.28×10^{-4}	-4.49×10^{-4}
Cents/°C	-0.10	-0.14
Ih/°C	-0.33	-0.46
At 550°C: (%Δk/k)/°C	-1.99×10^{-4}	-0.58×10^{-4}
Cents/°C	-0.03	-0.018
Ih/°C	-0.10	-0.060
Buffer		
At 20°C: (%Δk/k)/°C	-3.97×10^{-4}	-
Cents/°C	-0.066	-
Ih/°C	-0.200	-

[a]Net coefficient: Doppler coefficient plus expansion coefficient for driver fuel only heated.
[b]Reactivity change due to heating the VTRZ (core and axial reflector from a uniform 20°C temperature to 550°C).
[c]Net coefficient: Doppler coefficient plus expansion coefficient.

Table 39 also gives the reactivity change or defect due to heating the VTRZ core and axial reflector from a uniform 20°C to the operating temperature of 550°C. For both assemblies, there is a net loss in reactivity of about 30 ¢. Thus, the heatup of the VTRZ is expected to present no problems in terms of excess reactivity available during startup operation.

The reactivity worths given in Table 40 for sodium, fuel, and fully loaded drawers are of importance during the construction and operation of the VTRZ assemblies. The drawer and fuel worths indicated the relative importance of core materials at various locations in the assemblies. Figures 92 and 93 show the flux and flux adjoint as a function of radial position for VTRZ-1 and VTRZ-2, respectively.

TABLE 40. Material Worths

Material	VTRZ-1 %Δk/k	VTRZ-1 Cents	VTRZ-1 Ih	VTRZ-2 %Δk/k	VTRZ-2 Cents	VTRZ-2 Ih
Sodium Voided from:[a]						
Central calandria can	0.94×10^{-3}	0.16	0.48	4.10×10^{-4}	0.13	0.42
Calandria can at edge of VTRZ[b]	0.95×10^{-3}	0.16	0.48	4.85×10^{-4}	0.15	0.50
Entire VTRZ	-2.65×10^{-1}	-43.7	-135.0	-1.39×10^{-1}	-43.7	-143.0
Entire driver	-	-	-	-1.31	-412.0	-1350.0
Entire assembly	-2.65×10^{-1}	-43.7	-135.0	-1.45	-456.0	-1490.0
Drawer Worths[c]						
Central calandria can	4.34×10^{-2}	7.15	22.1	2.17×10^{-2}	6.82	22.4
Calandria can at edge of VTRZ[b]	3.73×10^{-2}	6.15	19.0	1.87×10^{-2}	5.88	19.3
Buffer	-3.64×10^{-2}	-6.00	-18.5	-	-	-
Outer edge of driver	1.95×10^{-1}	32.2	99.2	7.30×10^{-3}	2.30	7.5
Fuel Worths[d]						
Central calandria can	3.10×10^{-2}	5.11	15.8	1.73×10^{-2}	5.44	17.8
Calandria can at edge of VTRZ[b]	2.76×10^{-2}	4.55	14.1	1.53×10^{-2}	4.81	15.8
Buffer	1.04×10^{-1}	17.2	52.9	-	-	-
Center of driver	-	-	-	6.35×10^{-2}	20.0	65.4
Outer edge of driver	5.94×10^{-2}	9.70	30.2	1.06×10^{-2}	3.34	10.9

[a]Sodium at 100% density used for these calculations.
[b]Calandria can located at the axial center along the outer edge of the VTRZ.
[c]Reactivity change due to the addition of a fully loaded drawer or calandria can.
[d]Reactivity change due to the addition of fuel pins to a calandria can or fuel plates to a drawer. Note that the buffer region contains no fuel plates; the worth reported here assumes ^{235}U fuel plates loaded into a buffer drawer.

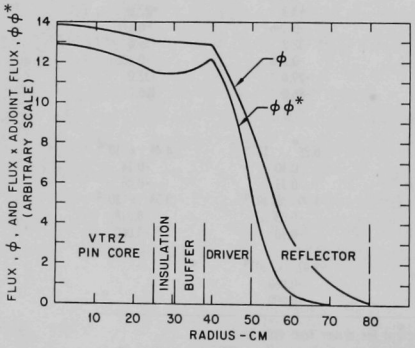

Fig. 92. Radial Flux and Adjoint-flux Distributions for VTRZ-1

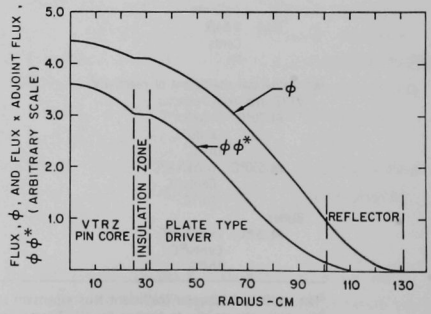

Fig. 93. Radial Flux and Adjoint-flux Distributions for VTRZ-2

During the operation of the VTRZ assemblies, measurements of the central worths of materials will form part of the experimental program. The worths obtained from these measurements will be interpreted as being indicative of the properties of large fast power reactors. It is therefore important that an asymptotic spectrum be established at the center of the VTRZ. The influence of the insulation zone on the central spectrum was investigated by computing central spectra for VTRZ-2 with and without the insulation zone. The results, shown in Table 41, demonstrate that the presence of an insulation zone has little effect on the central spectra.

TABLE 41. Real and Adjoint Flux at Center of VTRZ for VTRZ-2 with and without Insulation Zone[a]

Group	Lower Energy Bound, MeV	VTRZ-2 with Insulation Zone		VTRZ-2 without Insulation Zone	
		φ	φ^*	φ	φ^*
1	3.63	1.406	5.158	1.416	5.164
2	2.23	2.739	5.021	2.760	5.022
3	1.35	3.865	4.652	3.886	4.649
4	8.21×10^{-1}	4.839	4.218	4.854	4.214
5	4.98×10^{-1}	9.448	4.118	9.483	4.114
6	3.02×10^{-1}	8.979	4.004	9.007	4.002
7	1.83×10^{-1}	11.784	3.899	11.824	3.898
8	1.12×10^{-1}	11.180	3.800	11.217	3.800
9	6.74×10^{-2}	10.207	3.686	10.224	3.687
10	4.09×10^{-2}	8.513	3.596	8.509	3.597
11	2.48×10^{-2}	6.852	3.580	6.833	3.583
12	1.50×10^{-2}	6.141	3.641	6.115	3.643
13	9.12×10^{-3}	4.446	3.784	4.419	3.785
14	4.31×10^{-3}	3.735	3.964	3.703	3.965
15	2.61×10^{-3}	0.729	4.334	0.723	4.334
16	2.03×10^{-3}	0.494	4.440	0.489	4.440
17	1.23×10^{-3}	0.182	4.518	0.179	4.518
18	9.61×10^{-4}	0.714	4.778	0.701	4.777
19	5.83×10^{-4}	1.025	5.193	0.998	5.193
20	2.75×10^{-4}	0.766	5.843	0.740	5.843
21	1.01×10^{-4}	0.281	6.383	0.269	6.384
22	2.90×10^{-5}	0.041	7.388	0.038	7.388

[a]VTRZ-2 without insulation zone assumes insulation zone filled with driver material.

During the experimental program, it may be necessary to introduce various materials into the insulation zone: electrical cables containing organic compounds including hydrogen, wire leads, stainless steel equipment pieces, etc. The influence of such materials present in the insulation zone

upon the central worths in the VTRZ was studied by computing central worths for various amounts of hydrogen, stainless steel, and insulation material in the insulation zone. It was found that:

(1) Only sodium central worths are appreciably changed by changes in the insulation region.

(2) The sodium central worth was decreased 10% with the presence of a large amount of hydrogen (about 0.2 wt %) in the insulation zone and increased by 20% by doubling the amount of stainless steel in the insulation zone.

(3) Adding or subtracting 25% of the insulation material had a negligible effect on central worths.

9.3 Calculations of Core-distortion Effect

Core distortion due to structural failure of the outer matrix assembly and central zone bridge combination is an extremely unlikely event. However, to perform hypothetical accident analyses, certain reactivity changes caused by gross core distortions have been calculated. The results of accident analyses based on these calculations are given in Sec. 4.3.6 of ANL-7638. The accident analyses in ANL-7638 are intended as worst-case scoping calculations and, as such, use as input the maximum reactivity change caused by uniform inward radial compression of the buffer and driver regions radially inward to the edge of the core. This uniform decrease of the outer radius of the insulation zone along the entire length of the zone is called a "uniform insulation annulus compression." The calculated reactivity changes resulting from uniform insulation-annulus compression shown in Table 42 are intended as upper limits of hypothetical accidents rather than estimates of the reactivity effect of any actual compression of the insulation zone.

TABLE 42. Reactivity Effect due to Collapse of Insulation Zone[a]

	%Δk/k	
Extent of Collapse[b]	VTRZ-1	VTRZ-2
1/4	-	+0.43
1/2	-	+0.71
3/4	-	+1.01
Full collapse	+0.59	+1.10

[a]Buffer and driver regions collapse uniformly through the insulation zone toward the core.

[b]1/4 collapse means buffer and driver regions have advanced one-quarter of the distance through the insulation zone toward the core. Full collapse is accomplished when insulation-zone materials have been compressed to the density of stainless steel.

The maximum possible reactivity changes caused by insulation-annulus compression, 0.59% $\Delta k/k$ for VTRZ-1 and 1.10% $\Delta k/k$ for VTRZ-2, are less than the 2% $\Delta k/k$ minimum safety-rod shutdown margin required for reactor operation. It is probable, therefore, that if a partial collapse of the insulation annulus did occur, a reactor scram would terminate any excursion before appreciable flux heating could occur.

To define the worst possible core-distortion accident, a core collapse was analyzed assuming no rod- or table-motion reactivity subtraction, i.e., assuming the core distortion disables all normal mechanical-scram reactivity-reduction methods. The analysis is discussed in detail in Sec. 4.3.6 of ANL-7638. The collapse of the insulation annulus was assumed, for purposes of defining the worst possible accident, to occur with free-fall velocity. Even with the above very conservative assumptions, the consequences of an insulation-annulus collapse were shown to be less than the consequences of the usual design basis accident. Even a worst possible core collapse, therefore, can be contained within the limits set forth for the ZPR reactor cells. It should further be noted that while even a partial annulus collapse is an extremely unlikely event, a complete insulation-annulus collapse like the one postulated is essentially impossible. Any actual collapse would occur in only a fraction of the insulation annulus, probably no more than one-quarter of the total annulus. Further, any actual collapse of the core would proceed by relatively slow sagging, in terms of reactivity removal rates during scram, of the outer matrix. It is likely, therefore, that even if an annulus collapse did occur, no fuel would be melted and no sodium boiled, so that there would be no damage to the reactor cell and no radiological hazard.

ACKNOWLEDGMENTS

We wish to acknowledge the contributions of the following persons to the Variable Temperature Rodded Zone and to the writing of this report:

Applied Physics Division

C. E. Till, G. K. Rusch, D. M. Smith, D. J. Kilsdonk, T. W. Johnson, R. D. Shields, W. J. Grajek, F. L. Willis, and D. R. MacFarlane.

Electronics Division

W. P. McDowell, J. M. Paul, A. L. Winiecki, and H. W. Helenberg.

Plant Engineering Division

L. J. Kelly.

Central Shops Department

J. J. McKinney, A. A. Frigo, E. F. Bielick, D. A. Cassidy, R. F. Hall, E. F. Lewandowski, and the other shop personnel in the Building 316 and Building 20 shops who made valuable contributions to this project.

Laboratory Director's Office

F. H. Martens.

Engineering and Technology Division

T. J. Lucitt and R. A. Banike.

REFERENCES

1. Merit P. White *et al.*, *Argonne Advanced Research Reactor Seismicity Report Phase I* (1967). (Copies available from ANL QAM Group)

2. W. Y. Kato, G. K. Rusch, L. R. Dates, C. E. Till, A. Ancarani, J. van Doorninck, C. L. Cheever, and E. M. Bohn, *Final Safety Analysis Report on the Use of Plutonium in ZPR-6 and -9*, ANL-7442 (Feb 1970).

3. W. Y. Kato, G. J. Fischer, and L. R. Dates, *Safety Analysis Report, Argonne Fast Critical Facility (ZPR-VI)*, ANL-6271 (Dec 1963).

4. W. Y. Kato and L. R. Dates, "Design and Construction of the Argonne Fast Critical Facility (ZPR-6)," *Physics of Fast and Intermediate Reactors*, IAEA, Vienna (1962).

5. L. R. Dates, *Design, Construction Details, and Preoperational Testing of the Argonne Fast Critical Facility*, ANL-7195 (Apr 1966).

6. C. E. Cohn, G. S. Rosenberg, L. R. Dates, W. B. Loewenstein, and G. H. Golden, *Safety Analysis for the ZPR-9 Facility* [*An Addendum to ANL-6271, Safety Analysis Report, Argonne Fast Critical Facility (ZPR-6)*], ANL-7166 (Feb 1966).

7. D. A. Meneley, L. C. Kvitek, and D. M. O'Shea, *MACH1, A One-dimensional Diffusion-theory Package*, ANL-7223 (June 1966).

8. G. J. Duffy, H. Greenspan, S. D. Sparck, J. V. Zapatka, and M. K. Butler, *SNARG-2D, A Two-dimensional, Discrete-ordinate, Transport-theory Program for the CDC-3600*, ANL-7426 (Mar 1968).

9. B. J. Toppel, A. L. Rago, and D. M. O'Shea, *MC^2, A Code to Calculate Multigroup Cross Sections*, ANL-7318 (June 1967).